

A Thesis Submitted for the Degree of PhD at the University of Warwick

Permanent WRAP URL:

<http://wrap.warwick.ac.uk/133202>

Copyright and reuse:

This thesis is made available online and is protected by original copyright.

Please scroll down to view the document itself.

Please refer to the repository record for this item for information to help you to cite it.

Our policy information is available from the repository home page.

For more information, please contact the WRAP Team at: wrap@warwick.ac.uk

The Influence of Metallic Surface Topography towards Adhesion of Gram- positive & Gram-negative Bacteria

by

Ahmad Johari Mohamad

A thesis submitted in partial fulfilment of the requirements for the
degree of
Doctor of Philosophy in Engineering

University of Warwick, School of Engineering
May 2019

TABLE OF CONTENTS

ACKNOWLEDGEMENT	v
DECLARATION	vi
ABSTRACT	vii
List of Abbreviations	viii
List of Figures	x
List of Tables	xiv
Chapter 1 Introduction	15
1.1 Problem Statement	15
1.2 Background of the Study	18
1.3 Motivation for the Study	20
1.4 Aims	21
1.5 Project Objectives	22
1.6 Organisation of the Thesis	24
Chapter 2 Literature Review	26
2.1 Learned from nature	26
2.1 Biomaterial and the Application	28
2.2 Surface topographies	30
2.3 Surface Wettability	31
2.4 Surface finishing techniques	33
2.4.1 Polishing	33
2.4.2 Wire EDM	34
2.4.3 Laser Fabrication	35
2.6 Mechanism and Factors Governing Bacterial Adhesion	38
2.6.1 Bacterial properties	39
2.6.2 Surface properties	40
2.6.3 Environmental Condition	44
2.6.4 Micro-organisms: <i>S. aureus</i> , <i>E. coli</i> and <i>B. subtilis</i>	45
2.6.5 Wire Electrical Discharge Machine (WEDM)	47
2.6.6 Laser-assisted technique	48
2.6 Biological	49
2.7.1 Optical density (OD)	51
2.8 Chapter Summary	54
Chapter 3 Bacterial Characterisation & Process Screening	55
3.1 Introduction to Partial Characterisation of Micro-organism	55

3.2	Growth curve	56
3.3	Partial characterisation of the model organism.....	59
3.3.1	Determination of Cell Size.....	61
3.3.2	Determination Cell Surface Hydrophobicity (CSH)	63
3.3.3	Determination of Bacteria Zeta Potentials	68
3.4	Screening of the Process Condition for Bacterial Adhesion on Glass	68
3.4.1	Preliminary adhesion of <i>E. coli</i> and <i>B. subtilis</i> on the glass substrata.	69
3.4.2	Effect of Cell Concentration on the Percentage of Adhesion	77
3.4.3	Effect of Culture Age on the Percentage of Adhesion	80
3.5	Chapter Summary	87
Chapter 4 Polished Surface Characterisation with respect to Contact Angle Measurement and Bacterial adhesion.....		88
4.1	Introduction.....	88
4.2	Polished Surface Characterisation	89
4.2.1	Polished Surface Height Characterisation.....	89
4.2.2	Spatial and Hybrid Parameter Analysis	94
4.3	The Correlation between Contact Angles and Surface Roughness.....	97
4.4	Bacteria-Surface Adhesion	100
4.5	Bacterial Adhesion on Control sample	101
4.6	Bacterial Adhesion on Polished Stainless-Steel.....	103
4.7	Bacterial Adhesion on Polished Titanium.....	105
4.8	Correlation Between Surface Parameter, Contact Angle and Bacterial Adhesion.....	106
4.9	Chapter Summary	112
Chapter 5 WEDM Surface Characterisation with respect to Contact Angle Measurement and Bacterial adhesion		113
5.1	Introduction.....	113
5.2	WEDM Surface Characterisation.....	116
5.2.1	WEDM Height Parameter Characterisation.....	116
5.2.2	Spatial and Hybrid Parameter Characterisation	119
5.3	The Correlation between Contact Angle Measurement and Surface Topography Parameter.....	123
5.4	Bacteria-Surface Adhesion	126
5.5	Bacterial Adhesion on WEDM stainless-steel	126
5.6	Bacteria Adhesion on WEDM titanium	129
5.7	Correlation Between Surface Parameter, Contact Angle and Bacterial Adhesion.....	130
5.8	Chapter Summary	137

Chapter 6 Laser-Assisted Surface Characterisation with respect to Contact Angle Measurement and Bacterial Adhesion.....	138
6.1 Introduction.....	138
6.2 Laser-Assisted specimen: The correlation of surface topography and wettability	140
6.2.1 Height Parameter Analysis.....	141
6.2.2 Laser scan Speed correlation with Sa and Sv	145
6.2.3 Spatial and Hybrid Parameter Characterisation	146
6.3 The correlation of Contact Angle with Surface Topography Parameter.....	149
6.4 Bacterial adhesion on Stainless Steel that has undergone laser treatment	153
6.5 Bacterial adhesion on Titanium that has undergone femtosecond laser treatment	155
6.6 Discussion on the effect of modified properties towards bacterial adhesion	159
6.7 Viewing the adhesion patterns using SEM	165
6.8 Correlation of Wettability and Surface Topographies with Bacterial Adhesion	176
6.9 Chapter Summary	182
Chapter 7 Conclusions and Recommendations.....	183
7.1 Conclusions.....	183
7.2 Recommendations for future studies.....	188
REFERENCES.....	190

ACKNOWLEDGEMENT

First and foremost, I would like to thank Prof X. Liu for her excellent supervision, guidance and the never-ending support throughout the completion of this study. I would also like to extend my gratitude to Prof Elizabeth Wellington for allowing my work to be carried out in her laboratory at the School of Life Sciences University of Warwick. Martin Davis deserves a mention for his assistance in handling the analytical instruments at the metrology laboratory, School of Engineering.

I would like to acknowledge the collaborators of the FABSURFWAR projects from the Karlsruhe Institute of Technology (KIT) Germany, Dr W. Pfleging, Alexandra Reif, and Jan Rakebrandt for their help in laser fabrication and helpful guidance on the effect of laser's parameter towards the surface patterning.

I would like to thank my late father Mohamad Hussin, my lovely mother, Rafiah Ab Rahman, brothers and sisters, my lovely wife, Dr Wan Salwanis Wan Md Zain, all my children, Ayyash Mukhlis, Anas Mukhlis, Asra Imani, Afra Imani and Adra Imani for their steadfast support, encouragement and undivided help during the hard times in the completion of this study. Without them, all this wouldn't be possible to complete. Not to forget all my friends in Coventry, especially Abang Fuad, Kak Shidah and family who have been very good companions.

A heartfelt appreciation goes to my Sponsors, Universiti Malaysia Pahang (UMP) and the Ministry of Higher Education Malaysia (MOHE) for the chance and financial support for this study. Last but not least, my foremost gratitude goes to Allah SWT Who has made all this possible. Alhamdulillah.

DECLARATION

I hereby declare that the thesis is my original work and it has been written by me in its entirety. I have duly acknowledged all the sources of information which have been used in the thesis.

This thesis has also not been submitted for any degree in any university previously

Ahmad Johari b Mohamad

May 2019

ABSTRACT

The presence of bacteria on metals is considered a serious source of potential contamination for domestic and industrial environments. Possible contributing factors to the formation of biofilm are related to the surface properties of materials used such as surface topography and hydrophobicity. Surface topography and hydrophobicity will be the focus in this investigation towards Gram-positive and Gram-negative bacteria (*S. aureus*, *E. coli* and *B. subtilis*) adhesion. Modified surfaces of 316L stainless-steel and Ti6Al4V, titanium prepared by polishing, WEDM and laser-assisted technique and the as-received substrates were also considered in the study. The corresponding surface topography and contact angle measurement were assessed by Bruker Optical Profilometry and Kruss DSA, Germany. The number of adhered bacterial on metal surfaces was determined by O.D, CFU and Fluorescent Microscopy. Polished, WEDM and laser-assisted surfaces managed to mitigate bacteria adhesion as opposed to controlling surfaces but increased the adhesion of *E. coli* on both stainless steel and titanium. The introduction of laser-assisted technique using argon gas successfully combatted the adhesion of both Gram-positive and Gram-negative bacteria, revealing the lowest adhesion for *S. aureus* and *E. coli*, surpassing those on polished surface and WEDM. The success factor was presumably contributed by the ability to suppress oxidation, while contours and nanograin surface effects prevent entrapments of bacteria whilst inducing an antibacterial property through contact killing mode.

List of Abbreviations

AFM	Atomic Force Microscopy
<i>B. cereus</i>	<i>Bacillus cereus</i>
<i>B. subtilis</i>	<i>Bacillus subtilis</i>
<i>B.cereus</i>	<i>Bacillus cereus</i>
CA	Contact angle
CAM	Contact angle measurement
CFU	Colony Forming Unit
CLSM	Confocal Laser Scanning Microscopy
CO ₂	Carbon Dioxide
<i>E. coli</i>	<i>Escherichia coli</i>
EPS	Extracellular Polymeric Substance
Fe ²⁺	Iron
HCl	Hydrochloric acid
K ₂ HPO ₄	Dipotassium Phosphate
KCl	Potassium Chloride
KH ₂ PO ₄	Monopotassium Phosphate
LP	Laser parameter
LP _x	Laser parameter step x, x = 1-4
MgSO ₄	Magnesium Chloride
NaCl	Sodium Chloride
NaOH	Sodium Hydroxide
OD	Optical Density
PBS	Phosphate Buffer Solution
PIA	Polysaccharide Intercellular Adhesion
<i>S. aureus</i>	<i>Staphylococcus aureus</i>
<i>Sa</i>	Roughness average
<i>Sds</i>	Summit density
<i>Sdr</i>	Developed Interfacial Area Ratio
<i>Sdq</i>	RMS Surface Slope

<i>Str</i>	Texture Aspect Ratio
<i>E. coli</i>	<i>Escherichia coli</i>
SEM	Scanning Electron Microscope
<i>Sku</i>	Kurtosis
<i>Sq</i>	Root mean square roughness
SS	Stainless steel
SSC	Stainless steel - control (mirror finish)
SSE	Stainless steel undergone EDM
<i>Ssk</i>	Skewness
SSL	Stainless steel undergone laser
SSL-Air	Stainless steel undergone laser fabrication in air
SSL-Ar	Stainless steel undergone laser fabrication in argon
SSP	Stainless steel undergone polishing
TI	Titanium
TIC	Titanium – control (mirror finish)
TIE	Titanium undergone EDM fabrication
TIL	Titanium undergone laser fabrication
TIL-Air	Titanium undergone laser fabrication under air
TIL-Ar	Titanium undergone laser fabrication under argon
TIP	Titanium undergone polishing process
WEDM	Wire-Electrical discharge machine

List of Figures

Figure 1-1 Scope of the experiment.....	23
Figure 2-1: Schematic set up of laser fabrication of bioactive glass where the laser beam was passed through the neutral density filter (NDF) and lens (L = 5 cm focal lengths) before hits the sample on the computer-controlled X-Y stages.	36
Figure 2-2 Factors that influence the development and biology of a biofilm.....	44
Figure 2-3 SEM's image of a) <i>S. aureus</i> , b) <i>E. coli</i> and c) <i>B. subtilis</i> (Carr, 2007)	45
Figure 3-1 The growth curves of a) <i>S. aureus</i> , b) <i>E. coli</i> and c) <i>B. subtilis</i> , grown in 250 mL flask containing LB medium for 24 hours, with shaking at 200 rpm and 37°C.[OD , CFU]...	57
Figure 3-2: Images of the exponential phase-cells of a) <i>S. aureus</i> , b) <i>E. coli</i> and c) <i>B. subtilis</i> from 10 hours culture, observed under SEM at magnification between 2500x - 3000x.....	60
Figure 3-3 Images from Gram staining analysis of a) <i>S. aureus</i> , b) <i>E. coli</i> and c) <i>B. subtilis</i>	60
Figure 3-4 Close up pictures of a) <i>S. aureus</i> , b) <i>E. coli</i> and c) <i>B.subtilis</i> under 4000x magnification using SEM.	62
Figure 3-5 Bacterial adhesion on solvent a) hexadecane, b) hexane, c) chloroform, and d) ethyl acetate. Adhesion was carried out using bacteria at the exponential phase and the late stationary phase using 10-hour culture and 66 hours culture, respectively.	65
Figure 3-6 Percentage adhesion of <i>S. aureus</i> , <i>E. coli</i> and <i>B. subtilis</i> on the glass substrates. Samples were immersed in bacterial suspension (OD = 1.0) for 24 hours.	69
Figure 3-7 Number of cells adhered on the glass substrata after immersion in the bacterial suspension with initial OD of 1.0 (containing approximately $\sim 10^8$ CFU/mL of active cells in the exponential phase). Bacteria were quantified at 4, 8, 12 and 24 hours.	71
Figure 3-8 The images show the adhered <i>S. aureus</i> on the glass slide viewed under light microscopy at a) 4 hours, b) 8 hours, c) 12 hours and d) 24 hours.	75
Figure 3-9 The images show the adhered <i>E. coli</i> on the glass slide viewed under light microscopy at a) 4 hours, b) 8 hours, c) 12 hours and d) 24 hours.	76
Figure 3-10 The images show the adhered <i>B. subtilis</i> on the glass slide viewed under light microscopy at a) 4 hours, b) 8 hours, c) 12 hours and d) 24 hours.	76
Figure 3-11 Numbers of remaining bacteria in the PBS solution during 24 hours of exposure on the glass substrate.	77
Figure 3-12 Number of cells adhered on the glass substrata after 24 hours immersion in the bacterial suspension with initial OD of 0.8, 1.0 and 1.2 containing active cells in the exponential phase. Bacteria were viewed using a light microscope.....	78
Figure 3-13 The adhered cells after 24 hours exposure to the glass surface at OD a) 0.8, b) 1.0 and c) 1.2. Bigger flocs were formed at higher cell concentration.	79
Figure 3-14 : <i>E. coli</i> (A) and <i>B. subtilis</i> (B) with contact on the glass surface for 24 hours at initial cell concentration of 1.2.	80
Figure 3-15 Percentage adhesion of, <i>E. coli</i> and <i>B. subtilis</i> on the glass substrates after 24 hours exposure to the bacteria solution containing active () and stationary-phase () cells.....	81
Figure 3-16 Number of adhered cells per mm ² area; exponential-phase cells () and stationary phase-cells () on the glass substrates after 24 hours exposure with bacterial suspension in PBS buffer with initial OD of 1.0 containing cells at $\sim 1 \times 10^8$ /mL.	82
Figure 3-17 Light microscopy images showing adhered exponential phase cells of a) <i>S. aureus</i> , b) <i>E. coli</i> and c) <i>B. subtilis</i> , on glass substrates at 24 hours exposure to bacterial solution (approximately 1×10^8 CFU mL) while (b), (d) and (e) are the adhered stationary phase cells, respectively.	84

Figure 3-18: Adhered cells (<i>B. subtilis</i>) on the glass substrate for cells in the exponential phase (a & b), cells in the stationary phase (c & d).	85
Figure 4-1 Graph of the height parameters on 316L and Ti6Al4V with respect to A) <i>Sa</i> and <i>Sq</i> , B) <i>Sku</i> and <i>Ssk</i>	90
Figure 4-2 Graph of the height parameters on 316L and Ti6Al4V with respect height surfaces parameter, <i>SP</i> (max peak height), <i>Sv</i> (max valley depth) and <i>Sz</i> (max height of surface)	91
Figure 4-3 Bruker images on polished stainless-steel and titanium.....	92
Figure 4-4 Correlations between graph A) <i>Sa</i> and polished grit and B) kurtosis (<i>Sku</i>)and skewness (<i>Ssk</i>). $R^2 > 0.7$ indicated strong correlation, $R^2 = 0.5 - 0.69$ represented moderate correlation and $R^2 = 0.49 - 0.3$ poorly correlated and $R^2 < 0.29$ provided no correlation.....	93
Figure 4-5 3D optical profilometry images with spatial parameter data.....	95
Figure 4-6 Auto-correlation on polished stainless-steel specimen.....	96
Figure 4-7 Auto-correlation on polished titanium specimen	96
Figure 4-8 Graph of contact angle measurement on metallic polished specimen.....	97
Figure 4-9 Correlation between a), average roughness, <i>Sa</i> b) kurtosis, <i>Sku</i> c) skewness, <i>Ssk</i> d) auto-correlation length, <i>Sal</i> e) developed interfacial area ratio. <i>Sdr</i> h) summit density, <i>Sds</i> with water contact angle on 316L and Ti6Al4V Specimen.	98
Figure 4-10 Number of bacterial adhered on stainless steel and titanium undergone surface polishing technique (mirror finishing) after four hours t at 37°C and CFU ~ 1 x 10 ⁸ CFU/mL.	101
Figure 4-11 Graph of bacterial adhesion on the polished-stainless steel	103
Figure 4-12 Graph of bacterial adhesion on the polished titanium	105
Figure 4-13 Correlation between CA, <i>Sa</i> and <i>Sds</i> with bacteria adhesion (<i>S. aureus</i> ■ , <i>E. coli</i> ■ and <i>B. subtilis</i> ■) on SSP a), c), e) and on TIP b), d), f).....	108
Figure 4-14 Correlation between <i>Sku</i> and <i>Ssk</i> and bacteria adhesion (<i>S. aureus</i> ■ , <i>E. coli</i> ■ and <i>B. subtilis</i> ■) on SSE a), c), e) and TIE b), d), f).....	110
Figure 4-15 Fluorescent images of a) SSP-without bacteria, b) <i>S. aureus</i> on SSP, c) TIP without bacteria, and d) <i>S. aureus</i> on TIP e) <i>E. coli</i> on SSP, f) <i>B. subtilis</i> on SSP, g) <i>E. coli</i> on TIP and h) <i>B. subtilis</i> on TIP.	111
Figure 4-16 SEM images of <i>E. coli</i> on titanium specimen at different magnification, a) 5000x, b) 1000x and c) 500x	111
Figure 5-1 WEDM stainless-steel morphology a) SSE-01 (10mm/min), b) SSE-02 (12mm/min), SSE-03 (20mm/min) and d) SSE-04 (22mm/min).....	114
Figure 5-2 WEDM titanium morphology a) TIE-01 (10mm/min), b) TIE-02 (12mm/min), TIE-03 (20mm/min) and d) TIE-04 (22mm/min).....	115
Figure 5-3 Graph of the height parameters on 316L and Ti6Al4V with respect to A) <i>Sa</i> and <i>Sq</i> , B) <i>Sku</i> and <i>Ssk</i>	117
Figure 5-4 Graph of height parameter on 316L and Ti6Al4V with respect to maximum height surface parameter, <i>SP</i> (max peak height), <i>Sv</i> (max valley depth) and <i>Sz</i> (max height of surface)	118
Figure 5-5 3D optical profilometry for TIE-02 with <i>Sa</i> = 3.30 μ m, <i>Sku</i> = 3.34, <i>Ssk</i> = 0.38, <i>SP</i> = 33.48, <i>Sv</i> = -15.99 and <i>Sz</i> = 49.48.....	118
Figure 5-6 Correlations between a) average roughness, <i>Sa</i> (μ m) and machine feed rate (mm/min) b) maximum height surfaces, <i>Sz</i> (μ m) and machine feed rate (mm/min) on WEDM stainless-steel and titanium. $R^2 > 0.7$ indicated strong correlation, $R^2 = 0.5 - 0.69$ represented moderate correlation and $R^2 = 0.49 - 0.3$ poorly correlated and $R^2 < 0.29$ provided no correlation.	119

Figure 5-7 3D optical profilometry images for a) Ti6Al4V with Std = -81.23, Str = 0.10 and b) Ti6Al4V with Std = n/a, Str = 0.85.....	121
Figure 5-8 ACF on WEDM stainless-steel specimen	122
Figure 5-9 ACF on WEDM titanium specimen	123
Figure 5-10 A graph of contact angle measurement on EDM specimen	123
Figure 5-11 The correlation between a), average roughness, <i>Sa</i> b) kurtosis, <i>Sku</i> c) skewness, <i>Ssk</i> d) auto-correlation length, <i>Sal</i> e) developed interfacial area ratio. <i>Sdr</i> h) summit density, <i>Sds</i> with water contact angle on 316L and Ti6Al4V specimen.....	125
Figure 5-12 A graph of bacteria adhesion on WEDM stainless-steel specimen (SSE)	127
Figure 5-13 Graph of bacteria adhesion on WEDM titanium (TIE)	129
Figure 5-14 Correlation between <i>Sa</i> , <i>Sku</i> , <i>Ssk</i> and bacteria adhesion (<i>S. aureus</i>  , <i>E. coli</i>  and <i>B. subtilis</i> ) on stainless-steel (a), (c), (e) and on titanium (b), (d), (f).....	132
Figure 5-15 Correlation between <i>Sku</i> and <i>Ssk</i> and bacteria adhesion (<i>S. aureus</i>  , <i>E. coli</i>  and <i>B. subtilis</i> ) on stainless-steel (a), (c), (e) and on titanium (b), (d), (f).....	135
Figure 6-1 Images for the titanium undergone femto-second irradiation techniques showing all the available features on the modified surfaces viewed with SEM.....	139
Figure 6-2 Graph of height parameter on 316L and Ti6Al4V with respect to a) <i>Sa</i> and <i>Sq</i> , b) <i>Sku</i> and <i>Ssk</i> and c) SP (max peak height), <i>Sv</i> (max valley depth) and <i>Sz</i> (max height of surface) ..	142
Figure 6-3 Graph of height parameter on 316L and Ti6Al4V with respect to a) <i>Sa</i> and <i>Sq</i> , b) <i>Sku</i> and <i>Ssk</i> and c) SP (max peak height), <i>Sv</i> (max valley depth) and <i>Sz</i> (max height of surface) ..	144
Figure 6-4 Correlation between A) average roughness, <i>Sa</i> and laser scan Speed (mms^{-1}) on 316L (air) and 316L (argon), B) average roughness, <i>Sa</i> and laser scan Speed (mms^{-1}) on Ti6Al4V (air) and Ti6Al4V (argon).....	145
Figure 6-5 Correlation between A) max height surface, <i>Sz</i> and laser scan Speed (mms^{-1}) on 316L (air) and 316L (argon), B) max height surface, <i>Sz</i> and laser scan Speed (mms^{-1}) on Ti6Al4V (air) and Ti6Al4V (argon).....	146
Figure 6-6 3D optical profilometry images on SSL-01 (Air) and SSL-01 (Ar).....	148
Figure 6-7 The difference between dominant lay surface and isotropic surface of Ti6Al4V ...	149
Figure 6-8 Graph of water contact angle on laser-assisted on 316L and Ti6Al4V	150
Figure 6-9 Correlation between contact angle and A) average roughness, <i>Sa</i> on 316L C) surfaces kurtosis, <i>Sku</i> on 316L, E) surface skewness, <i>Ssk</i> on 316L, B) average roughness, <i>Sa</i> on Ti6Al4V, D) surface kurtosis, <i>Sku</i> , F) surface skewness, <i>Ssk</i>	151
Figure 6-10 Correlation between contact angle and A) summits density, <i>Sds</i> , C) developed interfacial area ratio, <i>Sdr</i> on 316L, B) summits density, <i>Sds</i> , D) developed interfacial area ratio, <i>Sdr</i> on Ti6Al4V.....	152
Figure 6-11 Numbers of adhered bacteria on lasered surfaces (stainless steel) after exposure to bacterial suspension (1×10^8 CFU/mL) for four hours at 37°C. (SA- <i>S. aureus</i> ; EC – <i>E. coli</i>)	154
Figure 6-12 Numbers of adhered bacteria on lasered surfaces (titanium) after exposure to bacterial suspension (1×10^8 CFU/mL) for four hours at 37°C. (SA- <i>S. aureus</i> ; EC – <i>E. coli</i>)	157
Figure 6-13 Adhesion of <i>S. aureus</i> on three difference parts of the multi scales stainless steel surfaces undergone laser treatment (air)	167
Figure 6-14 Adhesion of <i>S. aureus</i> on three difference parts of the multi scales stainless steel surfaces undergone laser treatment (argon)	168
Figure 6-15 Adhesion of <i>S. aureus</i> on three difference parts of the multi scales titanium surfaces undergone laser treatment in (air)	168
Figure 6-16 Adhesion of <i>S. aureus</i> on three difference parts of the multi scales titanium surfaces undergone laser treatment in (argon).	169

Figure 6-17 Adhesion of <i>E. coli</i> on three difference parts of the multi scales stainless steel surfaces undergone laser treatment (air)	171
Figure 6-18 Adhesion of <i>E. coli</i> on three difference parts of the multi scales stainless steel surfaces undergone laser treatment (argon)	172
Figure 6-19 Adhesion of <i>E. coli</i> on three difference parts of the multi scales titanium surfaces undergone laser treatment (air)	173
Figure 6-20 Adhesion of <i>E. coli</i> on three difference parts of the multi scales titanium surfaces undergone laser treatment (argon)	173
Figure 6-21 Formation of cells clusters by <i>S. aureus</i> on the unstructured area of a) SS and b) TI fabricated in air.	174
Figure 6-22 Fluorescence images of <i>S. aureus</i> on the SSL-02-Ar (a-b) and <i>E. coli</i> on the TIL4-Ar (c-d) showing more cells were retained on the unstructured area than the LIPSS.	175
Figure 6-23 The SEM images showing the shape of <i>S. aureus</i> and <i>E. coli</i> on the structured (LIPSS) and unstructured stainless steel and titanium fabricated in air and argon. a) Polished sample, b) <i>S. aureus</i> -air, c) <i>S. aureus</i> -argon, d) <i>E. coli</i> air and e) <i>E. coli</i> -argon.....	177
Figure 6-24 Correlation between CA, S_a and S_{ds} on the adhesion of <i>S. aureus</i> and <i>E. coli</i> on SS (a, c, and e) and TI (b, d and f) in air and argon fabrication. () SA-Air, () SA- AR, (an) EC-Air and (X) EC-AR.	178
Figure 6-25 Correlation between S_{sk} and S_{ku} on the adhesion of <i>S. aureus</i> and <i>E. coli</i> on SS (a and b) and TI (c and d) in air and argon fabrication. () SA-Air, () SA- AR, (an) EC -Air and (X) EC-AR. $R_2 > 0.7$ indicated strong correlation, $R_2 = 0.5 - 0.69$ represented moderate correlation and $R_2 = 0.49 - 0.3$ poorly correlated and $R_2 < 0.29$ provided no correlation.	181

List of Tables

Table 3-1 Size of bacteria at the exponential and stationary phase	61
Table 3-2 Determination of electron acceptor/donor properties [131]	67
Table 3-3 Surface charge of the bacteria in exponential and stationary phase	68
Table 4-1 Spatial and Hybrid Parameter Data on Polished Metallic Specimen.....	94
Table 4-2 Size of bacteria at the exponential stage.....	100
Table 4-3 Data on Surface Topography Parameter, Contact Angle and Bacteria Adhesion	102
Table 4-4 Total number of bacteria adhered on stainless steel and titanium	106
Table 5-1 WEDM topography data on a spatial and hybrid parameter for 316L stainless-steel and Ti6Al4V, titanium	121
Table 5-2 Data on Surface Topography Parameter, Contact Angle and Bacteria Adhesion undergone WEDM fabrications	128
Table 5-3 Total number of bacteria adhered on stainless steel and titanium	130
Table 6-1 Laser parameter for different surface topographies.....	140
Table 6-2 Laser parameter for different surface topographies.....	141
Table 6-3 Spatial and hybrid parameter data on 316L and Ti6Al4V.....	147
Table 6-4 Data for control and laser Specimen (stainless steel).	156
Table 6-5 Data of bacterial adhesion for control and laser Specimen (titanium).....	158
Table 6-6 Summations of bacteria in all process with respect to metal.....	160

Chapter 1

Introduction

1.1 Problem Statement

The presence of bacteria colonies or ‘biofilm’ on inert surfaces can be both advantageous and destructive. Nitrogen fixation and the bioremediation of wastewater are the beneficial functions of microbial biofilms. However, biofouling mechanisms such as the fluid flow blockage in conduits, over surfaces, filters, heat exchangers, and corrosion, are major economic liabilities in the oil, gas, maritime, manufacturing and food industries [1]. In general, a biofilm is often regarded as the colonisation of submerged surfaces by undesirable organisms such as algae, bacteria, and barnacles. This colonisation has damaging effects on exposed surfaces, e.g. in shipping and leisure vessels, heat exchangers, oceanographic sensors and aquaculture systems [2]. There are many problems caused by this biofilm phenomenon, including biofouling and bio-corrosion. For example, the development of biofouling on the hull of ships reduces their speediness by ~10% and raises fuel consumption, which has an impact on operational costs and leads to more greenhouse gases production. The accumulation of algae/bacteria also increases the surface roughness of the hull, which in turn causes increased frictional resistance and fuel consumption while decreasing the maximum speed and range [3].

In European countries, biofouling causes a lot of damage in the aquaculture industries. This often results in additional costs in terms of operational and maintenance procedures. In farm industries, biofouling significantly reduces the efficiency of materials and equipment such as netting and buoys, onshore equipment, cages and structures such as pipelines, pumps, filters and holding tanks. Annual cost estimates due to unwanted biofouling growth comes up to nearly €100,000 per farm.

The use of membrane technology, micro and ultra-filtration in wastewater treatment systems exposes them to widespread fouling caused by micro-organisms and organic molecules. This limitation can lead to a significant decline of the permeate flux, higher-energy consumption and eventually, failure to meet regulatory standards. In addition, regular cleaning of the surfaces is costly and may damage the materials/layers. The cost of fixing the biofilm issue in membrane applications at a water factory caused an increase of 30% in operating costs. Due to the biofilm problem, membrane life-time is reduced from three years to one year and the replacement of the membrane alone cost around USD 1.17 million/year [4].

In power plants, biofouling has accounted for 20% of all-inclusive fouling in energy generation. Biofouling generally occurs in the intake structures, i.e. screen, seawater cooling pipeline and heat-exchanger tubes in the salt removal system, thus causing an extensive decline in plant efficiency at great economic cost. For example, the presence of a biofilm on the transfer surfaces of heat exchangers cooled by seawater reduces the heat transfer rate by 20-50% and incurs a global expenditure of over \$15 billion per annum to control the problem. It is estimated that the worldwide cost for biofilms in desalination reaches billions of US dollars annually [5].

Meanwhile, the formation of biofilm in the bio-medical field is highly associated with health and safety issues. 5% of disease infection cases involving chronic issues are due to pathogen adhesion on instruments and devices causing fatal illnesses. For example, *Staphylococci* SP are among the most important pathogens causing bloodstream infections that are associated with implanted medical devices. Controlling the bacterial adhesion to material surfaces is important for the prevention of biofilm formation and biomaterial-associated infections [6].

Bio-corrosion is caused or promoted by micro-organisms, occurs in both metallic and non-metallic materials, and is often evident either as layers of metal sulphide or a hydrogen sulphide smell which may contribute to health issues. On cast iron, a graphitic corrosion selective leaching may be the result, with iron being consumed by the bacteria,

leaving a graphite matrix with low mechanical strength in place. To combat corrosion, various kinds of corrosion inhibitors can be used such as benzalkonium chloride, which is common in the oilfield industry. Apart from metal, microbial corrosion also occurs in plastics, concrete, and many other materials: two examples are nylon-eating bacteria and plastic-eating bacteria. These micro-organisms can directly or indirectly affect the integrity of many of the materials used in industrial systems. Most metals, including iron, copper, nickel, aluminium, and their alloys, are susceptible to damage. Only titanium and its alloys appear to be generally resistant to microbial attack.

The possible contributing factors that induce biofilm formation are related to the surface properties of the materials used, such as the surface topography, surface chemistry and the hydrophobicity. Hydrophobicity has often been regarded by researchers as the main factor that governs cell-surface adhesion. Hydrophobic bacteria prefer hydrophobic surfaces, and this hydrophobic attachment is stronger compared to the adhesion of hydrophilic bacteria-hydrophilic surface. However, making these surfaces superhydrophobic has adverse effects on the bacterial adhesion. Superhydrophobic surfaces repel water to a degree that is a few orders of magnitude stronger than normal hydrophobic surfaces, thus preventing any attachment of microstructures (dirt/bacteria) onto its surfaces. Superhydrophobic surfaces wash off water from their surfaces; therefore, they create a phenomenon called self-cleaning. These superhydrophobic surfaces can be produced via several approaches, which are mainly dominated by two aspects: i) roughness surface modification and ii) chemical modification. This self-cleaning property (bacterial adhesion repellent surface) is beneficial in reducing the formation of biofilm and avoiding water corrosion [7].

Biofilm formation has caused severe problems in many engineering applications; therefore, any comprehensive innovation which leads to the process of removal or blocking of the formation of biofilm, will affect many industrial sectors and directly impact many important areas. Billions of dollars could be saved yearly if biofouling could be kept to a minimum. Since bacterial adhesion is a complex process and involves a combination of micro-organism properties, surface properties and environmental factors, the solution provided to rectify this issue could eventually be misleading and less

accurate. Therefore, extensive research needs to be carried out to save billions of dollars for the industries involved. The biofouling can be best prevented by controlling the initial bacterial adhesion, starting at the initial stages of adhesion prior to biofilm formation. Understanding the mechanisms as well as the time and length scales of bacterial adhesion with respect to the effect of the surface properties might allow for the control of bacterial adhesion. This control can be achieved by engineering the surfaces for adhesion and controlling the properties that increase repulsion towards bacterial adhesion.

1.2 Background of the Study

Our environment has complex systems and processes that function from the macro to the micro scales. This creates the possibility of a great diversity of practical applications and benefits for human beings in all aspects of existence, since many features of nature can be adapted to contribute meaningfully to the world; e.g. through physical structures, chemical compounds, manoeuvrability as well as material description. The process of manipulating nature's strategies into human technology is called 'biomimetics'.

Biomimetics is a term invented in the 1950s by Schmitt for the transfer of ideas from biology to technology. It has produced many significant and successful concepts and devices in the past 60 years, but is still empirical [8]. Therefore, this emerging technology is still effective and is experiencing progress in many studies seeking to embed nature into human technological innovation. The term biomimetics has been defined as a process of gathering and merging biological characteristics in order to mimic biology or nature for technological innovation [9, 10]. It is obvious that the properties of biological materials and surfaces create a process of interplay between surface topography, wettability and chemical properties [10-15].

In theory, biomimetic research is derived from nature; e.g. bacteria, plants, insects, spiders, lizards, aquatic animals, birds, seashells, spiders' webs, moth-eyes, the fur and skin of polar bears, and biological systems [11]. This is often useful to create an add-on value to the existing technology for specific purposes. For example, in the plant category, the lotus leaf (scientifically known as *Nelumbo nucifera*) plays an important role in many innovations and applications of superhydrophobic materials with a self-cleaning architecture. The technology embedded within its properties has been utilised and manipulated in various applications, e.g. in transparent and anti-reflective superhydrophobic coatings, super-hydrophobicity, self-cleaning surfaces, energy conversion, bacterial adhesion, thermal insulation, sensory aid, biological self-assembly, fluidic drag reduction, enhancing a water supporting force, the controlled transportation of fluids, superhydrophobic valves, bio-surfaces, anti-biofouling, the prevention of water corrosion, battery and fuel cell applications, humidity-proof coatings for electronic devices, superhydrophobic textiles, oil-water separation and micro condensation [11, 12, 14-17].

The hydrophobicity effect of the lotus leaf and the ability to repel water and self-cleaning properties has provoked a substantial area of interest due to their many applications [18-23]. It has induced more thoughtful and motivating investigations for researchers to make more significant discoveries. The reason for the significant potential of lotus leaf as a self-cleaning surface lies in the micro/nano-structures and hierarchical roughness (micro-bumps) [24-26]. A micro-level scale investigation of the lotus leaf in 1997 has shown that the hydrophobicity effect of the leaf was contributed by rough scale of wax crystalloids of varied composition [13-16]. Therefore, numerous follow-up studies have confirmed that this combination of micrometre-scale has more benefits in engineering applications. *S*-scale roughness, along with a low surface energy material, leads to an apparent water contact angle greater than 150°, a low sliding angle (hysteresis) and the self-cleaning effect [16]. Materials with these properties are called *superhydrophobic* surfaces [27]. Other bio-inspired natural phenomena such as dragonflies and geckos exhibit an antibacterial property due to their sharp nanopillar arrays which can damage the bacterial cell wall when it meets the skin and have been referred to as model surfaces for various applications [28].

1.3 Motivation for the Study

It is becoming increasingly difficult to ignore the impact of a self-cleaning phenomenon in worldwide industries. It plays a key role in several areas and is gradually expanding into new applications such as health and safety, environmental concerns and food industries. The study of this self-cleaning innovation leads to many other process studies such as the fabrication of surfaces and surface characteristics. Self-cleaning surfaces, as mentioned above, are materials derived from increased surface topography. Currently, there is a growing interest within various industries for self-cleaning surfaces in applications as diverse as aerospace, skyscrapers, food packaging, automobiles and bio-medical engineering. Over the past decade, many attempts have been invested in this field with empirical studies trying to understand the mechanism of this unique phenomenon and thus the possible applications are limited. In this new global economy, the self-cleaning innovation is believed to have a key role in generating economic impact by improving the biofilm effects of many surfaces. The contribution of the self-cleaning innovation affects several issues in that it increases product quality and quantity, avoids material damage, increases the efficiency of process performance, prevents the use of biocides and increases the lifetime of the components due to extended cleaning.

Self-cleaning surfaces can be utilised in many potential areas such as on antifouling surfaces in the marine, pharmaceutical, textile, bio-surface, sustainable energy, environmental, bio-medical transplant material, and cleaning industries [16]. The use of antifouling (AF) coatings to control the problem of fouling in marine vehicles saves the US Navy around USD 2.1 billion per annum [3]. Organ transplantation generates around £15 billion of business worldwide each year through the production of biomaterials to replace non-functioning human organs. Surface roughness plays into a key aspect of biomaterial function; it creates more adherence to human tissues to ensure that the material is well accepted by the human body. The annual cost for organ transplantation and health infection is estimated to be in the billions of dollars in the US, with about 2 million fracture-fixation devices being inserted yearly [29].

The fishing industries also benefit significantly from self-cleaning innovation surfaces [30], while pipe corrosion and fouling require USD 6–8 billion for cleaning purposes. Bridge corrosion costs around USD 7 billion annually. It is estimated that the 100 main biomimetic products generated approximately US \$1.5 billion over 2005–2008. Annual sales are expected to continue to increase dramatically [11]. As a result, these markets are worth billions of pounds annually worldwide. There will be an increase in the volume in many sectors, strongly motivating any significant and comprehensive study into self-cleaning innovation surfaces.

Undoubtedly, this self-cleaning phenomenon benefits many industries and is becoming gradually more popular due to increases in economic factors as well as in health and safety issues. However, to date there has been little discussion of the relationships between surface topography, contact angle and bacterial adhesion. Therefore, in this study, the concept of the lotus leaf phenomenon has been used to investigate the effect roughness on the self-cleaning property surfaces [31]. Further investigation will be focused on the effects of surface topography parameter, wettability and bacterial adhesion on metallic surfaces. This will be supported by evidence from the surface roughness parameter by quantifying and determination of the adhesion kinetics based on three distinct types of bacteria which are *S. aureus*, *E. coli* and *B. subtilis*.

1.4 Aims

The aim of the research is to establish strong relationship between surface topography, wettability and bacteria adhesion on metallic surfaces that have undergone several fabrications methods. It is designed to investigate the effect of surface topography parameters towards the contact angle and leads to the effect of bacterial adhesion, which can be used further for developing a material that resists bacterial adhesion for hygiene, safety and cost-effective purposes. This study also aims to provide sound, blended information concerning the effect of surface roughness, hydrophobicity, environmental factors as well as bacterial properties and the adhesion of bacteria on stainless steel and titanium surfaces. The merged knowledge of these properties with respect to bacterial adhesion will be beneficial in the preparation of a material with self-cleaning properties and is of utmost importance, especially in domestic and medical applications.

1.5 Project Objectives

The project is expected to achieve:

- i) *Fabrication of various stainless-steel and titanium surfaces topography*
According to the theory of the *lotus leaf*, the effective contact angle can be increased by increasing the roughness of the surface, which will subsequently increase the surface hydrophobicity. There are two factors influencing the critical surface properties of materials, which are: i) the non-wetting (hydrophobicity) and ii) the surface attachment point (organisms smaller than the scale of the surface microstructure). To achieve a surface with the properties mentioned above, various substrates were rendered through the processes of surface roughness modification. The roughness can be tailored by the mechanical processes of grinding, milling, sandblasting, chemical etching or laser etching to obtain micro-indentations that are arranged in a specific pattern.

- ii) *Characterisation of the substrates' surfaces in terms of surface wettability.* The study will investigate the parameters of the surfaces such as roughness, skewness and kurtosis and the wettability of the surfaces. These surface parameters are expected to play an important role in bacterial adhesion due to the shape, peakedness, and surface attachment point. Widening the surface area contact with the bacteria furthers the ability of the bacteria to attach to the surface and form a colony.

- iii) *Bacterial Characterisation:* This concerns understanding and applying the proper techniques for the handling, culturing and analysis of the bacteria. The bacteria were partially characterised to understand the effect of the bacteria's properties and their influence on the adhesion process.

- iv) *Effect of Physical Factors on the Bacterial Adhesion Process:* This concerns identifying the bacterial adhesion behaviour based on the effect of certain environmental factors such as temperature, agitation, time of exposure, the concentration of the bacteria and age culture on the adhesion processes using standard experimental procedures.

- v) *Effect of Surface Properties on the Bacterial Adhesion:* The physical aspects of the surfaces (surface contact angle with respect to non-wetting properties or hydrophobicity) were thoroughly studied to determine the effect of the materials and their hydrophobicity properties and their influence on the adhesion mechanism.

To summarise the scope of the research, a graphic relationship is shown in Figure 1-1 below.

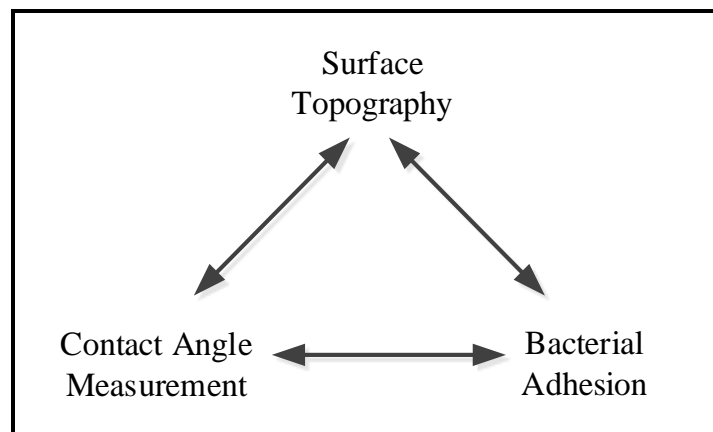


Figure 1-1 Scope of the experiment

1.6 Organisation of the Thesis

The thesis consists of several chronological chapters that were derived to provide a detailed understanding of the bacterial adhesion on the modified surfaces with controlled properties. The introductory chapter explains the motivation for the study by addressing the problems associated with bacterial adhesion. It has also addressed how the desirable features of any newly proposed system must be fabricated to achieve the objectives of the research. The remainder of this thesis is organised into eight chapters as follows:

- i) CHAPTER 2 presents a literature review of biomimetic innovation, hydrophobicity, surface characterisation and the factors that affect bacterial adhesion on metallic surfaces.
- ii) CHAPTER 3 presents a preliminary characterisation of the sample micro-organisms (*S. aureus*, *E. coli* and *B. subtilis*) such as the bacterial growth curve, surface properties and sizes. The adhesion of these bacteria was also thoroughly examined using glass substrate to observe the varying adhesion orientations with respect to different types of bacteria.
- iii) CHAPTER 4 – discusses the surface characterisation of metallic polished specimens' surface topography parameter with respect to contact angle measurement and bacterial adhesion.
- iv) CHAPTER 5 – discusses the surface characterisation of metallic WEDM specimens' surface topography with respect to contact angle measurement and bacterial adhesion. A comparison will be made between polished and WEDM specimens on surface topography, contact angle and bacterial adhesion.

- v) CHAPTER 6 discusses the surface characterisation of polystyrene and metallic laser-assisted specimens' surface topography with respect to contact angle measurement and bacterial adhesion. A comparison will be made between polished, WEDM and laser-assisted specimens on surface topography, contact angle and bacteria adhesion.

- vi) CHAPTER 7 discusses the overall contributions and conclusions from the results achieved in this study. Some recommendations are highlighted for future studies to generate improvements and more significant findings with respect to the related issues.

Chapter 2

Literature Review

2.1 Learned from nature

There is a large volume of published studies describing the role of nature in engineering applications [32]. This phenomenon has become more interesting in the last five decades since Richard P. Feynman presented a technological vision of extreme miniaturisation in 1959 [33]. Learning from nature was broadened with the help of the first commercial Scanning Electron Microscope (SEM) in 1965 by the Cambridge Scientific Instrument Company [34], that enabled researchers to have a deeper knowledge of the nano-realm and the magnificence of nano-creatures [35-38]. The identification of the characteristics of nano-creatures has led researchers to design numerous engineering applications through broad disciplines, and the practice is known as bio-mimetic study [17, 39].

Historically, biomimetic study started thousands of years ago when the Chinese craved for artificial silk [40]. It became recognised when historians found that the ancient Chinese used lotus leaves in their cultural activities and emphasised the greatest self-cleaning behaviour of the leaf [41]. Since then, it has become one of the key interests for scientists to focus on and has expanded the knowledge of nature for human daily applications [13, 24, 27, 42]. In other words, biomimetics is related to the concept of using ideas from nature and manipulating the hidden engineering aspects in various fields such as automotive industries, aerospace, food packaging, textile and bio-medical engineering [43-48]. The term ‘bio mimetic’ was derived from the Greek term *bios* or *life* and the suffix mimetic means the ability for mimicry [10]. Scientists focus on the structures that embody the object while exploring the functionalisation of these structures in nature’s daily operation.

Numerous studies have attempted to explain the intensifying of biomimetic engineering [49]. There has been an increase in the level of exploration since the 1960s. It is projected to grow broadly in the next 10 years (year 2020) and expand into many areas of research such as biomaterials, gel-artificial muscle, mechanic-biomimetic, biomimetic chemistry, and neuropsychology. The most likely cause of the increase might have come from the discovery of the lotus effect by Wilhelm Barthlott and C. Neinhuis officially in 1965 [50]. This is because there is evidence of the increasing number of publications on the lotus effect (super hydrophobicity) since the 1990s due to the possibility of building superhydrophobic surfaces with desired properties when the technology matured [17, 24, 27, 39]. Figure 2.2 clearly depicts that the number of published papers increased exponentially from the 1990s until the 2010s. The citation count in biomimetic engineering also presented a significant increase and reflected the trend of published papers. This trend shows the substantial value and relevance of biomimetic engineering in the future and benefits many other research disciplines. Therefore, it can be concluded that interest in biomimetics has become more significant and there will be more exploration and development activities in this topic.

In addition to the increasing literature publication, the real evidence to show the expansion in biomimetic and nanotechnology study is the research spending allocations by the world governments. Based on a US National Nanotechnology Initiative report in 2000, almost every developed and developing economy had initiated their own nanotechnology programs [51]. The world governments are spending \$10 billion per annum on nanotechnology research and development, and this amount is estimated to grow by 20% over the next three years. This spending by the governments reflect the potential benefits behind the biomimetic engineering field.

Many countries have allocated money in their budgets for nanotechnology research and development. Starting from 1997, the United States, Western Europe and Japan has spent about USD 687 million in total. This amount will increase significantly in the next five years when all the countries start to make investments in nanotechnology research. In 2002, Japan led the investment by spending around USD 750 million compared to the United States with USD604 million. The amount of budget allocation all over the world for nanotechnology research and development has totalled USD 2,274

million dollars since 2002. This trend shows the importance and expansion of nanotechnology research and development. It also shows that governments have demonstrated interest and are allocating huge amounts for research and development in nanotechnology.

2.1 Biomaterial and the Application

The development of biomaterials was inspired from nature and the environment as summarised by Nosonovsky and Bhushan [52] who demonstrated their selected contributions. [10]. Materials that possess compatibility with living cells/organism are termed as biomaterials. They range from plastics to polymers, metals and composites to ceramics. Implants are one of the biomaterials that are often associated with severe bacterial infection [53]. Numerous efforts have been expended to develop a smart implant with the ability to support the growth of tissues, whilst hindering bacterial adhesion and colonisation by either preventing the attachment or killing the micro-organisms upon contact with the surfaces. Other biomaterials possess a selective barrier which permit the transport of a specific component, whilst resisting the other, i.e. in the dialysis process for patients with damaged kidneys. There are other functions of biomaterials that are being continuously exploited for various purposes.

Material selection for biomaterials is based not only upon the usability, strength, and durability but also on their antibacterial properties. Metals are often selected as load bearing materials, ranging from pure compounds to various alloys invented for specific purposes [53]. Metals and alloys which have high melting points and specific gravity are often chosen due to their excellent thermal, electrical and mechanical properties. Besides that, metals are strong and highly durable against wear making them an excellent choice for use as implants and bone joints. Stainless steel and titanium/titanium alloys are often selected owing to their strength and chemical stability to undergo various fabrication techniques while posing negligible cytotoxicity for human use [54]. Stainless steel is generally known for its high corrosion resistance due to the formation of a thin passive chromium-oxide film [55]. New metals that are gaining interest are Mg, ZnO and Cu as they possess antibacterial properties that disrupt the cellular membrane and subsequently

killing the bacteria when coming into contact. The release of ionised Mg/Cu/Zn that can travel through the membrane and bind with the DNA while inhibiting enzyme activity, increases the bacterial fatality rate [56].

Synthetic polymeric materials have been widely used in disposable medical supplies, prosthetic materials, dental materials, implants, dressings, extracorporeal devices, encapsulates, polymeric drug delivery systems, tissue engineered products, and orthodontic facilities. They have been associated with various infection cases in hospitalised patients which require the removal of the infected devices, thus causing trauma and long hospitalisation periods [53]. Wenzel [57] reported that 10% of 40 million admitted patients were infected with nosocomial infections involving the urinary tract, surgical site, bloodstream and lungs from the use of polymeric medical apparatuses. The main problem regarding the use of the plastic made biomaterials is caused by the difficulty to sterilise the materials, either associated with their low tolerance towards thermal processing or to withstand strong chemical agents. Godoy-Gallardo, Mas-Moruno [58] stated that the current effective treatment for fighting infection in tooth implants was to use antibiotics before proceeding with the removal and replacement of the infected implant.

The current study employed two types of metallic surfaces which are austenitic stainless steel (316L) and titanium vanadium alloy (Ti6Al4V). The 316L SS has found wide applications due to its excellent ductility and corrosion resistance and is used for the fabrication of cardiovascular stents and equipment for the food industry. It contains 18% Cr and 8% nickel and is the most commonly used stainless steel. Chromium when exposed to air and water forms an oxidised layer which prevents the metal from corrosion by stabilising the ferritic content of the SS. The chemical stability is contributed by the inert oxy-hydroxide layer which maintains the surface smoothness (no additional anchoring point), thereby inhibiting biofilm growth during long-term exposure [55]. Besides, its competitive price comparative to titanium has increased the uses of this substance in daily operations. Meanwhile, Ti6Al4V is made from aluminium, vanadium and titanium and is often utilised in the fabrication of high strength prosthetic implants because of its recognised osseointegration and biocompatibility. It is also used for manufacturing equipment in chemical processing and airframe structural components

owing to its chemical inertness, high strength and its property as a lightweight material [59]. In addition, it is used to fabricate many surgical tools as it can reduce fatigue symptoms in surgeons during long operations [60].

2.2 Surface topographies

The next step after surface fabrication is the process of surface characterisation for identifying the surface parameters such as height parameter, spacing parameter and hybrid parameters [61]. Previously, surface parameters for 3D measurements were denoted by ‘*R*’ but has been changed to ‘*S*’ according to the new ISO25178 standard. These parameters can be measured using two types of measurements, i) contact mode and ii) non-contact mode. Contact mode measurement can be determined using Taylor’s Hobson, AFM, and Tribological Probe Microscope (TPM), while optical profilometry is used for the non-contact mode [62, 63][48, 49]. The advantages of optical profilometry such as WYKO, Bruker and the stylus measurement lies in their ability to cover more measurement areas and producing additional information whilst exploring the deep valley.

For the parameter analysis, 3D areal texture measurement gives more information compared to 2D parameter analysis. The 2D profiles, even if properly controlled, will give an incomplete description of the real topography. With the use of areal parameters, the texture shape and direction, attributing features can be accurately estimated and connected. Isolated features can be differentiated, while with traditional profile parameters it is limited to manufacturing process control and cannot be used to diagnose product functional performance. Areal parameters use all the available data from the texture surface while 2D profiles only use data from previously identified segments from the texture surface.

Height distribution parameters of skewness and kurtosis are also taken for comparison purposes. Skewness (Ssk) is defined as the degree of symmetrical height distribution and is characterised by positive or negative values, indicating more material on peaks or valleys, respectively. It cannot distinguish if the profile spikes are evenly distributed above or below the mean plane and is strongly influenced by isolated peaks or isolated valleys. The direction of the Ssk is dependent on whether the bulk of material is above the mean plane (negative skew) or below the mean plane (positive skew). If $Ssk < 0$, it indicates that the surface has more valleys or pits, whereas $Ssk > 0$ shows a surface with dense peaks. If the peaks and valleys are normally distributed the $Ssk = 0$ according to Gaussian distribution. A negative skewness (often specified between -1.6 and -2.0) is used as a criterion for a good bearing surface. The measurement for Ssk is shown below,

Meanwhile, kurtosis (Sku) describes the sharpness of height distribution and takes a value of 3 for a Gaussian distribution surface. A surface with a narrow height distribution has a kurtosis value greater than 3, while a surface that has a well spread out structure has $Sku < 3.0$. Or in other words, if the Sku is < 3 , it indicates a random structure while a value above 3 shows an ordered or organised surface structure. Furthermore, hybrid parameter-summit density (Sds) is used to characterise a modified surface, representing the number of peaks (summits) per unit area making up the surface. In the current study, this parameter is used to explain the hydrophobic properties of the surface and the alteration of the contact point between bacteria-surface. It is used in accordance with the parameters for a detailed impact of surface topography to repel adhesion.

2.3 Surface Wettability

Wettability involves the measurement of contact angle (CA) as the primary data, which indicates the degree of wetting when a solid and a liquid interact. Wetting phenomena of the surface is also used to evaluate the surface free energy measured using static measurement. Technically, hydrophobicity can be defined as the measurement of energy dissipation during the flow of a droplet along a solid surface. They can be divided into four stages such as super hydrophilic, hydrophilic, hydrophobic and super

hydrophobic. If the contact angles are greater than 90° , they are called hydrophobic surfaces and if below 60° , they are defined as hydrophilic surfaces. With contact angles greater than 160° , a surface is considered as super hydrophobic and when less than 10° , it is known as super hydrophilic, subsequently evaluated as surfaces with low and high surface energy, respectively [64].

Contact angle is defined as the angle formed by the intersection of the liquid-solid interface and the liquid-vapour interface is measured using the sessile drop method. The calculations based on measured contact angle values yield an important parameter such as the solid surface tension, which quantifies the wetting characteristics of a solid material.

Contact angle measurement can be achieved by considering a droplet of liquid settling on a flat horizontal surface. Ideally, the shape of a liquid droplet is determined by the surface tension of the liquid. Each molecule in the bulk is pulled equally in every direction by neighbouring liquid molecules, resulting in a net force of zero. However, the molecules exposed at the surface do not have neighbouring molecules in all directions to provide a balanced net force. As a result, the liquid voluntarily contracts its surface area to maintain the lowest surface free energy. The intermolecular force to contract the surface is called the surface tension, and it is responsible for the shape of liquid droplets. Historically, Thomas Young (1805) described the contact angle of a liquid drop on an ideal solid surface is defined by the mechanical equilibrium of the drop under the action of three interfacial tensions referred to as Young's equation. In 1936, Wenzel proposed a modified version of contact angle equations based on Young's equations as follows.

The equilibrium contact angle, r is the surface roughness ratio given by ($r = \frac{a}{A} = \left(\frac{da}{dA}\right) \geq 1$). θ_a is the apparent contact angle, a = actual surface area, and A = apparent area, or geometrical area of the surface. The validity of the equation lies in the assumption that the surface features of the substrate are insignificant compared to the drop dimensions.

2.4 Surface finishing techniques

2.4.1 Polishing

Mechanical polishing is one of the oldest processing methods, associated with the removal of unnecessary surface imperfections in various materials from metals [65] to polymers [66] and composites [67]. Polishing is grouped as wet and dry polishing and is targeted to generate surfaces with very high tolerances in geometry, surface integrity, and roughness characteristics. Polishing particles remove macro/micro elements and produce a smoother surface or flatness in low discrepancies by rubbing the polishing particles on a rotating disk. Polishing uses a larger number of multi point or random cutting edges for effective material removal. Abrasive finishing processes are used in a wide range of material applications and industries, i.e. in aerospace, automotive, mechanical seals, fluid handling, and many others precision engineering industries.

The polishing process is controlled by varying the speed, contact pressure [68], temperature, grit size and chemical usage [69]. Wet polishing reduces the fracturing rate, inhomogeneity and crack formation during mechanical grinding of composite materials [67]. During dry polishing, temperature effects are very significant especially for materials with low thermal tolerance e.g. polymers and bio composites. The surface defects can be greatly reduced due to the softening of the material's surface caused by augmented temperature. Meanwhile, the grit size affects the final roughness of the surfaces, where a rougher surface can be produced by grinding with high grit size, presented by more fractured zone and polishing streak. In a diamond finishing study, increasing the contact pressure and speed increases wear and surface defects [68]. Studies on the effects of the polishing process and polished material for preventing bacterial adhesion have also been reported by many authors. Bacterial adhesion onto polished Ti alloy-based implants was reduced after the roughness was kept to nanometre level ($Sa = 350-540$ nm) and was also due to the formation of a thin surface oxide layer on the titanium that aided in mitigating the transport of bacteria onto the surface [69]. A study by Skovager, Whitehead [70] reported that polished stainless steel caused more adhesion of *Listeria monocytogenes* but showed the lowest retainment during the cleaning process

compared to other rougher surfaces. Kang, Choi [71] reported a positive and negative correlation relating to surface roughness and adhesion of *Streptococcus mitis* between two different polished substrates using various types of polishing kits. In a collective review by Hu, Zhang [72], the polishing process alters the surface morphology, chemical composition, wettability [69] and subsequently affected the post modification activities.

2.4.2 Wire EDM

The wire electrical discharge machining (WEDM) is a non-traditional machining preferable in small scale production as it offers a cheap and fast method for cutting tough alloy materials with high hardness and impact resistance [73]. WEDM is widely utilised in modern industries such as aerospace, automotive, precision instruments, moulds etc [74, 75]. It is a non-contact, force free and thermal process where an ionised channel between the nearest point of the work and tool is generated by the applied voltage. WEDM can be utilised to create a surface with specialised and difficult contours, but it suffers from a few limitations such as poor surface finish and high tool cost that affects the production cost of the finished products. Good workmanship is measured by the electrode wear rate, size precision, efficient material removal rate (MRR), chemical and surface topography quality (i.e *Sa*, peaks, cracks etc) [76]. A better finishing quality by WEDM was reported by combining with an ultrasonic or magnetic field where surface roughness, irregularities, and surface cracks were successfully reduced compared to a conventional WEDM process [77].

WEDM process is a thermal-utilising-process using electrical discharge to erode certain parts of the conductive materials, which leads to melting-vaporisation-ionisation of the wire electrode at the pulse discharge point. The conductive materials are immersed in the dielectric liquid, and wire brass with a varied diameter (0.02 – 0.3 mm) is usually used as the electrode [76], often facing high wearing rate. The process generates recast layers, protruding peaks of molten metal, discharge craters and cracks. Moreover, the remaining debris that failed to be removed by the dielectric fluid accumulates in the

discharge channel and machining gap, subsequently affecting the stability of the discharge pulse, thus producing a surface with poor finishing [76].

Despite the precision control over difficult sizes and shapes, the operating procedures consisted of various parameters, and the synergistic change of more than one parameter often revealed a significant output. The set-up for the machine parameters are often complex and the detailed input factor and their heat treatment is yet to be understood. The effects of pulse on/off time [78], voltage, wire tension, cutting speed, cut directions and electrolyte flushing pressure [79] have been reported in the literature as affecting the properties of surface finishing and the wearing rate of the electrode wire. Optimising these process parameters aids in prolonging the shelf life of the wire electrode, increasing cutting efficiency and reducing surface imperfections. The reduced abrasive/adhesive wear and anti-erosion properties of an aluminium oxide film was obtained by Cheng, Nakamoto [80], by employing high speed WEDM. Torres, Puertas [78] reported that the lowest Sa value was obtained by keeping the current load at 4A and pulse time of 50 μs , which were the lowest values in the range tested. Meanwhile, reduced peaks and irregularities (*cleaner surface*) were attained at the highest pulse time (150 μs). A better surface finishing was associated with higher material removal rate (MRR), achieved by varying the current density and further enhanced by introducing the magnetic field and ultrasonic vibration [77]. Despite many studies on optimising the processing parameters of WEDM to produce a good surface finishing, to the best of our knowledge, this surface finishing has not been reported with intensity for bacterial adhesion.

2.4.3 Laser Fabrication

Implant failure due to the presence of bacteria and biofilm often requires a secondary surgery to remove the infected component causing a possible threat to patient health and can lead to fatality. It has been a long search for a universal surface that would facilitate the growth of tissue, while preventing the adherence of most pathogenic bacteria. Such a surface is still at an early stage since the phenomena of adhesion is yet to be understood. Although numerous reports have been published relating to bacterial

adhesion with surface modification, failure to carry out comprehensive analyses on the surface and bacterial properties has resulted in a deficient conclusion on the properties of surfaces that can be manipulated for preventing adhesion.

Femtosecond laser fabrication offers a very flexible 3D positional control with high accuracy of energy deposition at a scale range down to sub- μm resolutions. Unlike nanosecond laser, femtosecond laser produces a clean surface finishing, eliminating the heat affected zone during processing [72]. It can be used to design a surface from a wide range of materials, where the post modification textures often offer high thermal and mechanical stability against abrasion which are some of the many important features to be attained in load bearing implants [72]. Laser processing techniques are compatible and can be utilised to complement other laser-based techniques i.e. interference lithography and micromachining. Figure 2-1 illustrates the simple laser technique used by Ma, Tong [81].

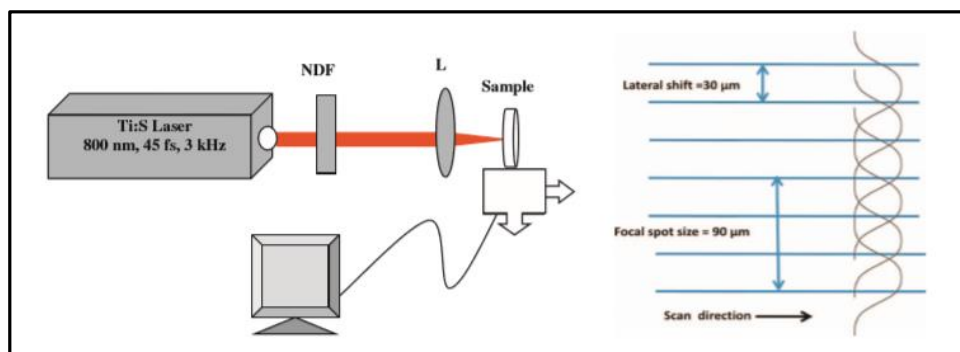


Figure 2-1: Schematic set up of laser fabrication of bioactive glass where the laser beam is passed through the neutral density filter (NDF) and lens ($L = 5 \text{ cm}$ focal lengths) before hitting the sample on the computer-controlled X-Y stages.

Surface texturing with an ultrafast laser offers simplicity, flexibility, controllability and reproducibility of results and is also easy for scaling up [82]. Laser fabrication has been gaining interest and is a widely exploited method to achieve a surface with varying functionalisation's. Laser fabrication has been utilised for micro polishing [83] and to produce surfaces with emerging textures [58], controlled wettability (REF), biofunctionalization [84], low reflection etc. The evolution of LIPSS emerged after the

laser fabrication could be varied to suit various applications. LIPSS can be tailored by varying the laser power (P), number of pulses [58], laser speed (V) [72], temperature [85], laser spot diameter (D), [84], wavelength [85] etc. These parameters will determine the laser fluence, F which represents the amount of energy per unit area as follows: -

$$F = \frac{P}{V \times D} \quad \text{Equation 2-1}$$

Where F in (J/mm²), P (mW), V (mm/s) and D (mm).

The effect of laser fluence determines the melting rate of the metal surface after the laser incidents. A very low F results in an incomplete melting of the exposed surface subsequently reducing the strength attachment of the molten layer on the substrate. Reducing the scanning speed will expand the formation of the heat affected zone and overlapping may occur if the hatch distances are kept at minimum. Besides that, the vaporisation rate of the metal was increased and blown off through laser bombardment leaving a deep gap between the protrusions Hu, Zhang [72]. The overlapping ratio needs to be set accurately to have a good balance between surface homogeneity and processing efficiency. An overlapping ratio that's too high or too low may lead to overheating thus increasing cladding inefficiency or causing surface inhomogeneity, respectively [84]. According to Du, Ai [86], increasing the laser fluence $> 5.5 \times 10^3 \text{ W/mm}^2$ in accordance with an increased pulse overlap produced a polyimide surface with hydrophilic character, while increasing these parameters produced a superhydrophobic characteristic. The two extreme conditions arise due to its surface topography and changes in its surface chemistry. In a combination of laser texturing and chemical treatment that produced a circle shape texture pattern, the super hydrophobicity of SS surface was reduced with an increasing ratio of P/D from 1.0 to 1.8 due to the increased flattened area on the modified surfaces [81].

2.6 Mechanism and Factors Governing Bacterial Adhesion

Bacterial adhesion is influenced by the properties of both the bacteria and the substratum surface. Bacterial characteristics that are highly influential in directing the adhesion mechanism are hydrophobicity [87], surface charge, motility, pH, chemical agents [88], biofilm rheology, temperature [89] and the excretion of extracellular substances such as polysaccharides/protein. The adhesion and colonisation of bacteria are being recognised to be of significant socio-economic interest throughout the world. Bacterial contamination and biofilm growth affect many aspects of society, ranging from bio-induced corrosion of industrial piping and other materials, to serious health implications in infected individuals [90]. Biofilms are particularly durable and persistent, being responsible for 65% of hospital-acquired infections in the US. Cleaning with chemical disinfectants not only threaten the environment but may create new strains that are more robust and resistant to antibiotics. Besides that, the use of disinfectants is tightly controlled by local authorities, often incurring a very high cost for environmental-friendly solvents, yet often failing to achieve the complete elimination of biofilms. Thereby, the effective action to limit the impact of bacterial adhesion is to prevent the initial formation rather than employing remediation.

The adhesion of micro-organisms on the surface is associated with hydrophobic interaction, cell communications, specific interactions of the relevant properties of the substratum such as hydrophobicity, zeta potential, surface texture, surface energy etc. [91]. The influence of the surface free energies of the substratum and the bacterium can be modelled using a thermodynamic approach. The extended-DLVO [92] theory accounts for Lifshitz–Van der Waals, electrostatic, and short-range acid–base interaction energies between the surface and the bacterium as a function of their separation distance. The mechanistic knowledge of bacterial adhesion obtained from the extended-DLVO theory provides guidelines for the development of surface coatings exhibiting minimal adhesion of bacteria.

Adhesion on the surface is initiated by the formation of a conditioning aqueous layer on the solid surfaces that are rich in nutrients, subsequently attracting the sessile organism. The establishment of bacteria-surface interaction consists of four stages[93]. The first stage is the initial attachment-involving interaction between the bacterial cell-surface. Stage two occurs when the binding proceeds with specific and non-specific interactions between the surface proteins and binding molecules on the biomaterial. After adhesion is secured, the micro-organisms predominantly grow as communities on the surfaces (stage 3) and continuous colonisation is depicted by the irreversible adhesion or biofilm formation. A rapid multiplication of the species occurs with the formation of biofilm and the adhered bacteria becoming the source of nutrient for the biofilm community, thus maintaining their viability.

2.6.1 Bacterial properties

An important feature of the bacterial cell membrane is related to the composition that leads to its multiple responses when interacting with inert surfaces or biological compounds. The composition and types of the polysaccharides, lipids and proteins attached to the cell membrane vary significantly with different types of bacteria and are categorised based on the Gram positive or negative grouping. The cell walls of Gram-positive bacteria are mainly a network of long sugar strands consisting of a thick layer of stretchable peptidoglycan approximately ~25 nm, cross-linked with amino acids a). The peptidoglycan cell wall is comprised of multiple inter-connected sheaths of cross-linked glycan strands that form the general shape of the bacterial cell. In contrast, the membrane of Gram-negative bacteria consists of lipopolysaccharides, comprised of an inner and outer membrane separated by a periplasmic space and a thinner layer of peptidoglycan. b). The peptidoglycan layer is linked to the outer membrane via lipoprotein, is thinner than the one in the Gram-positive bacteria and vulnerable against shear.

It is important to note that the bacterial properties are highly dependent on their surrounding (pH, medium and nutrient availability, temperature, salinity etc.) and on the growth stages. Protein and lipid composition on the bacterial surfaces vary according to the growth stages, subsequently changing its hydrophobicity and surface charge, thereby affecting adhesion. Proteinaceous appendages including pili and flagella also initiate the bacterial adhesion by establishing a strong binding between surface and cell. Bacteria often carry a negative charge in an ionic solution above and below their isoelectric values, and upon contact with biomaterial surfaces which usually have a negative charge the repulsion effect is activated. But at around 15 nm, van der Waals and hydrophobic forces are exerted and the repulsion is overcome.

Others have reported that the effect of the electrostatic interaction between the negatively charged-bacterial cell and positively charged substratum surpassed the attraction caused by hydrophobic attraction. In addition, the forces caused by electrostatic interaction are far greater resulting in a stronger adhesion for cell-metal surface interaction [94]. Bacteria with a high surface energy show low preference for hydrophobic surfaces (low surface energy) but perform a strong bonding with hydrophilic surfaces [95]. An adhesion study on polymeric composites using two different types of rod-shaped Gram-positive and Gram-negative bacteria showed a significant difference in magnitudes of adhesion, where the Gram-positive bacteria was a greater coloniser than the Gram-negative *Sp* [55].

2.6.2 Surface properties

The effects of surface patterns [96], surface roughness [93], surface energy [97], chemical composition and wettability [98] were the most widely reported as very influential aspects for adhesion. Primarily, the adhesion magnitude is debated based on the modified roughness and wettability before the other factors as these parameters can be easily altered and undergo a simple analysis method as discussed previously. However, when these parameters often failed to provide a consistent observation for different types of bacteria or surfaces, other factors such as surface chemistry and energy was evaluated.

The studies often concluded that alterations of adhesion were a contribution of two or more synergistic factors and are strain dependent.

The ability of surfaces to repel bacteria is often associated with the increased/reduced wettability of the modified surfaces. It is widely accepted that the resistance for adhesion increases when the CA are beyond $\theta = 160^\circ$, where a super hydrophobicity character is pronounced. Yoon, Rungraeng [99] reported that despite different chemical properties, superhydrophobic TI/SS has been proven to reduce the adhesion capacity in comparison to its control experiments ($CA < 100^\circ$), but slightly below a similar surface with $CA = 143^\circ$ [99]. The increased cleaning ability achieved with hydrophobic/superhydrophobic surfaces is contributed by the rolling off effect of the water droplets that produces a minimal contact between the liquid/cells with the surface, thus minimising the adhesion. Super hydrophobicity can be easily fabricated to increase the resistance to mass transfer, thus can minimise the proliferation of the adhered bacteria and avoid the formation of biofilms in long operations. However, the effectiveness of the superhydrophobic surface are still dependent on the types of bacteria, types of material, the surrounding conditions and poor in stability. Superhydrophobic surfaces can be attained using various physical and chemical methods, or a combination of both. Super hydrophobicity has been established by authors using various techniques such as nano-structuring [54], plasma technique [100], coatings and chemical functionalisation [101], lithography, or a combination of these processes. The question that arises with the approaches concerns the reproducibility and the durability of the surface. The effect from chemical functionalisation often lack stability linked with the leaching process. The increased wettability effect achieved using nano-structuring often produce a variety of results, which are caused by the synergistic effects from multiple factors which have yet to be understood.

Surface texturing is one of the methods that was proposed to reduce the bacteria adhesion. A pitted surface increases the wettability of the surface, thus serving as a sink/strainer for bacterial adhesion. On the other hand, a surface with protruding features works differently from a surface with valleys and grooves. Many researchers have reported that reduced adhesion was attained since bacterial attachment was prevented on

the patterned area, and adhesion was limited at the valley between the protruding texture [96]. Lu, Zhang [102] reported that micro patterning with sizes smaller than bacteria prevented the adhesion of *S. aureus*, *P. aeruginosa* and *E. coli* on the PDMS surface fabricated with electron beam lithography [102]. The textures must be designed to be smaller than the size of bacteria, else it will facilitate the adhesion by offering more binding site area vertically. Lu, Zhang [102] mentioned that the patterning effects work to reduce adhesion for both hydrophobic and hydrophilic surfaces, which concluded that micro patterning alone are effective measures for bacterial mitigation without associating with the increased hydrophobicity level. It is best to note that the adhesion took place at the grooves, thereby adding more protruding features (size < bacteria size) per unit area would be beneficial to reduce preferred sites for bacterial adhesion.

The effect of topography provides significant information on the reduction of bacterial adhesion, with many associated with the modified Sa. Some authors reported that preference towards roughened surfaces occurred because of the increased surface area which provided more binding sites for the bacteria either vertically or horizontally. This condition is true related to the size and shape of bacteria. The vertical surfaces, the microstructures and roughness add protection that minimised the shear stress in the dynamic environments, thus strengthening the binding through time. The work by Truong, Lapovok [103] showed increased preference towards fabricated (ECAP) titanium surfaces for *S. aureus*, *E. coli* and *P. aeruginosa* but at different magnitudes. In laser fabrication, the emerging random structures provided a coarse surface with multiple contours (peak and valleys/crevices) at varying heights. The spatial distribution between the contour lines increased the resistance for bacterial adhesion.

A strong relationship between higher bacterial adhesion with increased roughness have been reported while others have found the opposite. A collection of review articles from Han, Tsoi [95] concluded that the effect of roughness works differently between the preference to bacterial adhesion and the effect on the osseointegration. Most papers found that surfaces with roughness $Sa > 5 \mu\text{m}$ encouraged the adhesion for both bone tissue and bacteria colonisation. Reducing the Sa to $< 1.5 \mu\text{m}$ managed to mitigate the adhesion for Gram-negative/positive bacteria but failed to support the bone growth on the tested

implant [95]. This is supported by the earlier finding of Korber, Choi [104], that a rough surface increases surface area or contact point for the bacteria-surface interactions and enhanced cell to cell communications which leads to biofilm development. However, more bacterial attachment was observed on the weld metal of 304L SS compared to its base metal, where a strong correlation between the adhesion and the average grain size was successfully reported. Another observation by Little, Edelman [105] showed that smoother and rougher surfaces enhanced the bacterial adhesion of four different bacterial strains on the 304-SS surface with Sa ranging from 0.03 to 0.89 μm . Minimal adhesion was observed at $Sa = 0.16 \mu\text{m}$ while both smoother and rougher surfaces were shown to attract more bacteria.

In laser fabrications, adhesion of *E. coli* on SS that has undergone nanosecond laser was hindered on a surface with roughness Sa between 0.006 μm and 33.00 μm with coverage area reduced to $< 10\%$. Conversely, bacterial coverage increased to more than 50% on a surface with roughness between 0.83–11 μm . A study on PPMA also shows increased *S. aureus* adhesion on a surface displaying roughness in the range of 0.3–1.86 μm . Finer and rougher surfaces with roughness 0.04 μm and 7.89 μm displayed an increased antibacterial property, respectively. An increase in the roughness of SS from 0.04 μm for a polished sample to 0.30 μm for an abraded sample, increased bacterial adhesion strength more than a larger increase in surface roughness from 0.04 to 0.96 μm for the polished stainless steel. This means that under the same tip-surface force during scanning with an atomic force microscopy tip, more cells remained on abraded stainless steel than on unpolished/polished stainless steel. Although no absolute value of roughness has been reported to be the standard for controlling the adhesion phenomena, the roughness that similar to the size of the bacteria are often referred to as the threshold values. Others have reported $Sa = 0.2 \mu\text{m}$ to be the threshold value since any further reduction of Sa did not contribute towards reducing adhesion on the dental implant Han, Tsoi [95].

2.6.3 Environmental Condition

Sheng, Ting [106]) studied the adhesion forces of two anaerobes (*D. desulfuricans* and *D. singaporenus*) and an aerobe (*Pseudomonas* SP.) to stainless steel in different aqueous systems. They observed that the nutrient and ionic strength of the solutions affected the bacteria-surface interactions. A stronger ionic strength in the solution resulted in a larger bacteria-stainless steel adhesion force, which is due to the stronger electrostatic attraction force between the positively charged metal surface and the negatively charged bacterial surface. The pH of the solutions affected the synthesis of protein, thus altering the bacterial responses. A sudden increase/decrease of pH can be fatal to the bacteria, but some bacteria can survive in extreme pH with gradual exposure [89]. The bacteria-surface adhesion forces reached its highest value when the pH of the solution was near the isoelectric point of the bacteria. The maximum adhesion at the isoelectric point was explained by the change in the ionisation state of bacterial cell surface functional groups. The adhesion forces at pH 9 were higher than at pH 7 due to the increase in the attraction between Fe ions and negative carboxylate groups. Figure 2-2 summarises the interaction factors between bacterial surface-inert surface-surroundings that contribute significantly towards the development of bacteria biofilm.

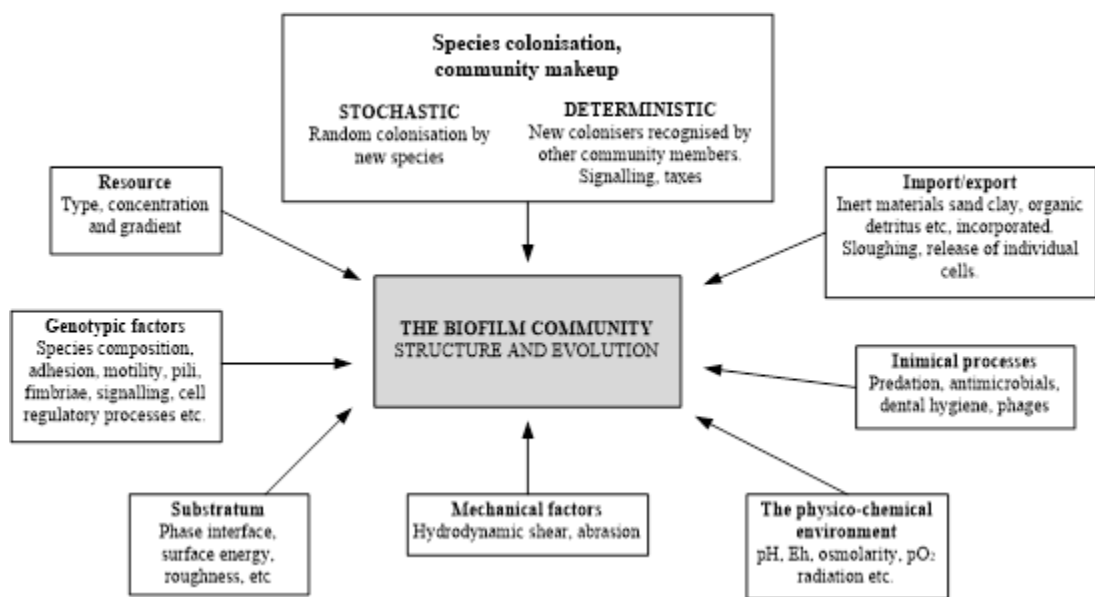


Figure 2-2 Factors that influence the development and biology of a biofilm

2.6.4 Micro-organisms: *S. aureus*, *E. coli* and *B. subtilis*

The *Staphylococci* family are Gram-positive bacteria, possessing a coccoidal shape with a diameter of 0.5–1.5 μm , and often appears in clusters like bunches of grapes (Figure 2-3a) rather than individual *cocci*. *S. aureus* are facultative anaerobes i.e. can grow well in the presence or absence of oxygen. They are non-motile, non-spore forming anaerobes and are virulent compared to *S. epidermis*, despite their phylogenetic similarities. Their cell wall is hydrophobic, made up from a tough amorphous coat with a thickness of about 20-40 nm. The growth and survival of this bacteria are dependent on their cells' ability to adapt to environmental changes. They have evolved many mechanisms to overcome the changes.

Staphylococcus sp are a mild pathogenic strain, causing infections in human with lower resistance, with *S. aureus* and *S. epidermis* being the most reported in the literature. *S. aureus* are widely found in food, some strains can produce toxins which cause acute gastrointestinal diseases if ingested. The enterotoxin produced by *S. aureus* is a heat-stable protein, which survives heating at 100°C for 30–700 minutes. Staphylococci can grow at low water activity (approx. 0.86), corresponding with a salt content of about 14%. The main reservoirs of *S. aureus* are humans and animals where healthy people carry the organism in their nose, throat, hands and in open cuts or wounds.



Figure 2-3 SEM's image of a) *S. aureus*, b) *E. coli* and c) *B. subtilis* (Carr, 2007)

Escherichia coli (*E. coli*) is a Gram-negative, rod-shaped, non-spore forming, motile with peritrichous flagella or non-motile, and grows well in LB media (Figure 2-3b). The normal length of the bacteria is between 1.0–1.5 μm , while the shorter end is 0.45–0.8 μm and can reach up to 2–3 μm in length. *E. coli* expresses different types of pili that stretch 5–10 nm long, which aid the bacteria to fasten themselves to a surface, thus preventing shearing when external forces are applied [107]. *E. coli* can be found in the human body with the ability to grow under both aerobic and anaerobic conditions Morgan and Wilson [108]. Most strains of *E. coli* are harmless and are a part of the normal intestinal microflora, synthesising vitamins to efficiently retard the growth of harmful organisms. An overpopulation of intestinal *E. coli* causes sickness and diarrhoea with vomiting. The worst case associated with *E. coli* infection is causing bloody diarrhoea which can lead to kidney failure and fatality, with more cases observed in children and people with low immunity. The optimal conditions for *E. coli* growth occur at a pH between 6.0 to 8.0, with temperatures between 30° to 39°C. However, growth can occur in as low as pH 4.3 and as high as pH 10 and is a strain-dependent property [109].

B. subtilis is a Gram-positive spore forming bacteria shaped like a rod (Figure 2-3 c). *Bacillus* with spore forming ability grow well in an aerated medium and start to produce end spores when nutrient and oxygen availability becomes limited. These strains are widely studied due to its lack of pathogenicity effect on humans, animals and plants. The adhesion of *B. subtilis* is facilitated by EPS enhanced cellular adhesion and the abilities vary with the stage of growth [110]. *Bacillus* are exploited for the manufacture of various enzymes, secreting extracellular proteins which are beneficial for many industrial purposes. Besides that, *B. subtilis* are suitable to be used as a mini factory for synthesising a product of interest, achieved by inserting foreign genes to produce the product of interest. The major concern with the spore forming bacteria is due to its ability to thrive in unfavourable conditions and are resistant to heat, chemicals, pH, nutrient limitation, dehydration etc, thus causing persistent contamination [111].

The length of mature *B. subtilis* cells range between 1.2–2.4 μm with a diameter of approximately 0.5–0.75 μm . Its oval-thick skin end spore is slightly smaller with a dimension of 0.6–0.9 μm , is highly resistant to extreme environments such as chemicals, radiation and insusceptible to enzyme attack. The matured cells are made by thick

capsules of heteropolymer matrix of peptidoglycan. Its thicknesses range between 20–50 nm, attached to anionic polymers such as teichoic and teichuronic acids, 10x thicker than that of typical Gram-negative bacteria such as *E. coli*. The highly negative charge of the *B. subtilis* induces bonding towards metallic surfaces with an opposite charge. This is attributed to the anionic polymers and the un-substituted carboxyl groups of muramyl peptide that covers the surfaces contributing to its negative surface charge. Besides that, *B. subtilis* also synthesises lipoteichoic acid which contains polyanionic hydrophilic chains.

2.6.5 Wire Electrical Discharge Machine (WEDM)

The spark theory on wire electrode discharge machining (WEDM) is basically the same as that of the vertical EDM process. In wire EDM, the conductive materials are machined with a series of electrical discharges (sparks) that are produced between an accurately positioned moving wire (the electrode) and the work piece. High frequency pulses of alternating or direct current is discharged from the wire to the workpiece with a very small spark gap through an insulated dielectric fluid [112].

The mechanism of WEDM puts impulse voltage between the electrode wire and the workpiece through an impulse source controlled by a servo system, to get a certain gap, and realise impulse discharging in the working liquid between electrode wire and workpiece. Numerous tiny holes appear due to the erosion of impulse discharging, and therefore gets the needed shape of workpiece [113]. The electrode wire is connected to the cathode of the impulse power source, and the workpiece is connected to the anode of the impulse power source. When the workpiece is approaching the electrode wire in the insulating liquid and the gap between them gets smaller to a certain value, the insulating liquid is broken through; very shortly, discharging channel forms, and the WEDM method involved using an electric voltage to produce rough surfaces. The Wire Electric Discharge Machine (WEDM) uses a single pulse discharge machine equipped with an IGBT wave generator to produce a surface roughness below 10 μm . For this study, experiments were carried out using a pulse range between 100–500 ms, with the electrode distance kept in

the range of 10 mm to 22 mm to obtain four different degrees of roughness. The pulse duration was controlled manually by changing the program parameters of the single chip, and the waveform produced was recorded using an oscilloscope for further analysis. The voltage and current were set at their typical values of 200 V and 10 A, respectively. The shape of the electrode chosen during machining was also varied, either using a needle or disk type.

2.6.6 Laser-assisted technique

For the laser-assisted technique, the surfaces of both metals (stainless steel and titanium alloy) were treated using the laser ablation technique. The laser treatment was performed at the Karlsruhe Institute of Technology (KIT, Germany) using a micro-machining workstation (PS450-TO, Optec, Belgium) equipped with an ultrafast fiber laser (Tangerine, Amplitude Systems, France) operating with an average power of 35 W. In order to accommodate the biological tests, the modified surfaces were fabricated using a metal surface of size 2.0 cm x 2.0 cm and was polished to mirror finishing before undergoing laser treatment. The metal surfaces were then crafted with 4 different surfaces of size 5 mm x 5 mm, using four (4) laser parameters. The laser surface texturing was carried out under two conditions, i) ambient air and ii) in argon; with a central wavelength of 515 μm , a laser pulse duration of 380 fs and a repetition rate of 200 kHz. The laser beam scanning speed towards the metals was set at between 10–50 mm/s while the average laser power was varied between 80 mW - 1200mW, with a single or double pass. Between two laser pulses, the sample is moved in the scanning direction with a length of about 2.75 μm . The generation of the LIPSS was guided through a beam expander (2-fold) and the scan head was from Newson Engineering BV, Belgium. This was used together with an f-theta lens with a focal length of 100 mm [7]. After the laser treatment, the surface structure achieved was characterised by scanning electron microscopy (SEM) (Carl Zeiss, SEM EVO 50).

2.6.7 Surface Characterisation

All specimens were characterised prior to adhesion testing using both qualitative and quantitative analysis. Surface characterisations were tested and analysed for surface topography and the surface wettability (contact angle). Surface structures were measured by using an optical interferometer profiler (Contour GT-K0 3D Profiler, Bruker), which provides a fast and high-resolution measurement (0.1 to 10 mm) over a large scanning area up to $50 \times 50 \text{ mm}^2$. This profiler has a vertical resolution of 0.1 nm and a lateral resolution of 0.13 μm . In this study, the topography measurements for each specimen were obtained under a magnification of 10 to 27.5 over an area of $0.5 \times 0.5 \text{ mm}^2$ with a stitching facility. High magnification measurements were also taken over a smaller area of $100 \times 100 \mu\text{m}^2$ to provide some finer features. For comparison purposes, surface structures on as-received surface areas were also measured. Surface data validity was achieved with a minimum of three (3) sets of measurements taken at different places; averaged values of surface roughness, and their height distribution parameters were recorded and analysed in Chapter 4.

2.6 Biological

There are two parts involved in the biological experiment: i) bacterial characterisation and ii) the bacterial adhesion test. The types of bacteria selected for the surface adhesion experiment were chosen from non-harmful strains of *S. aureus*, *E. coli* and *B. subtilis*. They were chosen based on their size, shape (coccus/oval/rod), Gram type, hydrophobicity and surface charges.

For the bacterial-surface adhesion on glass surfaces, the experiment was carried out in two conditions; i) Adhesion of active young cells (cells at the exponential phase) and ii) adhesion of old cells (cells in the stationary phase) using a 66-hour culture. To obtain young and active cells, *E. coli/S. aureus/B. subtilis* was cultivated in LB broth for 10 hours to ensure a maximum viable cell count located

in the middle of the log phase. In contrast, the study of bacterial adhesion with old cultures was carried out by prolonging the bacterial cultivation for 66 hours, where the bacteria cell was starved due to the exhaustion of nutrients. At this stage, the growth ceased, and the viable bacteria continued to live with very minimal cell activity. For the preparation of the bacterial suspension, the culture broths for both conditions were centrifuged at 5000 rpm, and the cell was washed twice using a saline solution. The cells were suspended in a 0.1 M Phosphate buffer saline (PBS) pH ~7.0 and made-up to an OD of 1.0 (measured with UV VIS). This bacterial suspension was then used for the subsequent adhesion experiments. This procedure was carried out in order to ensure the equivalent number of bacteria was used for every experiment to avoid discrepancies in the data.

The *E. coli*, *S. aureus* and *B. subtilis* specimens were obtained from the Science Lab, School of Biosciences, University of Warwick. For long term preservation, these cultures were kept in 20% (v/v) glycerol, and stored in a freezer at -80°C. For use in subsequent microbial work, these bacterial stocks were stored at -20°C, transferred to an agar plate and incubated for 24 hours at 37°C before preparing the seed culture.

The samples collected at specified time intervals were quantified using a plating method for the determination of the numbers of live cultures. The sample was diluted up to 10⁻²-10⁻⁶ dilution using sterilised distilled water to obtain countable colonies. 10 µL of aliquots was then transferred to an agar plate and incubated at 37°C for 24 hours. The number of colonies formed on the agar surface were counted and measured as CFU/ml. The procedures were carried out in a strictly sterile environment.

2.7.1 Optical density (OD)

The optical density (OD) of the samples was determined using a UV Spectrophotometer (Hitachi) for measuring the concentration of micro-organisms in the samples for both live and dead cells. The samples were diluted using distilled water, and the OD was read at wavelength 600nm against the fermentation media as a blank. The results were plotted against time for the growth curve.

A smear of bacterial culture was prepared and fixed to the surface of a clean glass slide. The bacteria smear was air dried at room temperature and passed through a flame very quickly several times for heat fixation. A drop of crystal violet was smeared on the bacterial sample and left for 1 minute and the process was continued by washing with distilled water from a wash bottle. The smear was then covered with Gram's iodine for 1 minute. The iodine was washed off by tilting the slide and squirting water above the smear so that the water ran over the smear. A 95% ethyl alcohol solution was run through the smear to decolourise the surface until no large amounts of the purple wash came out. Finally, safranin was added for 1 minute, and removed by washing with distilled water. Excess water was removed by blotting with a paper towel or adsorbent paper, which was pressed lightly on the smear. The stained smear was then examined microscopically using low (10 – 20x), high-dry (40x), and oil immersion (100x) lenses. Upon the staining of the bacteria, the stock solution was diluted using DMSO to a final concentration of 50-20 nM and was stored at -20°C. This must be done in a plastic vial to prevent the stain from sticking to the wall (e.g. glass). Drops of diluted dye were applied on the adhered bacteria, and the slide was tilted to make sure that it covered most of the respective area. The sample was left for 5 minutes in a dark room to allow time for the dye to penetrate the bacterial cell. The slide was then rinsed with distilled water to remove the excess dye and allowed to dry. The smear was covered with a glass coverslip before being visualised with a fluorescent microscope.

During the observation of the sample with a microscope, several different counting methods can be used to evaluate the number of adhered bacteria. In general, a suitable approach simply involves dividing the area of interest into sections, counting the number of bacteria in each section and taking the average overall number. However, the counting process can be extremely difficult in some cases when there are many cells and/or congregations of a bacterium. However, to optimise the accuracy of the measurement, statistical analysis was carried out to increase the degree of confidence.

Viewing of a micro-organism under light microscopy was done using oil immersion lenses with 100x magnification. The microscope was connected to an eyepiece, and viewing can be done through the computer screen, and images can be captured and saved. Measuring the size of bacteria was done manually with the help of the software, Dino® version 3.

Visualisations were carried out in the dark room since Syto®9 is a light sensitive dye. The stained cells appeared green when viewing with a fluorescent microscope (Hitachi). Images were visualised using 10x, 20x, 40x and 100x lenses. The viewed images were captured using software (DenQ) for the determination of the number of adhered cells on the solid surfaces. The image grey levels were modified to obtain high contrasts between the cells and the background. This can help in either counting the individual cells, or if these are too numerous, in determining the percentage area covered by the bacteria.

Viewing with a SEM (Zeiss) was carried out for the observation of the adhered bacteria on the solid surfaces. It also provides close-up images of the bacteria for the determination of sizes and shapes. Samples were coated with gold prior to viewing, and images were captured using 250x, 500x, 1000x, 2000x and 5000x magnifications.

Determinations of shapes and sizes were carried out by viewing and capturing the images using microscope. The sizes were measured using ImageJ from an average of 50–100 different images, and the average values with standard deviation were recorded. All micro-organisms were grown from the 10-hour and 72-hour cultures to study the cells' surface characteristics during the exponential and stationary phases. Four types of solvents were used, hexadecane, chloroform, ethyl acetate and decane, for the determination of the electron donor/acceptor properties of the cells. 3 ml of bacterial suspension (OD of 1.0) was added to 3 ml of solvent (1:1 ratio). The mixture was then mixed and vortexed for 60 seconds and allowed to separate at room temperature for 15 minutes. The OD of the bacterial suspension against the fresh PBS buffer, after the phase separation, was measured at 600 nm and the affinity towards the solvent was calculated using the following equation. All measurements were carried out in triplicate and the results presented were the average values.

The quantitative evaluation of the adhered cells on the solid surfaces was performed using fluorescence microscopy (Zeiss) with the help of software Open Lab 4.0.2 using the established protocol. The software assisted in quantifying the number of adhered cells by evaluating the cell coverage in terms of integrated density [I.D. = $N \times (M-B)$], where N is the pixel in the area covered by the microscope, and M and B are the average grey area and common pixel, respectively. The densities of the cells were determined by the numbers of bacteria adhered per area covered.

This chapter reviewed the development of biomimetic study and the current scenario that creates a new dimension of biomimetic phenomenon. It covers the surface finishing techniques (polishing, WEDM and laser) and the quality of surface finishing. The effects of varying the process parameters on the properties of modified surfaces were thoroughly reported. The mechanism of bacterial adhesion on the biomaterials were deeply reported, and factors affecting the interaction of bacteria i.e bacterial properties, surface properties and surrounding effects were appropriately addressed.

2.8 Chapter Summary

The methodological approach engaged in this study combined two major fields: surface at engineering and biological works. The combination will provide a comprehensive evidence of the behaviour of bacterial adhesion on inert surfaces such as metals and polymers. Knowledge of the bacterial adhesion phenomenon will lead the researcher to understand the major parameters influencing the interaction between the surface and micro-organism mechanism. To scientifically demonstrate the interactivity between surfaces and biological organisms, several quantitative and qualitative experimental works have been conducted according to the standard procedures.

For the entire thesis, four (4) major experiments were involved and have been classified as: i) the fabrication process, ii) surface characterisation, iii) bacterial characterisation and iv) adhesion testing works. The results of each stage were closely monitored to ensure the validity of the data to be used in the next experimental stage, whereby the final correlation of bacteria adhesion can be concluded in the last experiment (adhesion test). The uniformity of substrate topography parameters will determine the constructive correlation of the adhesion phenomena while bacterial characteristics varied the trend and adhesion degree on these surfaces. These aspects were thoroughly studied and analysed to relate the adhesion with the properties of the surfaces. Correlations between surface topography and bacteria adhesion contributed significantly to the determination of the major parameters that governed the adhesion process.

Chapter 3

Bacterial Characterisation & Process Screening

3.1 Introduction to Partial Characterisation of Micro-organism

This chapter discusses the effect of bacterial properties on the adhesion on a solid surface (borosilicate glass). The work was dedicated to searching for some patterns concerning adhesion involving distinctive bacteria, which are *S. aureus*, *E. coli* and *B. subtilis*. The bacteria underwent a partial characterisation which includes a determination of *shape* and *size*, *cell-surface characterisation* and *Gram types*. The solid surfaces (glass) were fully immersed in a 100 mL bacterial suspension (containing approximately $\sim 1 \times 10^8$ CFU/mL of active/stationary phase cells) and shaken for a predetermined time and condition. A typical borosilicate glass with dimensions of 25.4 x 76.2 mm was used in this study and cleansed with ethanol followed by immersion in an ultrasonic bath for 10 minutes.

Biofilm development can occur under both low and highly dynamic environments. The properties of the biofilms are relatively different from each other, with the latter being the most difficult to be treated even after the combined use of biocides and mechanical handling (scraping and brushing). Thus, the best way of cleaning the surfaces is to prevent the formation of biofilms. Therefore, preparing a surface that resists bacterial adhesion is a multi-million-dollar industry which not only saves on yearly maintenance costs, but can also prolong the shelf life of the equipment. The preliminary adhesion studies involved the screening of the physical parameters that contributed to the adhesion, including the exposure time, bacterial concentration and culture age. The results of the study were used for further works in the search for the possibility of manipulating the physical properties of the targeted surfaces, namely the wettability, roughness and surface topography. Prior to that, experimental works on the growth curve of the bacteria were carried out to

determine a suitable time for harvesting the cells in their exponential and stationary phases.

3.2 Growth curve

The growth kinetic of different bacterial strains was examined.

Figure 3-1 (a – c) illustrates the growth stages of the bacteria over a 24-hour incubation in a Luria broth, occurring at 37°C. Absorbance data and a colony forming unit from three replications were used to measure the growth of the bacteria. Figure 3-1 (a) represents the growth stages of *S. aureus*, showing the absence of the stationary phase. The cells grew exponentially for up to 12 hours, followed by a sudden decline up to the 24-hour mark. A similar trend was also observed in the colony forming unit, where the numbers dropped by half, from the optimum value of 200×10^8 to less than 100×10^8 CFU/mL at the end of the incubation period. In contrast, the growth curves for the *E. coli* [Figure 3-1 (b)] and *B. subtilis* [Figure 3-1 (c)] show the typical growth curves with clear exponential, stationary and death phases. The overall results show that the maximum number of CFU for all three types of bacteria varies accordingly. The highest number of active cells was found with *B. subtilis* ($\sim 350 \times 10^8$ CFU/ mL), which was greater by 67% and 75% as opposed to *S. aureus* ($\sim 210 \times 10^8$ CFU/ mL) and *E. coli* ($\sim 200 \times 10^8$ CFU/ mL), respectively. LB mediums are used widely for culturing *B. subtilis*, and the current study shows that an appropriate growth was achievable with the same medium for growing *E. coli* and *S. aureus*. Therefore, the LB medium was used as the culturing preparation throughout the study for all three species.

After transferring the starter culture into the new medium, the cell is in the lag phase which occurs within 0 to 4 hours maximum. The lag phase often serves as the adaptation period for the bacteria to become familiar with the new environment, thus growth is limited in this stage. Following the lag phase, the cells continued to grow and produced newer cells efficiently due to the availability of mineral and essential substrates for growth. This stage went on for 12 – 16 hours for all the tested bacteria before entering the stationary or death phase. The deterioration of growth for *S. aureus* occurred at $t = 12$ hours, while for *E. coli* and *B. subtilis* it was delayed slightly, occurring at $t = 14$ and

$t = 16$ hours, respectively. The reduced number of CFU in the culture medium resulted from the inability of the bacteria to survive in the nutrient-deprived medium which has lost its culturability. After most of the nutrients had been used up, the bacteria were forced to enter the stationary phase, which occurred between 12 – 16 hours after the initiation of culture and the numbers of surviving cells decreased continuously.

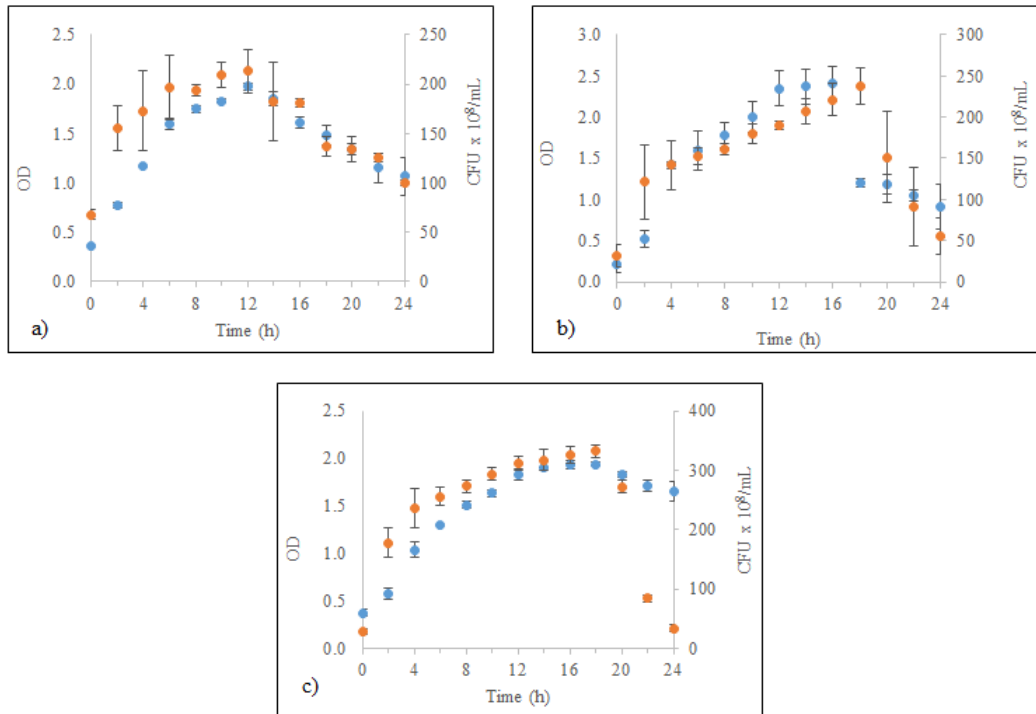


Figure 3-1 The growth curves of a) *S. aureus*, b) *E. coli* and c) *B. subtilis*, grown in a 250 mL flask containing LB medium for 24 hours, with shaking at 200 rpm and 37°C. [OD ■, CFU ■]

The growth of the population is limited by one or multiple factors, which could be the exhaustion of the available nutrients, the accumulation of inhibitory metabolites/end products, the possibility of the exhaustion of space, or combinations of these factors. In the current study, both OD and the numbers of viable bacteria are interrelated and show a good data correlation. It is best to note that during the period of 16–18 hours, data fluctuation was observed for *E. coli* and *B. subtilis*. The fluctuation, which can be interpreted as a poor correlation between OD and CFU analysis, shows the independent value between the number of live cells (with the ability to reproduce) and the actual intact cells (both dead/live) available in the culture broth. At this stage, after the maximum population had been reached during the exponential stage, the rate of death escalated due to the previously mentioned reason, which was dictated by the low CFU count [(c)], but the OD reading remained uninterrupted. The OD readings, however, represent the number of intact cells, both active and dead cells. *B. subtilis* has a thick outer membrane (peptidoglycan), which possibly makes the cell lysis rate very slow compared to the other bacterial strains in the study. Therefore, the intact non-living cells in the culture were still detected during the OD analysis. The OD reading remained high while the CFU count decreased with time.

Referring the best time to harvest all three bacteria to obtain the cells in their exponential phase would be between 8 to 10 hours, where cells were still in their mid-exponential phase. Conversely, the best time to harvest the intact cells in their late stationary/death phase must be beyond 30 hours. Therefore, all the bacterium for the adhesion purposes was grown in LB media, cultured up to 10 hours for the exponential phase and prolonged up to 72 hours to obtain cells in their late stationary phase.

3.3 Partial characterisation of the model organism

Viewing under SEM for the 10 hr cultures (exponential phase) shows that *E. coli* and *B. subtilis* SP. possessed a common rod shape, meanwhile the *S. aureus* apparently is a typical coccus shape (Figure 3-2). When viewed microscopically, *S. aureus* appears in clusters, like bunches of grapes, and this was confirmed with the images from the gram staining shown in Figure 3-2 (a). *E. coli* appears as a slightly ovalis cylinder, with a very similar look to *B. subtilis* but from the Gram-negative group, from its pink staining as shown in Figure 3-2 (c). *S. aureus* and *B. subtilis* are of positive types, dictated by their purple hue when observed using the light microscope (Figure 3-2). The major differences between Gram-negative and Gram-positive bacteria depend on the cell wall structure. The Gram-negative bacteria are unable to retain the crystal violet dye after the ethanol washing step due to their thinner peptidoglycan layer [114], where the counterstain (safranin) was added afterwards to re-stain with a pink shade for easy visualisation. Besides this, the thin outer membrane was easily disrupted during the decolourisation step [115]. In contrast, the capability of the Gram-positive bacteria to retain the crystal violet stains is due to their thick peptidoglycan and secondary polymer layer in conjunction with an impermeable wall that resists decolourisation during the washing step [115, 116].

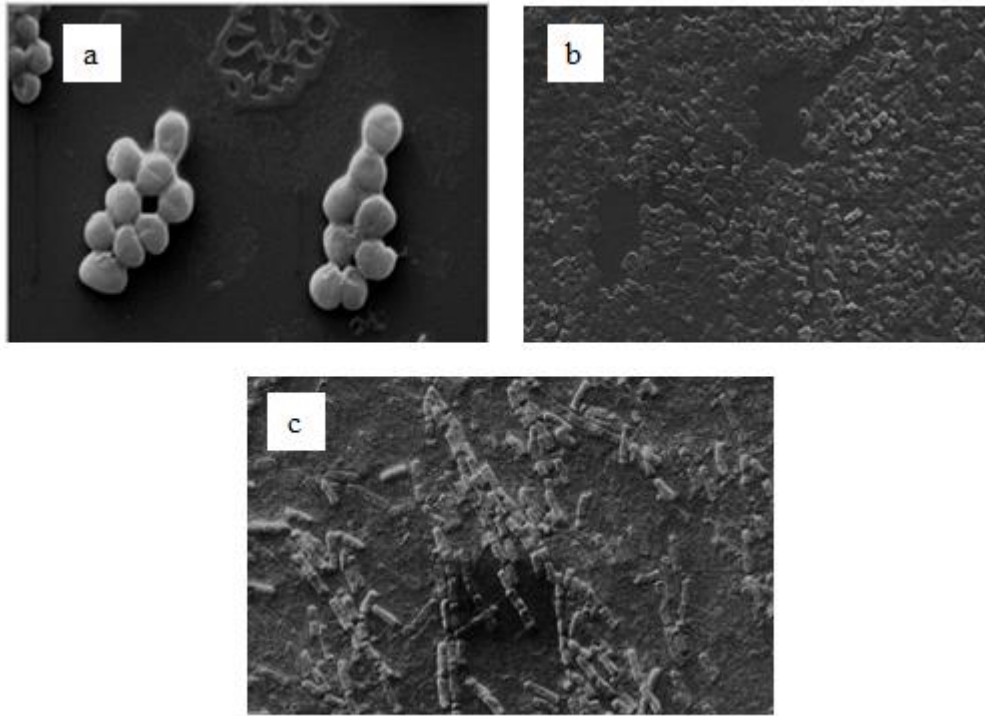


Figure 3-2: Images of the exponential phase-cells of a) *S. aureus*, b) *E. coli* and c) *B. subtilis* from a 10 hour culture, observed under SEM at magnification between 2500x - 3000x.

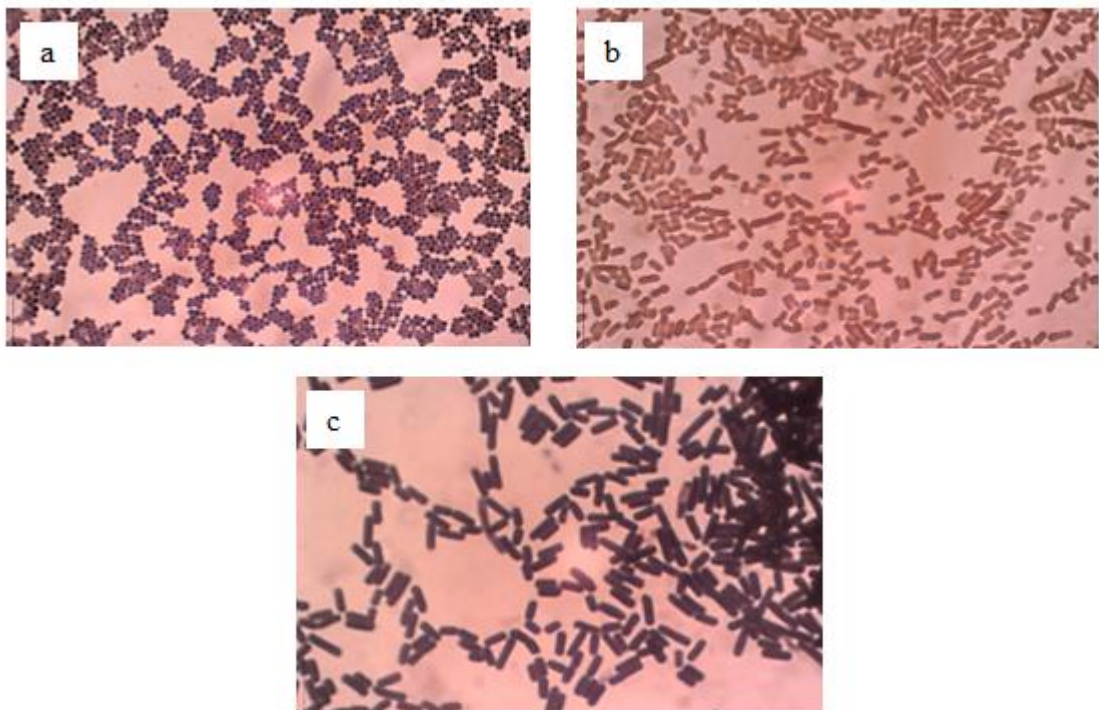


Figure 3-3 Images from Gram staining analysis of a) *S. aureus*, b) *E. coli* and c) *B. subtilis*

3.3.1 Determination of Cell Size

Microscope images of the micro-organisms were taken from 10 and 66-hour shake flask cultures to study the size and the morphology of cells in the exponential and stationary phases, respectively. The measurement was done using 100 cells for each micro-organism, and the mean averages were taken as a result. Table 3-1 shows the sizes of both young and active cells in their active exponential stage, and the aged cells in their late stationary phase. The results show the differences in the cell sizes of the bacteria in the two phases. For *B. subtilis* and *E. coli*, the size of the cells in the stationary phase was apparently bigger in comparison to the young and active cells in the exponential phase. The sizes of *E. coli* and *B. subtilis* at the exponential phase were $1.23 \pm 0.07 \mu\text{m}$ and $1.69 \pm 0.18 \mu\text{m}$ and increased by $\sim 54\%$ and $\sim 25\%$ in the death phase giving the mean value of $1.89 \pm 0.10 \mu\text{m}$ and $2.11 \pm 0.06 \mu\text{m}$, respectively. The change of size was reported for many other bacteria, which might be contributed by the changes in the osmotic pressure in the surrounding environments due to the consumption of nutrients. Consequently, this results in the passive transport of water molecules crossing the semi-permanent membrane and causing the bacteria to swell. However, starving the soil bacteria in a low nutritional medium does not reduce or increase the size, but the cells lose their culturability [117]. In addition, the size of the bacteria was generally dictated by the type of medium and the nutrient availability. Bacteria cultured in nutrient- rich complex media appeared larger by 40% in comparison to bacteria cultured in defined low nutritional media. The increased size in the *E. coli* species, as they shifted from the exponential to the stationary stage was also observed [118].

Table 3-1 Size of bacteria at the exponential and stationary phase

Bacteria	Gram types	Shape	Cell Size (μm)		¹ %
			Exponential	Stationary	Difference
<i>S. aureus</i>	Positive	Coccus	0.75 ± 0.12	0.65 ± 0.14	-13.3
<i>E. coli</i>	Negative	Short rod	1.23 ± 0.07	1.89 ± 0.10	53.6
<i>B. subtilis</i>	Positive	Long rod	1.69 ± 0.18	2.11 ± 0.06	24.9

¹ Size changes with reSPect to the exponential phase

An observation of the size of *S. aureus* in the stationary phase revealed a contradictory result to the sizes of *B. subtilis* and *E. coli*. Based on the image from SEM analysis (Figure 3-4), the average diameter of *S. aureus* in the stationary phase was $0.65 \pm 0.14 \mu\text{m}$ and apparently, this was smaller compared to the cells in the exponential phase. The mean size during the active phase was $0.75 \pm 0.12 \mu\text{m}$ and reduced by 13.3% (Table 3-1) in the stationary phase to an average of $0.65 \pm 0.14 \mu\text{m}$. The bacteria responded differently to changes in their environments. More often, Gram-negative bacteria were recorded to reduce in size and became more spherical they have in a nutrient-deprived environment for a prolonged period [119]. However, this was not the case in the current study. The current study revealed that the increased/decreased sizes were more prominent in the Gram-negative bacteria (*E. coli*) compared to the Gram-positive bacteria (*B. subtilis* and *S. aureus*). This was presumably owing to the thickness of the cell wall allowing the transport of osmotic components in and out of the cells, that an increment of cell length of ~6% was observed for *E. coli* in the stationary phase ($0.93 \mu\text{m}$) as opposed to exponential phase-cells ($0.87 \mu\text{m}$) [120].

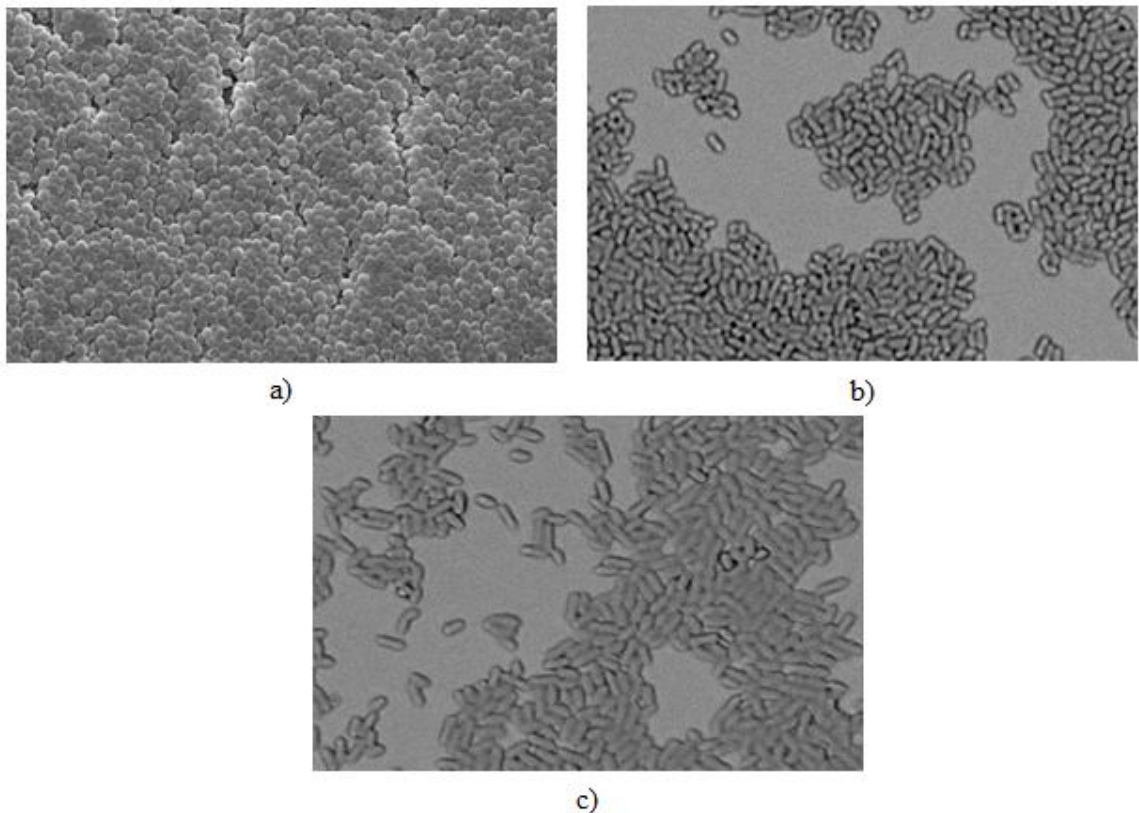


Figure 3-4 Close up pictures of a) *S. aureus*, b) *E. coli* and c) *B. subtilis* under 4000x magnification using SEM.

The mechanism of the cell's dimension difference was long thought to be the growth rate mechanism, and medium/nutrition independent, where bacteria with high growth rates were three times bigger than their slow-growing counterparts [121]. However, recent research has found that the size of the bacteria is a rather complex, multifactorial phenomenon. The nutritional availability that contributes to the high growth rate dictates the cell size, which is also a function of cell expansion and cell cycle progression [122]. It was reported that the cell sizes were more affected by the nutritional value through the medium rather than the growth rate. This is supported by the observation that the growth rates of *B. subtilis* and *E. coli* were able to be maintained in the nutrient-deprived environment, but this reduced the cell sizes by approximately 35% and 25%, respectively, in comparison to culturing in a carbon-rich medium. During growth in a nutrient-rich medium, cell division was delayed while cells continued to grow in size [122]. However, the condition is not generally true for other microbes, where other researchers have reported otherwise, and the actual mechanisms are far from clear.

3.3.2 Determination Cell Surface Hydrophobicity (CSH)

The wettability of a surface is now more generally expressed in a reverse sense and is referred to as hydrophobicity. There are several methods available for the determination of cell surface hydrophobicity, ranging from the highly accurate yet laborious and pricey, to simplistic and straight-forward measurements. Contact angle measurement (CAM) [123], atomic force microscopy (AFM) [124] and hydrophobic interaction chromatography (HIC) [125] are more specific and accurate, whilst the technique of bacterial adherence to hydrocarbons (BATH) provides speedy results with simple preparation steps at fairly low cost [123, 125-127]. A few authors reported that a good correlation was achieved between HIC and BATH [125, 128], while others achieved a contradictory result between BATH and CAM. Although there are continuous debates and questions arising concerning the accuracy of the BATH test, this method still achieves wide acceptance, it is a good correlation for the electron donor properties achieved for the BATH technique and when using CAM for the *E. coli* strain [129]. However, weak and contrasting results were discovered for *S. aureus* and *B. subtilis*. Nonetheless, the adhesion of cells onto a solid surface is affected by three important components: i) the

physicochemical properties of the micro-organisms, ii) the surface characteristics and iii) the surroundings (e.g. medium, hydrodynamic properties, temperature, shear stress, exposure time, size of inoculum). The physiochemistry of the micro-organisms is long thought to be the important or the main driving force, which interacts differently for a given surface and process conditions [130]. It is very useful to determine the properties of the interacting bacteria in terms of electron donating/electron accepting properties as this will also influence the adhesion process and provide a better understanding of the directions of the mechanism in terms of the specific interaction with the surfaces. Apart from this, strain types, particle shape, surface wettability and surface charge are some of the important factors that initiate cell-surface adhesion [131-133].

The BATH results obtained for the three bacteria using four types of solvents (hexane, hexadecane, chloroform and ethyl acetate) showed the diversity of their surface properties. Figure 3-3 depicts that the bacteria exhibited a broad range of affinity towards these solvents, ranging between 6%-47%. The adhesions to hexadecane were considered as the measurement for the hydrophobicity since this omitted the effects of electrostatic owing to its uncharged properties [134, 135]. It also shows that CSH varied differently as the cells moved from the exponential to the stationary phase, with the percentage of difference varying from 4% to 85%. *B. subtilis* and *E. coli* are relatively hydrophilic in nature as they adhered weakly towards the polar solvent (hexadecane) with less than 30% adhesion for both the active and stationary phase-cells. On the other hand, a strong hydrophobic character was shown by *S. aureus* as their affinity towards hexadecane was more than 45%. Meanwhile, *B. subtilis* was the most hydrophilic bacteria, with the lowest affinity towards hexadecane (~11%). Upon shifting from the exponential stage to the stationary growth phase, the hydrophobicity of the cells reduced for *S. aureus* and *E. coli* with the percentage of reduction varying from 50-70%, as denoted by the weaker adhesion towards hexadecane [Figure 3-4 (b)]. Contrarily, there was a slight increase in the CSH level for the *B. subtilis* stationary phase-cells, measured to be 11% higher than the cells in the exponential phase. The order of hydrophobicity for the active cells in increasing levels is as follows: *B. subtilis* < *E. coli* < *S. aureus*, while for the stationary phase-cells it is: *E. coli* < *B. subtilis* < *S. aureus*.

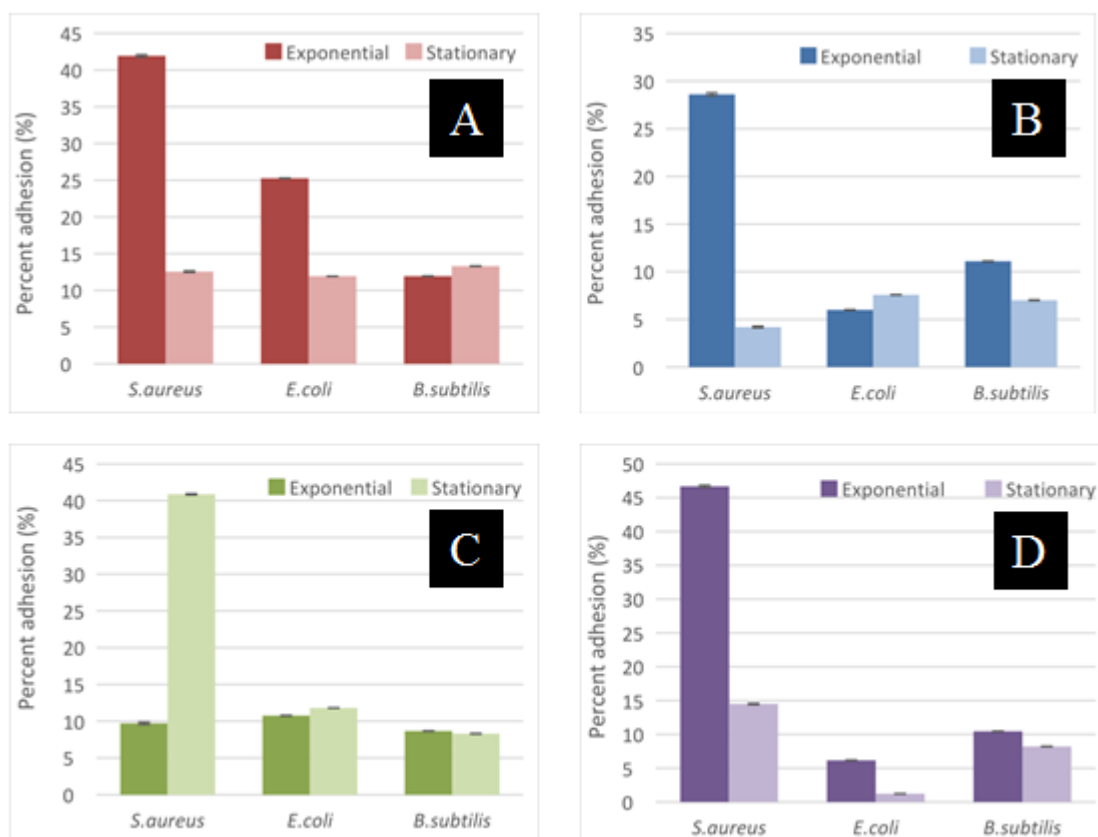


Figure 3-5 Bacterial adhesion on solvent a) hexadecane, b) hexane, c) chloroform, and d) ethyl acetate. Adhesion was carried out using bacteria at the exponential phase and the late stationary phase using 10-hour culture and 66-hour culture, respectively.

The variabilities of the CSH are highly influenced by the physicochemical component on the surface. This is dictated by the type and amount of protein available on the surface, while the hydrophilic character is often contributed by the polysaccharide components. The Gram-negative bacteria are often less hydrophobic (more hydrophilic compared to Gram-positive) in nature due to the presence of markedly hydrophilic constituents at the cell envelope [136]. The changes of CSH in the recent study are in line with other findings that have stated that this property will alter accordingly with growth stages and cell age [123, 137, 138]. However, cells in the stationary phase are generally more hydrophobic due to the alteration of the wall and cell composition [14]. The present findings reveal that the *S. aureus* forms big clusters (when examined under microscope and SEM) in the stationary phase due to its hydrophobic character, thus preventing it from being attracted to the solvents, hence showing declining CSH. A reduction in CSH was also observed for the *Pseudomonas fluorescens*, where the highest hydrophobicity was

observed during three hours after incubation and this declined gradually between 12 to 48 hours. The starvation of the cells during the stationary phase (nutrient deprived medium) caused the consumption of a certain amino acid on the cell wall as the energy source for the metabolism process, thus reducing the CSH [138, 139]. This could also occur due to the degradation of wall proteins, which is due to nutritional stress [138].

Interestingly, *B. subtilis* exhibited a conflicting trend to the previously mentioned bacteria where the adherence towards hexadecane was slightly increased in the cells in the stationary phase. At matured stages, where often the nutrient availabilities in a medium are very low, the cell envelope and exosporium of *B. subtilis* consist mainly of proteins. Lipids and phospholipids will be thickened, thus contributing to the increased hydrophobicity level of the *Bacillus* [140, 141]. At these stages, spore formation will take place, and it is best to note that the composition of the protein on the surface often varies between strains, and thus also the CSH level. Care should be taken as the CSH level is easily provoked by single/multiple effects of environmental factors such as substrate concentration, surfactants (sorbitol, tween 80, etc.), temperature, etc., thus imposing different adhering ability onto the surfaces [87, 136, 142, 143].

From the study, eight out of 12 isolates of *Staphylococcus* Sp. possessed moderate to highly hydrophobic surfaces, dictated by their high affinity towards xylene (34.07–81.25%) [125]. Despite the result, care should be taken since the BATH tests are prone to erroneous output due to its different responses to ionic strength and the covalent compounds of the buffer [125]. Some hydrophilic bacteria may possess hydrophobic characteristics due to their hydrophobic hyphae, fibronectin, flagella, etc. *B. subtilis* showed a diverse range of CSH levels, varying between 6-66% when tested using the BATH technique [128].

The BATH method is often regarded as the combination effects of both hydrophobicity and electrostatic interaction and, therefore, it is best used to measure adhesion rather than determine the hydrophobicity level [135] [134, 142]. A higher affinity to chloroform when compared to hexadecane is indicative of the predominance of basic properties on the cell's surface, while a higher adhesion to the basic solvent ethyl acetate compared to hexane indicates that the cell's surface presents more acidic properties. The electron donor/acceptor property of bacteria varies significantly and relies heavily on the strain, type of media, ionic strength, etc. [109, 134].

The electron donor and electron acceptor properties were also measured for the bacteria using the method discussed by Hamadi et al. (2005). The electron donor character was determined by the difference between the affinity to chloroform and hexadecane, while the electron acceptor property was determined by the differences between the affinity towards ethyl acetate and hexane. Referring to Table 3-2, the percentage difference between ethyl acetate and hexane showed that the active cells of *S. aureus* carried basic and electron acceptor character. In contrast, the cells in the stationary phase showed a higher affinity towards chloroform, a marked difference with the hexadecane of around 38%. This indicates that the electron acceptor property was dominant for the non-active/non-living cells of *S. aureus*.

Table 3-2 Determination of electron acceptor/donor properties [131]

Bacteria	Chloroform	Hexadecane	Electron donor ²	Ethyl acetate	Hexane	Electron acceptor
Exponential phase						
<i>S. aureus</i>	9.7	42	-	46.5	4	42.5
<i>E. coli</i>	10.8	25	-	6	6	0
<i>B. subtilis</i>	9.2	11.5	-	10.2	11.5	-1.3
Stationary phase						
<i>S. aureus</i>	40.5	12.5	38	14.5	4.5	10
<i>E. coli</i>	11.2	11.5	-	3	7	-4
<i>B. subtilis</i>	8.7	13	-	8	6.5	1.5

² Electron-donor character was determined by the difference between the percentages of affinity to chloroform and hexadecane. The standard deviation is given in parentheses. oA high affinity to hexadecane means a high hydrophobicity

3.3.3 Determination of Bacteria Zeta Potentials

The surface of the bacteria was tested using bacterial suspension at physiological pH ~7 in a PBS buffer with molarity of 0.01M. The suspension was prepared using cultures at the exponential stage ($t=10$ hrs) and at near the death phase, ($t=72$ hrs) and the OD reading was set at 1.0 reading 600 nm. The zeta potentials of the bacteria in the exponential and stationary stages are presented in Table 3-3 below. The surface charge of the *S. aureus* increased slightly to 17.1 mV when cells were in the stationary phase, an increase of 31.5% although the value was not statistically significant. On the other hand, the negativity charges of *E. coli* and *B. subtilis* were reduced to 23.6 mV and 34.4 mV, which marked a reduction of less than 10% relative to the cell in the exponential phase.

Table 3-3 Surface charge of the bacteria in exponential and stationary phase

Bacteria	Exponential (mV)	Stationary (mV)
<i>S. aureus</i>	$\sim 13.0 \pm 0.8$	$\sim 17.1 \pm 0.6$
<i>E. coli</i>	$\sim 24.6 \pm 1.0$	$\sim 23.6 \pm 1.1$
<i>B. subtilis</i>	$\sim 35.2 \pm 2.0$	$\sim 34.4 \pm 1.0$

3.4 Screening of the Process Condition for Bacterial Adhesion on Glass

The adhesion process on the glass substrata (hydrophilic surface) was carried out for 24 hours, with initial cell concentration fixed at OD 1.0 ($\sim 10^8$ cfu/mL) containing active young cells in their exponential phase. The bacteria were suspended in a PBS buffer (non-nutritious media) to prevent the cells from multiplying during the incubation time. Samples were withdrawn at 2, 4, 8, 12 and 24 hours to check on the remaining OD of the bacterial suspension and the number of adhered cells using a fluorescence microscope. The adhesion is measured by the percentage of adhesion (%) and the number of adhered cells per centimetre square area (no of cells/cm²). The percentage of adhesion was measured as follows: **Percent adhesion** (%) = $\frac{OD_i - OD_{t=t}}{OD_i} \times 100\%$...Equation 3-1

The adhesion capacity was also determined by quantifying the number of adhered bacteria on the glass substrata. Since the adhesion experiment was carried out in triplicate, five (5) randomly selected images were taken for each sample, giving a total of 15 images per surface. The adhered cells were presented as the number of adhered cells per cm² area taken as the average counted from 15 images. The kinetic adhesion of the adhered cells per hour was also determined graphically during the exponential phase adhesion.

3.4.1 Preliminary adhesion of *E. coli* and *B. subtilis* on the glass substrata.

To evaluate the adhesion for all the bacteria species on the glass surfaces, the adhesion procedure was developed and maintained throughout the study based on the exposure of a fixed concentration of active live bacteria to a surface for a fixed time. All experimental variables, except the bacterial strain cell types (active or live cells), were held constant, including the cell concentration, exposure time, shaking speed, container size and solution volume. Data for the percentage of adhesion based upon the reduction of the OD reading is presented in Figure 3-6.

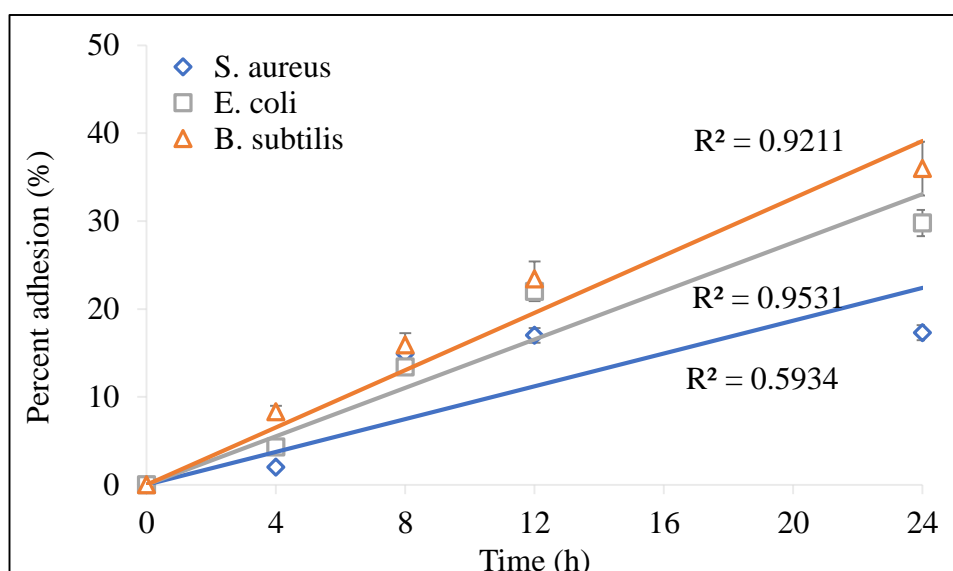


Figure 3-6 Percentage adhesion of *S. aureus*, *E. coli* and *B. subtilis* on the glass substrates. Samples were immersed in bacterial suspension (OD= 1.0) for 24 hours.

Figure 3-6 presents data with respect to the percentage difference of OD reading over the initial OD. It was assumed that the greater the percentage of the OD difference (which will be referred onwards as percentage adhesion), the higher the bacterial adhesion to that surface. All adhesion with the tested bacteria shows that the percentage adhesion increased almost linearly with time during the first 12 hours of incubations. A speedy increase of adhesion for *S. aureus* was observed in the first 8 hours of exposure and reached a maximum at $t = 12$ hours (17%) and remained on a plateau afterwards until $t = 24$ hours. *E. coli* adhesion also sped up and increased linearly with time, up to 24 hours ($R^2 = 0.95$). The maximum adhesion was achieved at $> 35\%$ and showed no evidence of slowing down. Meanwhile, the adhesion of *B. subtilis* shows an increasing trend, which is linear up to 12 hours of exposure ($R^2 = 0.92$), with signs of slowing down, and maximum adhesion was achieved at 29%. Despite being in different gram groups, a close competition was observed between *E. coli* and *B. subtilis* (hydrophilic species), and the final adhesion percentage was the lowest for the most hydrophobic species, *S. aureus*. The order of adhesion is as follows, *S. aureus* $<$ *E. coli* $<$ *B. subtilis*.

The adhesion of the bacteria on the glass surfaces was also viewed under a microscope, and the result was analysed thoroughly for the adhered cells on the glass surface. The data on the quantified adhered cells presented in Figure 3-7 shows a similar profile regarding adhesion percentage but differs in terms of order. A speedy increase in the number of adhered *S. aureus* cells was observed in the first 8 hours of exposure, and this reached a maximum at $t = 12$ hours with no significant increase until the end of fermentation. On the other hand, the adhesion of *E. coli* and *B. subtilis* sped up between 4-8 hours of incubation, with a gradual increase up to 24 hours. All three profiles suggested that the adhesion saturations/equilibrium were achieved after 12 hours of incubation, for all the bacteria tested. There were negligible changes in the numbers of adherent cells counted at $t = 12$ h and $t = 24$ h, varying only between 2–6%. However, it was observed that the decreasing rate of adhesion for *B. subtilis* occurred much earlier, at $t = 8$ h. The order of adhered cells was highest in *S. aureus*, followed by *E. coli*, and the lowest adhesion was attained with *B. subtilis*, which provides a good agreement with the level of hydrophobicity index for the bacteria species (Figure 3-7). The number of adhered cells increased in parallel with the degree of hydrophobicity of the bacteria. *S. aureus* (Gram-positive) is the most hydrophobic species and adhered most to the glass

accounting for $\sim 1.5 \times 10^3$ bacteria/ mm^2 , followed by *E. coli* (Gram-negative) at $\sim 0.9 \times 10^3$ bacteria/ mm^2 and *B. subtilis* ($\sim 0.7 \times 10^3$ bacteria/ mm^2). *S. aureus* was the greatest coloniser of all the tested strains owing to the CSH level ($\sim 45\%$), which was the highest among all the other strains. *B. subtilis*, which has the lowest CSH at 11% affinity towards hexadecane, adhered the least to the glass surfaces. Doubling the value of the CSH level of *E. coli* at 25%, increased the adhesion by 30% compared to *B. subtilis*. Many studies have reported that hydrophobic bacteria are greater colonisers compared to their hydrophilic counterparts.

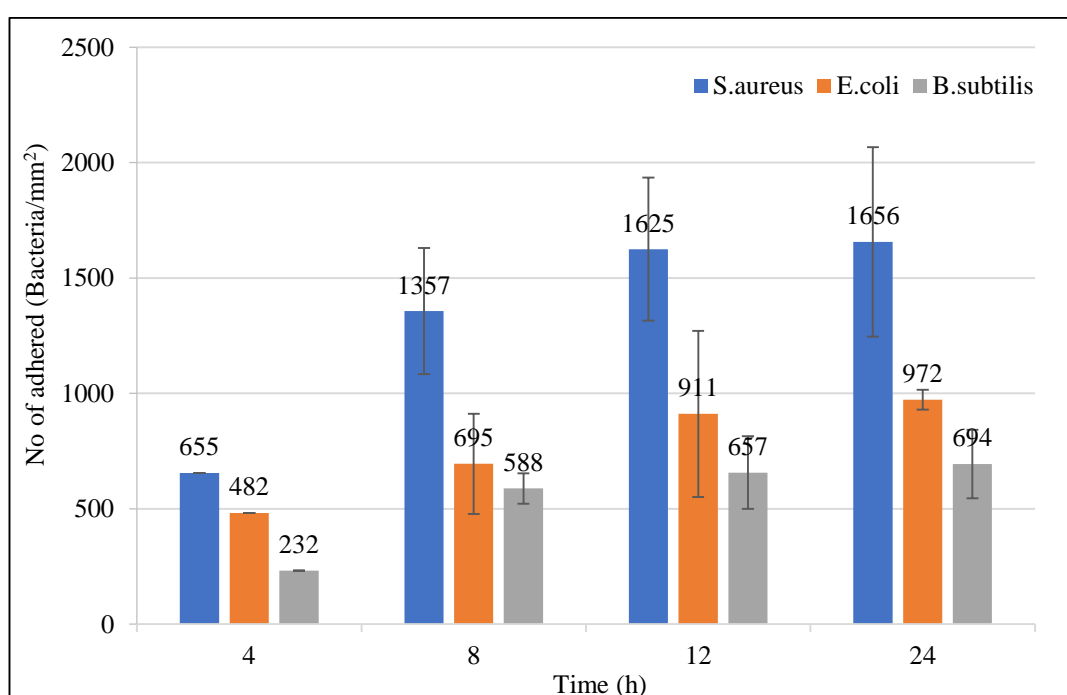


Figure 3-7 Number of cells adhered on the glass substrata after immersion in the bacterial suspension with initial OD of 1.0 (containing approximately $\sim 10^8$ CFU/mL of active cells in the exponential phase). Bacteria were quantified at 4, 8, 12 and 24 hours.

Apart from the hydrophobicity correlation between CSH and the number of adhered cells, the adhesions were believed to be correlated with the surface charge of the bacteria. The zeta potential of the exponential phase-cell in the near physiological pH was the highest for *B. subtilis*, which might explain why there was the least number of cells adhered to the glass surface. A greater repulsion existed between the negatively charged glass surfaces and the highly negative *B. subtilis* ($z = \sim 35 \pm 2.0$ mV). This is followed by *E. coli* with a surface charge of $z = \sim 24 \pm 1.0$ mV and the lowest negativity of *S. aureus*

($z = \sim 13 \pm 0.8$ mV), subsequently resulting in the highest adherence to the glass surface associated with the lowest repulsion. Statistical analysis shows that the final number of adhered bacteria on the glass surfaces varies significantly between the three bacterial species (confidence level = 95%) with respect to the zeta potential. Other than that, the influence of the biological component on the bacterial surface might aid in enhancing/reducing the adhesion. The adhesion of *E. coli* and *S. aureus* on the inert surfaces was attributed to the presence of an extracellular polymeric substance (EPS) and lipopolysaccharide (LPS), which aid in the adhesion process. Despite being the most hydrophilic bacteria, due to the lack of LPS, *B. subtilis* is the least adhered on the glass surface. Studies reported that hydrophilic bacteria will adhere more onto hydrophilic surfaces [131]. However, the situation did not occur here, thus it was expected that despite its highly hydrophilic surface, limited adhesion was observed in Bacillus, possibly due to the non-existence of the molecular structure on its surfaces (e.g: LPS) to aid the adhesion and due to repulsion effect.

The current findings agree with the earlier studies which stated that the availability of LPS and its length dictated the degree of adhesion, thus in some cases it demolished the effect of hydrophobicity/hydrophilic attraction [144]. Others have reported that the truncation of the carbohydrate chain on the LPS structure reduced the adhesion capacity of *E. coli* on the hydrophilic surfaces (glass and mica) but showed attraction towards hydrophobic surfaces e.g. polystyrene and Teflon due to its increased CSH level [145]. Little variation was also expected from the electrostatic interaction between the bacteria and the glass surface, since the experiment was conducted in the low ionic strength buffer and nearly neutral pH. At this stage, the hydrophilic-hydrophilic interactions are disabled and the effect of electrostatic (either repulsion or attraction) is augmented, which subsequently dictated the adhesion phenomena.

Statistical analysis also shows that the adhesion capacity also varies with a significant difference ($p < 0.05$) between the *S. aureus* and *E. coli*, representing the Gram-positive and negative types, respectively. Meanwhile, the increment in the number of adhered *B. subtilis* with respect to time was not statistically significant, and in fact showed the lowest adhesion compared to the other species. The increasing bacteria count on the

glass showed that the attachment on the inert surface escalated with time, thus explaining the reduction of the colony in the CFU plating as shown in Figure 3-6. Following the same gram type (*S. aureus* and *B. subtilis*), it showed a significant difference of attraction between these two species towards glass surfaces. In this case, the hydrophobicity of the *S. aureus* empowers the law of attraction towards the glass therefore increasing the adhesion capacity by ~ 60% compared to *B. subtilis*. Quite often, the adhesion and the hydrophilic surface do not provide a good correlation between the number of adhesion and the increased CSH of the bacteria. Studies have revealed that the interaction between the adhered *Zymomonas mobilis* 113S on the glass surface was inversely related with the increased CSH level of the cell [136] However, when the study was performed on hydrophobic surfaces, the number of adhered cells increased proportionally with the CSH level, providing a linear relationship. In addition, a report by Cunliffe, Smart [146] shows that there was a considerable difference in the attachment of several bacteria to the hydrophilic surface. Meanwhile, a report by van Hoogmoed, van der Kuijl-Booij [88] show that the adhesion of *S. aureus* was higher on the hydrophilic substrate than on the hydrophobic surface. These findings were in contradiction to Chan, Carson [147] who observed that hydrophobic *S. aureus* adheres preferentially onto hydrophobic surfaces rather than hydrophilic surfaces. The current findings suggest that the effects of interaction towards the hydrophilic glass surface increased with increasing hydrophobicity, which might also be contributed by the reduction of the repulsive interaction through the reduction of the zeta potential value of these bacteria. The magnitude of the percentage increase of the adhered cells was followed closely by the percentage difference of the bacterial zeta potential with respect to *B. subtilis*.

S. aureus selected for this study was considered as having a strong electron-acceptor property, shown by the strong affinity towards chloroform (> 45%). Because of the attractive effect from the electron-acceptor/electron-donor interactions (although the interactive nets for bacteria and the surface are both negative); the adhesion was high, even though there should be an additional repulsive effect from the differences due to hydrophobic CSH and the hydrophilic properties of the glass surfaces. Bellon-Fontaine, Rault [148] has reported that proteins can adsorb onto a very hydrophilic surface, such as clean glass, even though macroscopically the net interaction is repulsive. The reason for this lies in the microscopic acid-base interactions between the strong electron-donor sites

of the protein with discrete electron-acceptor patches of glass. This explains the maximum adhesion observed between the strong electron-donor character of *S. aureus* and the considerable electron-donor character of glass in the range of pH 4 to pH 6. Besides hydrophobicity and acid-base interactions, the electrostatic interactions have also been shown to play an important role in microbial adhesion to a surface. The present results demonstrate that the hydrophobic and acid–base interactions also participated in the adhesion of *S. aureus*, *B. subtilis* and *E. coli* and strongly dictated the capability of these bacteria to colonise the glass surface.

Visual representations under light microscopy are shown in Figure 3-8–Figure 3-10 following the adhesion of the bacterial species on the glass substrata. It is observed that the cell density on the glass surface for all the bacteria increased with increasing exposure time (Figure 3-8–Figure 3-10), thus explaining the reduction of the colony in the CFU plating (Figure 3-7). The adhesion was more individualistic and scattered homogenously on the surfaces during the first 8 hours, despite the ability or preference to form small colonies for *S. aureus* and *B. subtilis*, respectively. At $t = 24$ hours, *Staphylococcus* were often attached in colonies, whereas *B. subtilis* and *E. coli* were more homogenously spread on the inert surface on an individual basis. This is certainly the case with *S. aureus* and *S. epidermidis*, as they are both known to grow in clusters rather than homogenous planktonic cells.

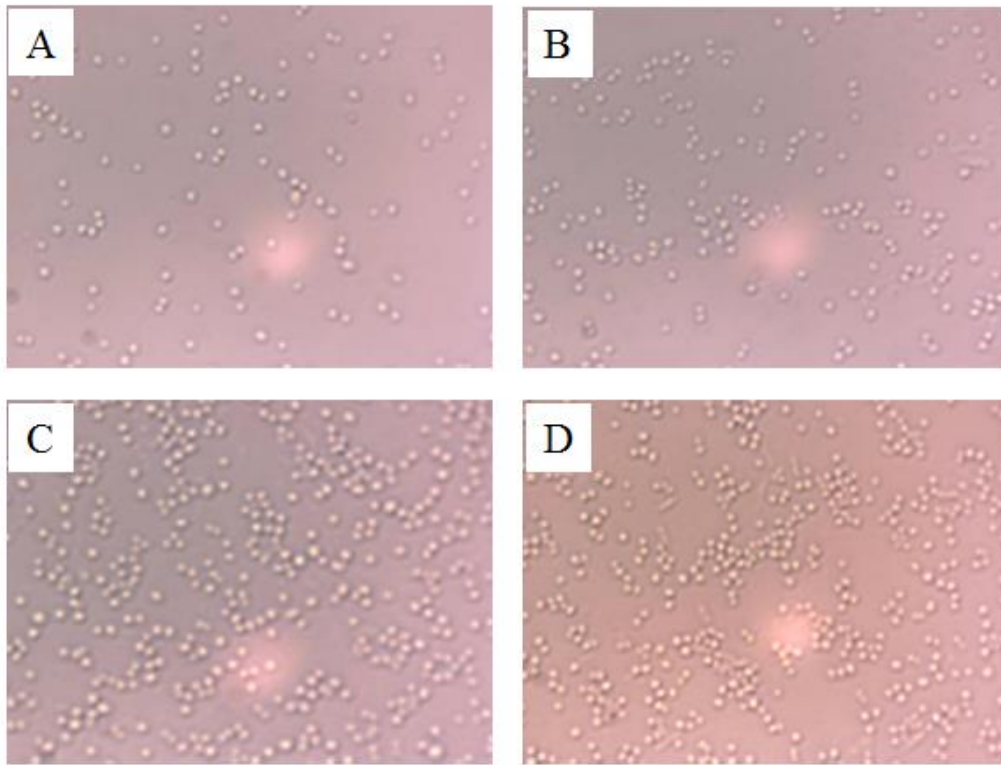


Figure 3-8 The images show the adhered *S. aureus* on the glass slide viewed under light microscopy at a) 4 hours, b) 8 hours, c) 12 hours and d) 24 hours.

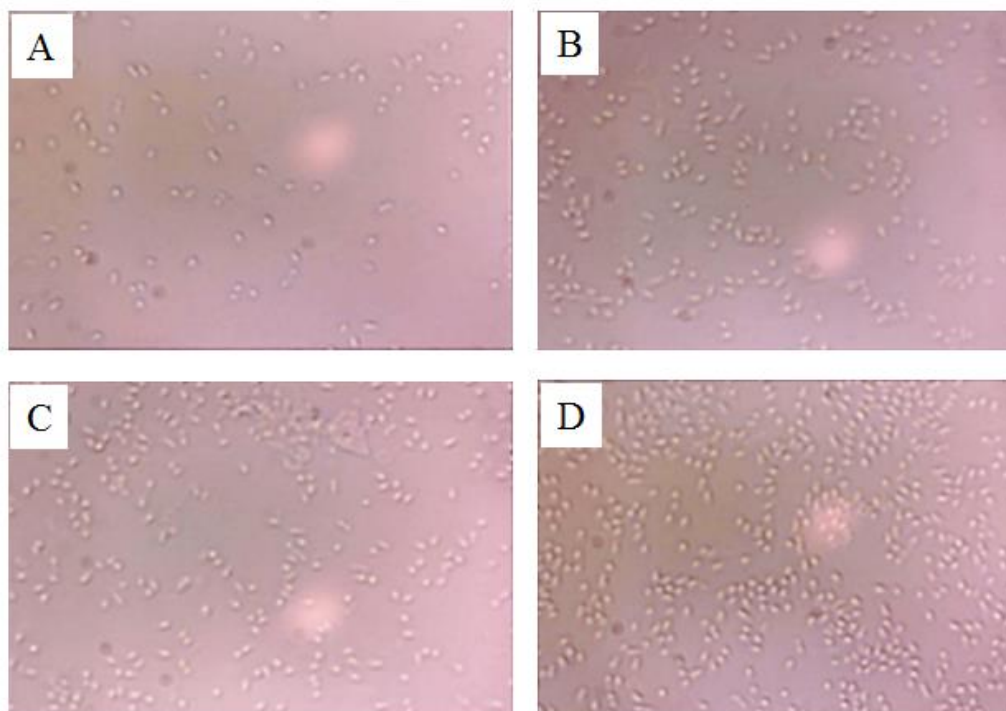


Figure 3-9 The images show the adhered *E. coli* on the glass slide viewed under light microscopy at a) 4 hours, b) 8 hours, c) 12 hours and d) 24 hours.

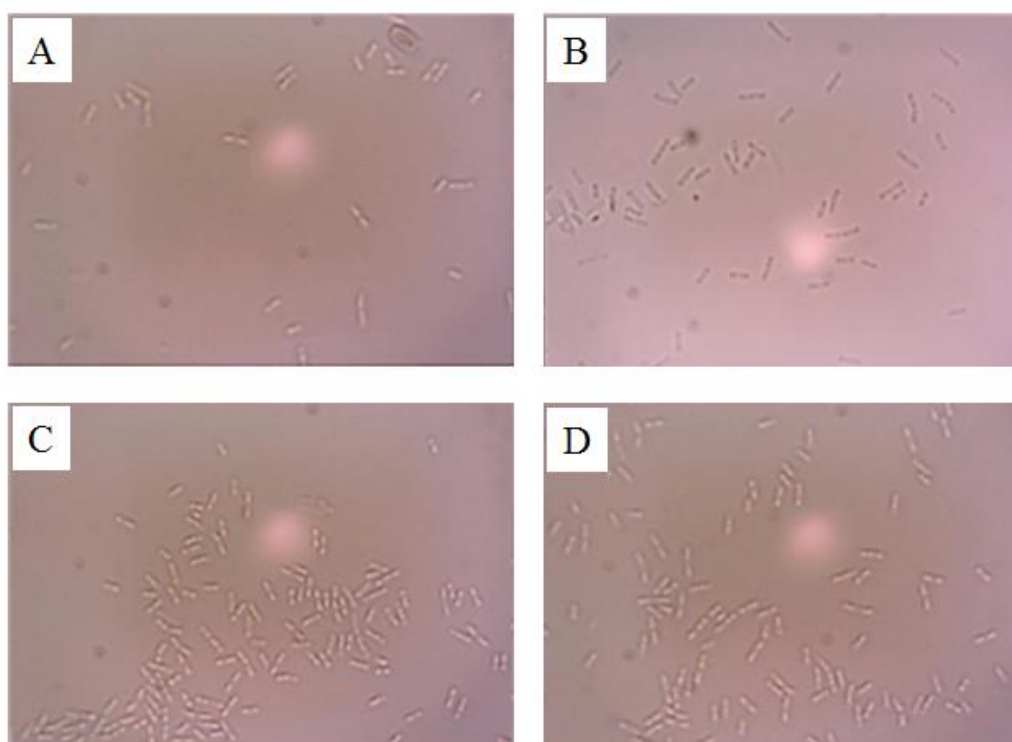


Figure 3-10 The images show the adhered *B. subtilis* on the glass slide viewed under light microscopy at a) 4 hours, b) 8 hours, c) 12 hours and d) 24 hours.

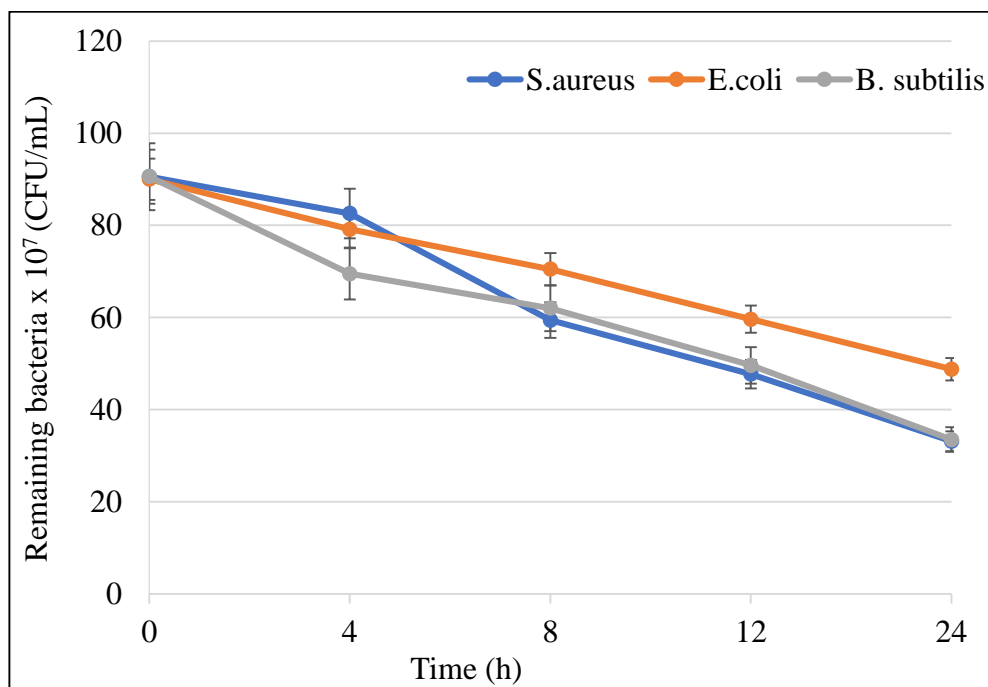


Figure 3-11 Numbers of remaining bacteria in the PBS solution during 24 hours of exposure on the glass substrate.

3.4.2 Effect of Cell Concentration on the Percentage of Adhesion

An experiment with respect to the varying of the initial cell concentration was carried out to investigate the possibility of an increased coagulation probability of the bacteria, which subsequently affects the adhesion. The experimental steps were carried out over 24 hours, and the glass substrates were exposed to the bacterial suspension at initial OD of 0.8, 1.0 and 1.2 with continuous shaking. Data were taken at the end of the experiment (one-time sampling) and the number of the adhered cells were quantified from three replicates. The results are presented in Figure 3-12.

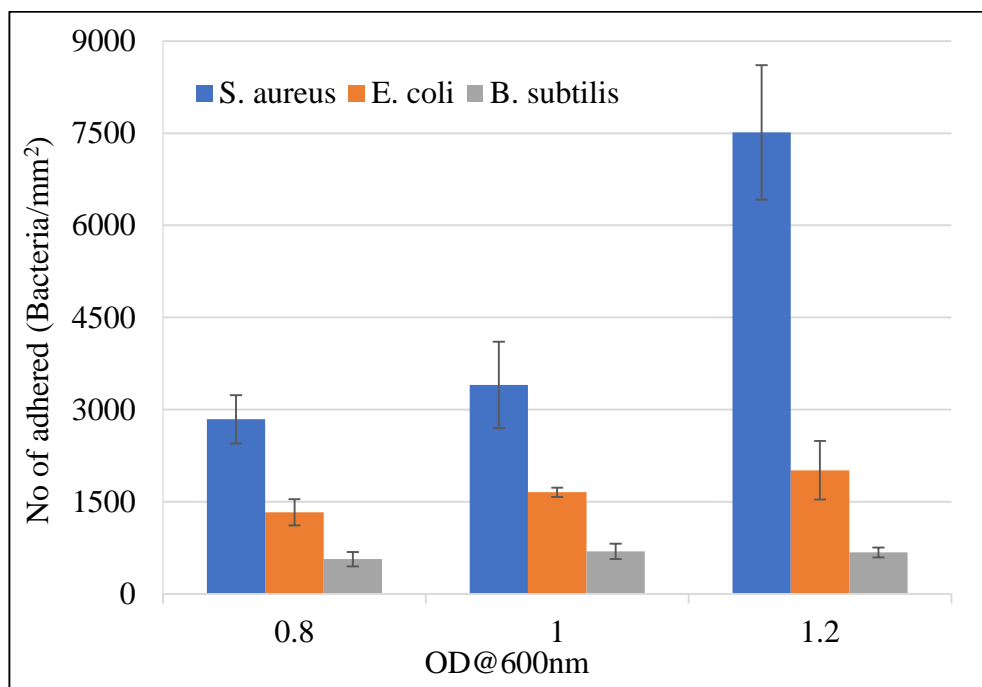


Figure 3-12 Number of cells adhered on the glass substrata after a 24 hour immersion in the bacterial suspension with initial OD of 0.8, 1.0 and 1.2 containing active cells in the exponential phase. Bacteria were viewed using a light microscope.

Figure 3-12 shows that the number of adhered cells for all three bacterial strains increases with increased cell concentration. A steep increase ($p > 0.05$) was observed in *S. aureus*, where the number of cells increased from $\sim 2900/\text{mm}^2$ at 0.8 to $3400/\text{mm}^2$ at 1.0, which was $\sim 85\%$ higher than the cells at 0.8. Increasing the cell concentration to 1.2 resulted in a 3-fold increase of the bacteria retained on the glass slide ($7500/\text{mm}^2$) as opposed to bacteria at 0.8. The increase of the *Staphylococcus* species can be associated with their greater ability to form micro-colonies due to the high cell concentration. The ‘quorum sensing’, cell to cell communication, was enhanced where the distances between cells were reduced at a high cell concentration, thus promoting the formation of aggregates [149]. The micro-colonies, which presumably had a lower electronegativity compared to the planktonic cells, might reduce the repulsion force with respect to the glass surfaces, subsequently allowing more adhesion on the glass. The number of adherent cells increased with an increase in the cell concentration in the medium, due to its ability to form clusters, thus facilitating the adhesion on the glass surface [150]. Figure 3-12 shows the adhesion behaviour of *S. aureus* on the glass surface with respect to the cell concentration, viewed with light microscopy.

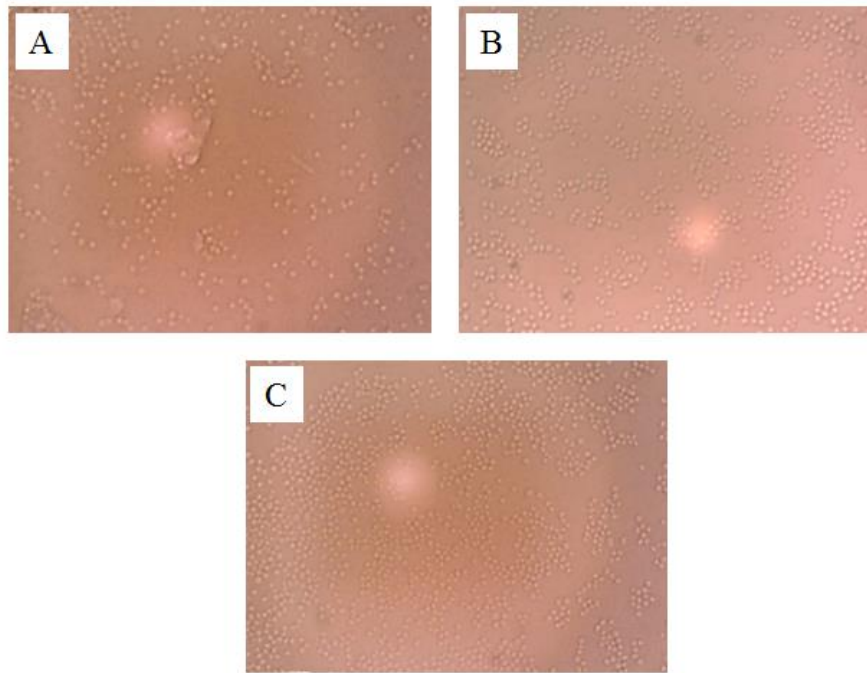


Figure 3-13 The adhered cells after 24 hours exposure to the glass surface at OD a) 0.8, b) 1.0 and c) 1.2. Bigger flocs were formed at higher cell concentration.

The dependence of the degree of adhesion on the cell concentration is not surprising, as an increase in the factor will lead to numerous collisions between the bacteria on the glass surface, hence allowing more chances for attachment. However, the degree of the *E. coli* adhesion with respect to increased bacterial concentration occurred at a much lower percentage compared to *S. aureus*. The number of adhered cells for *E. coli* at 0.8 and 1.0 cell concentrations was reduced by half when compared to *S. aureus*. A further increase of cell concentration to 1.2 marked a greater difference in the number of adhesions between these two species. Conversely, the adhesion of *B. subtilis* on the glass surface shows negligible differences with respect to bacteria concentration and was the least adhered at all tested levels. Unlike *S. aureus*, the adhesion of *B. subtilis* and *E. coli* at higher cell concentrations does not provide any evidence of augmented cell clustering. Figure 3-14 shows *E. coli* and *B. subtilis* with contact on the glass surface for 24 hours at an initial cell concentration of 1.2.

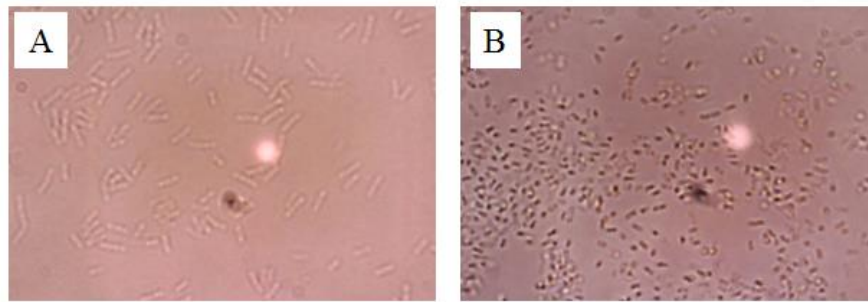


Figure 3-14 : *E. coli* (A) and *B. subtilis* (B) with contact on the glass surface for 24 hours at initial cell concentration of 1.2.

3.4.3 Effect of Culture Age on the Percentage of Adhesion

Experiments were carried out to test the capability of the old/dead bacteria to adhere to the glass surface. Since the bacteria in the death phase underwent a shift in their physicochemical properties, the adhesion to the glass surface is also affected accordingly. The adhesive capacity of the cells in the exponential and stationary phases was studied within 24 hours of exposure to the glass surfaces using cells at $t = 10$ hours and $t = 66$ hours to represent the exponential active phase and the stationary cells (old), respectively. Previously, the characterisation analysis in section 3.1 revealed that the properties of the bacteria were affected as the bacterial cells moved from the active phase to the stationary phase, i.e. the hydrophobicity level, the electron donor/acceptor properties and the sizes. Although the percentage difference varies independently with the types of bacteria, current studies have revealed that the adhesion capacities between the species were affected (although not statistically significant) in accordance with the differences in the physicochemical properties, as analysed in the earlier findings.

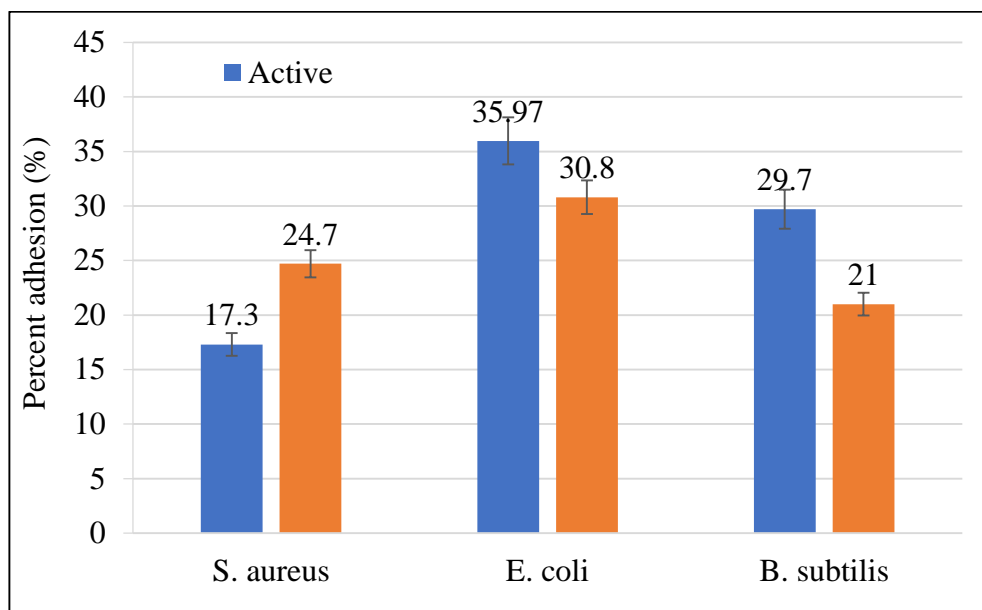


Figure 3-15 Percentage adhesion of, *E. coli* and *B. subtilis* on the glass substrates after 24 hour exposure to the bacteria solution containing active (■) and stationary-phase (■) cells.

Figure 3-15 shows that the adhesion capacity of *S. aureus* in stationary phase increased by 41% compared to the cells in the exponential phase. However, both *E. coli* and *B. subtilis* showed a decrease in adhesion by 14% and 29%, respectively. A greater reduction was observed in the *B. subtilis*, which was in parallel with the increasing hydrophobicity level of the CSH (section 3.3.2) in the stationary-phase cells. It is best noted that the adhesion for the stationary-phase cells also showed the same trend with the previous observation, for the percentage of adhesion (Figure 3-13) and the number of adhered cells (Figure 3-15). Figure 3-15 depicts that the order of adhered stationary phase cells was the highest with *E. coli* accounting for 1374 cells per mm² area. This is followed by *S. aureus*, with 1118 cells/ mm² and the least adhered was *B. subtilis* amounting to only 587/mm². The ability of the bacteria to adhere to the inert surface was not related to the growth rate or the adhesion incubation time [151]. The different levels of bacterial adhesion occurring with changes in the growth rate and phases were probably associated with surface changes and not directly dependent on the physiological activity, particularly since the adhesion did not decrease with the death phase cells. It was observed that the adhesions of *E. coli* and *S. aureus* at both the exponential and stationary state were still higher than the adhesion by *B. subtilis*.

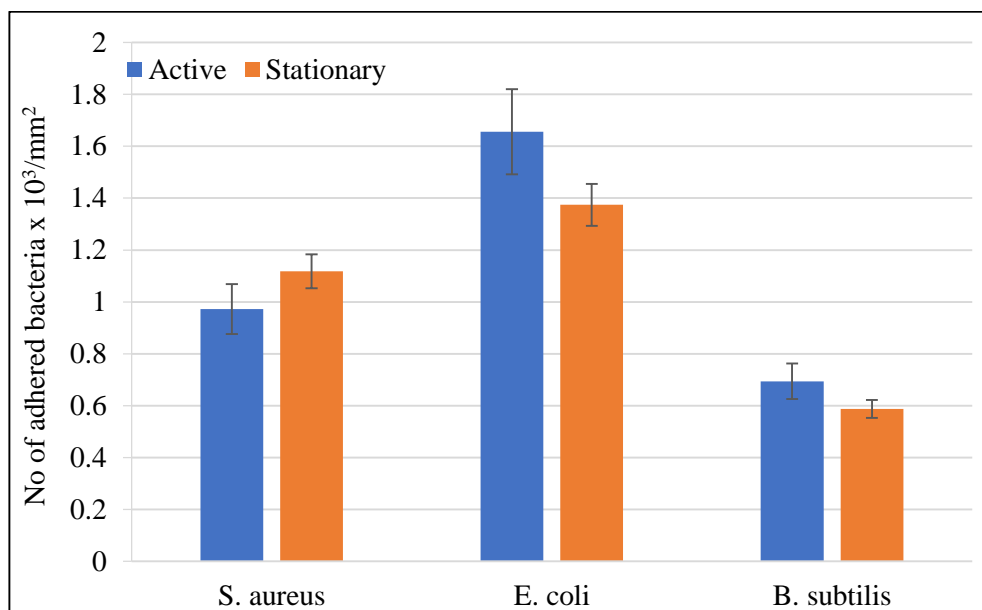


Figure 3-16 Number of adhered cells per mm² area; exponential-phase cells (■) and stationary phase-cells (■) on the glass substrates after 24 hours exposure with bacterial suspension in PBS buffer with initial OD of 1.0 containing cells at $\sim 1 \times 10^8$ /mL.

The growth phase has been shown to influence the surface charge characteristics, the hydrophobicity and the adhesion ability of different species. Similarly, all the previously mentioned properties, i.e. bacterial adhesion, surface at charge, hydrophobicity and extracellular polymer production, were also influenced by the individual growth rate of the bacteria species. It was observed that the stationary-phase *S. aureus* was markedly more adhesive than in the active phase, depicted by the increasing number of adhered cells and the percentage adhesion. The behaviour was partly attributed to the reduction in the hydrophobicity level of the bacteria, thus increasing the rate of adhesion. It is speculated that this situation was also contributed by the non-uniform distribution of the local charge on the outer membrane, resulting in less repulsion force between the cells and the inert surface, which consequently increased the adhesion [120]. In contrast, a more uniform charge distribution with the active cells imposed greater repulsion, thus hindering the adhesion onto the inert surface. Meanwhile, the other strains (*E. coli* and *B. subtilis*) showed a decrease in the adhesion level for the stationary phase-cells, which was in parallel to the reduction of the hydrophilicity of these bacterial strains. A study based on the in vitro adhesion of *S. aureus* on mammalian cells also concluded that the degree of adhesion is provoked by factors such as the growth media, the growth

phase and the types of host, and the localisation is highly influenced by the in-vitro micro-environment [152].

Changes in cell morphology were first observed during the characterisation part of the active and stationary phase cells. Viewing the SEM images, together with a qualitative observation of the adhered cells, also provided a good agreement, which indicates the increased size for the stationary phase cells adhered to the glass surfaces (Figure 3-17). These findings are true for the *E. coli* and *B. subtilis* strains, with an average increase as the cell volume varied between ~30% and ~18%, respectively. The cells in the stationary phase appeared larger, and with greater volume, compared to the adherent cells in the exponential phase. Notably, the reduction in size was observed for the *S. aureus* in the exponential phase, even though the changes were less than 10%. Morphological changes in the adhered cells on the glass slides were also observed under light microscopy. The current findings suggest that the changes in size might well have resulted in an increased/reduced number of adhered cells. Increases in adhered *S. aureus* might be contributed by the increasing strength of adhesion, related to the size reduction. The smaller size increases the contact area between the bacteria and the glass, thus strengthening the adhesion and, consequently, preventing detachment due to the external force exerted by the dynamic environment. Collectively, more cells were retained in the glass over the 24-hour incubation, thus marking an increase in the adhered cells, in comparison with incubation with active cells. Meanwhile, augmented volumes of stationary phase cells of *E. coli* and *B. subtilis* could have prevented cell adhesion, due to an increasing individual cell weight, thus weakening the cell-substrate interaction and promoting cell detachment from the surface.

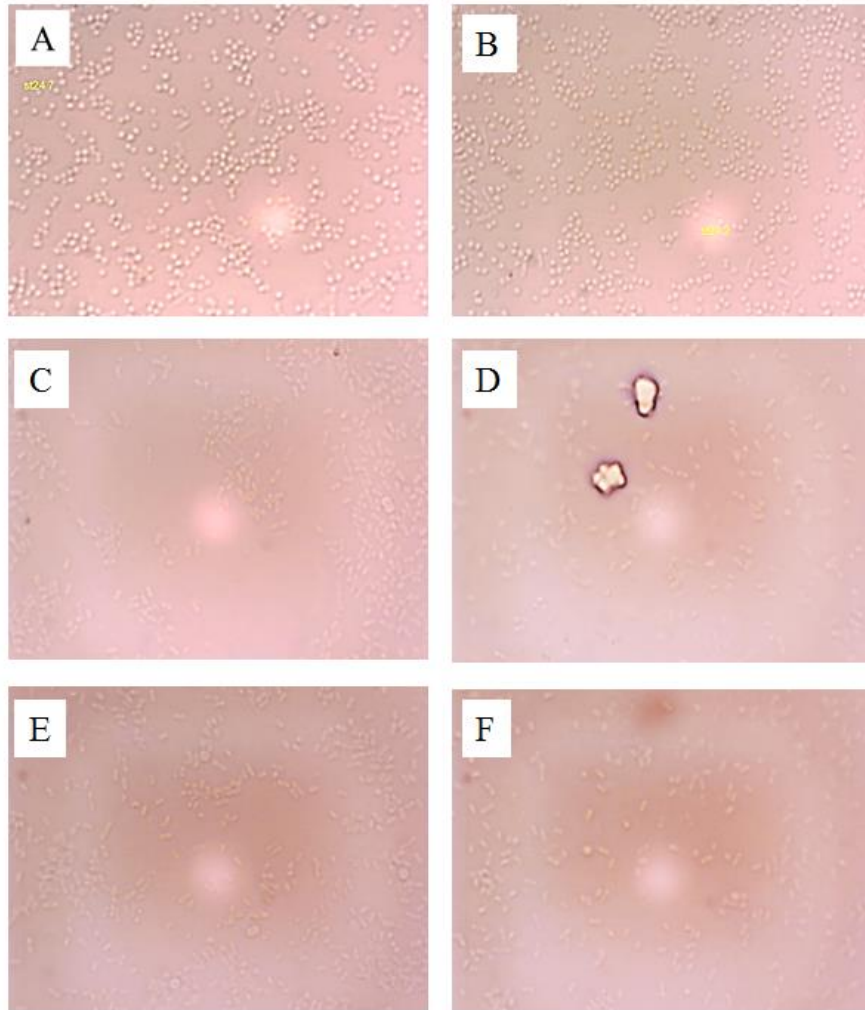


Figure 3-17 Light microscopy images showing adhered exponential phase cells of a) *S. aureus*, b) *E. coli* and c) *B. subtilis*, on glass substrates at 24 hours exposure to bacterial solution (approximately 1×10^8 CFU mL) while (b), (d) and (e) are the adhered stationary phase cells, respectively.

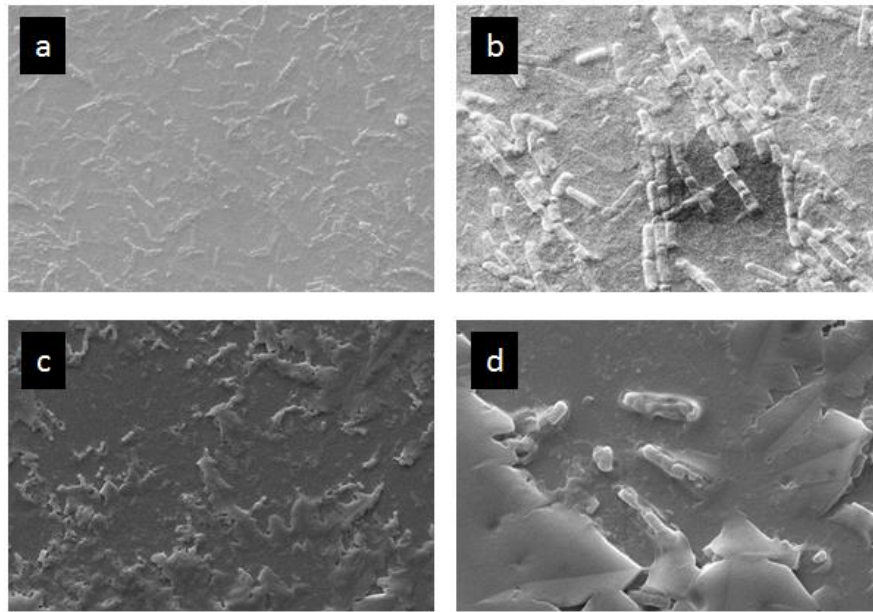


Figure 3-18: Adhered cells (*B. subtilis*) on the glass substrate for cells in the exponential phase (a & b), cells in the stationary phase (c & d).

Various authors have reported varying degrees of adhesion with respect to changes in the bacteria's physical factors. In the current study, it is speculated that the increased adhesion for the stationary phase *S. aureus* correlated with 1) a reduction of sizes, ii) strengthening of the hydrophilic-hydrophilic interaction due to reduced CSH [131], iii) improved electron donor properties [131] iv) increased zeta potentials [153]. Further analysis revealed that the zeta potential of the *S. aureus* increased from $\zeta_{\text{exp}} = -13.1 \text{ mV}$ to $\zeta_{\text{stat}} = -17.2 \text{ mV}$ for cells in the exponential and stationary states, respectively. The increase, which was over 30%, could have contributed to the increased number of adhered cells. A study revealed that *E. coli* strains with the highest negativity were the greatest colonisers on PMMA surfaces compared to strains with lower zeta potentials, and presented the highest initial adhesion rate as well as the highest equilibrium value [153]. This attempts to relate the percent of adhesion with the zeta potential, however, it failed to produce a significant correlation between these properties [154].

When the surface hydrophobicity of a bacterial cell is increased, the charge at the cell surface will be reduced, subsequently diminishing the repulsive forces which normally exist between two negatively charged bodies. This phenomenon will either increase the chances of adhesion or simply strengthen the interaction between the bacteria and the inert surfaces. The increased adhesion observed in the stationary phase *E. coli* was presumably due to the fimbriae adhesions, which are composed of hydrophobic amino acids, and which increase the surface hydrophobicity and reduce the cell-surface charge. Bacterial cell adhesions can be ranked based on their hydrophobicity with recognised pathogenic *Escherichia coli* showing a greater surface hydrophobicity than other non-pathogens.

Increases in cell sizes due to the adhesion phenomenon were also observed due to cell adaptation owing to the augmented roughness of the modified glass surfaces [132]. The bacteria *P. issacchenkonii* appeared bigger on an altered glass surface (high roughness) compared to cells on a smooth glass surface. Analysis with AFM and CSLM revealed that excessive granular EPS production was provoked due to changes in the surface topography, thus increasing the size of the cells by relatively 20-40% in length, width and height. The cell alteration was their sustenance strategy on the rough surfaces. The excess EPS coating could be the means for an extra protection to the outer membrane, preventing it from being ruptured due to the 'brushing' effect of the rougher surfaces. Increased adhesion in the stationary phase growth was also observed in *B. cereus* on stainless steel due to an increased CSH level in the stationary phase cells. Stainless steel possesses a hydrophobic character and attraction towards a similar surface property as the main driving force is highlighted. The present study is also consistent with the general hypothesis; both reduction/increases of adhesion for the stationary phase cells were in parallel to the differences in the CSH level and the attraction law towards hydrophilic surfaces (glass, $\theta = 52^\circ$) [154].

3.5 Chapter Summary

This chapter provided a preliminary understanding of the extent of adhesion in three (3) bacteria with different properties towards inert surfaces (glass). At this stage, the bacterial properties for all the strains were crucially examined to search for the determining single or multiple factors associated with bacterial properties that governed the adhesion, e.g. the CSH level, Gram type, sizes, and surface charge (zeta potential) of the bacteria. These factors were monitored when the adhesion experiments were tested using bacteria at different growth stages. The findings revealed that the bacteria with hydrophobic surfaces (*S. aureus*) are very adhesive in nature, compared to the bacteria with hydrophilic surfaces (*E. coli* and *B. subtilis*) regardless of the Gram type. The adhesion capacity of bacteria onto the glass surface was in parallel with the increasing CSH level, and thus against the theory of the preference of adhesion for hydrophilic-hydrophilic interaction. Apart from this, the adhesion to the glass surfaces (negatively charged) was also contributed by the bacterial surface charge, where lower repulsion was observed in bacteria with a lower zeta potential, thus enhancing the adhesion. The changes in sizes might contribute towards adhesion, where bacteria with a huge volume (bigger in size) were expected to have a lower adhesion strength on the surface, therefore reducing their ability to remain attached at the surface in dynamic environments (hydrodynamic forces).

Chapter 4

Polished Surface Characterisation with respect to Contact Angle Measurement and Bacterial adhesion

4.1 Introduction

The discussion in this chapter is focused on metallic surface characterisation (316L and Ti6Al4V) with respect to contact angle measurement and the number of cell attachment on the modified surface. To investigate the systematic correlation between these three areas (surface characterisation, wettability and cell adhesion), the use of 3D Optical Profilometry (*Bruker*, UK), Drop Shape Analyzer (*Kruss*, Germany) and standard cell-attachment experiments with the right process are essential. The main objectives of producing a metallic polished specimen with sub-micron roughness (0.10 μm to 0.20 μm) were to assess the behaviour of the cells towards micro-size roughness and the hydrophobicity of the surfaces. On surface characterisation, three groups of measurement were used in the data analysis. These were height, spatial and hybrid parameters. Normally, height parameters are used to construct the relationship between hydrophobicity surfaces. However, trusting those values only is not enough; therefore, an extension to analyse spatial and hybrid parameters is essential. Consequently, there are ten parameters that will be used for the whole thesis from the three groups of measurements. For wettability phenomena, a distilled water sessile drop was used to measure the contact angle of water. And lastly, for cell-adhesion, *S. aureus*, *E. coli* and *B. subtilis* were used as the test objects for bacterial adhesion experiment due to their Gram-type and shape as discussed in Chapter 4.

4.2 Polished Surface Characterisation

Using the polish method, smooth surfaces on 316L stainless-steel and Ti6Al4V titanium were produced by using polishing grit paper with sizes of 240, 320, 800 and 1200. The expected roughness of the modified metal specimens was between 0.10 to 0.20 μm on S_a . These ranges of roughness are important to be used in conjunction with the sizes of bacteria for the whole discussion in the thesis, from as small as 0.75 μm (*S. aureus*) to a maximum of 2.11 μm for *B. subtilis* as further discussed in section 3.3.1.

4.2.1 Polished Surface Height Characterisation

From the height parameter data as shown in Figure 4-2 (A - C), the average data reduction was high compared as-received and the modified specimens were labelled as SSP-01, SSP-02, SSP-3 and SSP-04. The average roughness reduction happens between 96.6% to 97.8% where SSP-01 with grit 240 shows the highest reduction of 0.17 μm and SSP-04 shows the lowest roughness with 0.11 μm . Another two specimens, SSP-02 and SSP-03 had the values of 0.16 μm and 0.15 μm respectively. A drastic reduction can be seen between SSP-03 and SSP-04, from 0.15 to 0.11 μm while the decrease from SSP-01 to SSP-02 was small with a 0.01 μm difference. It was an indication that the higher the polished grit, the lower the S_a of the metallic surfaces. As for 316L, the hard metal properties contributed to small changes of S_a compared to polishing grit. As in 316L, the Ti6Al4V polished specimens showed the same pattern of S_a reduction. With the percentage of reduction between 98.3 to 99%, the values of S_a for Ti6Al4V were 0.17 μm , 0.14 μm , 0.11 μm and 0.10 μm for TIP-01, TIP-02, TIP-03 and TIP-04 respectively. In contrast with 316L, the Ti6AL4V S_a reduction showed a difference of 0.03 μm from grit 240 to 320. This drastic reduction is due to their differences in terms of mechanical properties and composition plus the ability to respond to the grinding process.

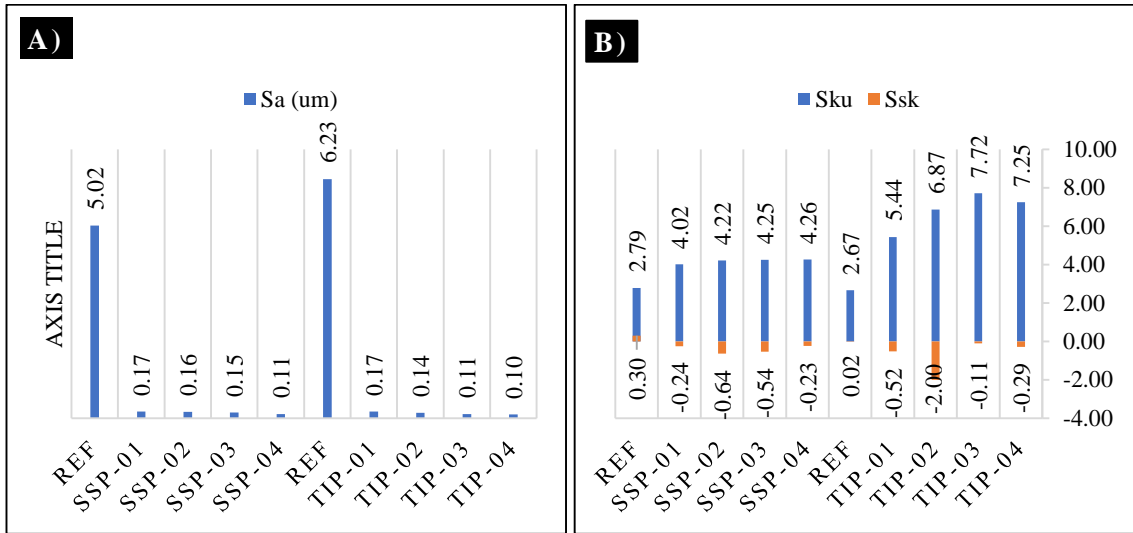


Figure 4-1 Graph of the height parameters on 316L and Ti6Al4V with respect to A) S_a and S_q , B) S_{ku} and S_{sk}

Despite the S_a values, surface kurtosis is used to describe the distribution peaks on the modified surfaces for both metallic polished specimens. From the graph in Figure 4-2 B), S_{ku} increased gradually from grit 240 to 1200 for both specimens with values greater than 3. Ti6Al4V shows a higher S_{ku} compared to 316L which results in more peaks with different sizes on titanium compared to stainless-steel. Again, the hardness of the 316L specimen made it difficult to polish and resulted in a regular size and pattern of surface peaks. Further statistical data on structure distribution was demonstrated by the value of skewness, S_{sk} as the degree of symmetry between peaks and valleys on the surfaces. Figure 4-2 B) shows the measured values of S_{sk} where all modified specimens reveal negative skewed surfaces which translate to more deep valleys for the modified surfaces compared to as-received substrates as shown in Figure 4-3 [155].

Therefore, in summary, the height parameter topography of modified 316L and Ti6Al4V shows the reduction of S_a is inversely proportional with polish grit size 240, 320, 800 and 1200. The larger the polish grit the lower the S_a values. On the other hand, surface kurtosis is proportional with polish grit where a higher polish grit resulted in the gradual increase of S_{ku} for both metallic specimens.

The main aim of the study was to establish the correlation between surface topography with contact angle and cell-adhesions. The interaction of water droplets on the surface and the attraction of cells start with the structure of the inert surfaces. Therefore, it is essential to identify the profile of the surface especially the length of peaks (Sp), valleys (Sv) and the overall height length of the surfaces (Sz). These important values determine the measured value of contact angle as well the degree of cell-attachment especially when dealing with the number of deep valleys. This is because the high number or deep length of the valleys makes it possible to entrap the cells inside the holes resulting in the formation of a biofilm/colony. In contrast, more peaks influence the hydrophobicity of the surfaces and influence the attachment of the cells by reducing the contact points. Therefore, the information concerning Sp , Sv and Sz were essential to be used in the discussion of contact angle (CA) and cell-adhesion correlation with surface topography.

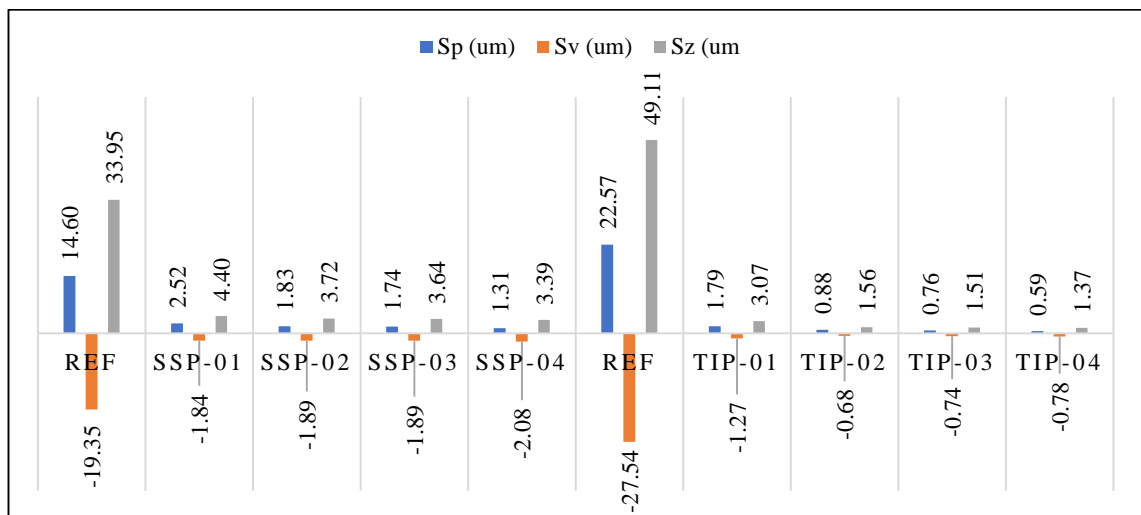


Figure 4-2 Graph of the height parameters on 316L and Ti6Al4V with respect to height surfaces parameter, Sp (max peak height), Sv (max valley depth) and Sz (max height of surface)

Figure 4-2 demonstrates height surface values where for the peaks on the surfaces, Sp values were 2.52 μm , 1.83 μm , 1.74 μm and 1.31 μm for SSP-01, SSP-02, SSP-03 and SSP-04 respectively and 1.79 μm , 0.88 μm , 0.76 μm and 0.59 μm for TIP-01, TIP-02, TIP-03 and TIP-04 respectively. Overall, Ti6Al4V has lower Sp compared with 316L. The variations between high and low peaks was 1.21 μm for 316L and 1.17 μm for Ti6Al4V. As for the distribution of valleys in both metals, Sv values were -1.84 μm , -1.89

μm , $-1.89 \mu\text{m}$ and $-2.08 \mu\text{m}$ for 316L and -1.27μ , -0.68μ , $-0.74 \mu\text{m}$ and $-0.78 \mu\text{m}$ for Ti6Al4V. The variations were not too much different in S_p as reflected in the discussion of the skewness parameter in the previous paragraph (-ve skewed plane). Finally, for the overall length between S_p and S_v , the maximum height of surfaces, S_z for both metals shows the values of $4.40 \mu\text{m}$, $3.72 \mu\text{m}$, $3.64 \mu\text{m}$ and $3.39 \mu\text{m}$ for 316L and $3.07 \mu\text{m}$, $1.56 \mu\text{m}$ $1.51 \mu\text{m}$ and $1.37 \mu\text{m}$ for Ti6Al4V respectively. By comparing between these metals, Ti6Al4V shows a high variation of S_z ($1.01 \mu\text{m}$) compared to 316L with the highest S_z of $4.40 \mu\text{m}$ and the lowest of $3.39 \mu\text{m}$. while for Ti6Al4V, the variation of S_z was $1.7 \mu\text{m}$.

Therefore, in summary of height of surfaces values, both metals show relatively low values of S_p , S_v and S_z with respect to as-received substrates. However, with the negative skewed surfaces, it is expected to demonstrate that both metals produced kurtosis and skewness values which are in the region of negative skew with deep valley kurtosis. For the same S_a , ($0.17 \mu\text{m}$) between both metals, titanium produced more smooth surfaces compared to stainless-steel as shown by the Bruker images in Figure 4-3.

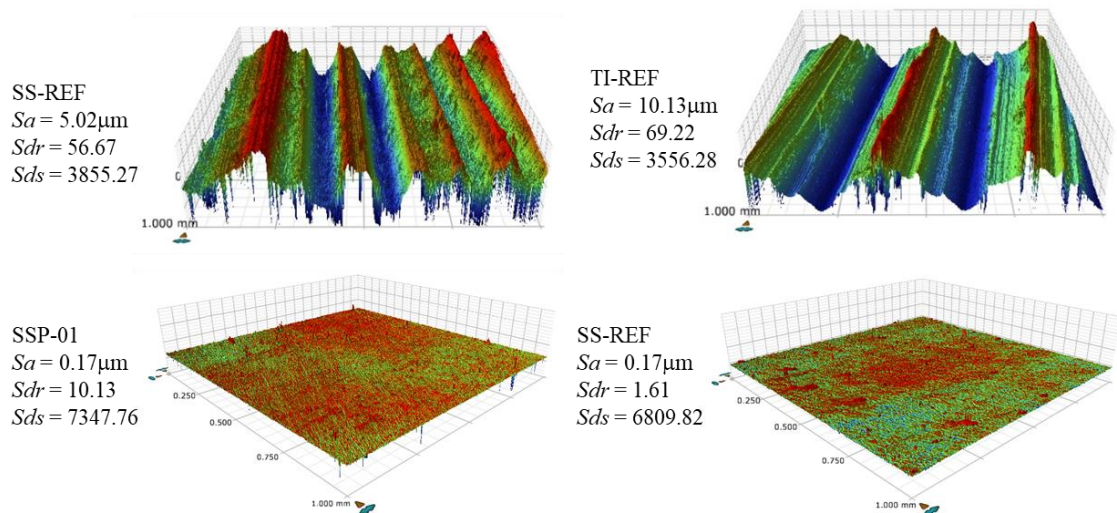


Figure 4-3 Bruker images of polished stainless-steel and titanium

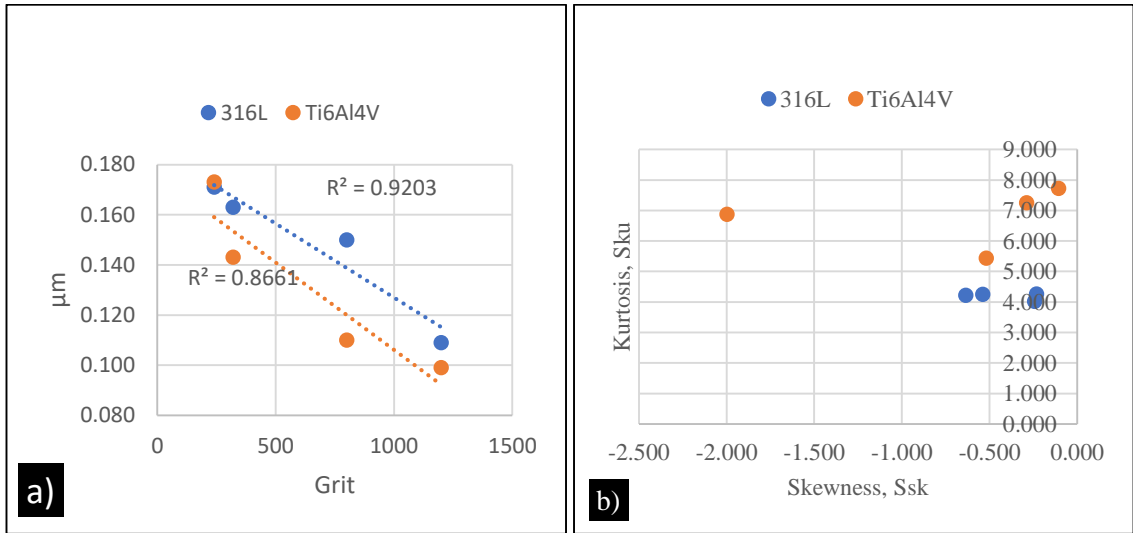


Figure 4-4 Correlations between graph A) Sa and polished grit and B) kurtosis (Sk_u) and skewness (Ssk). $R^2 > 0.7$ indicated strong correlation, $R^2 = 0.5 - 0.69$ represented moderate correlation and $R^2 = 0.49 - 0.3$ poorly correlated and $R^2 < 0.29$ provided no correlation.

To establish the correlation between polished grit and average roughness, Sa , the measured values of Sa and polished grit were plotted as shown in Figure 4-4. It is clear from the graph that both metals showed a negative strong correlation between polished grit and water contact angles, with R^2 equal to 0.9203 and 0.8661 for stainless-steel and titanium respectively. The strong correlation is derived from the material and mechanical properties of both metals. 316L stainless steel is known as a hard metal that tends to harden if machined too quickly. Grinding with 18 LBS/N – 30 LBS/N at 20–60 rpm, resulted in gradually reduced Sa values. For Ti6Al4V titanium in general, the metal is a little soft compared to 316L, and removing parts is higher and make the grinding process more difficult. On the other hand, titanium is a soft metal where is easier to remove the metal when it changes from grit 240 to grit 320 with 0.03 μm as discussed in the above paragraph. With grinding technique, both metals produced deep valley surfaces where the kurtosis values were greater than 3.00 ($Sk_u > 3$) and skewness values were negative as shown in Figure 4-4 (B). The grinding process removed the peaks of the as-received substrates and flattened the surfaces, and the deep valleys that remained caused the surface to be more hydrophilic.

4.2.2 Spatial and Hybrid Parameter Analysis

Surface height parameters alone do not represent enough dimensional features. Therefore, further analysis under the spatial family parameters will provide some extra information on the spacing and wavelength of the surface which will represent the properties of all wavelengths, or spatial size of the feature; also known as a surface texture descriptor. From this analysis, the auto-correlation function will determine and reflect on the overall texture of the surface, whether isotropic or anisotropic [156]. From Table 4-1, a lower value of *Sal* means a lower ACF distance from the surfaces. Both polished metals have a low *Sal* where SSP-01 on stainless-steel has a value of 5.78 μm . For titanium, the distance is much longer with SSP-01 producing 10.58 μm . The *Sal* values show a lower distance of ACF. Texture direction, *Std*, shows the existence of small-angle ranges from 1.71 to 6.38 for stainless-steel and 0.42 to 1.90 for titanium. These values indicated that the surfaces had a small surface direction where the stainless-steel shows a higher degree compared to titanium. To strengthen the data, with the help of texture aspect ratio, *Str*, both specimens show a value which tends to approach 0, which indicates the surface has a dominant lay because *Str* is approaching 0. For polished specimens, dominant lay the surface with low values were expected due to the direction of the grinding machine. Overall, with the ACF diagrams demonstrated in Figure 4-6 and Figure 4-7, all specimens show an identical shape of ACF, which means the texture was similar in the direction of ACF and has a correlation.

Table 4-1 Spatial and Hybrid Parameter Data on Polished Metallic Specimen

Specimen	Spatial Parameter			Hybrid Parameter			
	<i>Sal</i> (μm)	<i>Std</i> (deg)	<i>Str</i>	<i>Sa</i> (μm)	<i>Sdr</i> (%)	<i>Sds</i>	
316L	REF	48.25	87.18	0.06	5.02	70.06	3050.75
	SSP-01	3.78	1.98	0.43	0.17	10.13	7347.76
	SSP-02	2.62	1.88	0.40	0.16	8.05	7044.39
	SSP-03	1.96	1.75	0.35	0.15	12.37	6954.23
	SSP-04	1.68	1.71	0.36	0.10	4.29	6765.32
Ti6Al4V	REF	81.62	81.23	0.10	6.23	119.91	3146.75
	TIP-01	10.58	1.90	0.35	0.17	1.61	6809.82
	TIP-02	7.36	0.52	0.37	0.14	3.65	6695.45
	TIP-03	5.56	0.71	0.35	0.11	2.97	6531.13
	TIP-04	3.31	0.56	0.39	0.10	3.45	6313.32

For the hybrid measurement of the metallic specimen (Sdr , Sds), the modified 316L with low Sa and indicating a low Sdr associated with as-received substrates had a finer spaced texture while the REF substrates have a wider SPACED texture as shown in Figure 4-5. The Sdr for modified stainless-steel is lower compared to as-received substrates (REF). Thus, a higher Sa in as-received substrates with a wider spaced texture, have a lower Sdr value than a lower Sa but finer spaced texture, as displayed above due to the polishing process that produced finer surfaces and even peak structures. For the summit density, both metals show higher Sds values with respect to low Sa . It is because Sds which is derived from the peaks has a higher number in polished specimens due to the compressed fine surface removed by grit paper during the process. Both hybrid parameters agreed with the theoretical definition of the parameters.

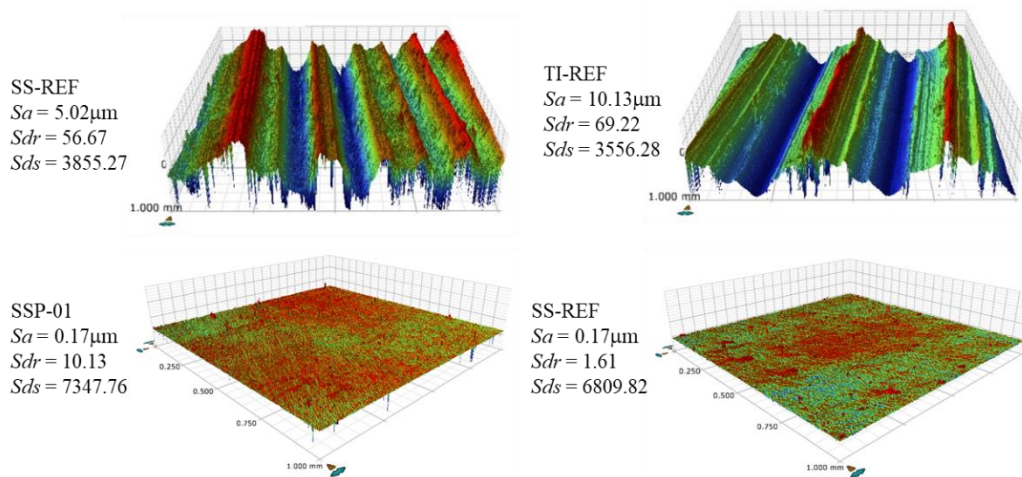


Figure 4-5 3D optical profilometry images with spatial parameter data

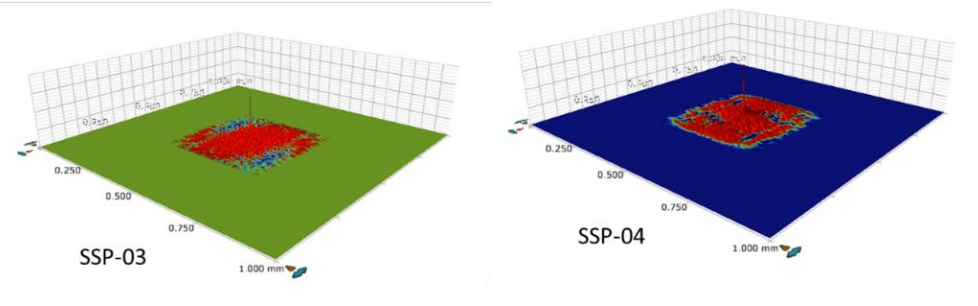
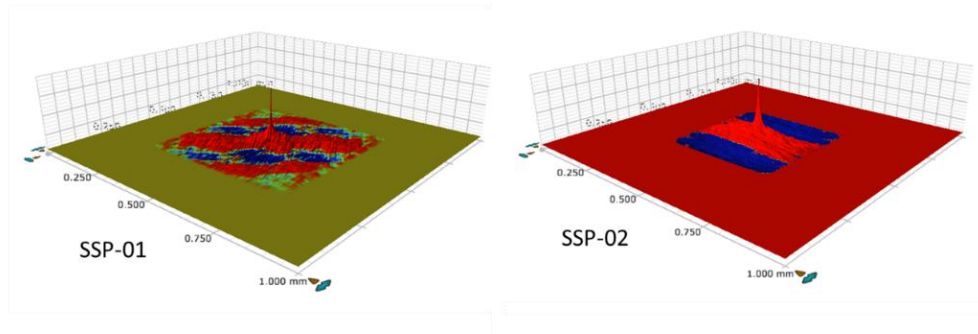


Figure 4-6 Auto-correlation on polished stainless-steel specimen

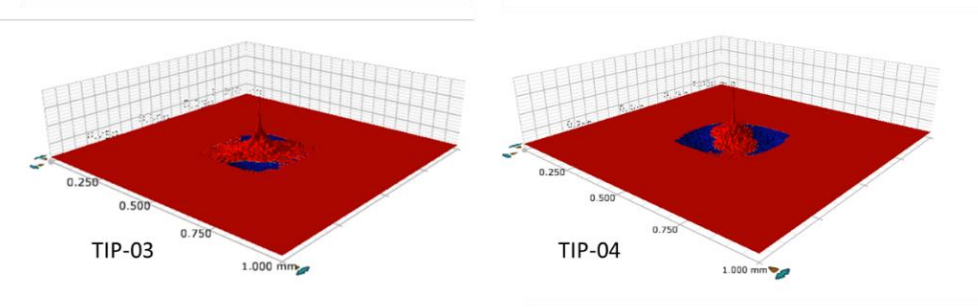
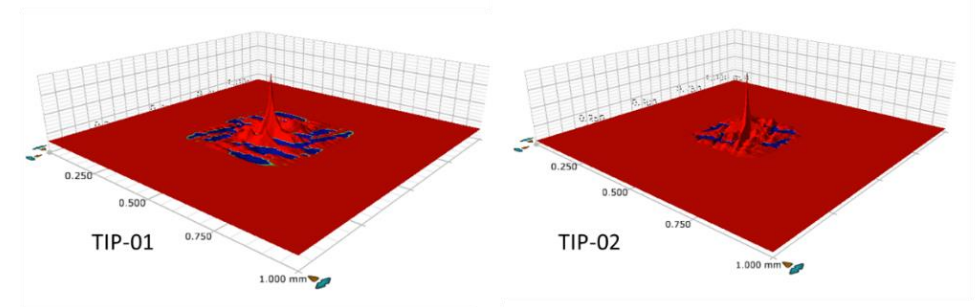


Figure 4-7 Auto-correlation on polished titanium specimen

4.3 The Correlation between Contact Angles and Surface Roughness

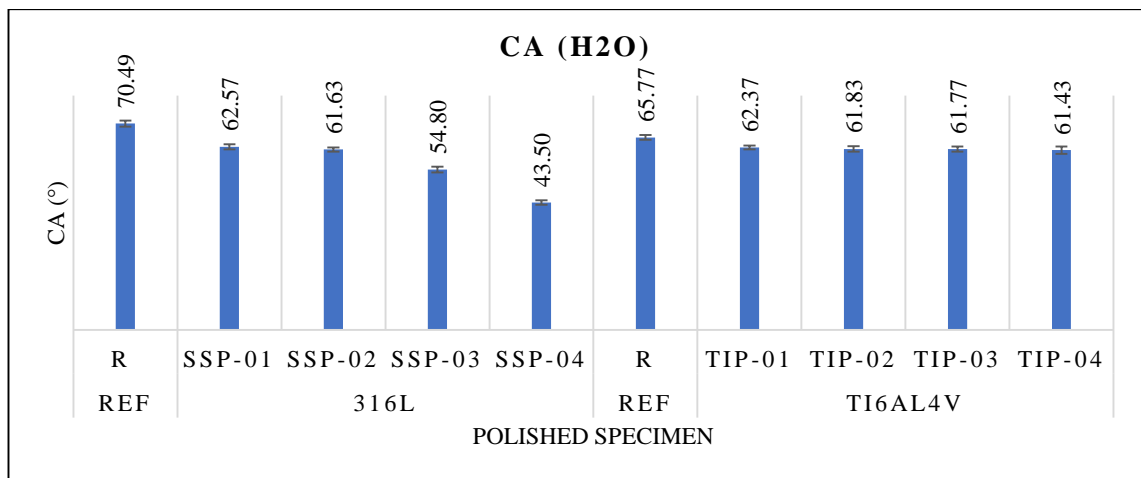


Figure 4-8 Graph of contact angle measurement on metallic polished specimen

From the overall data on metallic polished specimens, the surface profile shows the Sa with sub-micro roughness, negative skew, short distance of Sal , and higher value of Sds compared to as-received substrates (REF). In summary, metallic polished specimens (316L and Ti6Al4V) exhibit flat surfaces with negative skew and high summit density. Figure 4-8 shows the CA measurement with the values of 62.57°, 61.63°, 54.80°, and 43.50° for 316L and 62.37°, 61.83°, 61.77° and 61.43° for titanium where all specimens demonstrate low contact. All CA measured for polished specimens were hydrophilic, as any surface with $CA < 70^\circ$ are considered hydrophilic [39]. The difference between higher and lower CA measurements for 316L was 19.07° while for Ti6Al4V it was 0.94°. 316L shows the wider range of CA measurement, which means the structure was not affected much by polished grit from 240 to 1200 while for Ti6Al4V, titanium remains with a narrow variation as discussed in section 4.2.1. The Sa variation for 316L was 0.03 μ m and 0.01 μ m for Ti6AL4V. Wider roughness variations contribute significantly to the measurement of CA regardless of the type of material. For the kurtosis relationship with CA, the higher the kurtosis, the higher the CA measurement and a low Sku produces a low CA measurement. This is in contrast with surface skewness, where there is no significant relationship between Ssk values with the CA measurement for both metallic specimens. To quantify the relation for all parameters,

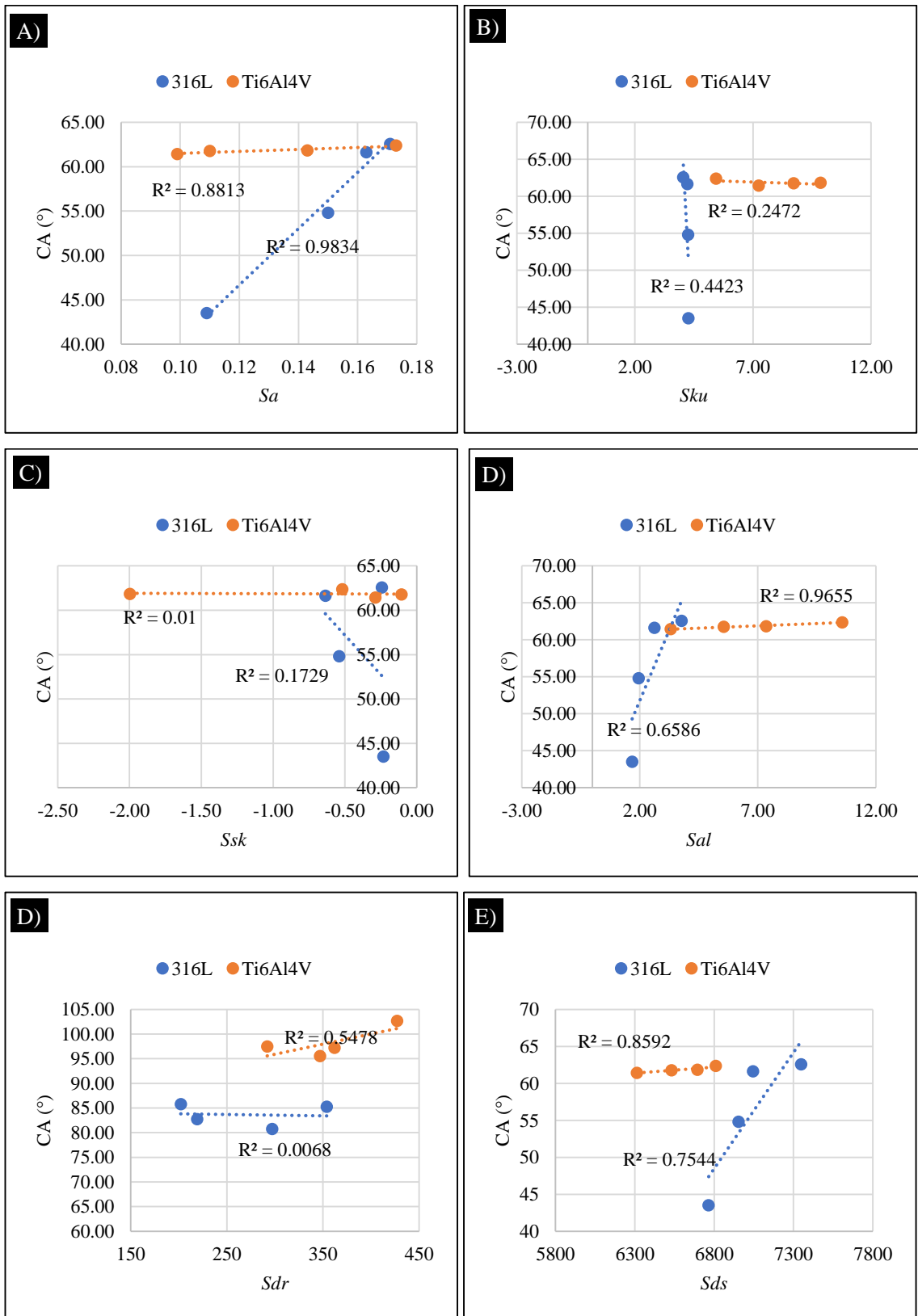


Figure 4-9 Correlation between a), average roughness, Sa b) kurtosis, Sku c) skewness, Ssk d) auto-correlation length, Sal e) developed interfacial area ratio, Sdr h) summit density, Sds with water contact angle on 316L and Ti6Al4V specimen.

The effects of surface properties on CA with respect to metallic polished fabrication were presented in Figure 4-9 [A) – E)]. The CA were plotted against Sa , Sku , Ssk , Sal , Sdr and Sds and a linear regression was plotted with R^2 values to indicate the accuracy of the correlation. R^2 values between 0.7–1.0 represented a strong correlation, $R^2 = 0.50–0.69$ for moderate, $R^2 = 0.3–0.49$ for poor and $R^2 < 0.29$ means no correlation was observed in the responses. Variations in responses with correlation between 0.01 to 0.9834 was observed towards contact angle values. A correlation of contact angle with Sa , Sku and Ssk [Figure 4-9 A), B) and C)] were carried out to identify any strong influence by surface profiles within the test ranges over $43.50^\circ–62.57^\circ$. 316L polished specimen provided the strongest correlation with R^2 of 0.9834, indicating the high influence of polished grit towards hydrophobicity. Sku shows a moderate correlation for 316L with R^2 of 0.4423 and no correlation for titanium with R^2 of 0.2472. The higher the Sku for titanium, the lower the correlation with CA measurements. Ssk showed the least influence on CA measurement where both metallic polished specimens show no correlation with R^2 below 0.01.

On the spatial and hybrid parameters, Sal , Sdr and Sds , the variations in responses occur with the regression (R^2) values between 0.0068 (no correlation) up to 0.9655 (strong correlation). The Ti6Al4V specimen showed a strong correlation with CA measurement on Sal and Sds with R^2 equal to 0.9655 and 0.8592 respectively and a moderate correlation on Sdr with R^2 equal to 0.5478. In contrast, the 316L specimen showed a strong correlation on Sds with R^2 equal to 0.7544, a moderate correlation on Sal with R^2 equal to 0.6586 and no correlation on the Sdr parameter. Therefore, surface texture indicates substantial influences towards surface wettability especially with the Sds parameters which showed strong correlations for both metallic polished specimens.

4.4 Bacteria-Surface Adhesion

Four different surfaces were produced for each metal that underwent the polishing technique using grit paper ranging from 240–1200, where the post-modification properties varied from those of received substrates. In the adhesion study, samples were cleaned and sterilised before being exposed to the bacterial suspension containing approximately 1×10^8 CFU/ mL of cells in the mid exponential phase for four (4) hours using three types of bacteria as in Chapter 4. The bacteria can be divided into Gram-positive bacteria (*S. aureus* and *B. subtilis*) and Gram-negative (*E. coli*) with varying properties i.e. coccus shape for *S. aureus* and rod-shaped for *B. subtilis* and *E. coli*. In this section, discussions about the bacteria adhesion measurement were carried out using fluorescent microscopy procedure as mentioned in Chapter 3. The effects of an altered surface topography including *Sa*, *Sds*, *Sku*, *Ssk* and wettability were discussed individually while observing the correlations between changing these parameters and their effects on the adhesion intensity. Table 4-3 shows the data from the surface topography parameter, water contact angle and the number of bacteria adhered to the specimens. It shows the range of measurement for both polished stainless steel and titanium specimens with height, spatial and hybrid surface parameters, contact angle of water against the number of bacteria counted on per-mm² areas. The effectiveness of the process was compared against the adhesion on the control specimens. The control specimens used was similar metal that have undergone fine polishing until a mirror finish surface was achieved, denoted by SSC for stainless steel and TIC for the titanium.

Table 4-2 Size of bacteria at the exponential stage

Properties	<i>S. aureus</i>	<i>E. coli</i>	<i>B. subtilis</i>
Gram Type	+	-	+
Shape	Coccus	Rod	Rod
Size (mm)	0.6-0.7	1.2-1.8 (L) 0.45 – 05 (D)	2 -2.5 (L) 0.5-0.75 (D)
CSH (%)	~42	~25	~12
Characteristic	Hydrophobic	Moderately hydrophilic	Hydrophilic

4.5 Bacterial Adhesion on Control sample

Control experiments were performed to be the standard for comparing the effectiveness of modified surfaces in repelling adhesion. The number of adhered bacteria retained by the SSC and TIC is presented by Figure 4-10. Comparable to adhesion on the glass surface, *S. aureus* (Gram-positive and hydrophobic bacteria) performed as the greatest coloniser depicted by the highest number of cells adhered on SSC and TIC, with $\sim 158 \times 10^3/\text{mm}^2$ and $82.6 \times 10^3/\text{mm}^2$, respectively. This was followed by *B. subtilis*, which is also Gram-positive but has a hydrophilic membrane, with $50.8 \times 10^3/\text{mm}^2$ and $45.8 \times 10^3/\text{mm}^2$ on SSC and TIC, respectively. In this study, the TIC showed a greater antibacterial effect, depicted by a lower bacterial retention for all three species. A greater repulsion was obtained for the *S. aureus*, as shown by the nearly $\sim 50\%$ reduction, while only less than 10% reduction was observed for *E. coli* and *B. subtilis*. Unlike the adhesion on glass, *E. coli* when exposed to metallic surfaces showed the lowest adhesion comparative to *S. aureus* and *B. subtilis*. This was not expected since the CSH level of *E. coli* was higher than *B. subtilis*, hence it was predicted to be the second greatest coloniser after *S. aureus*. Only $14.5 \times 10^3/\text{mm}^2$ and $13.5 \times 10^3/\text{mm}^2$ of *E. coli* was retained on the SSP and TIP after 4 hours exposure, respectively.

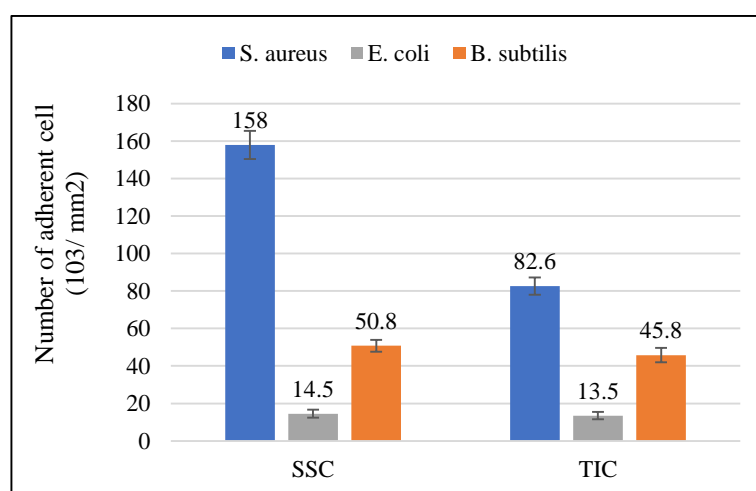


Figure 4-10 Number of bacterial adhered on stainless steel and titanium undergone surface polishing technique (mirror finishing) after four hours at 37°C and $\text{CFU} \sim 1 \times 10^8 \text{ CFU/mL}$.

Table 4-3 Data on Surface Topography Parameter, Contact Angle and Bacterial Adhesion

Specimen	Surface Topography Parameter					Contact Angle Measurement	Bacterial Adhesion/mm ²		
	<i>Sa</i> (μm)	<i>Sku</i>	<i>Ssk</i>	<i>Str</i>	<i>Sds</i>	CAM	<i>S. aureus</i>	<i>E. coli</i>	<i>B. subtilis</i>
SSP-01	0.17	4.02	-0.24	0.50	7347.76	62.57 ± 0.46	53800 ± 1000	31300 ± 2000	38600 ± 300
SSP-02	0.16	4.22	-0.64	0.20	7044.39	61.63 ± 0.50	65900 ± 2000	42500 ± 3700	61100 ± 4000
SSP-03	0.15	4.25	-0.54	0.35	6923.45	54.80 ± 0.54	30500 ± 1000	17600 ± 1100	15100 ± 1000
SSP-04	0.11	4.26	-0.23	0.38	6865.32	43.50 ± 0.11	62400 ± 1200	29200 ± 1000	26300 ± 1000
TIP-01	0.17	5.44	-0.52	0.35	7354.02	62.37 ± 0.31	69600 ± 1000	74400 ± 1000	50100 ± 1000
TIP-02	0.14	6.87	-2.00	0.40	7161.68	61.83 ± 0.65	37800 ± 2000	18700 ± 2000	38200 ± 1000
TIP-03	0.11	7.72	-0.11	0.36	7016.53	61.77 ± 0.32	55200 ± 2000	40600 ± 2000	48500 ± 2000
TIP-04	0.10	7.25	-0.29	0.40	6790.66	61.43 ± 0.85	54400 ± 2000	23800 ± 2000	29200 ± 1000

4.6 Bacterial Adhesion on Polished Stainless-Steel

All stainless-steel surfaces that have undergone polishing and exhibited hydrophilic character were exposed to *S. aureus*, *E. coli* and *B. subtilis* for four hours and the number of attached cells were recorded in Figure 4-11. It shows *S. aureus* (Gram-positive, hydrophobic) as being a greater coloniser compared to its counterparts *E. coli* (Gram-negative, hydrophilic) except for SSP-04. It was clearly observed that *S. aureus* were attracted to the polished stainless-steel, indicating a ~30% difference compared to *E. coli* and *B. subtilis*. After four hours of exposure, SSP-01, SSP-02 and SSP-04 allowed an adhesion of *S. aureus* between $53.8 \times 10^3/\text{mm}^2$ to $65.9 \times 10^3/\text{mm}^2$, while the highest repellence was attained by SSP-03 with only $30.5 \times 10^3/\text{mm}^2$ cells attached onto the surface. All SSP surfaces managed to reduce *S. aureus* adhesion by > 50% as opposed to SSC.

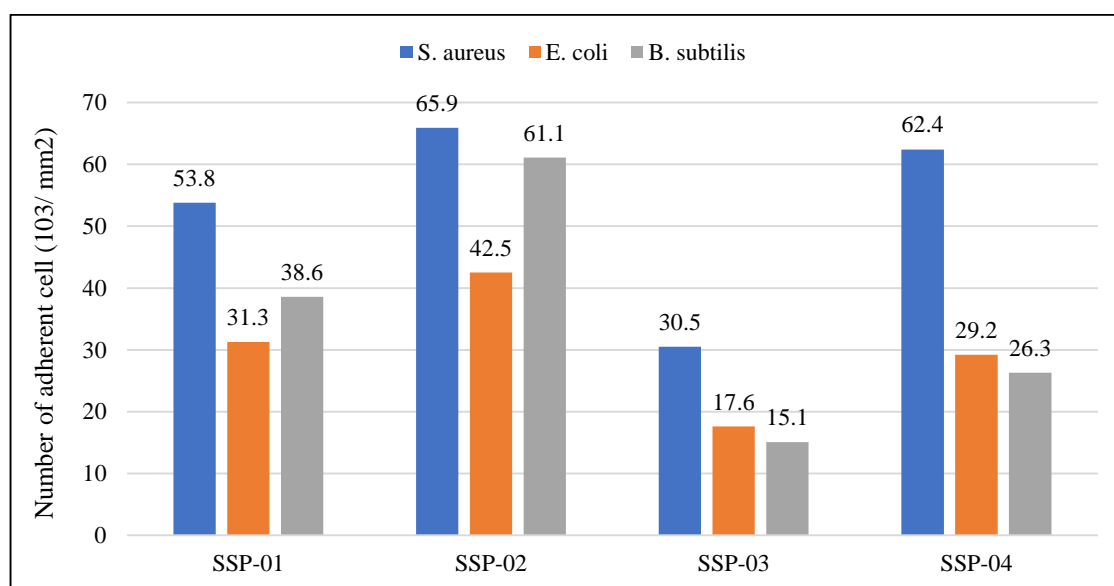


Figure 4-11 Graph of bacterial adhesion on the polished-stainless steel

When comparing the adhesion of the three tested bacteria, *E. coli* exhibited the lowest surface coverage, depicted by a cell count of between $17.6 \times 10^3/\text{mm}^2$ – $42.5 \times 10^3/\text{mm}^2$. The lowest repellence against *E. coli* was attained by surface SSP-03 ($17.6 \times 10^3/\text{mm}^2$), the highest adhesion was attained by SSP-02 with adhesion of $42.5 \times 10^3/\text{mm}^2$. Although the colonisation rate was the lowest, the SSP surfaces increased the attachment of *E. coli* 1.2–3 times compared to SSC. Ortega et al (2010) reported that *E. coli* was a slow coloniser, taking between 3-4 hours to establish a bacteria-surface interaction. The present study similarly showed that *E. coli* was a slower coloniser compared to *S. aureus*, taking 12 hours to reach a plateau of surface density, while other bacteria took 8 hours. This suggested that *E. coli* might require a longer time to establish the adhesion before irreversible attachment was secured. The ability of *S. aureus* and *B. subtilis* to stabilise themselves on the surface within seconds to minutes upon contact, explained the higher numbers of cells retained on the surface. Meanwhile *E. coli* adhesion remained the lowest, with only a slight competition with *B. subtilis* observed on SSP-03 and SSP-04.

B. subtilis (Gram-positive) which is the most hydrophilic strain in this study, was the second highest coloniser as depicted by the total numbers of adherent bacteria on SSP and TIP (Table 4-4). It is widely known that Gram-positive bacteria are better colonisers than Gram-negative SP, later discriminated based on the hydrophobic/hydrophilic CSH. The study once again proved the ability of colonising SSE surfaces, in decreasing order are as follows, *S. aureus* (Gram-positive and hydrophobic) > *B. subtilis* (Gram-positive and hydrophilic) > *E. coli* (Gram-negative and hydrophilic). Comparing with the adhesion on SSC, all SSP samples managed to scrap adhered *B. subtilis* by 60-72% relative to those on control. Overall, the current observation shows that SSP-03 prevented the anchoring of cells, with the lowest adhesion for all bacteria species occurring at 30.5×10^3 , 17.6×10^3 and 15.1×10^3 for *S. aureus*, *E. coli* and *B. subtilis*.

4.7 Bacterial Adhesion on Polished Titanium

Similar to those of SSP, TIP surfaces that have undergone similar polishing were exposed to *S. aureus*, *E. coli* and *B. subtilis* for four hours and the number of adhered cells are presented in Figure 4-12. The adherence of *S. aureus* on TIC ($82.6 \times 10^3/\text{mm}^2$) samples was reduced on all titanium surfaces, with the highest repellence ability shown by TIP-02 contributing with a figure of only $37.8 \times 10^3/\text{mm}^2$. In contrast to *S. aureus*, the adhesion of *E. coli* was promoted (relative to TIC), where the maximum adhering bacteria increased 6-fold (TIP-01). TIP-01 displayed the highest *E. coli* density, while the lowest adhesion was observed on TIP-04 ($18.7 \times 10^3/\text{mm}^2$), a ~40% increase relative to TIC. The increase in the number of *E. coli* on individual titanium surfaces surpassed those on the SS polished with the same grit number, suggesting the effect of affinity towards certain materials. Meanwhile, the lowest adhesion for *B. subtilis* occurred on TIP-04, presenting approximately $29.2 \times 10^3/\text{mm}^2$. Overall, the current observation shows that TIP-04 prevented the anchoring of rod-shaped cells, while TIP-02 was effective for the removal of coccus shape bacteria.

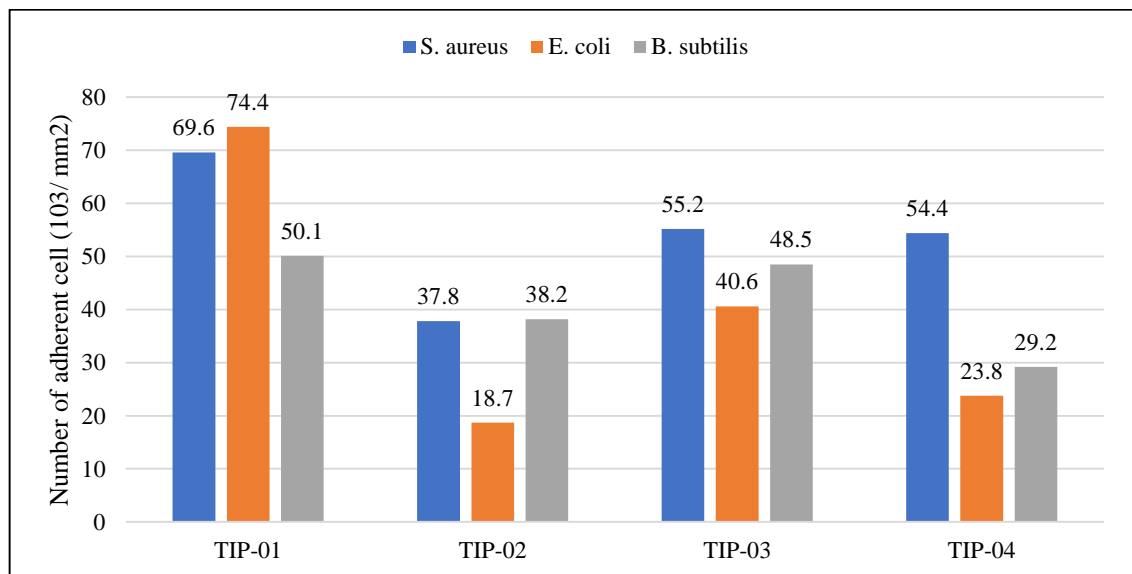


Figure 4-12 Graph of bacterial adhesion on polished titanium

4.8 Correlation Between Surface Parameter, Contact Angle and Bacterial Adhesion

Collectively, the total number of cells attached onto all polished stainless steel were 212.6×10^3 , 150.6×10^3 and $141.1 \times 10^3/\text{mm}^2$ for *S. aureus*, *E. coli* and *B. subtilis* respectively. Meanwhile the changes in total number of *S. aureus* adhesion was negligible on TIP, while *E. coli* and *B. subtilis* showed a reduction and increase in adhesion, respectively. Data from Table 4-4 shows that in every treatment, the bacterial density on the surfaces was as follows: *S. aureus* > *B. subtilis* > *E. coli*. The current finding is similar to those reported by Rodrigues-Contreras et al (2018), where *B. subtilis* adhered more than *E. coli* on SS surfaces. Collectively, the total number of adhesions for *S. aureus* on polished stainless steel was similar to polished titanium, showing a negligible difference. On the other hand, the adhesion of *B. coli* and *B. subtilis* was greatly reduced and enhanced on titanium, respectively, in comparison to polished stainless steel surfaces (Table 4-4).

Table 4-4 Total number of bacteria adhered on stainless steel and titanium

Fabrication/Metal		<i>S. aureus</i> ($10^3/\text{mm}^2$)	<i>E. coli</i> ($10^3/\text{mm}^2$)	<i>B. subtilis</i> ($10^3/\text{mm}^2$)
Control (Mirror Finish)	Stainless steel	158.1 ± 7.5	14.5 ± 2.1	50.8 ± 3.2
	Titanium	82.6 ± 4.6	13.5 ± 1.9	45.8 ± 3.9
Polished	Stainless steel	212.6 ± 7.8	150.6 ± 8.9	141.1 ± 11.5
	Titanium	217.1 ± 6.5	127.5 ± 12.6	165.70 ± 4.8

Figure 4-13 shows the relationship between bacterial adhesion with surface parameters, CA, *Sa*, and *Sds* on SSP and TIP. It is important to note that all the polished SSP and TIP exhibited $CA < 70^\circ$, ranging from $43.5^\circ - 62.57^\circ$ showing that the surfaces were moderate hydrophilic to poor hydrophilic. When hydrophobic bacteria interact with hydrophilic surfaces or vice versa, the adhesion behaviour becomes very difficult to predict. The hydrophobicity of the bacteria is expected to play an important role in the adhesion. Being similar Gram-positive bacteria, the magnitude of adhesion of *S. aureus* (CSH = 42%) exceeded the adhesion of *B. subtilis* (CSH = 12%). The adhesion of *S. aureus* was independent from increasing CA within the hydrophilic range, while *E. coli*

adhesion on SSP and TIP was negatively and positively correlated, given by $R^2 = 0.31$ and $R^2 = 0.28$, respectively, showing increased adhesion with increased hydrophobicity. Interestingly, increasing CA in SSP and TIP promoted the adhesion of *B. subtilis*. A linear correlation with $R^2 = 0.34$ and $R^2 = 0.74$ for SS and TI was developed depicting that correlation for Sa stretches from poor to strongly correlated, respectively.

Previous studies in the literature suggested the threshold value of Sa that discriminated between the ability to reduce or decrease bacterial adhesion was $0.2 \mu\text{m}$ (Chapter 2). The Sa of the polished metal for SSP ($Sa = 0.010\text{--}0.17 \mu\text{m}$) and TIP ($Sa = 0.11\text{--}0.17 \mu\text{m}$) were assessed to study the effects of Sa below the threshold value (Figure 4-13 C–D) with adhesion. In the case of SSP, adhesion of *S. aureus* and *E. coli* reduced with increasing Sa values from 0.10–0.17, while *B. subtilis* showed an opposing trend. Meanwhile, when tested on TIP, the adhesion of all species was promoted with increasing Sa values. *E. coli* adhesion with respect to varied Sa provided the strongest correlation above all with ($R^2 = 0.42\text{--}0.50$), while other species were not presented by the linear regression indicated by low $R^2 (< 0.20)$. Therefore, the adhesion of Gram-positive bacteria, regardless of its CSH and shapes, is independent from changes of Sa on smooth surfaces ($Sa < 0.2$).

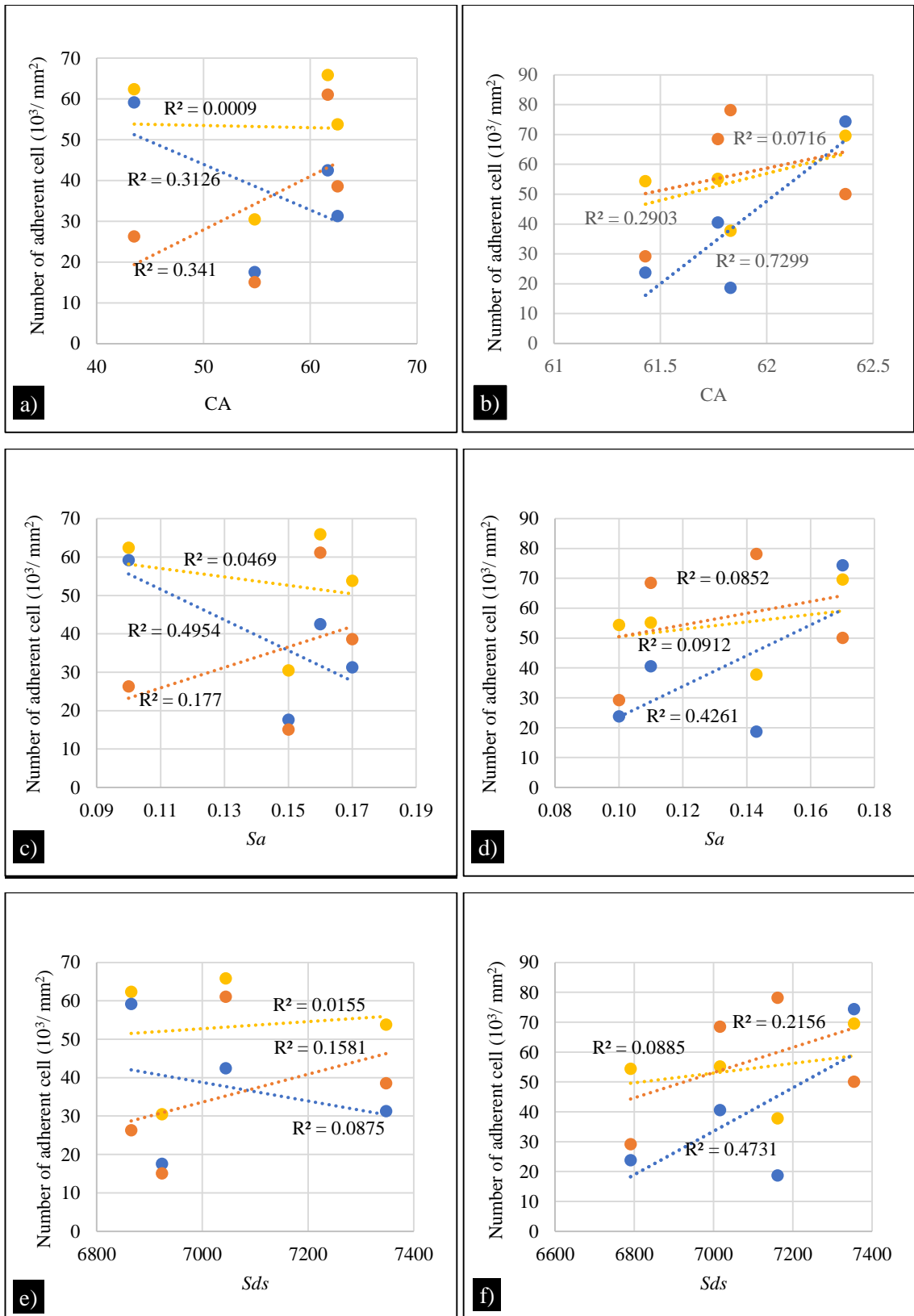


Figure 4-13 Correlation between CA, Sa and Sds with bacterial adhesion (*S. aureus* ■, *E. coli* ■ and *B. subtilis* ■) on SSP a), c), e) and on TIP b), d), f).

Figure 4-13 (E–F) shows the responses for bacterial adhesion on SSP and TIP with respect to the summit density parameter (Sds). Adhesion increased proportionally with increasing Sds in all bacterial species on both metals (with the exception of *E. coli* on SS), which agreed with the relationship between Sds and CA. Previously, it was found that Sds contributed to a higher contact angle (hydrophobicity) proven by a strong linear regression. Denser peaks per unit area (increase of Sds) in conjunction with low roughness enlarged the contact point of the bacteria with the surface. Although the adhesion increased with increasing Sds , the low regression observed within the tested range suggested that the adhesion process was independent of this variable. Nevertheless, the features correlated well for representing *E. coli* on titanium, given by $R^2 = 0.4731$.

It is worth mentioning that the responses in adhesion capability for all species with respect to changes of CA, Sa and Sds values were more sensitive on TIP than SSP, proven by the steeper line of the linear regression for the range studied. The slight difference (< 10%) between the properties of SSP and TIP with the use of similar grit paper can be neglected, therefore the gradient represented the sensitivity of the responses when small changes were applied. It was assumed that the polishing method might have affected the surface composition of the polished metal. Presumably, polishing thickened the oxide layer of the SSP, thereby the adhesion might have been controlled by the electrostatic interaction between the oxides and the bacteria. Unlike stainless steel, titanium is stable and chemically inert, suppressing the oxidising effect. Nevertheless, the effect of surface skewness and kurtosis (Figure 4-13) was evaluated to look out for a correlation between adhesion and surface topography (valleys and peaks).

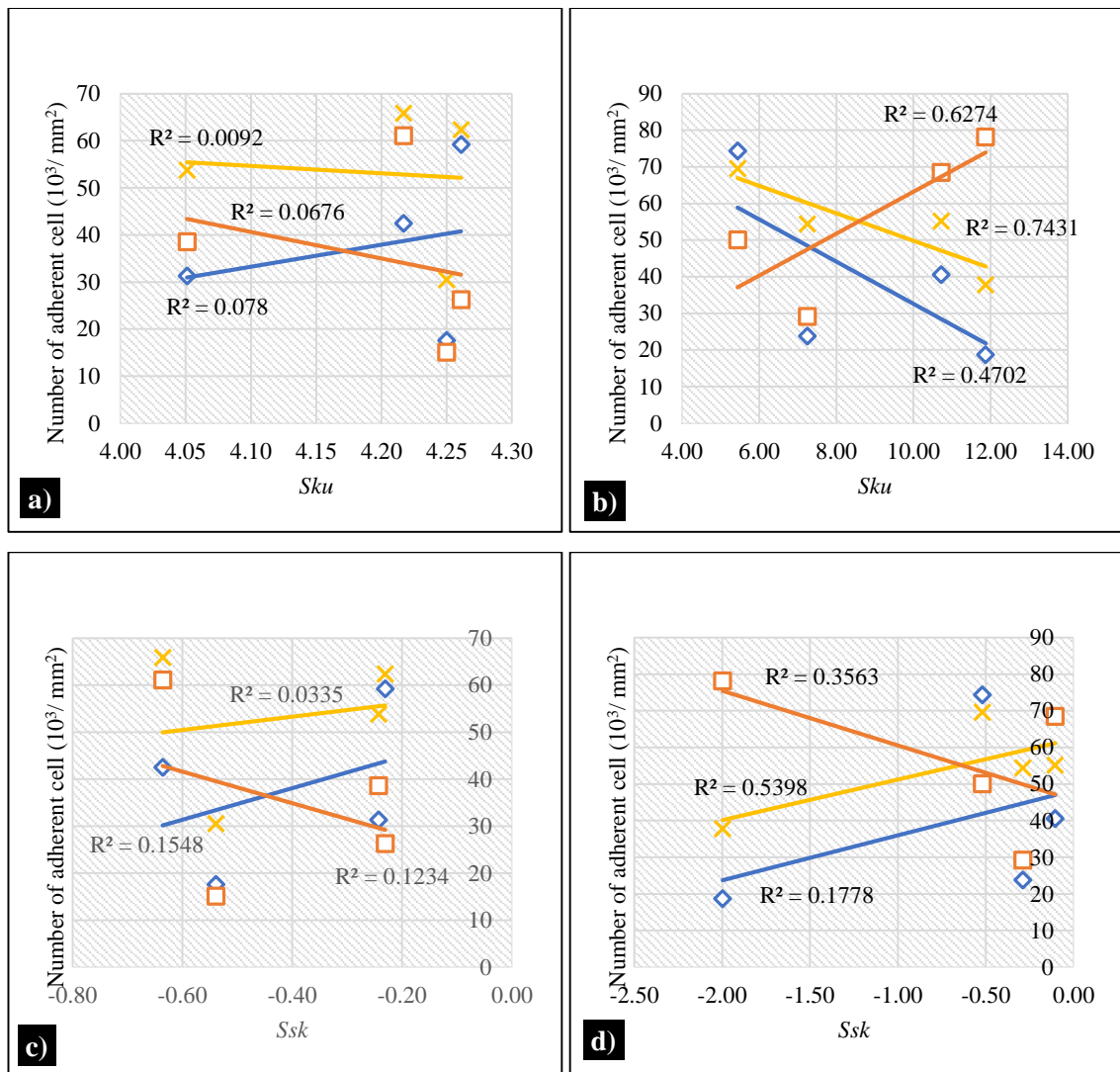


Figure 4-14 Correlation between *Sku* and *Ssk* and bacterial adhesion (*S. aureus* ■, *E. coli* ◆ and *B. subtilis* □) on SSE a), c), e) and TIE b), d), f).

Figure 4-14 shows the bacterial adhesion on the polished stainless-steel with respect to *Sku* and *Ssk*. In general, no concrete correlation based on *Sku* and *Ssk* for all three bacteria with respect to polished stainless-steel surfaces can be made due to very low R^2 (< 0.2). However, the effects of *Sku* and *Ssk* changed drastically when polished titanium was used. A moderate to strong correlation was established for all bacteria species with changes in both *Sku* and *Ssk*. Following the same fabrication technique, the *Sku* values for TIP were much higher than those of SSP, showing a high peakedness in TIP, made up by narrow and sharper peaks. The higher kurtosis values represented a wide range of peak height distribution and inhomogeneous surfaces thus increasing the resistance to adhesion. Meanwhile the *Sku* for SSE was narrowly distributed, suggesting

a controllable peak height. The adhesion of *E. coli* and *S. aureus* was reduced with increasing Sku value because the contact area between the bacteria and the peaks was subsequently reduced with increasing Sku. Figure 4-15 shows the images of bacteria on the SSP and TIP after a 4-hour exposure to bacterial suspensions. Meanwhile, Figure 4-16 shows the SEM images for *E. coli* adhered to stainless steel.

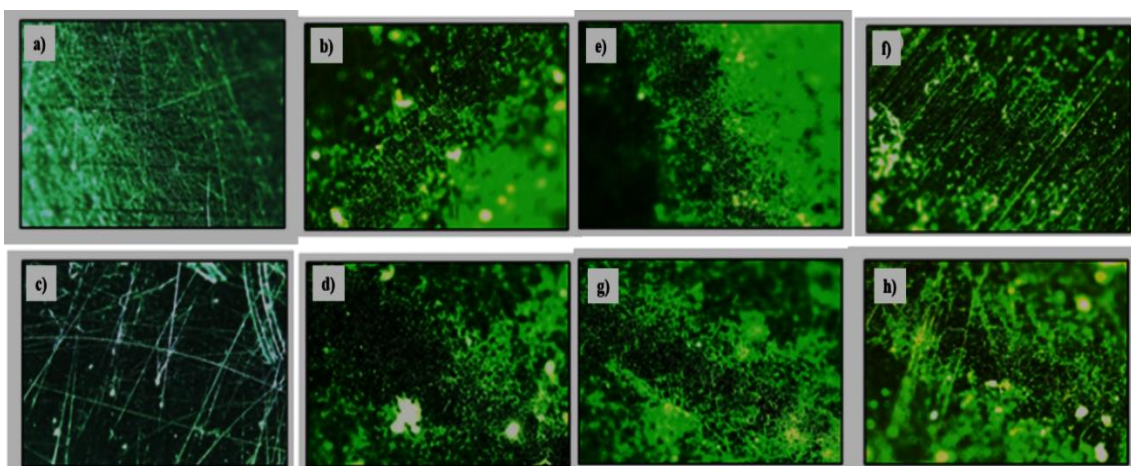


Figure 4-15 Fluorescent images of a) SSP-without bacteria, b) *S. aureus* on SSP, c) TIP without bacteria, and d) *S. aureus* on TIP e) *E. coli* on SSP, f) *B. subtilis* on SSP, g) *E. coli* on TIP and h) *B. subtilis* on TIP.

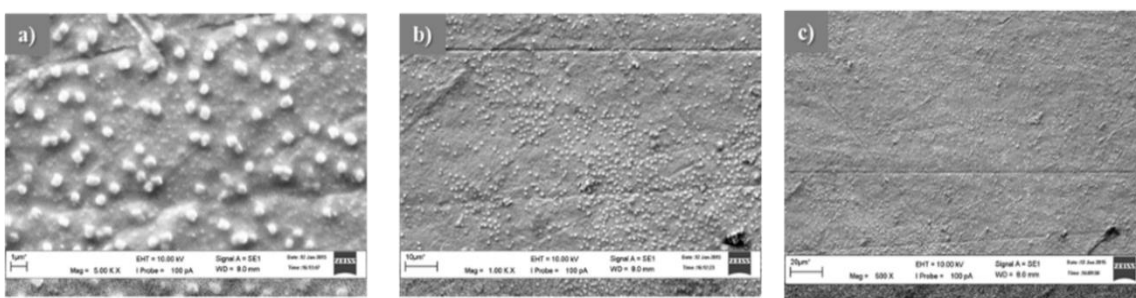


Figure 4-16 SEM images of *E. coli* on titanium specimen at different magnification, a) 5000x, b) 1000x and c) 500x

4.9 Chapter Summary

In summary, polished specimens reduced gradually with polishing grit paper size are in a negative correlation to average roughness Sa , while for Sku , it indicates a positive correlation and Ssk shows a weak correlation. Polished titanium produced fine surfaces compared to stainless-steel for height and hybrid parameter analysis. It is due to the difference in material structure between them. Titanium is soft compared to stainless-steel, which is a harder metal in physical condition. With respect to polishing grit, Sq and Sku show a strong correlation with a regression value of nearly 1.00 while for Ssk , a moderate correlation occurs with regression around 50% of Sa and Sku of the specimen. In conclusion, a higher polishing grit can lower the roughness and may increase the kurtosis of the surfaces. In terms of the wettability phenomenon, Sds demonstrated a strong positive correlation followed by Ssc with moderate regression values. Unfortunately, no significant correlation was indicated by Sdq and Str even though they are closely related to the texture of the surface. Therefore, Sds is the important parameter contributing to the surface wettability of the metallic specimen.

In general, the linear correlation between the surface properties (CA, Sa , Sds , Sku and Ssk) and the bacterial adhesion on SSE alone was either poorly correlated or insignificant. When observation was conducted on TIP, the regression value for the linear relationship was greatly improved showing a moderate to strong interaction existed. The variation in responses between these two surfaces was presumably due to the thickening of the oxide layer on the SSE surfaces that was formed after the polishing process. Being inert, oxidation was suppressed on the titanium surfaces, suggesting that the increase and reduction of adhesion displayed a sensitivity of the bacteria towards the parameters studied. It is appropriate to suggest that the natural effect coming from the hydrophilic-hydrophilic surface interaction does not seem able to surpass the effect due to hydrophobic bacteria (*S. aureus*). Thereby it is appropriate to suggest that the primary factor for adhesion was contributed by the hydrophobic CSH, while hydrophobic surfaces will augment the effect.

Chapter 5

WEDM Surface Characterisation with respect to Contact Angle Measurement and Bacterial adhesion

5.1 Introduction

The discussion in Chapter 5 will cover the relationship between sub-micron roughness with surface wettability and cell attachment on metallic surfaces. The parameters influencing surface wettability are Sa and Sds while *S. aureus* dominated the cells attached on stainless-steel and rod-shaped *B. subtilis* adhered more to titanium surfaces. In this chapter, the discovery continues from sub-micron on polished to micro level roughness with the same parameters fabricated using wire electrode discharge machining (WEDM). WEDM fabrication produced a surface roughness between 3 μm to 4 μm with a machine feed rate of between 10 mm/min to 22 mm/min. From the nature of the WEDM process, it was expected to provide a peak structure ($Ssk > 0$) contrasting with the polish technique with a deep valley structure ($Ssk < 0$) [155]. At the end of the discussion, wide-range conclusions need to be established in terms of the degree of influence on wettability and cell-attachment on both metallic surfaces.

At the end of the discussion, a wide-ranging conclusion on whether surface topography influences wettability and cell attachment with respect to *S. aureus*, *E. coli* and *B. subtilis* bacteria must be reached. The cutting operation is performed by Wire-cut Electrical Discharge Machining (WEDM) machine (SODICK VZ300L), surface characterisation was measured by using Bruker Optical Profilometry, contact angle by using Kruss DSA, Germany and the bacterial adhesion experiment followed the standard procedure as mentioned in Chapter 3. Wire electrical discharge machining (WEDM) is an important technology in the machining of very hard materials. The quality of an electrode machined surface determines the functionality of the metals.

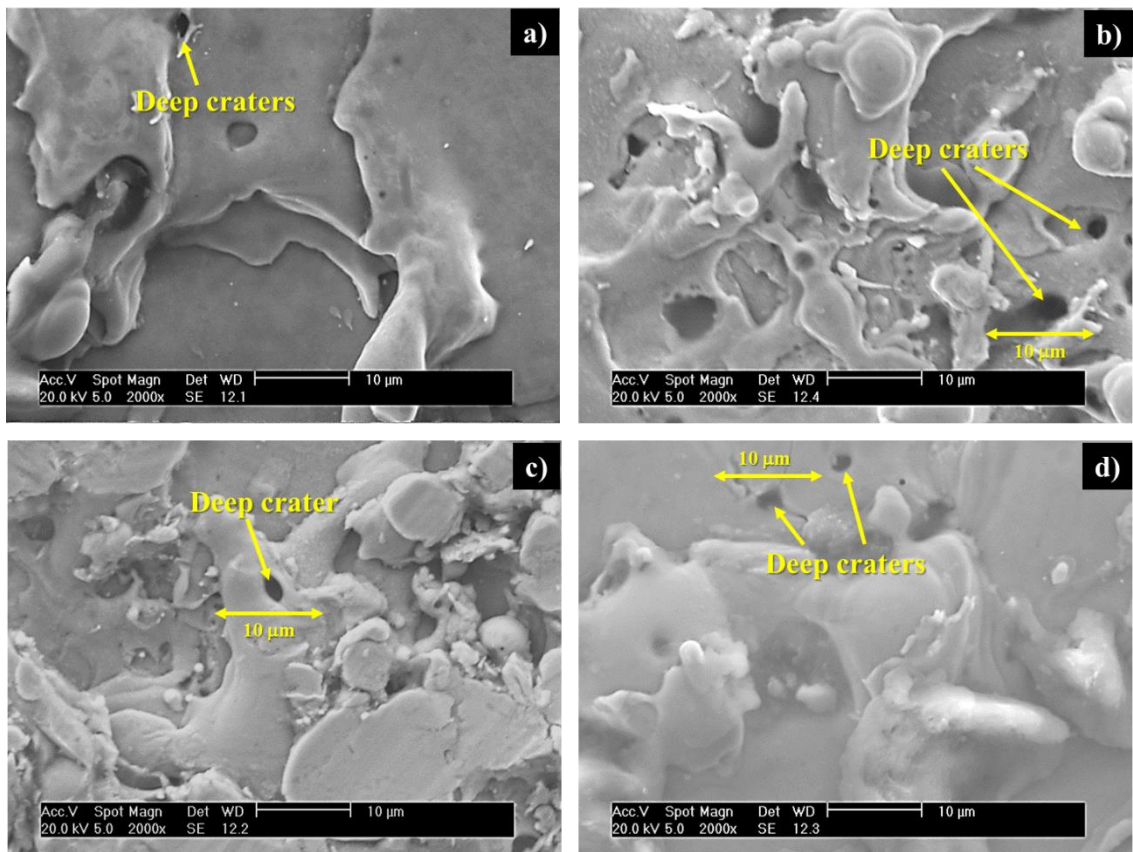


Figure 5-1 WEDM stainless-steel morphology a) SSE-01 (10mm/min), b) SSE-02 (12mm/min), SSE-03 (20mm/min) and d) SSE-04 (22mm/min)

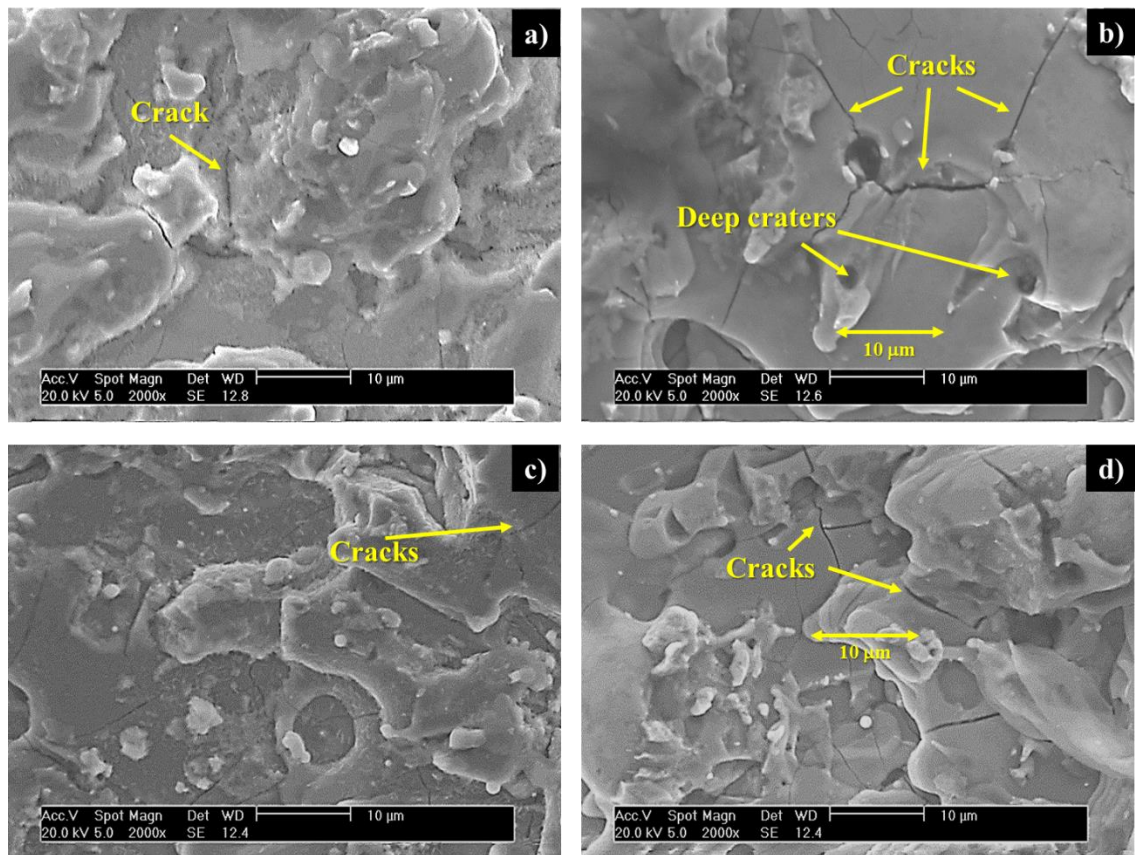


Figure 5-2 WEDM titanium morphology a) TIE-01 (10mm/min), b) TIE-02 (12mm/min), TIE-03 (20mm/min) and d) TIE-04 (22mm/min)

The morphology of 316L and Ti6Al4V surfaces machined using the wire electrode discharge machine is formed by many craters and micro cracks that resulted from individual electrical discharges and enormously rapid transformation of molten material into solid solution respectively [76]. Both morphology of the given area surface shows traces that are typical of material that was completely molten and subsequently rapidly cooled. With the help of scanning electron microscopy, the surfaces of 316L and Ti6Al4v were viewed under 500x, 1000x and 2000x magnifications as shown in Figure 5-1 (a – d) and Figure 5-2 (a–d). From the images, it is clear that craters and cracks formed on the surfaces vary greatly. For micro cracks, SSE-02 (12mm/min) showed the length of an individual crack exceeds 10µm followed by SSE-04 (22 mm/min). In contrast, SSE-01 (10 mm/min) and SSE-03 (20 mm/min) showed tiny lines of crack and can be considered acceptable.

With respect to the interaction with bacteria, the occurrence of craters might trap the bacteria, especially if the crater's diameter is larger than bacterial sizes. Due to the tiny line of the cracks, it is impossible for the bacteria to be trapped in the valley of the crack. However, it is perfectly possible for the fimbria of the bacteria to be attached or locked on the surfaces. It is plausible for bacteria to form a colony inside the craters (diameter = 3 to 5 μm) due to the diameter of the craters (3 to 5 μm) being bigger than the size of the bacteria (0.5 to 2 μm). All samples with electrode erosive machined to contain defects burned cavities, which means that the machine's parameter setting has no impact on its presence [76].

5.2 WEDM Surface Characterisation

5.2.1 WEDM Height Parameter Characterisation

The valuation of suitable surface parameters allowed the prediction of the peaks or deep-valley surfaces. Parameters involved by means of the profile method included average roughness (S_a), kurtosis (S_{ku}), skewness (S_{sk}), maximum height profile (S_z), maximum peak height (S_p), maximum valley depth (S_v). Area parameters allow the evaluation of the area quantitatively in all directions that are technically significant. Values of individual parameters for 316L and Ti6Al4V were plotted in diagrams shown in Figure 5-4 (A–C). Every average roughness, S_a show a reduction of around 33.4% to 51.2% from the as-received substrate (REF), from 5.02 μm to 3.34 μm , 2.50 μm , 2.91 μm and 2.47 μm for SSE-01, SSE-02, SSE-03 and SSE-04 respectively. Ti6Al4V also showed a reduction but the percentage of reduction was around 48.94% to 50.45% with S_a values of 3.36 μm , 3.30 μm , 3.34 μm , and 3.26 μm for TIE-01, TIE-02, TIE-03 and TIE-04 respectively. The S_a data shows that Ti6Al4V are not affected much by the machine feed rate variables because the S_a variation 0.10 μm while for 316L the variation was 0.84 μm . For kurtosis and skewness parameters, all the specimens established positive values with $S_{ku} > 3$ except for SSE-01 and SSE-03 ($S_{ku} < 3$). Surfaces with positive S_{sk} and S_{ku} greater than 3 demonstrated peaks/deep-valley structure as shown in Figure 5-5 (3D optical profilometry images). On the plane skewness, S_{sk} represents $S_{sk} > 0$ for all surfaces, which indicates the predominance of peaks on the surface [155].

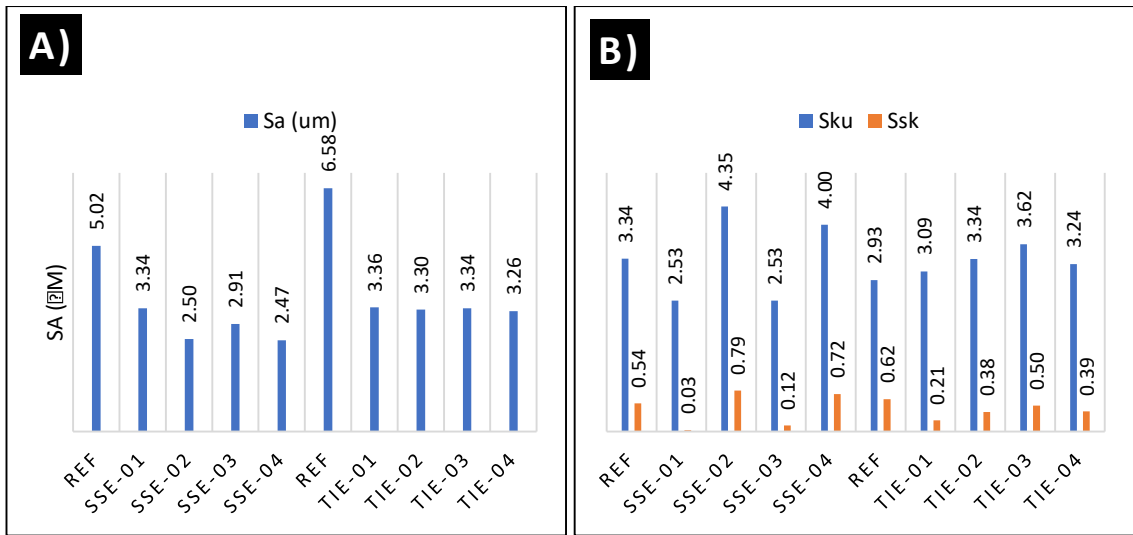


Figure 5-3 Graph of the height parameters on 316L and Ti6Al4V with respect to A) *Sa* and *Sq*, B) *Sku* and *Ssk*

As the aim of the study was to establish the relationship between surface topography, wettability and cell-adhesions, the profile of the surface was essential. For example, surfaces with deep valleys had a high potential to trap bacteria inside the valleys resulting in colony formation/early stage of biofilm. Conversely, high peaks influenced the reduction of the adhesion rate by reducing the contact point of cells with the flat surfaces. Therefore, the values of maximum peak height (*Sp*), the maximum valley depth (*Sv*) and the maximum height surfaces (*Sz*) were important to correlate with several cells attached to the surfaces. From Figure 5-4, as-received substrates for 316L and Ti6Al4V demonstrated high max height surface (*Sz*) with values of 61.58 μm and 59.14 μm respectively. The max height of peaks (*Sp*) for 316L (REF) was 31.91μm, slightly lower compared to Ti6Al4V (REF) with a value of 34.38. The max valley depths (*Sv*) for both specimens were -29.37 and -24.75 for 316L and Ti6Al4V respectively, which means 316L (REF) had a slightly deeper valley compared to Ti6Al4V (REF). For the modified surfaces, all the specimens showed a gradual reduction of *Sp*, *Sv* and *Sz*. The max height surfaces for SSE-01, SSE-02, SSE-03 and SSE-04 was 44.35 μm, 32.61 μm, 29.11 μm and 27.95 μm respectively. For TIE-01, TIE-02, TIE-03 and TIE-04, the values of *Sz* were 49.48 μm, 34.52 μm, 35.77 μm and 29.11 μm respectively. TIE-03 was slightly higher compared to TIE-02 with a 1.2 μm difference and the *Sa* for TIE-03 was slightly higher compared to TIE-02 with a 0.18 μm difference. On the whole, as a reflection from the *Sku* and *Ssk* values, all specimens exhibited higher peaks with deep valleys and this type of profile will be investigated in the cell-adhesion phenomenon.

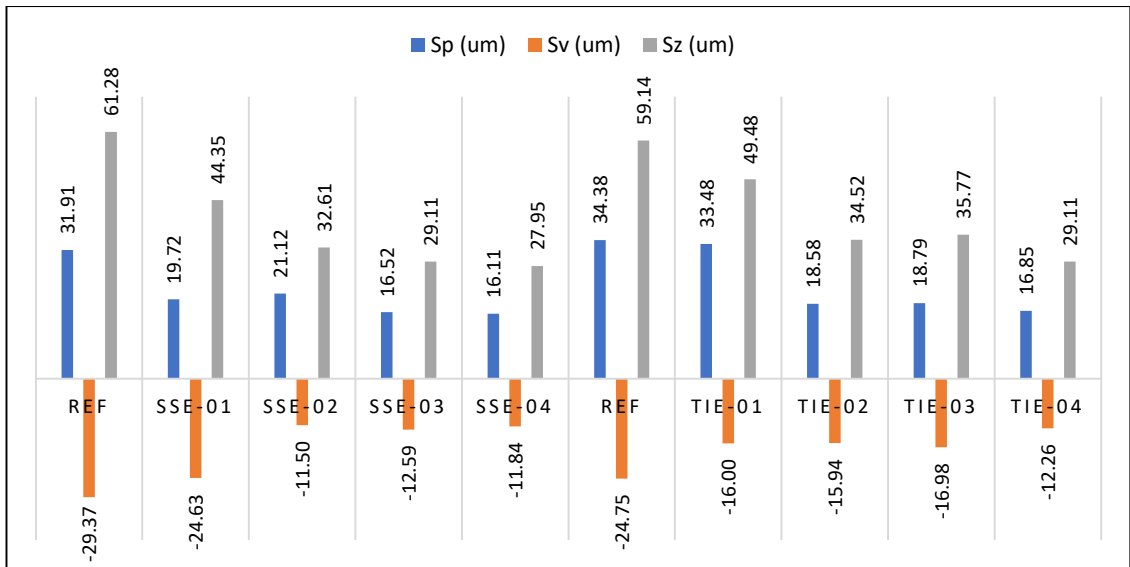


Figure 5-4 Graph of height parameter on 316L and Ti6Al4V with respect to maximum height surface parameter, SP (max peak height), Sv (max valley depth) and Sz (max height of surface)

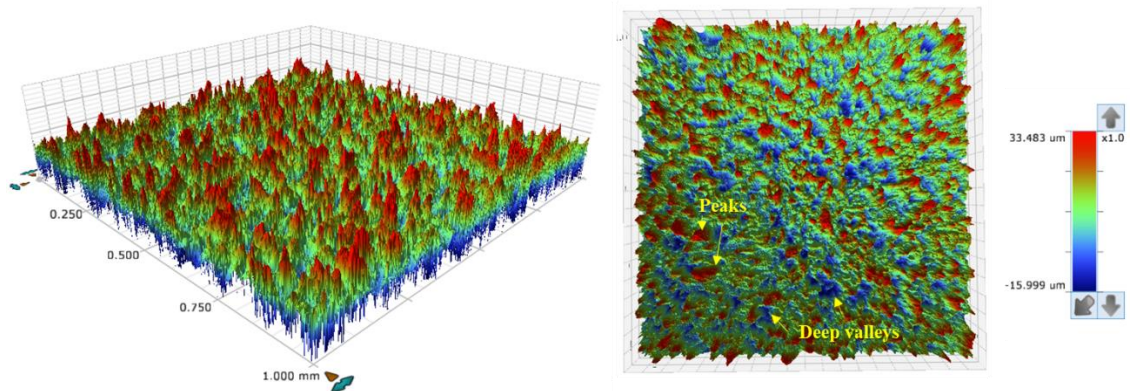


Figure 5-5 3D optical profilometry for TIE-02 with $Sa = 3.30 \mu\text{m}$, $Sku = 3.34$, $Ssk = 0.38$, $SP = 33.48$, $Sv = -15.99$ and $Sz = 49.48$

Figure 5-6 shows a graph of the machine feed rate correlated with average roughness, Sa and max height surface, Sz . Despite the gradual increase in the machine feed rate parameter from 10 mm/min up to 22 mm/min with other machine parameters set to constant, remarkably, the average roughness shows a low influence where the 316L specimen poorly correlated with the machine feed rate ($R^2 = 0.3415$) while Ti6Al4V showed no correlation ($R^2 = 0.2444$). Pragma Shandilya [157] reported that for optimum WEDM surface parameters, the machine feed rate had no substantial influence. There are

also two experiments conducted by Aniza Alias [158], investigating the correlation between the machine feed rate (mm/min) with Sa . The experiments concluded that no correlation transpired between them. However, when plotting the machine feed rate parameter against the maximum height of surfaces, Sz , surprisingly, 316L specimens showed strong correlation ($R^2 = 0.8616$) while Ti6Al4V showed a moderate correlation ($R^2 = 0.522$). It can be concluded that there is no significant correlation between machine feed rate with Sa but there is a strong correlation with the maximum height of surface, Sz for both specimens.

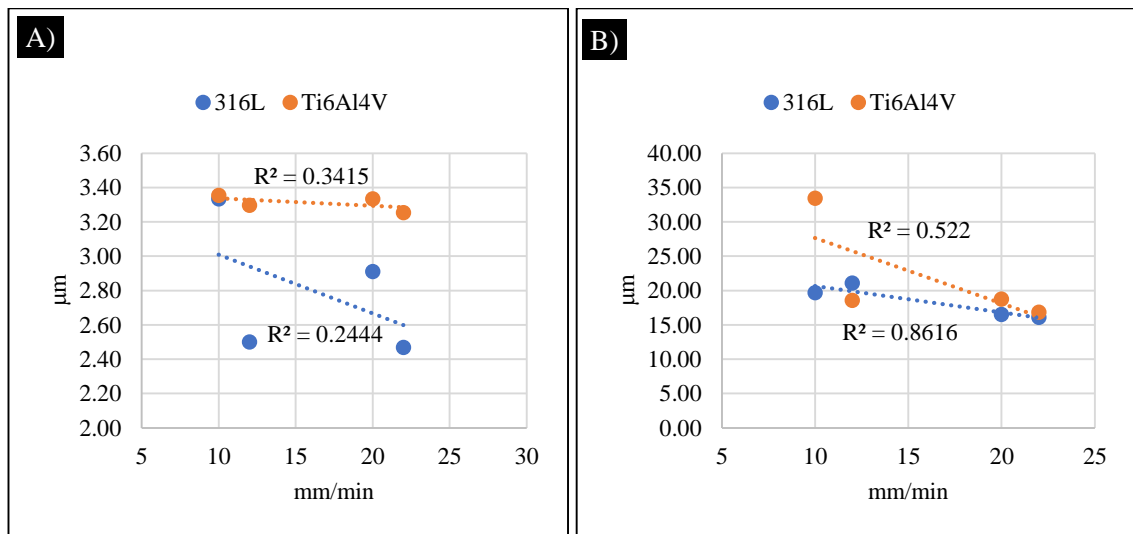


Figure 5-6 Correlations between a) average roughness, Sa (μm) and machine feed rate (mm/min) b) maximum height surfaces, Sz (μm) and machine feed rate (mm/min) on WEDM stainless-steel and titanium. $R^2 > 0.7$ indicated strong correlation, $R^2 = 0.5 - 0.69$ represented moderate correlation and $R^2 = 0.49 - 0.3$ poorly correlated and $R^2 < 0.29$ provided no correlation.

5.2.2 Spatial and Hybrid Parameter Characterisation

In section 5.2.1, the discussion covered how surface height parameters were influenced by the machine feed rate of WEDM. The outcome was there was no influence towards average roughness (Sa) and a strong influence on the maximum height of surfaces (Sz). Height parameters alone are not enough to represent the dimensional features of the profile. Therefore, a further characterisation under spatial and hybrid parameters is

needed to provide the spacing and texture information on the surface texture, whether isotropic or anisotropic [156].

Table 5-1 shows the spatial and hybrid data on 316L and Ti6Al4V WEDM specimens consisting of the auto-correlation length (*Sal*), texture direction (*Std*), texture aspect ratio (*Str*), developed interfacial area ratio (*Sdr*) and summit density (*Sds*) The *Sal* for 316L (REF) and Ti6Al4V (REF) are higher compared to the modified specimens with values of 48.25 μm and 81.62 μm respectively. These values decreased to 26.40 μm , 24.88 μm , 21.19 μm and 22.90 μm for the 316L and 19.11 μm , 17.19 μm , 16.33 μm and 17.89 μm for the Ti6Al4V specimens. Referring to Figure 5-8 and Figure 5-9 on ACF plot, both metals show the same pattern of ACF where 316L shows a slightly wider SPACED compared to Ti6Al4V with *Sa* values of around 3.00 μm . On the texture direction, *Std*, no data was recorded (*n/a*) for all modified specimens while for the as-received (REF), it shows 87.18° and -81.23° for 316L and Ti6Al4V respectively. No measured data on *Std* means the surfaces were isotropic (no dominant direction) while the as-received (REF) surfaces have a dominant lay with the angle $> 80^\circ$ as shown in Figure 5-7. The other parameter be discussed is the texture aspect ratio, *Str* which refers to the same dimensional surface measurement, either spatial isotropy or directionality texture surfaces. From Table 5-1, the *Str* for 316L were 0.77, 0.68, 0.60 and 0.63 with as-received (REF) value of 0.06 and for Ti6Al4V were 0.89, 0.85, 0.93 and 0.84 with as-received (REF) value of 0.10. With the *Str* close to 1.00, the surface texture is considered spatially isotropic.

Table 5-1 WEDM topography data on spatial and hybrid parameters for 316L stainless-steel and Ti6Al4V titanium

Specimen	Hybrid Parameter	REF	10 mm/min	12 mm/min	20 mm/min	22 mm/min
316L (spatial)	<i>Sal</i> (μm)	48.25	26.40	24.88	21.19	22.90
	<i>Std</i> (deg)	87.18	n/a	n/a	n/a	n/a
	<i>Str</i>	0.06	0.77	0.68	0.60	0.63
316L (hybrid)	<i>Sa</i> (μm)	5.02	3.31	2.43	4.22	2.39
	<i>Sdr</i> (%)	56.67	180.48	137.08	152.36	121.30
	<i>Sds</i>	3855.27	4876.28	4863.23	4786.86	3874.63
Ti6Al4V (spatial)	<i>Sal</i> (μm)	81.62	19.11	17.19	16.33	17.89
	<i>Std</i> (deg)	-81.23	n/a	n/a	n/a	n/a
	<i>Str</i>	0.10	0.89	0.85	0.93	0.84
Ti6Al4V (hybrid)	<i>Sa</i> (μm)	9.58	3.36	3.36	3.46	3.06
	<i>Sdr</i> (%)	69.21	203.78	296.67	256.89	215.80
	<i>Sds</i>	3556.28	4448.71	4372.52	4458.99	4809.01

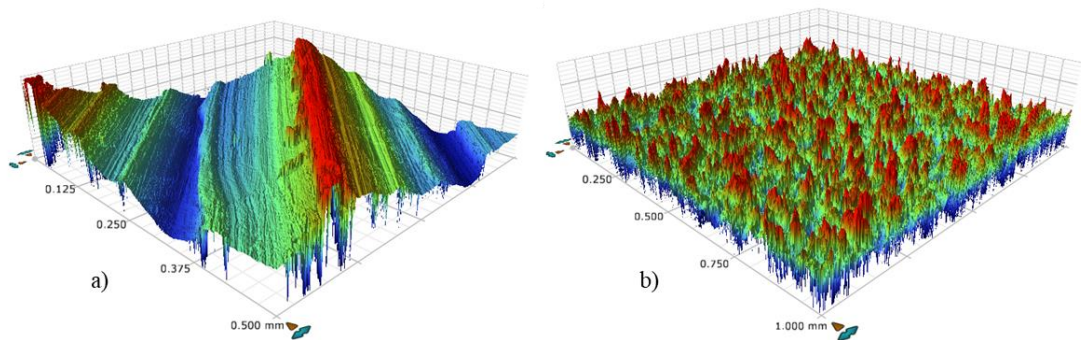


Figure 5-7 3D optical profilometry images for a) Ti6Al4V with $Std = -81.23$, $Str = 0.10$ and b) Ti6Al4V with $Std = n/a$, $Str = 0.85$

The discussion of hybrid parameters focuses on summit density (Sds) and developed interfacial area ratio (Sdr). Sds is the number of summits per unit area making up the surface while Sdr is an expressed percentage of additional surface area contributed by the texture as compared to an ideal plane the size of the measurement region. Typically, Sdr will increase with the spatial intricacy of the texture, whether or not Sa changes. From Table 5-1, the summit density for 316L (REF) is 3855.27 summits/mm, slightly low compared to modified surfaces with 4876.28 summits/mm, 4863.23 summits/mm, 4786.86 summits/mm, and 3874.63 summits/mm for SSE-01, SSE-02,

SSE-03 and SSE-04 respectively. For Ti6Al4V, the summit for as-received (ref) substrate is 3556.28 summits/mm, slightly low compared to modified specimens with 4448.71 summits/mm, 4372.52 summits/mm, 4458.99 summits/mm, and 4809.01 summits/mm for TIE-01, TIE-02, TIE-03 and TIE-04 respectively. Similar to Sds , Sdr (%) shows extremely higher differences between as-received (ref) and modified specimens with the increase being between 53.28% to 68.6% while for Ti6AL4V the increment is higher, between 66.03% to 76.67%. The higher values of Sdr meant a higher contribution of surface texture as compared to an ideal plane of the measurement region, regardless of the roughness value. For example, TIE-01 and TIE-02 shared the same Sa , 3.36 μm , however TIE-02 contributed more surface texture with 296.67% compared to TIE-01 with 203.78%. On the whole, Ti6Al4V has a higher Sdr compared to 316L.

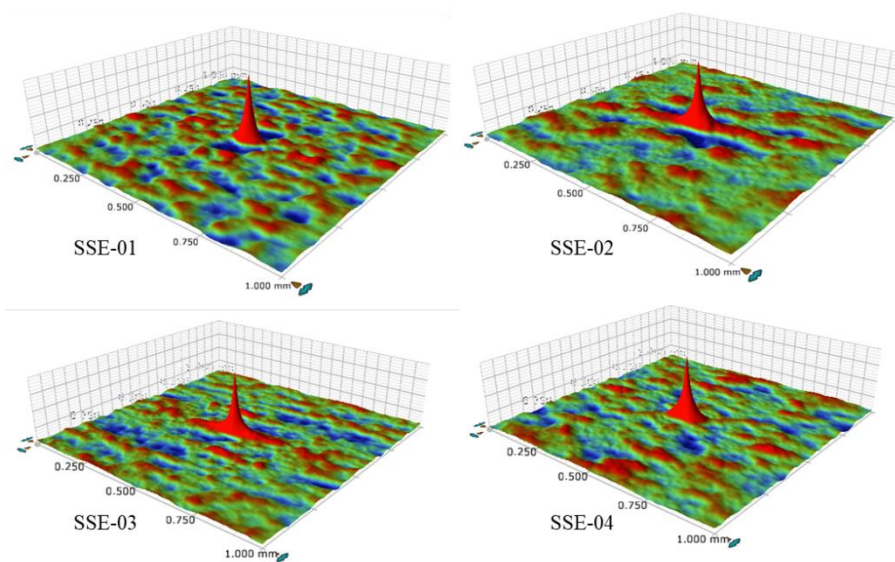


Figure 5-8 ACF on WEDM stainless-steel specimen

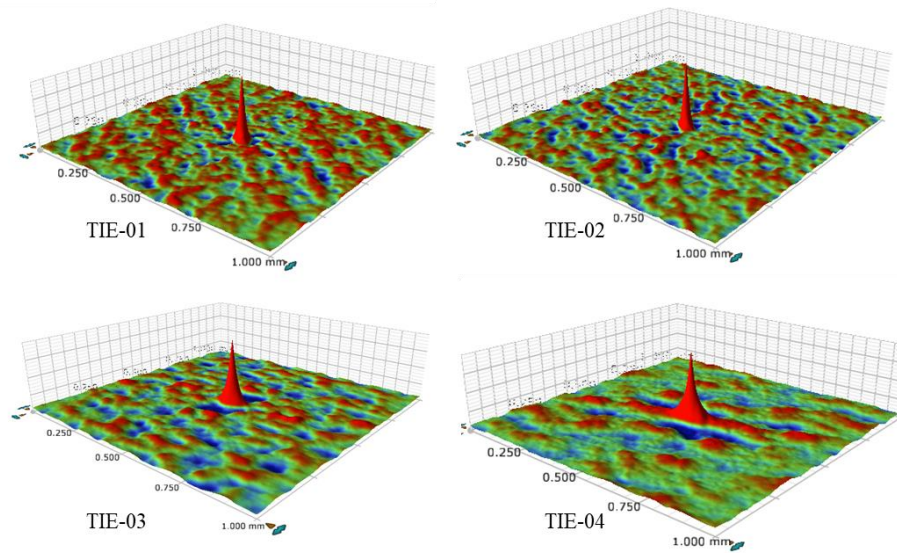


Figure 5-9 ACF on WEDM titanium specimen

5.3 The Correlation between Contact Angle Measurement and Surface Topography Parameter

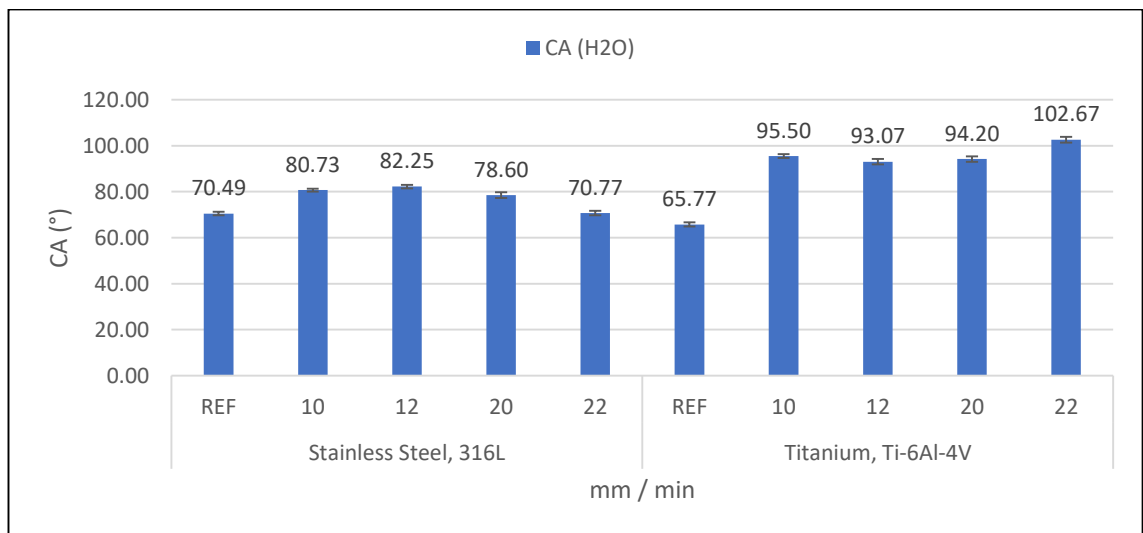


Figure 5-10 A graph of contact angle measurement on EDM specimen

In section 5.2, the characterisation of electro-erosive machined surface was discussed, which covered the height, spatial and hybrid parameters. On top of that, the aims of the thesis were to identify the influence of parameter contribution to a surface at hydrophobicity. Therefore, the measurement of water contact angle on the electro-erosive

machined surface has been made, and data was tabulated in Figure 5-10 presenting the contact angle versus machine feed rate of WEDM (mm/min). Generally speaking, all modified specimens show hydrophobic surfaces compared to polished specimens with low Sa values. Through increasing the Sa up to 3.36 μm , the surface becomes more hydrophobic compared to as-received (ref) value with 70.49° and 65.77° for 316L and Ti6Al4V respectively [39]. For SSE-01 to SSE-04, the contact angle increased to 80.73°, 82.25°, 78.60° and 70.77° and for TIE-01 to TIE-04, the values were 95.50°, 90.37°, 94.20°, and 102.67° respectively. The variation between the high and low measurement for 316L and Ti6Al4V specimens was 9.96° and 10.60° respectively, while the variation of Sa was 1.83 μm for 316L and 0.40 μm for Ti6AL4V.

The effects of surface properties on the CA measurement with respect to metal types and WEDM fabrications are presented in Figure 5-11 a) to f). CA measurements were plotted against Sa , Sku , Ssk , Sal , Str and Sds and linear regression was plotted to quantify the relationship between those parameters. Variations in responses with a correlation between 0.001 to 0.9792 was observed towards contact angle values. The relationship between contact angle with Sa , Sku and Ssk (Figure 5-11 A, B and C) demonstrated a poor correlation between Sa for Ti6Al4V with R^2 equal to 0.4812 while for 316L there was no correlation. For Sku , 316L shows a moderate correlation and Ti6Al4V shows no correlation. For the Ssk , both metals show no correlation at all with the contact angle measurement. The kurtosis, Sku , shows a poor correlation for stainless-steel and no correlation for titanium with R^2 of 0.4180 and 0.0159 respectively. A slight change in titanium's kurtosis resulted in poor Sku values while fluctuating kurtosis for stainless steel improved the correlation. For surface skewness, no correlation for both metal WEDM were found even though all Ssk values were positive. In the polished specimens, there was no correlation for Ssk due to negative values, but for the positive values (WEDM), there was no correlation at all. This means that there is no influence of skewness on the CA measurement whether it is positive or negative skewed surface. For the correlation with Sal , Sdr and Sds , Sds showed a strong correlation with R^2 equal to 0.9487 for 316L and 0.9792 for Ti6Al4V respectively. Sal and Sdr show either poor or no correlation with water contact angles.

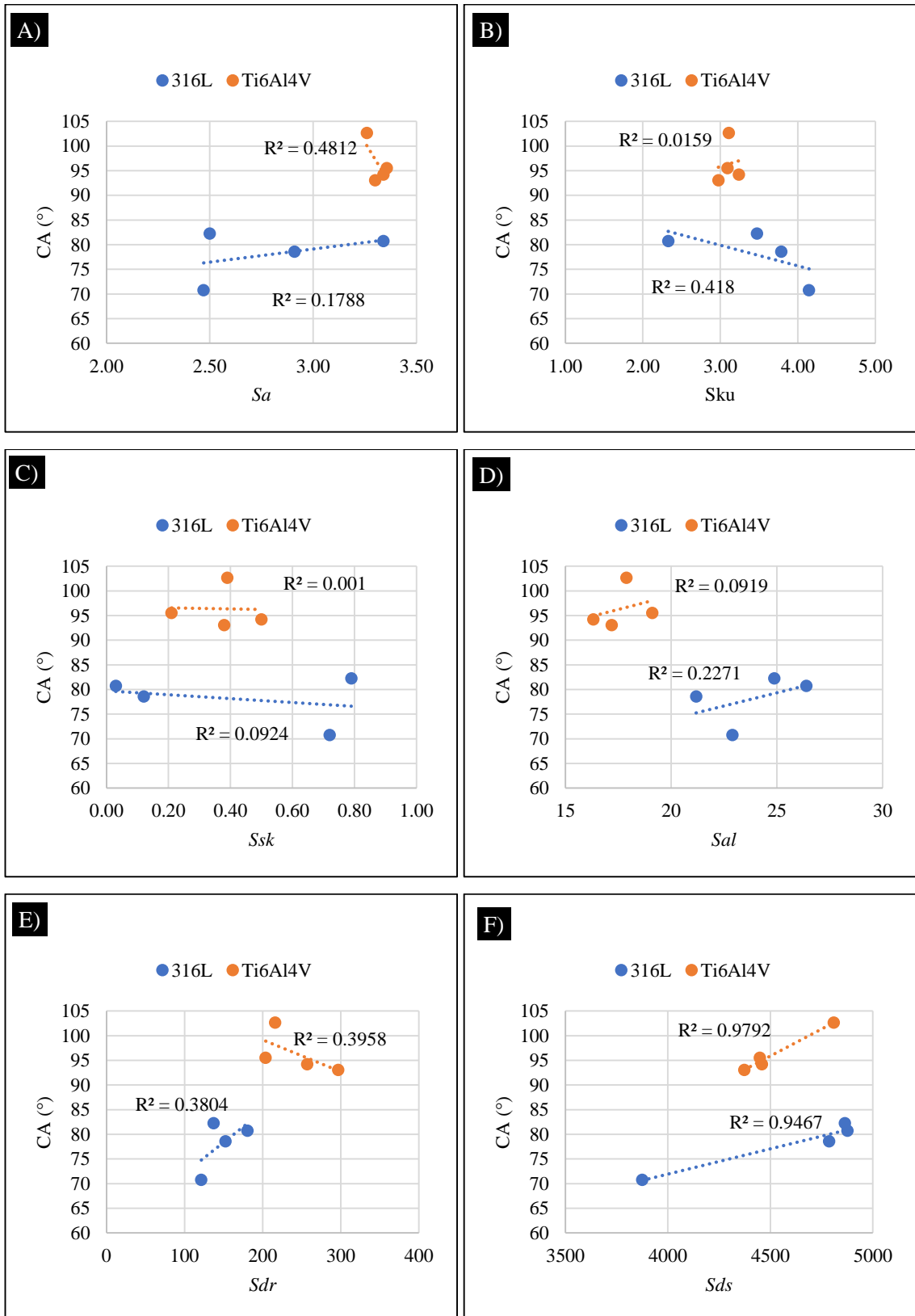


Figure 5-11 The correlation between a) average roughness, Sa b) kurtosis, Sku c) skewness, Ssk d) auto-correlation length, Sal e) developed interfacial area ratio, Sdr h) summit density, Sds with water contact angle on 316L and Ti6Al4V specimens.

5.4 Bacteria-Surface Adhesion

Four different surfaces were produced for SSE and TIE using the WEDM technique with different machine feed rates from 10 mm/min to 22 mm/min. The process produced surfaces with hydrophobic characteristics, with CA ranging from 80.73°–102.67° and roughness varying from 2.50–3.36 µm. These surfaces were exposed to a bacterial solution to determine the ability of the surface to repel adhesion, relative to the control process. Prior to the adhesion test, WEDM samples were cleaned and sterilised at 121°C for 20 minutes before being immersed into individual bacterial suspensions containing approximately 1×10^8 CFU/ mL of cells in the mid exponential phase for four (4) hours. The bacteria can be divided into Gram-positive (*S. aureus* and *B. subtilis*) and Gram-negative (*E. coli*) bacteria with varying properties i.e. coccus shape for *S. aureus* and rod-shaped for *B. subtilis* and *E. coli* (Table 3-1). In this section, a bacterial adhesion measurement was carried out using fluorescent microscopy procedure as mentioned in Chapter 3. The effects of an altered surface topography including S_a , S_{ds} , S_{ku} , S_{sk} and wettability were discussed individually while observing the correlations between changing these parameters and their effect on the adhesion intensity. The details in Table 5-2 show the data from the surface topography parameter, water contact angle and number of bacteria adhered to the specimens. It shows the range of measurement for both WEDM-stainless (SSE) steel and WEDM-titanium (TIE) specimens with height, spatial and hybrid surface parameters, and the contact angle of water against the number of bacteria counted on per-mm² basis. The effectiveness of the process was then compared against the adhesion on control specimens.

5.5 Bacterial Adhesion on WEDM stainless-steel

Metallic surfaces that were treated with WEDM and exhibiting poor to moderate hydrophobic character were exposed to *S. aureus*, *E. coli* and *B. subtilis* for four hours and the number of attached cells were recorded in Figure 5-12. Again, the surface areas of SSE-01 to SSE-04 were dominated by *S. aureus* (Gram-positive, hydrophobic), showed by the highest population ranging from $44.1 \times 10^3/\text{mm}^2$ to $98 \times 10^3/\text{mm}^2$, an increase of ~50% over those of *E. coli* and *S. aureus*. A very dense population of *S. aureus*

was observed on SSE-03, while SSE-02 provided the highest resistance to *S. aureus*. Although the WEDM fabrication increased the number of adhering bacteria relative to the polishing process, the adhesion was still low compared to the control specimen ($SSC-158 \times 10^3/\text{mm}^2$). A reduction of adhesion relative to control substrates was obtained in a range of 37.9%–72.1% for *S. aureus*.

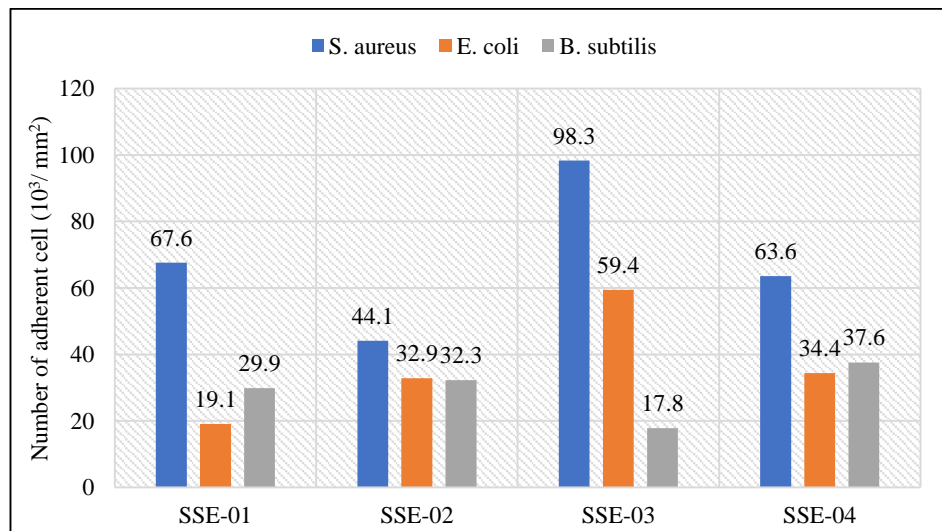


Figure 5-12 A graph of bacteria adhesion on WEDM stainless-steel specimen (SSE)

In general, the adhesion of *E. coli* was lower than *B. subtilis* on the SSE surfaces except for sample SSE-03, where *E. coli* density was ~3 times higher than *B. subtilis*. This finding is similar to Han, Tsoi [95], where in most surfaces, *B. subtilis* retained on SS was higher than *E. coli*. However, when compared with SSC, *E. coli* adhesion on SSE-03 was promoted by up to 4-fold, showing a very dense population of $59.4 \times 10^3/\text{mm}^2$. It adhered the least onto SSE-01, with only $19.1 \times 10^3/\text{mm}^2$, thus concluding that SSE metals failed to mitigate *E. coli* relative to control. In contrast, *B. subtilis* adhesion was successfully mitigated as showed by the low number of adhesions. *B. subtilis* adhesion was prevented on SSE-03 as shown by the $17.8 \times 10^3/\text{mm}^2$ cell count, correlating to 2 times lower than SSC. It is worth to highlight that *B. subtilis* was stabilised on SSE-01 to SSE-04 as showed by the low variation in the data, $17.8 \times 10^3/\text{mm}^2 - 37.6 \times 10^3/\text{mm}^2$. SSE-02 might provide a general with moderate anti bactericidal properties as the number of retained bacteria was reduced by half compared to the highest reading obtained in other surfaces. Alternatively, SSE-02, SSE-01 and SSE-03 were the best surfaces to repel individual adhesion by *S. aureus*, *E. coli* and *B. subtilis*, respectively.

Table 5-2 Data on Surface Topography Parameter, Contact Angle and Bacteria Adhesion undergone WEDM fabrications

Specimen	Surface Topography Parameter					Contact Angle Measurement	Bacterial Adhesion/mm ²		
	<i>Sa</i> (um)	<i>Sku</i>	<i>Ssk</i>	<i>Str</i>	<i>Sds</i>	CAM	<i>S. aureus</i>	<i>E. coli</i>	<i>B. subtilis</i>
SSE-01	3.34	2.53	0.03	0.77	4876.28	80.73 ± 0.25	67600 ± 1100	19100 ± 1000	29900 ± 2000
SSE-02	2.50	4.35	0.79	0.58	4863.23	82.75 ± 0.46	44100 ± 1000	32900 ± 4000	32300 ± 3400
SSE-03	2.91	2.53	0.12	0.57	4786.86	85.27 ± 0.95	98300 ± 1300	59400 ± 1000	17800 ± 1000
SSE-04	2.47	4.00	0.72	0.53	3874.63	85.77 ± 0.31	63600 ± 1000	34400 ± 1100	37600 ± 2000
TIE-01	3.36	3.09	0.21	0.89	4448.71	97.50 ± 0.12	42400 ± 2000	37700 ± 1000	17600 ± 3000
TIE-02	3.30	3.34	0.38	0.85	4372.52	97.23 ± 0.67	38400 ± 3000	51800 ± 1000	29100 ± 2000
TIE-03	3.34	3.62	0.50	0.93	4458.99	95.53 ± 0.74	43400 ± 6000	24100 ± 400	47100 ± 1000
TIE-04	3.26	3.24	0.39	0.84	4809.01	102.67 ± 0.23	34400 ± 3000	50200 ± 2000	17700 ± 1000

5.6 Bacteria Adhesion on WEDM titanium

TIE surfaces were exposed to *S. aureus*, *E. coli* and *B. subtilis* for four hours and the number of adhered cells were presented in Figure 5-13. Adherence of *S. aureus* ($82.6 \times 10^3/\text{mm}^2$) and *B. subtilis* ($45.8 \times 10^3/\text{mm}^2$) on TIE was successfully controlled by all TIE samples that went through the WEDM process. Comparable to the polishing process, *S. aureus* adhesion on TIE was greater than TIP as depicted by the lower adhesion on TIE-01, TIE-03 and TIE-04. The number of adhered *S. aureus* was $42.4 \times 10^3/\text{mm}^2$, $43.4 \times 10^3/\text{mm}^2$ and $34.4 \times 10^3/\text{mm}^2$, respectively. These figures were 40%, 22% and 37% lower relative to TIP-01, TIP-03 and TIP-04, respectively. Similarly, *E. coli* adhesion was also reduced on TIE-01 and TIE-03, contributing to 50% and 40% improvements over polished titanium. Shockingly, TIE-02 and TIE-04 induced *E. coli* adhesion, where the number of adhered cells increased by > 2 fold compared to TIP-02 and TIP-04. The adhesion of *E. coli* on these metals surpassed the adhesion by *S. aureus* and *B. subtilis*.

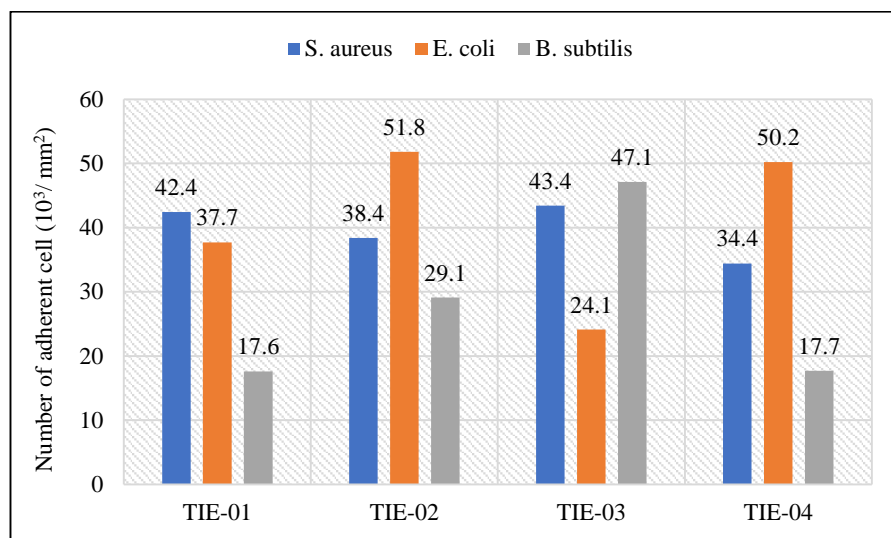


Figure 5-13 Graph of bacteria adhesion on WEDM titanium (TIE)

Similar to *S. aureus*, *B. subtilis*' adhesion on all TIE metals were also reduced when compared to polished titanium. When comparing the adhesion of the three tested bacteria, *B. subtilis* was successfully mitigated most TIE specimens, exhibiting the lowest surface coverage with the exception of TIE-03. The adhesion of *B. subtilis* varied between $17.6 \times 10^3/\text{mm}^2$ – $29.1 \times 10^3/\text{mm}^2$ on TIE-01, TIE-02 and TIE-04. The highest repellence of *B.*

subtilis was attained with in TIE-01 and TIE-04, both giving approximately $\sim 17.0 \times 10^3/\text{mm}^2$ of adhered cells. Meanwhile, the highest adhesion of *B. subtilis* occurred on TIE-02 ($47.1 \times 10^3/\text{mm}^2$), an increase of $\sim 2\%$ over the control ($45.8 \times 10^3/\text{mm}^2$). Overall, the current observation shows that TIE-04 repelled the adhesion of both Gram-positive bacteria, while TIE-03 prevented the anchoring of Gram-negative bacteria.

5.7 Correlation Between Surface Parameter, Contact Angle and Bacterial Adhesion

Collectively, the total number of cells attached onto all WEDM-stainless steel were 273.6×10^3 , 145.8×10^3 and $117.6 \times 10^3/\text{mm}^2$ for *S. aureus*, *E. coli* and *B. subtilis*, respectively. When compared to SSE, *S. aureus* marked a reduction, with only 158.6 retained on TIE. On the other hand, adhesion of *E. coli* increased to 163.8×10^3 while *B. subtilis* showed a negligible difference between TIE and SSE. When compared to polished titanium, WEDM-titanium marked a lower adhesion for *S. aureus* and *B. subtilis*, a reduction of 27.2 and 32.7%, respectively, while the adhesion of *E. coli* increased by 27.8% as shown in Table 5-3.

Table 5-3 Total number of bacteria adhered on stainless steel and titanium

Fabrication/Metal		<i>S. aureus</i> ($10^3/\text{mm}^2$)	<i>E. coli</i> ($10^3/\text{mm}^2$)	<i>B. subtilis</i> ($10^3/\text{mm}^2$)
Control (Mirror Finish)	Stainless steel	158.1 ± 7.5	14.5 ± 2.1	50.8 ± 3.2
	Titanium	82.6 ± 4.6	13.5 ± 1.9	45.8 ± 3.9
Polished	Stainless steel	212.6 ± 7.8	150.6 ± 8.9	141.1 ± 11.5
	Titanium	217.1 ± 6.5	127.5 ± 12.6	165.70 ± 4.8
WEDM	Stainless steel	273.6 ± 11.2	145.8 ± 8.4	117.6 ± 4.2
	Titanium	158.6 ± 2.1	163.8 ± 6.4	111.5 ± 7.0

Figure 5-14 shows the relationship between bacterial adhesion with surface parameters, CA, Sa , and Sds on SSE and TIE. It is important to note that all the WEDM-SSE and WEDM-TIE exhibited an enlarged hydrophobicity, with CA of $80.7^\circ < CA < 102.7^\circ$, showing that the surfaces were poor to moderately hydrophobic. It was found previously that adhesion of hydrophobic bacteria on hydrophilic surfaces was difficult to predict. This provided a very poor linear correlation between adhesion of hydrophobic bacteria with surface parameter. Previously, most of the properties studied were independent of surface properties, which was showed by very low regression values ($R^2 < 0.2$).

The effect of CA on the adhesions onto SSE and TIE are shown on Figure 5-14 (a & b). Previously in polishing, only bacteria with hydrophilic surfaces produced a linear correlation between the effect of CA with increasing number of adhesion (poor correlation). Current observations highlighted two important ones based on the SS. Firstly, similar to SSP, the effect of increasing CA, Sa and Sds on SSE failed to provide any correlation with the adhesion of *S. aureus* and *B. subtilis*. Secondly, the regression coefficient for linear correlation between *E. coli* and CA ($R^2 = 0.5408$) was higher than the regression on SSP-CA-*E. coli* ($R^2 = 0.341$), suggesting that *E. coli*, being moderately hydrophilic are compatible with the SSE despite it being moderately hydrophobic. The adhesion of *E. coli* on SSE increased linearly with increasing CA showing the affinity towards hydrophobic surfaces. Unlike *B. subtilis* which was purely hydrophilic, *E. coli* used in this study was considered to have moderately hydrophilic CSH, thus it may also generate an affinity towards hydrophobic surfaces similar to *S. aureus* within the tested range. ($< 90^\circ$). *S. aureus* in general has the highest adhesion rate on every specimen followed by *E. coli* and *B. subtilis*.

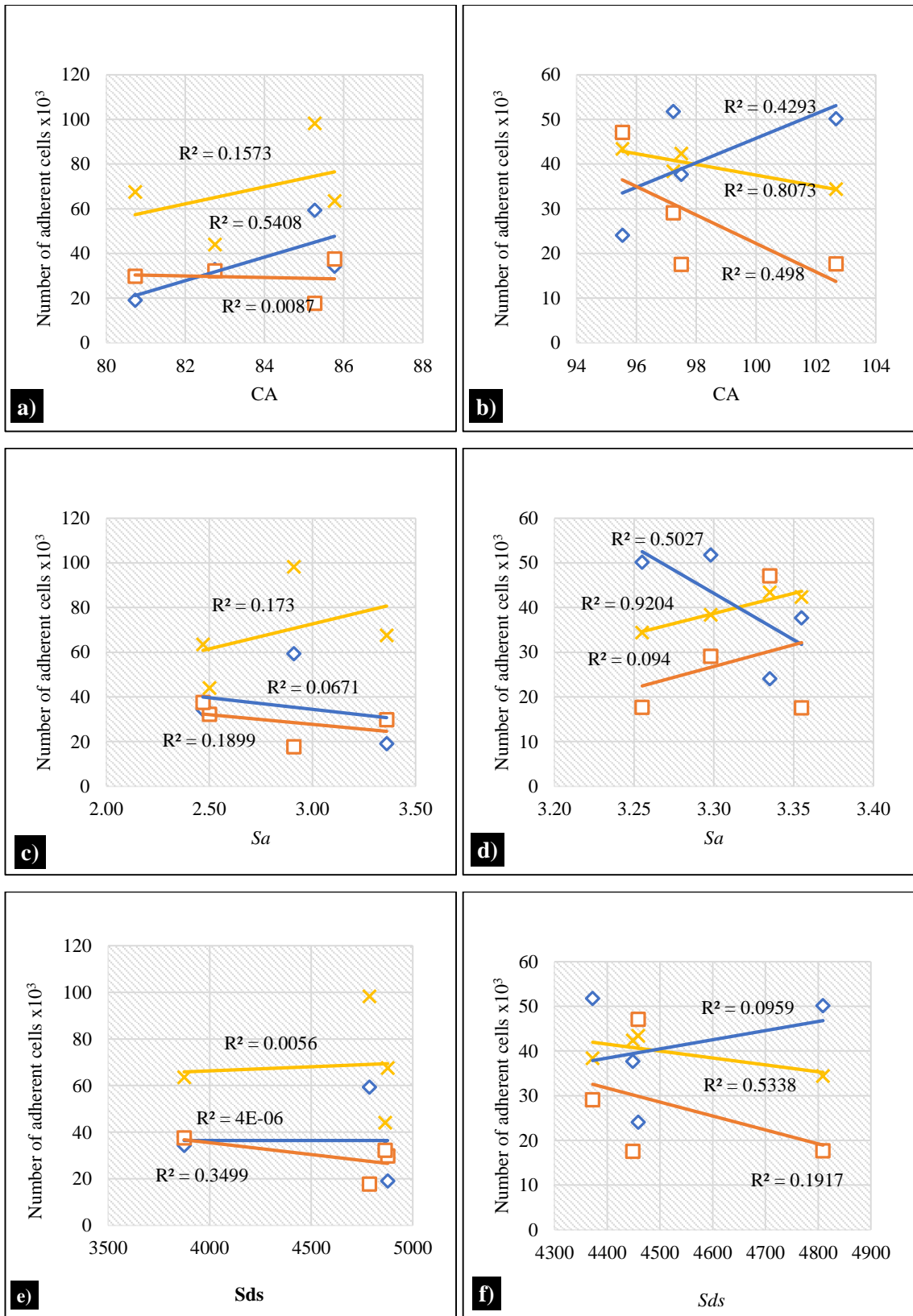


Figure 5-14 Correlation between S_a , S_{ku} , S_{sk} and bacteria adhesion (*S. aureus* ■, *E. coli* ◆ and *B. subtilis* □) on stainless-steel (a), (c), (e) and on titanium (b), (d), (f).

Interestingly, the adhesion of all species on TIE with respect to CA can be presented by linear regression with $R^2 = 0.81$, $R^2 = 0.43$ and $R^2 = 0.50$ for *S. aureus*, *E. coli* and *B. subtilis*, respectively. The CA of TIE surfaces are controlled at $95.2^\circ < CA < 102.7^\circ$ where a hydrophobic character was prominent. Following this, presumably the adhesion was merely controlled by the hydrophobic character of the surface. Figure 5-14 (b) shows that the adhesion of Gram-positive bacteria reduced with increasing CA, showed by moderate correlation, meanwhile the *E. coli* adhesion increased proportionally with increasing CA, represented by poor linear correlation. At this range of surface wettability, the adhesion mechanism might change slightly compared to adhesion with hydrophilic surface/mildly hydrophobic (SSP-TIP/SSE). On the hydrophobic surfaces, the adhesion mechanism might be contributed by the specific interaction of the hydrophobic proteinaceous component, where the effect of Gram type was more pronounced compared to the attraction between surfaces with similar characteristic (hydrophobic to mild hydrophobic). This might explain why a poor correlation was obtained for the effect of CA on *E. coli* adhesion, while other bacteria produced a moderate and strong correlation.

The *Sa* of the SSE and TIE ranged between 2.47–3.34 μm and 3.26–3.36 μm Figure 5-14 (c & d). It was mentioned previously that the adhesion capacity of the bacteria with *Sa* increased when $Sa >$ bacteria size, due to the additional contact area available for adhesion. The range used in this study since the size of *Bacillus Sp* reported can range up to 3 μm in length. As expected, the adhesion of all bacteria species on SSE was independent of *Sa*, suggesting that there were other properties that governed the adhesion. Meanwhile, a very strong correlation between *Sa* and *S. aureus* ($R^2 = 0.92$) and moderate correlation for *E. coli* ($R^2 = 0.50$) was observed with respect to TIE. In contrast, the adhesion behaviour of *B. subtilis* was independent of *Sa* suggesting that the *Sa* range was insufficient. Despite the low correlation for *S. aureus-Sa* on SSE, the number of adhering *S. aureus* increased with small changes in *Sa*, providing a positive correlation. On TIE, the relationship for *Sa-S. aureus* adhesion provided a positive strong correlation. Based on this observation, it is suggested that a new topography with emerging surface structures might increase the area for adhesion Bohinc, Dražić [159]. Being flexible and highly adhesive, *S. aureus* can easily position itself on both the horizontal and vertical planar.

The effect of Sds on adhesion is presented in Figure 5-14 (e & f). Sds value on SSE and TIE was in the range of 3900-4900/mm², much lower than that of polishing. While polishing flattened the surfaces by removing high peaks through grinding, the EDM process generates the formation of much higher peaks but is less dense. The effects of Sds can be easily explained by referring to adhesion on SSE-02 and SSE-04 for all three bacteria. The populations of *S. aureus*, *E. coli* and *B. subtilis* on SSE-04 ($Sa = 2.47 \mu\text{m}$, $Sk_u = 4.0$ and $Sds = \sim 3900/\text{mm}^2$) were $63.6 \times 10^3/\text{mm}^2$, $34.4 \times 10^3/\text{mm}^2$ and $37.6 \times 10^3/\text{mm}^2$, respectively. With nearly similar surface properties, the adhesion for these bacteria was reduced on the SSE-02 ($Sa = 2.5 \mu\text{m}$, $Sk_u = 4.0$ and $Sds = \sim 4900/\text{mm}^2$) to $44.1 \times 10^3/\text{mm}^2$, $32.9 \times 10^3/\text{mm}^2$ and $32.3 \times 10^3/\text{mm}^2$, lower by 31%, 5% and 14% than those on SSE-04, respectively. Predictably, the reduction occurred due to the increasing number of Sds to $\sim 4900/\text{mm}^2$. Nevertheless, the linear correlation for presenting the effect of Sds on adhesion was only available for *B. subtilis* on SSE and *S. aureus* on TIE, presenting a poor ($R^2 = 0.35$) and moderate correlation ($R^2 = 0.53$), respectively.

It is notable that the responses for adhesion capability in all species with respect to changes in CA, Sa and Sds values, were once again more sensitive on the TI metals than the SS metals, proven by the increased regression coefficient for the linear correlation based on the range studied. Previous observations showed that *B. subtilis* on TIP responded well to changes in CA and Sa , while current findings revealed that *S. aureus* on TIE reacted well to the changes in these properties within the tested range for individual metals. Nevertheless, the effect of surface skewness and kurtosis (Figure 5-15) on the bacterial responses was evaluated, where the effect of surface texture and irregularities was discussed (valleys and peaks).

In contrast with polished stainless steel and polished titanium ($Ssk < 0$), all metals that have undergone WEDM produced surfaces with positive skewness, ranging from 0.03 to 0.7. This shows that the post modification surfaces predominantly consisted of more peaks instead of valleys. However, the Sk_u values for these metals were narrowly distributed between 2.53–4.35, suggesting that the peak height distributions were controlled efficiently. Comparing SSE to SSP and TIE to TIP, the effect of skewness and kurtosis affected the adhesion mechanisms of bacteria. This owed to the distinct difference in surface morphology between polished samples and WEDM samples.

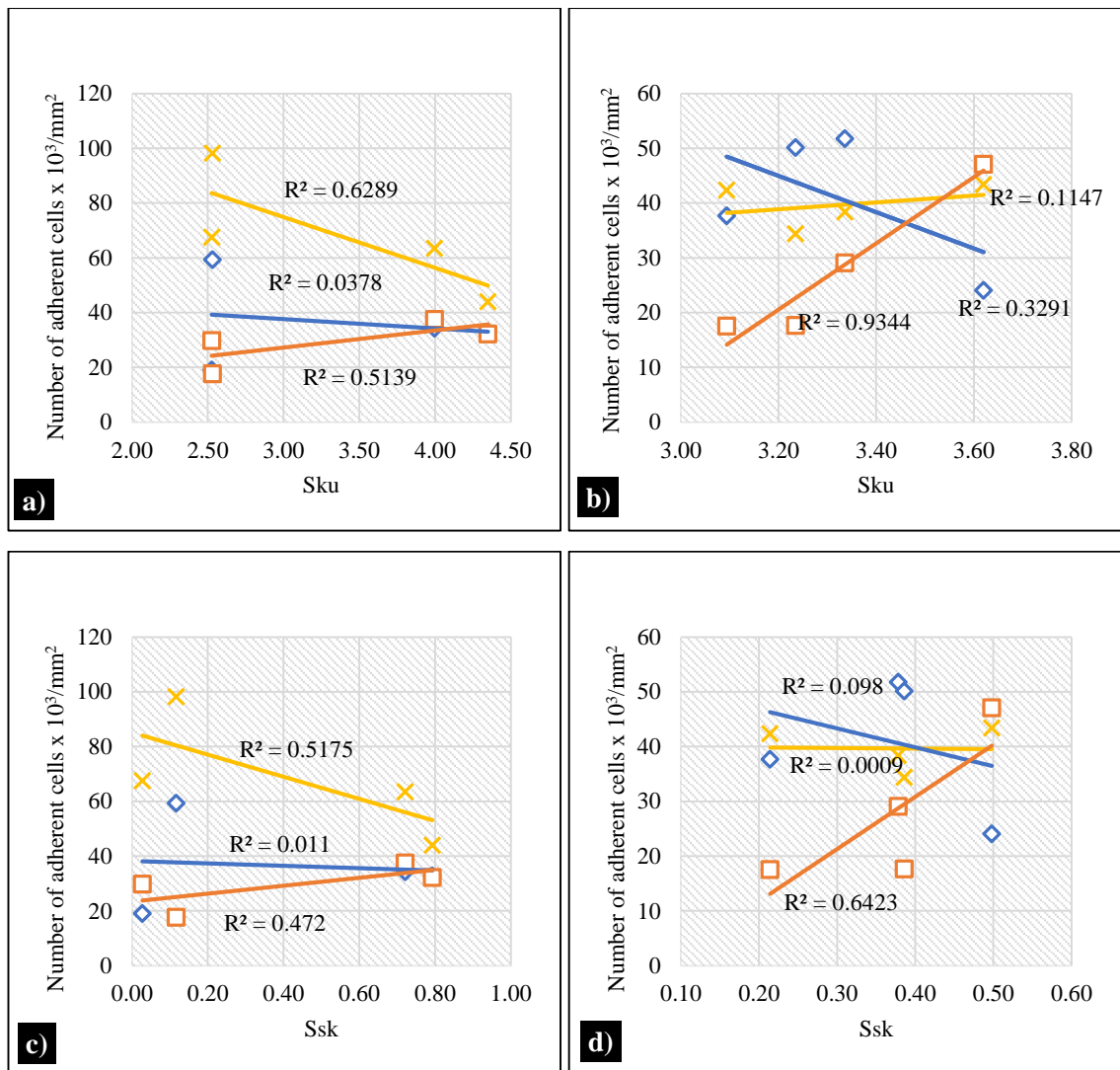


Figure 5-15 Correlation between Sku and Ssk and bacteria adhesion (*S. aureus* ■, *E. coli* ■ and *B. subtilis* ■) on stainless-steel (a), (c), (e) and on titanium (b), (d), (f).

When comparing the effect of Sku and Ssk after WEDM process on adhesion, the correlation revealed a different finding than those in polished metals. While the adhesion for three bacteria on SSP were independent of Sku, the opposite was true for SSE. Adhesion of both Gram-positive bacteria were highly correlated with changes in Sku. *S. aureus* adhesion reduced with increasing Sku, while *B. subtilis* adhesion increased proportionally with increasing Sku, depicted by R² = 0.63 and R² = 0.51, respectively. Conversely, *E. coli* once again proved that Sku in polishing and WEDM is not involved in adhesion on SSE and SSP, showed by very low R² < 0.2. Meanwhile, the effect of Sku on *B. subtilis* onto TIE revealed the strongest linear correlation, with R² = 0.93. Meanwhile, negative linear with poor correlation was obtained by *E. coli* on, whilst *S.*

aureus was not affected by the S_{ku} value within the tested S_a . Since the S_a value for TIE already exceeded the size of *S. aureus*, the range of peak height distribution does not inflict any control measures, and bacteria can easily adhere on any protruding features arising after the fabrications.

The effect of skewness was studied, and the results are shown in Figure 5-15 (c&d) for SSE and TIE, respectively. On both metallic surfaces, *E. coli* adhesion was not affected by the S_{sk} as shown by the very low regression coefficient. However, the *Bacillus subtilis* adhesion was highly affected by the distribution of peak to valley structures, given by the positive correlation for SSE ($R^2 = 0.47$) and TIE ($R^2 = 0.64$). Meanwhile, *S. aureus* adhesion on SSE reduced proportionally with increasing S_{sk} as shown by the moderate linear correlation ($R^2 = 0.52$). The behaviour of *E. coli* against the effect of either valley in polishing (-ve S_{sk}) or protruding texture of WEDM (+ve S_{sk}) proved that the topography of the surfaces does not directly influence the *E. coli* adhesion, which shows that it may use a different mechanism to attach to inert surfaces which is yet to be understood.

5.8 Chapter Summary

All WEDM specimens produced electro-erosive machined surfaces with Sa between 2.5 to 3.5 μm with positive skewness and Sku greater than 3. From the SEM images, more cracks and deep craters were observed on Ti6Al4V relative to 316L specimens. Cracks with sizes smaller than the bacterial size do not affect the adhesion performance while deep craters may contribute to the entrapment of bacteria due to the diameter being bigger than the bacterial dimension. As expected, the machine feed rate does not influence the average roughness, Sa (poor correlation). Meanwhile, Sz (max height of surfaces) showed a strong correlation, therefore this property can be controlled by varying the machine feed rate. Even though not all spatial parameters reflected a significant correlation with the CA measurement, Sds showed a strong correlation for both metals. Comparing against polished specimens, a higher Sds promotes hydrophilic surfaces while in WEDM, low Sds values with positive skewed surfaces promote hydrophobic surfaces by trapping air between the peaks.

The sensitivity of bacterial adhesion to changes in CA, Sa , Sds , Ssk and Sku was pronounced on the titanium surface. Unlike SSE, the relationship of these properties and the adhesion on TIE often produced a negative/positive linear correlation with a regression range from 0.4 to 0.9. Since the SSE and TIE ranged from mild hydrophobic to hydrophobic, it was observed to disturb the adhesion of mild hydrophilic bacteria and hydrophobic bacteria. Before any bacterial adhesion can be controlled through varying CA, Sa and Sds , the adhesion must be accomplished within the surface with similar properties, either hydrophobic-hydrophobic or hydrophilic-hydrophilic interaction. If the contact was between two opposite properties, the contribution of these properties towards increasing/reducing the adhesion was often insignificant. Apart from that, it is worth to note that the adhesion of Gram-negative bacteria on metallic surfaces after WEDM fabrication was more difficult to predict, because the effect of hydrophobic surfaces may provoke a specific binding based on the proteinaceous compound, which then must be discriminated based on the Gram types.

Chapter 6

Laser-Assisted Surface Characterisation with respect to Contact Angle Measurement and Bacterial Adhesion

6.1 Introduction

This chapter discusses the effect of additional features on metallic surfaces (textures and grains of stainless steel and titanium) that have undergone femto-second irradiation on the behaviour of bacterial adhesion using two model organisms, *S. aureus* and *E. coli*. Four different surfaces were produced for each metal that has gone through various irradiation techniques (has been detailed in Chapter 3 and Chapter 4) and were fabricated in air and argon. The modified surfaces were then cleaned and sterilised before being exposed to the bacterial suspension (initial OD set at 1.0), containing approximately 1×10^8 CFU/ mL of cells in the mid exponential phase for four (4) hours to determine the rate of adhesion. The surface morphologies before and after four hours of cultivation were captured by SEM and fluorescent microscope. For fluorescence imaging, the adhered bacteria were stained with Syto9 dye and data was taken from 15 randomly selected images of three replicates. The metal samples were also viewed under SEM using low and high magnifications (1000x–20,000x), where the adhesion density was thoroughly observed to examine the effectiveness of the nano-structures for preventing adhesion.

Following the laser treatment, the laser induced periodic surface topography (LIPSS) was termed as self-organised structures which refer to the spontaneous features formed under laser fluence and varied pulses [85]. The modified surface (Figure 6-1), with additional 3D topography, consisting of LIPSS and nano-grains was expected to increase the surface hydrophobicity, thus controlling the bacteria-surface interactions. The nano-surface will also alter the morphology of the adhered cells, thus affecting the

survivability and its proliferation. To obtain a surface with such features with an increased ability to repel adhesion, the treatment processes were carried out in two conditions, i) in air and ii) argon. The objective of the chapter was to use a physical method for producing a highly hydrophobic surface by surface texturing that is producible, robust and with increased ability to prevent bacteria adhesion. The effectiveness of the treatment was discussed by i) determining the bacterial adhesion on the fabricated surfaces and ii) finding the correlation between bacterial adhesion with surface topographies and wettability. The laser parameter and the description of the fabricated surfaces is presented in Table 6-1 for both stainless steel and titanium, while the SEM images are provided in Appendix A1.

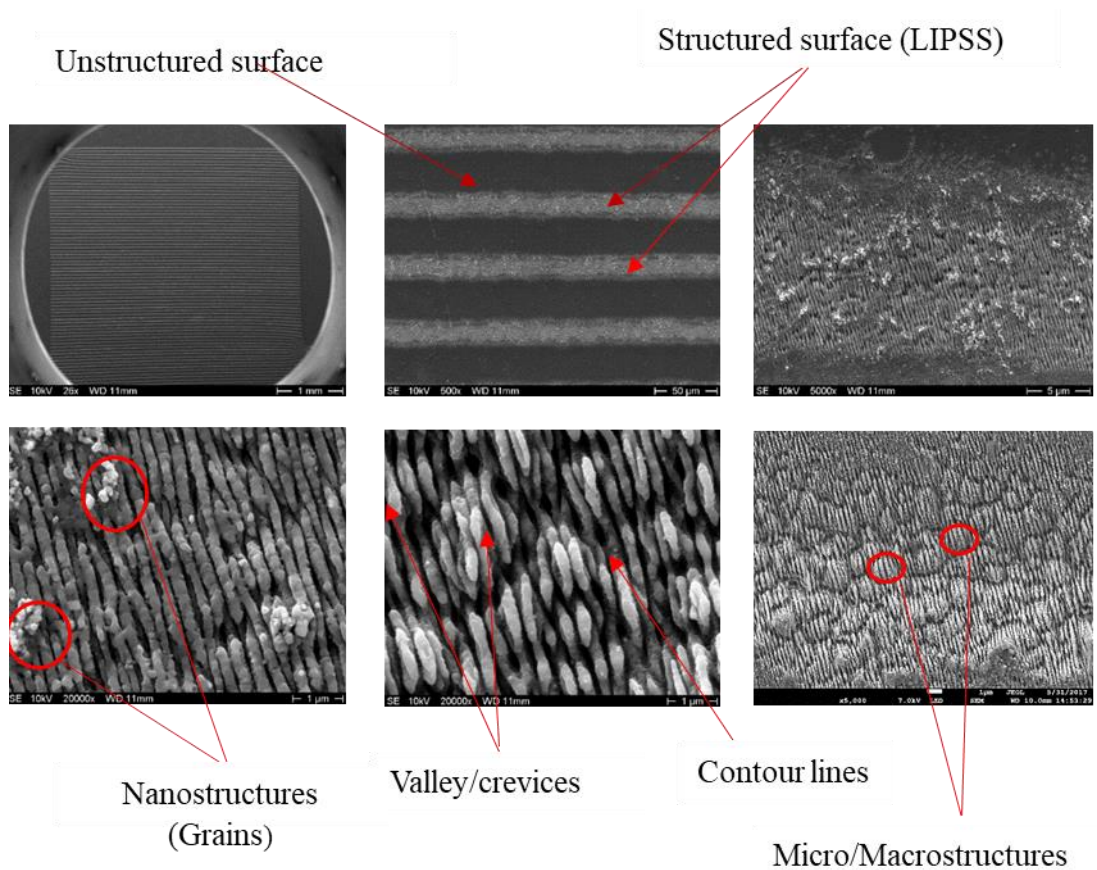


Figure 6-1 Images for the titanium that have undergone femto-second irradiation techniques showing all the available features on the modified surfaces viewed with SEM.

Table 6-1 Laser parameter for different surface topographies

Sample	Surface Description	Power (mW)	Scan speed (mm/s)	N
Control	316L Stainless steel undergone polishing.	-	-	-
SSL-01-/ TIL-01	The LIPPS form more convex micro to macrostructures with maximum waviness, very coarse line with nanograins made from molten metal.	120	10	1
SSL-02 /TIL-02	The LIPPS were more flatten with reduced waviness and shallow valleys between micro-macrostructures. The control lines were smoother.	120	50	1
SSL-03 /TIL-03	The LIPPS are flattened, reduced valleys and waviness, with longer and smoother contour lines.	120	50+50	2
SSL-04 /TIL-04	The LIPPS are flatten with reduced waviness, increased nanograins structures appeared on the top of the contour lines	80	10+50	2

6.2 Laser-Assisted specimen: The correlation of surface topography and wettability

Laser-assisted technique parameters vary on the power, velocity and number of laser-running on the stainless-steel and titanium surfaces as shown in Table 6-2. Both specimens of stainless steel and titanium were treated with air and argon gases after the scan process to examine the effect of oxidation on the metal surfaces. Surface topography data analysis will cover the height, spatial and hybrid family, while for the wettability test, data from water contact angle measurement were used in the analysis.

Table 6-2 Laser parameter for different surface topographies

Sample	Power (mW)	Scan Speed (mm/s)	Distance (μm)	N
LS-01	120	10	50	1
LS-02	120	50	50	1
LS-03	120	50	50	2
LS-04	80	10+50	50	2
LT-01	120	10	50	1
LT-02	120	50	50	1
LT-03	120	50	50	2
LT-04	80	10+50	50	2

6.2.1 Height Parameter Analysis

The assessment of suitable surface parameters allowed the prediction of the peaks or deep-valley surfaces. Parameters involved by means of the profile method included average roughness (Sa), kurtosis (Sku), skewness (Ssk), maximum height profile (Sz), maximum peak height (Sp), maximum valley depth (Sv). Area parameters allow evaluation of the area quantitatively in all directions that are technically significant. Evaluated values of individual parameters for 316L (Air & Argon) were plotted as shown in Figure 6-2 (A – C). Mixed values of were roughness recorded to demonstrate the higher value for Argon treated compared to Air treated specimens. SSL-01 (Argon) recorded a value of $0.56 \mu\text{m}$ while SSL-01 (Air) gave a value of $0.29 \mu\text{m}$ with an increment of about 48%. Another higher increase of Sa (61%) for stainless-steel was SSL-04 with Argon treated surface at $0.18 \mu\text{m}$ while for the Air treated, the Sa was equal to $0.07 \mu\text{m}$. For individual specimens, the increased roughness from the as-received samples based on the power and velocity of the laser was not too high where the values were $0.29 \mu\text{m}$, $0.17 \mu\text{m}$, $0.19 \mu\text{m}$ and $0.07 \mu\text{m}$ for SSL-01, SSL-02, SSL-03 and SSL-04 respectively

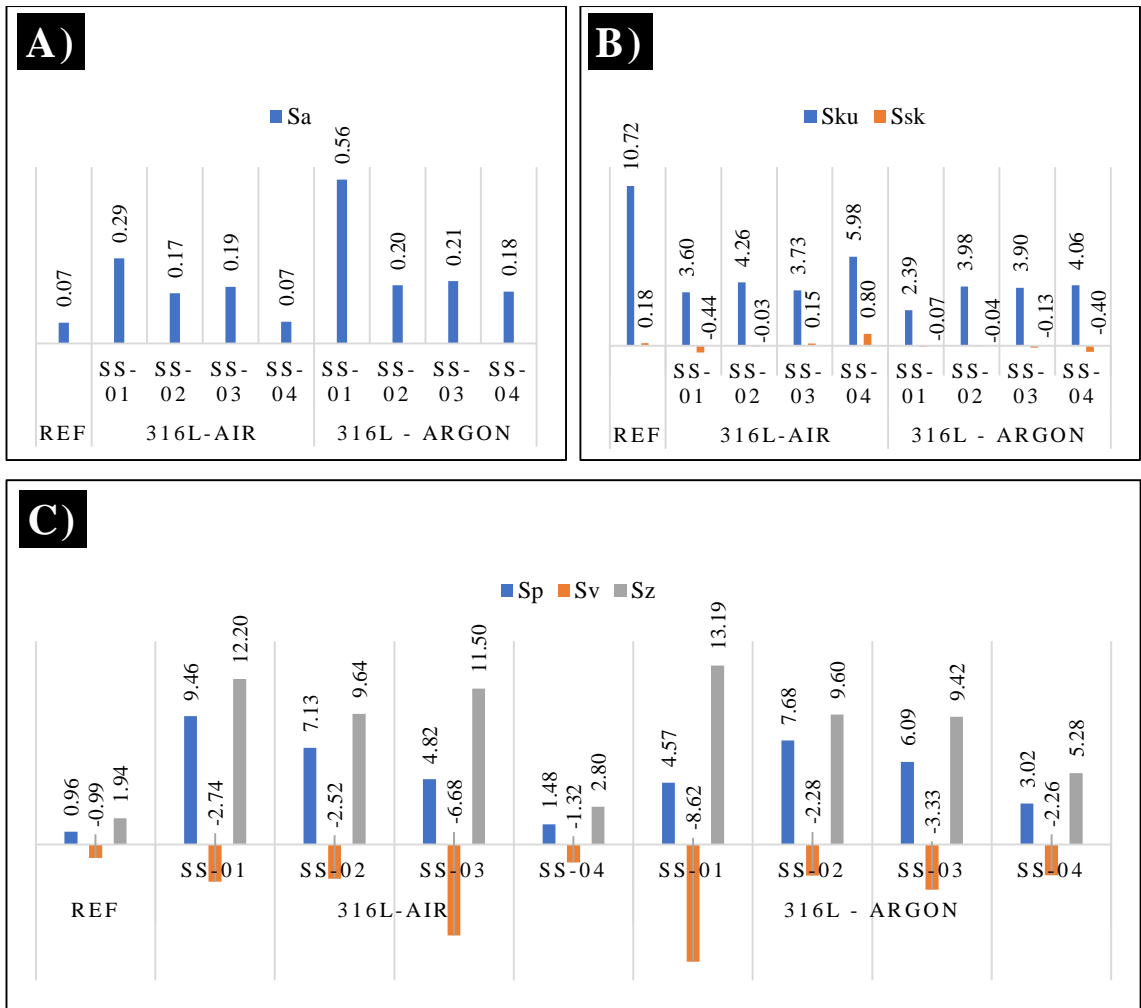


Figure 6-2 Graph of height parameter on 316L and Ti6Al4V with respect to a) S_a and S_q , b) S_{ku} and S_{sk} and c) S_p (max peak height), S_v (max valley depth) and S_z (max height of surface)

For Argon gas treated surface, the S_a was equal to 0.56 μm , 0.20 μm , 0.21 μm and 0.18 μm for SSL-01 (Ar), SSL-02 (Ar), SSL-03 (Ar) and SSL-04(Ar), respectively. Hence, the overall percentage increase from Air treated and Argon treated 316L was between 9.5% to 61%. For the height surface distribution, surface kurtosis shows values greater than 3 except for SSL-04 (Ar) with 2.39. All SSL-(Ar) had negative skewness compared to SSL-(Air) where only SSL-01 and SSL-02 had negatively skewed surfaces. On the summit value, S_p (max height peak) for Air treatment, SSL-01 to SSL-03 showed high values of peaks ranging between 4.82 to 9.46 μm and low on SSL-04 with 1.48 μm of peak height. For the valley depth (S_v), SSL-03 showed a deep valley with a value of -6.68 μm while the others showed -2.74 μm , -2.52 μm and 1.32 μm for SSL-01, SSL-02 and SSL-04 respectively. In contrast, for Argon treatment laser fabrication stainless-steel,

all specimens showed high peak height with values of 4.57 μm , 7.68 μm , 6.09 μm and 3.02 μm for SSL-01, SSL-02, SSL-03 and SSL-04, respectively. For the valley depth, it showed values of 8.62 μm , 2.28 μm , 3.33 μm and 2.26 μm for SSL-01, SSL-02, SSL-03 and SSL-04, respectively.

When comparing Air and Argon treated surfaces, the max height surface (S_z) for SSL-(Air) showed a fluctuation by height values according to the laser-scanned parameters. S_z values when compared to SSL-(Argon) and SSL-01 (Air) recorded a value of 12.20 μm followed by 9.64 μm , 11.50 μm and 2.80 μm for SSL-02 (Air), SSL-03 (Air) and SSL-04 (Air), respectively. Conversely, the same laser fabrication treatment with Argon gas showed values of 13.19 μm , 9.60 μm , 9.42 μm and 5.28 μm for SSL-01 (Ar), SSL-02 (Ar), SSL-03 (Ar) and SSL-04 (Ar) respectively. SSL-01 indicated an increase in S_a by 7.5% from Air to Argon treated surfaces. Unfortunately for SSL-03, S_a for Argon decreased by 16.5% roughness. In general, Argon gas treatment had no influence on the average roughness, S_z parameter. On the whole, as a reflection from the S_{ku} and S_{sk} values, all specimens exhibited higher peak surfaces with deep valleys. This type of profile will be investigated towards the cell-adhesion phenomenon.

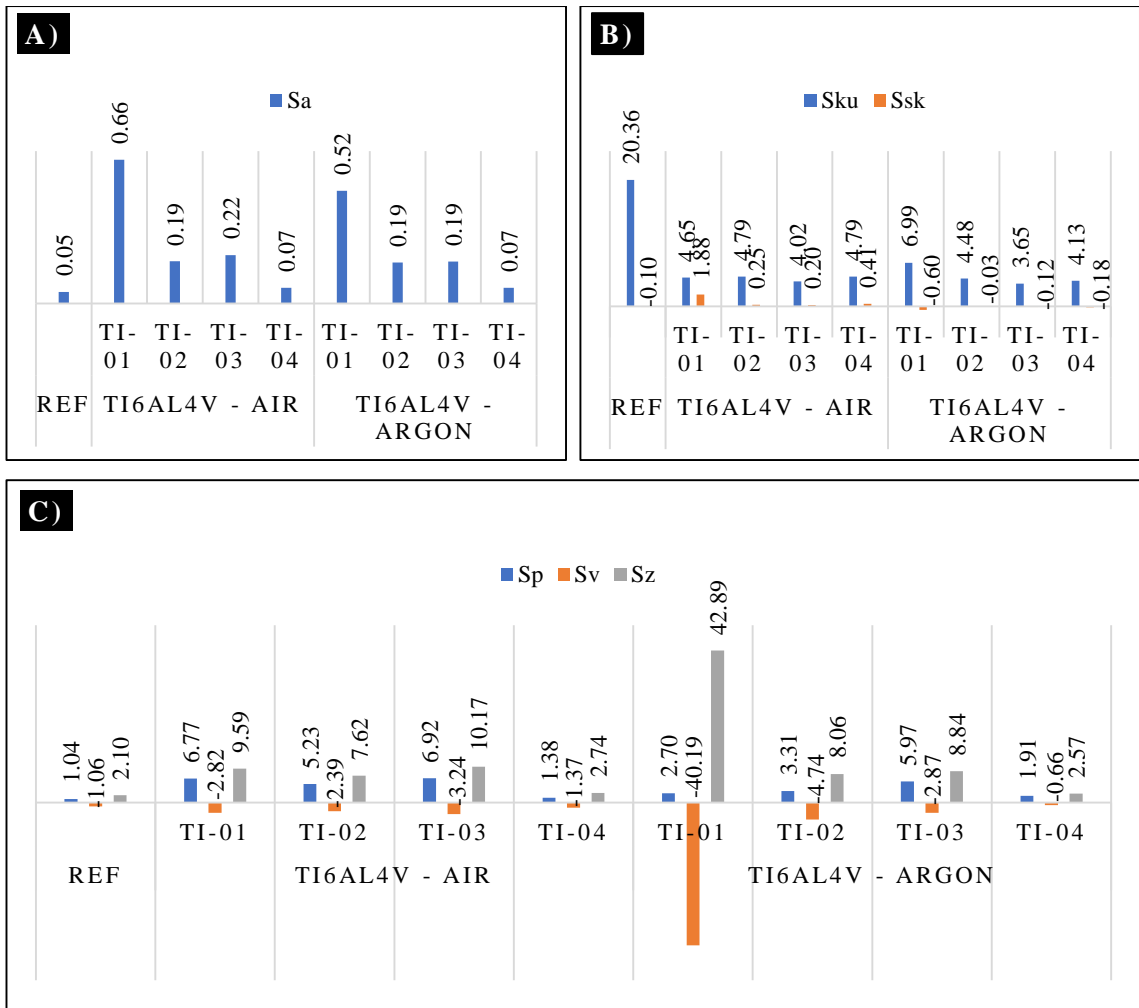


Figure 6-3 Graph of height parameter on 316L and Ti6Al4V with respect to a) *Sa* and *Sq*, b) *Sku* and *Ssk* and c) *Sp* (max peak height), *Sv* (max valley depth) and *Sz* (max height of surface)

Values of individual parameters for Ti6Al4V (Air & Ar) were plotted as shown in Figure 6-3 (A – C). Mixed values of roughness were recorded when comparing Argon and Air treatment surfaces. TIL-01 (Air) recorded a value of 0.66 μm while TIL-01 (Ar) recorded a value of 0.52 μm , a reduction of 21.2%. Another significant reduction happened at TIL-04 from 0.22 μm (Air) reduced to 0.19 μm . Interestingly, both TIL-02 and TIL-03 showed similar roughness for Air dan Argon treatment processes. All the specimens showed higher than 3.00 kurtosis values while for the skewness, the sign changed from +ve in Air to -ve in the Argon treatment fabrication. For the valleys and peaks analysis, SP (max height peak) for Air treatment, all TIL-01 for Air dan Argon treatment produced higher *Sz* compared to other specimens. The SP also showed all specimens formed

higher peaks with values ranging between 1.38 μm to 17.84 μm while on valley depth (S_v), all the specimens formed low -ve valleys except for TIL-01 (Ar) which had an extremely high S_v value of -40.19 μm .

6.2.2 Laser scan Speed correlation with S_a and S_v

Figure 6-4 below shows a graph of the correlation between laser scan speed and average roughness, S_a whereas all materials shows strong negative correlations with laser scan-speed. 316L (Ar) gives regression values of 0.9799 while for 316L (Air) the R^2 is equal to 0.8386. On Ti6Al4V, both metal treatment whether in Air or Argon, showed a R^2 close to 1.00. Therefore, laser scan speed plays an important role in average roughness, S_a either in Air or Argon gas treatment.

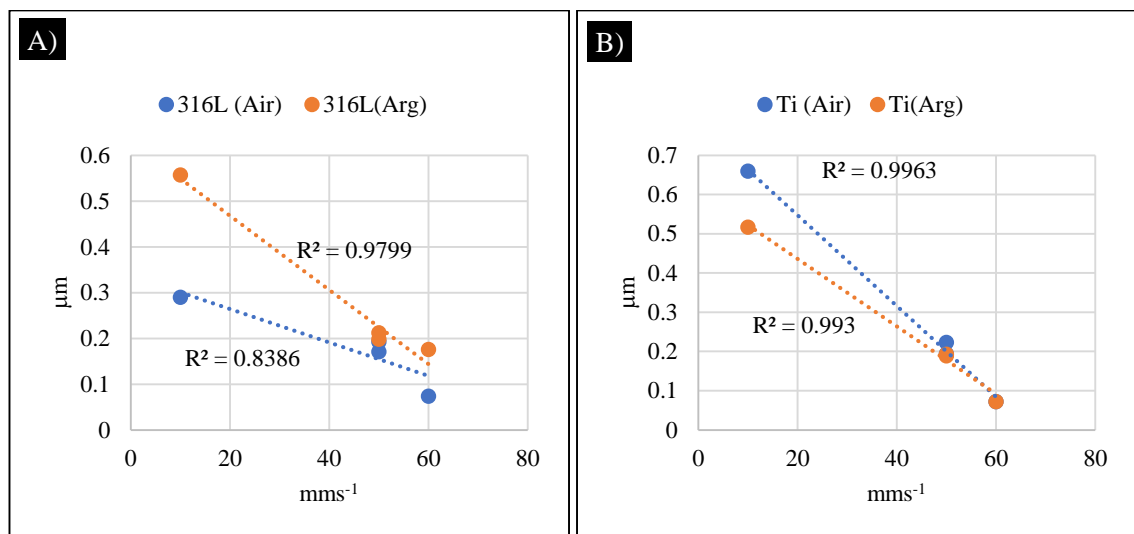


Figure 6-4 Correlation between A) average roughness, S_a and laser scan speed (mms⁻¹) on 316L (air) and 316L (argon), B) average roughness, S_a and laser scan speed (mms⁻¹) on Ti6Al4V (air) and Ti6Al4V (argon)..

Figure 6-5 shows the correlation between laser scan speed and maximum height surfaces (S_z). From the graph, 316L (Air) showed a moderate correlation while 316L(Ar) showed a strong correlation with the scan speed. For Ti6Al4V, both treatments show a strong correlation with scan speed with regression values 0.9553 and 0.9957 for Air and

Argon treatments respectively. In conclusion, laser scan speed highly influences the S_a and S_z of 316L stainless-steel and Ti6Al4V titanium surfaces.

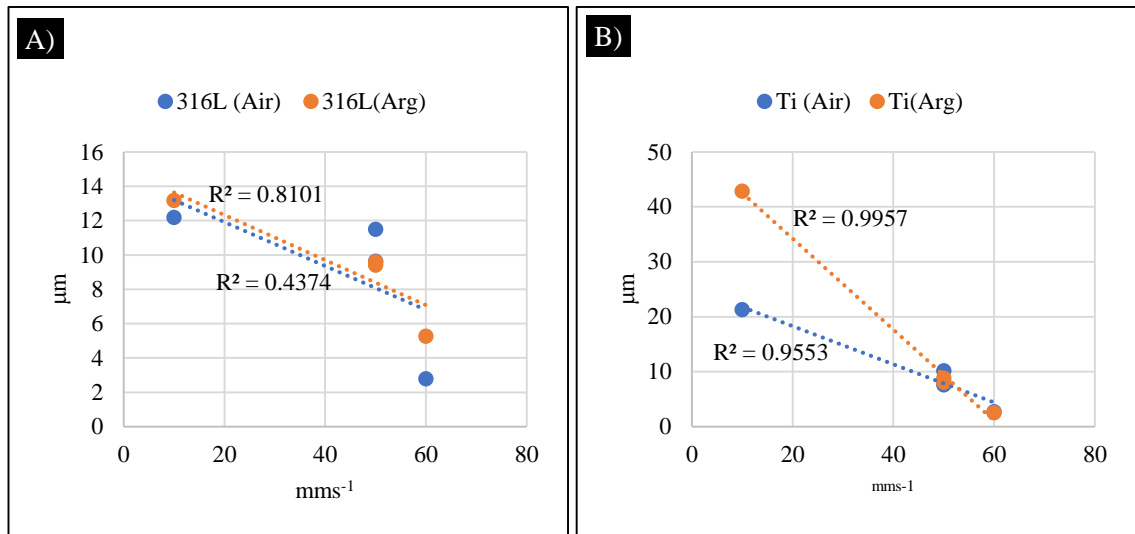


Figure 6-5 Correlation between A) max height surface, S_z and laser scan speed (mms⁻¹) on 316L (air) and 316L (argon), B) max height surface, S_z and laser scan speed (mms⁻¹) on Ti6Al4V (air) and Ti6Al4V (argon).

6.2.3 Spatial and Hybrid Parameter Characterisation

In section 6.2.1, the discussion covered how surface height parameters were influenced by laser scan speed where the results showed a strong influence on both metals. Besides that, for the surface texture analysis, spatial and hybrid parameters provide the spacing and texture information such as isotropic or anisotropic [156]. Therefore, in

Table 6-3, data on spatial and hybrid parameters for laser-assisted on 316L and Ti6Al4V presented with the information on the auto-correlation length (Sal), texture direction (Std), texture aspect ratio (Str), developed interfacial area ratio (Sdr) and summit density (Sds).

Referring to the table, it shows that *Sal* for 316L (Ar) had higher values compared to 316L (Air) in contrast with Ti6Al4V that showed an Air treated specimen had a slightly higher *Sal* compared to Argon gaseous treated specimens. The values for 316L(Air) reduced by 23.45%, 40.0%, 36.3% and 23.21% for SSL-01, SSL-02, SSL-03 and SSL-04, respectively. In contrast with 316L, the values for Ti6Al4V increased by 11.65% and 17.55% for TIL-01 and TIL-03, no change for TIL-02 and reduced by 40.81% for TIL-04. By referring to the *Std* and *Str* values for both specimens, all 316L specimens treated in Air or Argon showed a dominant surface lay whereas the *Std* had a low degree and *Str* approached 0. In contrast with Ti6Al4V specimens, whereas for an Air treated surfaces, all specimens showed dominant lay except for TIL-02 which produced isotropic surfaces with no available data for *Std* and *Str* greater than 0.50. No measured data on *Std* means the surfaces were isotropic (no dominant direction) while clearly for as-received (REF) they have dominant lay with the angle $> 80^\circ$ as shown in Figure 6-7.

Table 6-3 Spatial and hybrid parameter data on 316L and Ti6Al4V

Specimen	Spatial Parameter			Hybrid Parameter			
	<i>Sal</i> (μm)	<i>Std</i> (deg)	<i>Str</i>	<i>Sa</i> (μm)	<i>Sdr</i> (%)	<i>Sds</i>	
316L (Air)	SSL-01	2.87	88.62	0.02	0.29	60.83	26945.58
	SSL-02	0.99	-88.39	0.32	0.17	34.31	26409.43
	SSL-03	2.00	-1.82	0.11	0.19	37.61	26571.67
	SSL-04	0.89	-88.38	0.03	0.07	3.89	23026.09
316L (Ar)	SSL-01	3.75	87.26	0.01	0.52	61.64	24787.59
	SSL-02	1.67	87.57	0.21	0.19	40.07	27218.81
	SSL-03	3.14	87.18	0.19	0.19	41.22	26649.12
	SSL-04	1.16	87.46	0.30	0.07	1.76	24310.94
Ti6Al4V (Air)	TIL-01	3.26	3.03	0.01	0.66	76.63	19031.06
	TIL-02	1.07	n/a	0.60	0.19	48.54	26715.30
	TIL-03	1.54	-89.08	0.21	0.22	55.25	26770.31
	TIL-04	2.61	89.82	0.19	0.07	3.50	23618.40
Ti6Al4V (Ar)	TIL-01	2.88	-89.95	0.01	0.52	61.64	24787.58
	TIL-02	1.07	n/a	0.70	0.19	40.07	26649.12
	TIL-03	1.27	n/a	0.60	0.19	41.22	27218.81
	TIL-04	4.41	n/a	0.05	0.07	1.76	24310.94

The discussion on hybrid parameters focuses on summit density (Sds) and developed interfacial area ratio (Sdr). Sds is the number of summits per unit area making up the surface while Sdr is an expressed percentage of additional surface area contributed by the texture as compared to an ideal plane the size of the measurement region. Typically, Sdr will increase with the spatial intricacy of the texture, whether Sa changes or otherwise. From Table 6-3, the Sdr for 316L(Air) was lower compared to 316L(Ar) except for SSL-04. The Sdr for 316L(Air) were 60.83%, 34.31%, 37.61%, and 3.89% while for 316L(Ar), the Sdr were 61.64%, 40.07%, 41.22%, and 1.76% for SSL-01, SSL-02, SSL-03 and SSL-04 respectively. The Sds for 316L demonstrated higher values compared to polished and WEDM specimens with 26945, 26409, 26571, and 23026 for Air treated specimens and 24787, 26649, 27218, and 24310 for Argon treated specimens. In contrast, Ti6Al4V showed Sdr with values of 76.63%, 48.54%, 55.25% and 3.50% for Air treated surfaces and 61.64%, 40.07%, 41.22% and 1.76% for Argon treated surfaces.

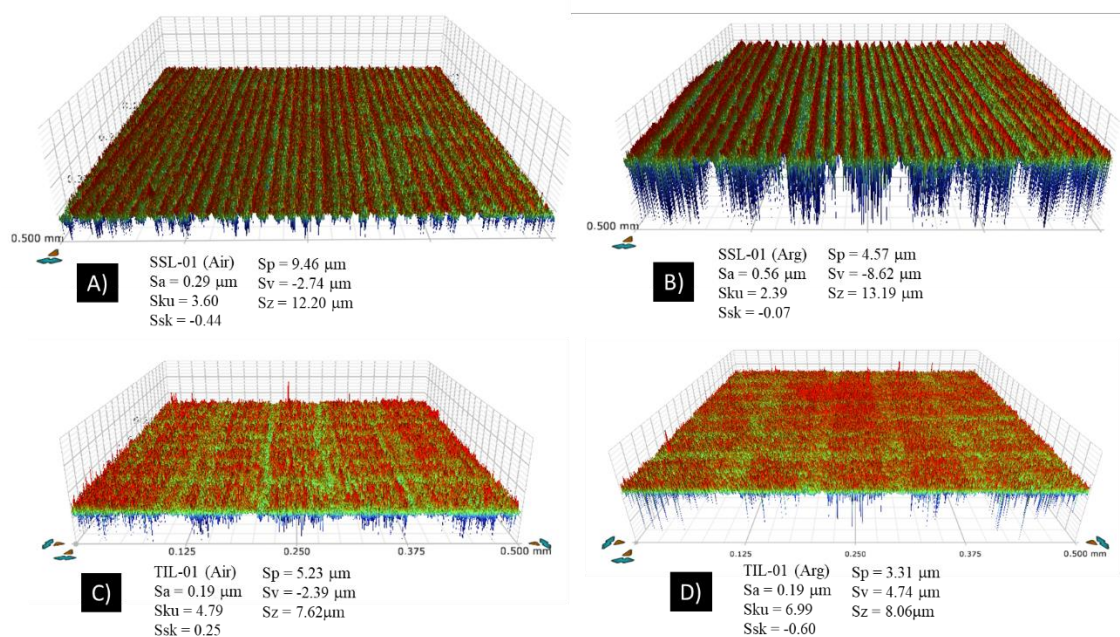


Figure 6-6 3D optical profilometry images on SSL-01 (Air) and SSL-01 (Ar)

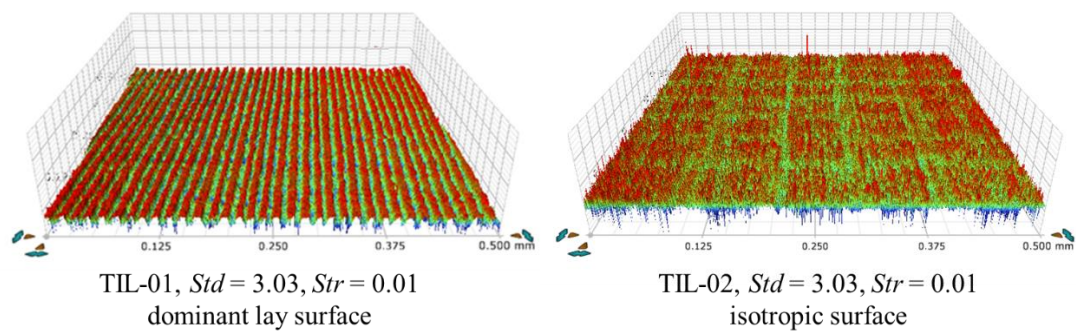


Figure 6-7 The difference between dominant lay surface and isotropic surface of Ti6Al4V

6.3 The correlation of Contact Angle with Surface Topography Parameter

The graph in Figure 6-8 shows the water contact angle measurement on 316L and Ti6Al4V laser-assisted fabrication treated with Air and Argon gas. In overall terms, all specimen showed an increase of contact angle with respect to as-received substrates (hydrophobic). 316L treated on Air produced hydrophobic surfaces with 129.5°, 104.4°, 133.8° and 127.3° CA. The figures for Argon treated surfaces were 134.2°, 104.7°, 130.2°, and 101.1° with respect to SSL-01, SSL-02, SSL-03 and SSL-04. For Ti6Al4V, on Air treated surfaces, the contact angle values were 135.7°, 138.6°, 128.7° and 129.6° while for Argon treated surfaces the values were 135.8°, 131.6°, 141.8° and 102.8° with respect to TIL-01, TIL-02, TIL-03 and TIL-04 respectively. As in the 316L contact angle, the argon gas resulted in a higher contact angle compared with an Air exposed surface.

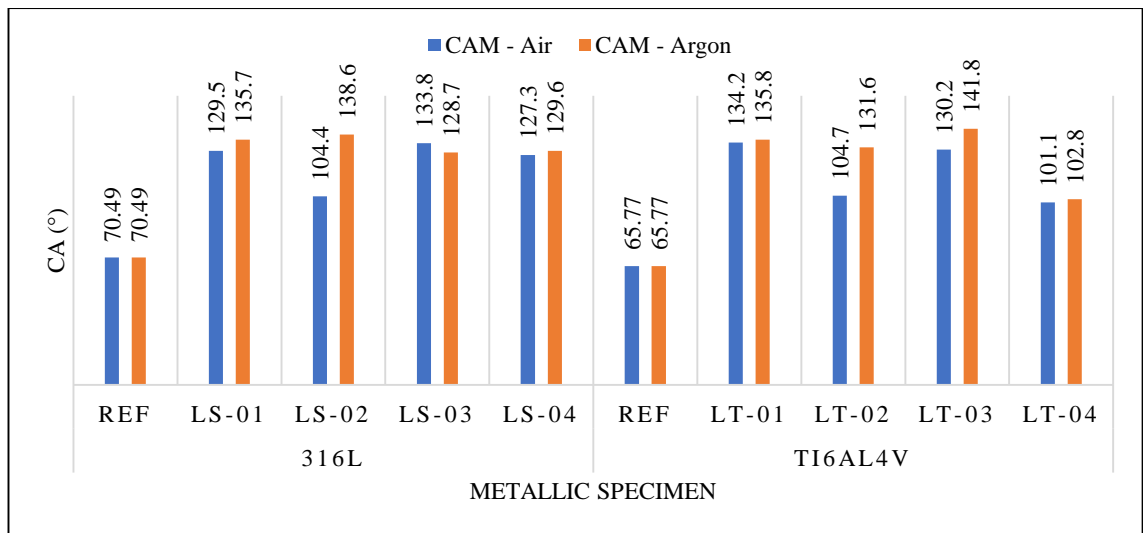


Figure 6-8 Graph of water contact angle on laser-assisted on 316L and Ti6Al4V

The effect of surface properties on the CA measurement with respect to laser-assisted process is presented in Figure 6-9 (A–E). Contact angle data plotted against Sa , Sku , Ssk , Sal , Sdr and Sds and linear regression was plotted with R^2 values to indicate the accuracy of the correlation. Variations in responses with correlation between 0.0052 to 0.7136 was observed towards contact angle values over 101.1° to 141.8° . The graph shows that Ti6Al4V (Ar) has a strong negative correlation with R^2 equal to 0.7136 and Ti6Al4V (Air) produced a moderate positive correlation with R^2 equal to 0.6022. For the kurtosis relationship with CA measurement, it shows no correlation for both 316L and Ti6Al4V specimens (Air & Ar). As for skewness, 316L(Ar) shows a moderate correlation with CA measurement with R^2 equal to 0.4607 but no correlation was recorded for 316L(Ar).

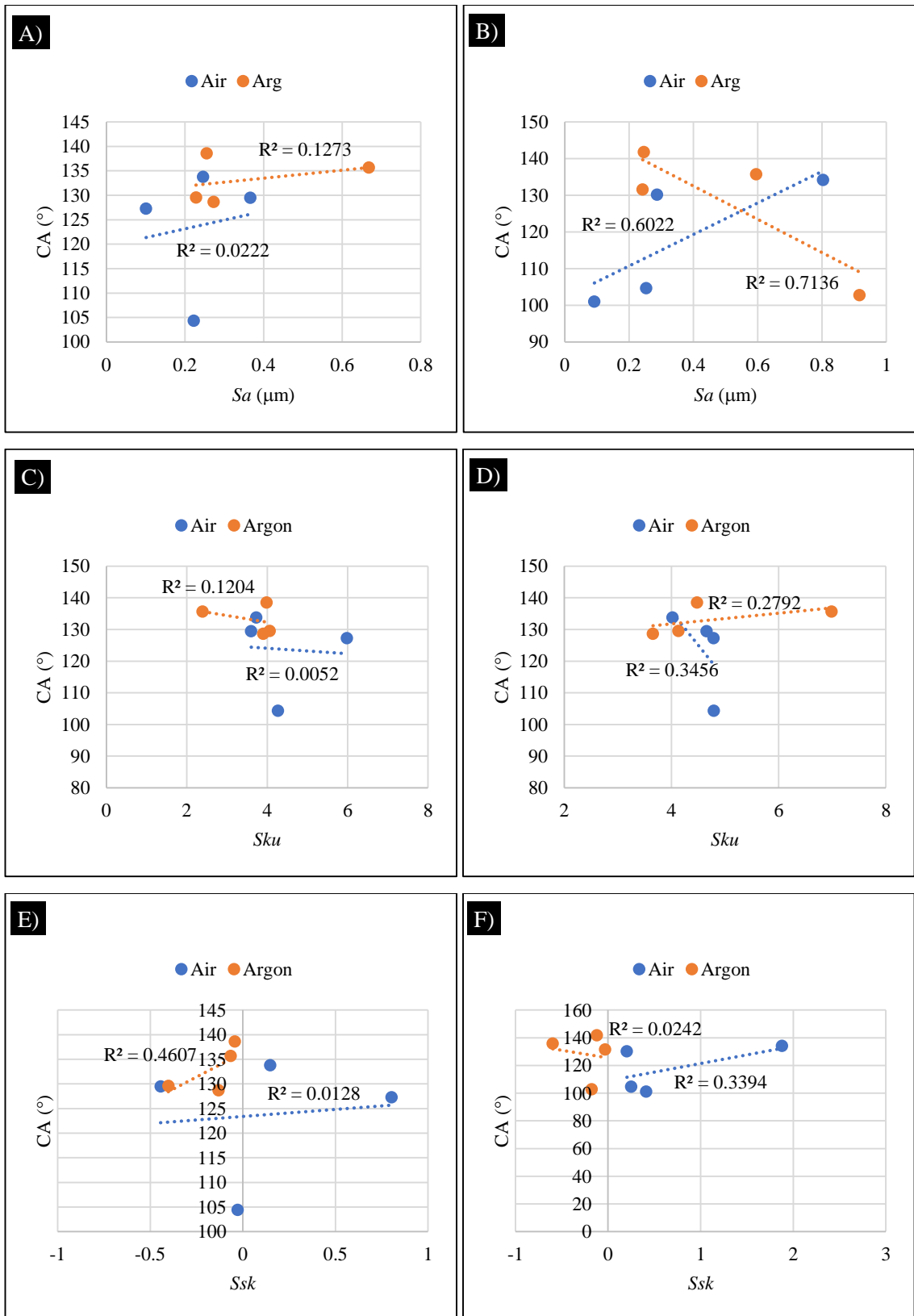


Figure 6-9 Correlation between contact angle and A) average roughness, Sa on 316L C) surfaces kurtosis, Sku on 316L, E) surface skewness, Ssk on 316L, B) average roughness, Sa on Ti6Al4V, D) surface kurtosis, Sku , F) surface skewness, Ssk .

In the other groups of parameters (*Sdr* and *Sds*), *Sds* shows a highly strong correlation with surface hydrophobicity with R^2 equal to 0.9792 and 0.9468 for Ti6Al4V and 316L respectively. *Sdr* shows a poor correlation for Ti6Al4V but a strong correlation for 316L for both types of surface treatment (Air and Argon). In summary, it can be concluded on the correlation between CA measurement and surface profile parameters that summit density (*Sds*) plays an important role in determining the hydrophobicity of the surfaces in laser-assisted methods.

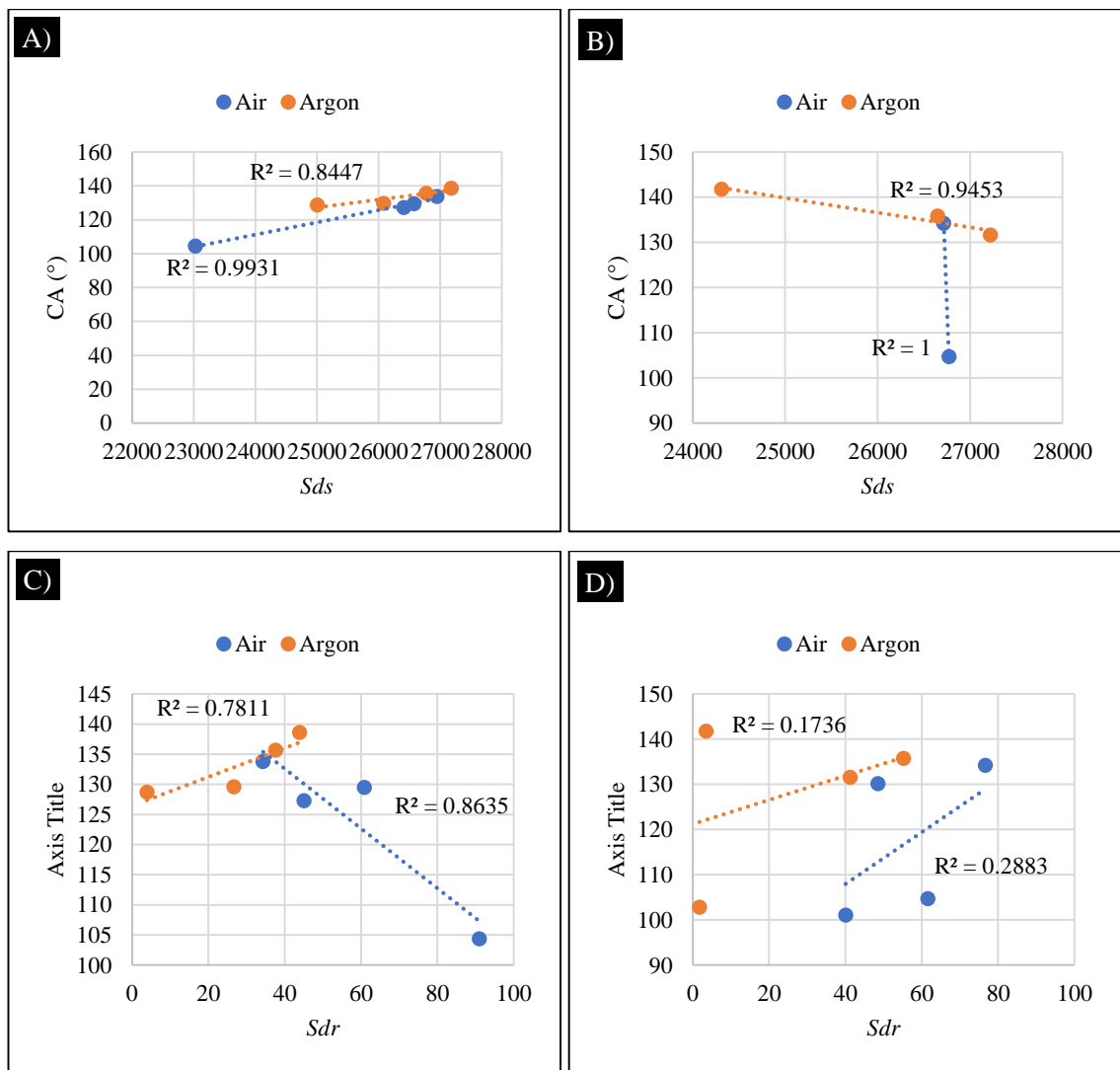


Figure 6-10 Correlation between contact angle and A) summit density, *Sds*, C) developed interfacial area ratio, *Sdr* on 316L, B) summit density, *Sds*, D) developed interfacial area ratio, *Sdr* on Ti6Al4V.

6.4 Bacterial adhesion on Stainless Steel that has undergone laser treatment

The femto-second laser irradiation techniques (in air and argon surroundings) produced an altered surface with multiple scales which are easily scalable to meet industrial requirements. This method was proposed to create a textural surface with varying surface properties. The texture formed during laser treatment was a spontaneous self-organised pattern, termed as Laser-Induced Periodic Surface Structures (LIPSS). Current observations revealed that the multi scale topography formed under both conditions has the potential to increase or reduce the bacteria adhesion when compared to the control specimens (SSC/TIC). Besides the formation of the additional features, the properties of the lasered surface were being altered compared to the control specimens in terms of increased contact angle (hydrophobicity), increased roughness in nanometre level, and increased hybrid parameter (*summit density*). Following that, the adhesion ability of these two model organisms on the metals was changing drastically compared to the control specimen and the previously discussed treatment (polishing and EDM). The numbers of adherent cells for both *S. aureus* and *E. coli* on certain lasered surfaces fabricated either in air or argon, showed a significant reduction as opposed to the polished surfaces. In addition, the bactericidal effects were more prominent on the surface fabricated under argon, with a greater extent observed in the repulsion of *S. aureus* SP. The adhesion data for both *S. aureus* and *E. coli* on all the surfaces that have undergone four different laser parameters in air and argon are presented in Figure 6-11.

The adhesion magnitude of *S. aureus* and *E. coli* on all eight lasered surfaces for stainless steel metal showed a significant difference ($p > 0.05$), with *S. aureus* (Gram-positive), being a greater coloniser compared to its counterparts (*E. coli*, Gram-negative). With respect to the stainless steel fabricated in air, the adhesion of *S. aureus* was > 50% higher than *E. coli* with the exception of laser parameter 3. Four hours exposure of SSL-1, SSL-02 and SSL-4 fabricated in air allowed the adhesion of *S. aureus* between $62 \times 10^3/\text{mm}^2$ - $65 \times 10^3/\text{mm}^2$, while the highest repellence was attained in SSL-3 with only $\sim 42 \times 10^3/\text{mm}^2$ cells attached onto the surface. These overall values represented a reduction of more than 50% as opposed to the polished stainless steel (Table 6-4). The anti-bacterial effect of the stainless-steel surface was further enhanced following treatment in argon, indicating a significant reduction in the adhered bacteria particularly

for *S. aureus*. Over 50% improvements in terms of reduced *S. aureus* adhesion were obtained for all stainless-steel surfaces fabricated in argon relative to the SSL-Air. The adhesion of *S. aureus* in the SSL-01-Ar, SSL-02-Ar, SSL-03-Ar and SSL-04-Ar were further reduced to $\sim 17 \times 10^3/\text{mm}^2$, $\sim 19 \times 10^3/\text{mm}^2$, $\sim 22 \times 10^3/\text{mm}^2$ and $\sim 32 \times 10^3/\text{mm}^2$, respectively. This indicated an improvement of over 72%, 70%, 47% and 48% compared to SSL-01-Air, SSL-02-Air, SSL-03-Air and SSL-04-Air, respectively.

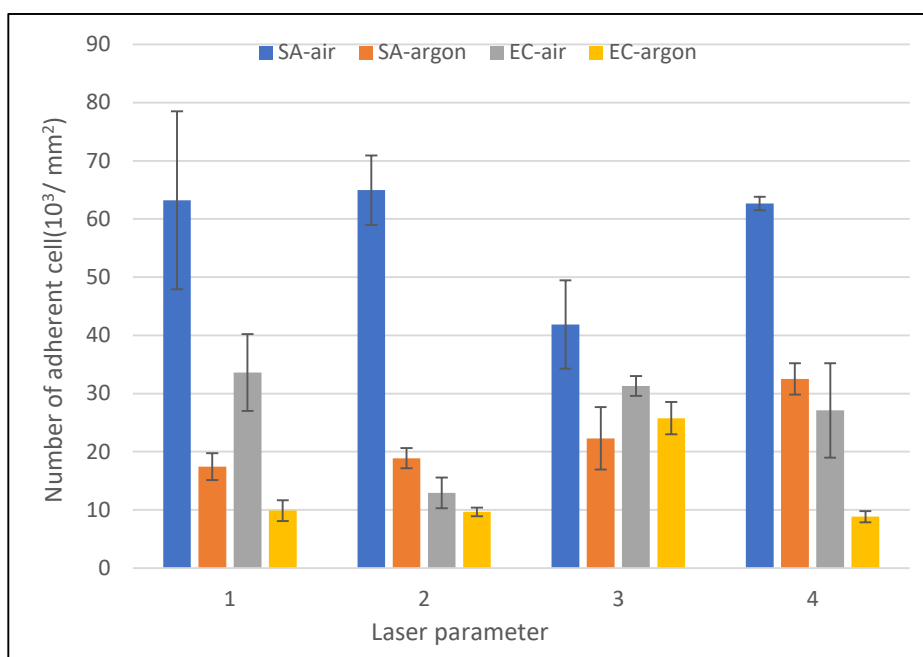


Figure 6-11 Numbers of adhered bacteria on lasered surfaces (stainless steel) after exposure to bacterial suspension (1×10^8 CFU/mL) for four hours at 37°C. (SA- *S. aureus*; EC – *E. coli*)

Being the least adhesive species, the adhesion of *E. coli* on the stainless-steel surface was much lower compared to the adhesion of *S. aureus*. In contrast with *S. aureus*, the adhesion of *E. coli* was enhanced in all the lasered stainless steel fabricated in air with the exception of SSL-03-Air (Table 6-4). *E. coli* adhesion increased between 87% to 32% for SSL-01-Air, SSL-03-Air and SSL-04-Air relative to the control sample. Except for SSL-02-Air, adhesion was reduced by 10% but it was not statistically significant. Comparing the effect of exposure during laser treatment, our finding for *E. coli* adhesion revealed a similar pattern to those of *S. aureus* where the repulsion in SSL-Ar was further increased compared to SSL-Air. *E. coli* retention was improved by 71%, 25%, 18 and 67% in SSL-01-Ar, SSL-02-Ar, SSL-03-Ar and SSL-04-Ar, respectively,

compared to SSL-Air. The ability to further prevent the colonisation of both species in SSL-Ar relies heavily on several adhesion factors, presumably contributed by the chemical composition of the altered surfaces as well as the effect from the altered surface topographies [100]. Our findings revealed that the lowest number of adhesion for *S. aureus* and *E. coli* were observed with SSL-01-Ar and SSL-04-Ar, with only $\sim 17 \times 10^3$ /mm² and 8800 /mm², respectively, an improvement of ~ 9.3 times and 40% against the control sample (Table 6-2).

6.5 Bacterial adhesion on Titanium that has undergone femtosecond laser treatment

Titanium surfaces that have undergone similar laser treatment to stainless-steel surfaces were exposed to *S. aureus* and *E. coli* for four hours and the number of adhered cells were presented in Table 6-4. In agreement with previous findings, the laser treatments managed to reduce the adhesion for *S. aureus* species in all fabricated titanium, both TIL-Air and TIL-Ar. However, the repulsion of *E. coli* species was only attained with TiL3 and TiL4 fabricated in argon, while the rest of the surfaces promoted adhesion as opposed to the control surfaces. Although the adhesion of *E. coli* was generally enhanced, total number of adhered *E. coli* remained lower than *S. aureus* as in the previous section in all eight titanium surfaces. This proved that the strain of *S. aureus* was prone to adhere to various surfaces compared to other bacteria species. When compared to the SS control surface, the adhesion of *S. aureus* decreased by 31%, 6%, 24% and 19% on the TIL1-Air, TIL2-Air, TIL3-Air and TIL4-Air, respectively. Repulsion capacity against *S. aureus* was further enhanced in TIL-Ar, increasing over 21%, 57%, 36% and 60% in TIL1-Ar, TIL2-Ar, TIL3-Ar and TIL4-Ar, respectively, relative to similar metal fabricated in air. The lowest *S. aureus* adhesion was produced by laser treatment 2 with only $\sim 33 \times 10^3$ /mm² cells retained on the surface, which indicated a 60% reduction compared to the control (82.6×10^3 /mm²).

Table 6-4 Data for control and laser specimen (stainless steel).

Metal	CA (°)	<i>Sa</i> (μm)	<i>Sq</i> (μm)	<i>Ssk</i>	<i>Sku</i>	<i>Sds</i> (1/mm ²)	<i>S. aureus</i> (10 ³ /mm ²)	<i>E. coli</i> (10 ³ /mm ²)
SSC	70.49	0.07	0.102	0.18	10.72	17600	158.1	14.5
SSL-01-Air	129.5	0.29	0.37	-0.44	3.61	26900	63.0	33.6
SSL-02-Air	104.4	0.17	0.22	-0.03	4.26	26400	65.0	12.9
SSL-03-Air	133.8	0.19	0.25	0.15	3.73	26600	42.0	31.3
SSL-04-Air	127.3	0.07	0.10	0.80	5.97	23000	62.7	27.1
SSL-01-Ar	135.7	0.56	0.67	-0.07	2.39	25000	17.0	9.9
SSL-02-Ar	138.6	0.20	0.26	-0.04	3.98	27200	18.9	9.7
SSL-03-Ar	128.7	0.21	0.27	-0.13	3.90	26800	22.3	25.8
SSL-04-Ar	129.6	0.18	0.23	-0.40	4.06	26100	32.5	8.8

- All data are represented as average taken from three replications

Meanwhile, the retention of *E. coli* species on all lasered titanium were much lower than those of *Staphylococcus*. However, when comparing to *E. coli* adhesion on the control titanium ($13.5 \times 10^3/\text{mm}^2$), most of the laser fabricated titanium induced the adhesion in a range of 9%-80%, with the exceptions of TIL3-Ar and TIL4-Ar. Such cases were also observed in stainless steel substrates, but the percent of increase was much higher than the titanium caused by different degrees of preference in different types of material. When comparing between the two fabrication methods, titanium fabricated in argon managed to reduce the number of adhesions as opposed to the similar laser treatment in air (Figure 6-12). The highest reduction of *E. coli* adhesion was contributed by TIL3-Ar and TIL4-Ar, scrapping nearly half of those adhered on the TIL3-Air and TIL4-Air. Currents findings revealed that the lowest number of adhesion for *S. aureus* and *E. coli* were observed in TIL2-Ar and TIL4-Ar, with only $\sim 33 \times 10^3 /\text{mm}^2$ and $5.2 \times 10^3 /\text{mm}^2$, respectively, giving an improvement of 60% and 61% against the control sample (Table 6-2).

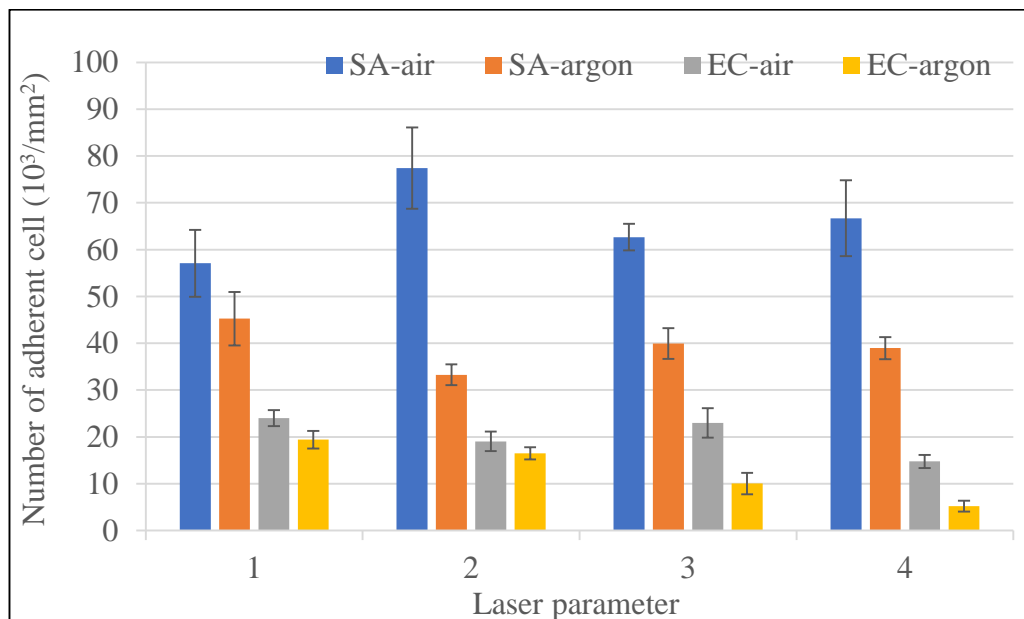


Figure 6-12 Numbers of adhered bacteria on lasered surfaces (titanium) after exposure to bacterial suspension (1×10^8 CFU/mL) for four hours at 37°C. (SA- *S. aureus*; EC – *E. coli*)

Table 6-5 Data of bacterial adhesion for control and laser Specimen (titanium)

T	CA (°)	Sa (µm)	Sq (µm)	Ssk	Sku	Sds (1mm ²)	<i>S. aureus</i> (10 ³ /mm ²)	<i>E. coli</i> (10 ³ /mm ²)
TIC	65.77	0.05	0.08	-0.10	20.36	13000	82.6	13.5
TIL1-Air	134.2	0.66	0.80	1.88	4.65	19000	57.1	24.0
TIL2-Air	104.7	0.19	0.25	0.25	4.79	26700	77.4	19.0
TIL3-Air	130.2	0.22	0.29	0.20	4.02	26800	62.7	23.0
TIL4-Air	101.1	0.07	0.09	0.41	4.79	23600	66.7	14.7
TIL1-Ar	135.8	0.52	0.60	-0.60	6.99	24800	45.2	19.4
TIL2-Ar	131.6	0.19	0.24	-0.03	4.48	26600	33.3	16.5
TIL3-Ar	141.8	0.19	0.24	-0.12	3.65	27200	40.0	10.0
TIL4-Ar	102.8	0.07	0.01	-0.18	4.13	24300	39.0	5.2

- All data are represented as average taken from three replications

6.6 Discussion on the effect of modified properties towards bacterial adhesion

Laser treatment with the parameters summarised in Table 6-5 had significantly modified the properties of both stainless steel and titanium. Overall, these treatments increased the roughness (0.07-0.66 μm), CAM ($>101.1^\circ$ - 141.8°), and the summit density of the hybrid parameter (23000 -27200/ mm^2) as opposed to the SS control (CA = 70.49° , Sa = 0.07 μm , Sds = 17600/ mm^2) and TI (CA = 65.77° , Sa = 0.05 μm , Sds = 13000/ mm^2). Any surface with CA $> 70^\circ$ were considered hydrophobic [64, 91, 160], therefore, the control surfaces for both stainless steel and titanium were considered as slightly hydrophilic. When comparing between the control surfaces of these two metals, the adhesion of *S. aureus* ($158.3 \times 10^3/\text{mm}^2$) and *E. coli* ($14.5 \times 10^3/\text{mm}^2$), showed higher retention onto stainless steel, with a significant difference observed in *S. aureus* ($p < 0.05$) (Table 6-6). The CA of the stainless steel was more hydrophobic than titanium, thus attracting more cells to the surface and securing the adhesion. Although both species showed a preference towards stainless steel, the difference between the number of adhered bacteria was very significant ($p < 0.05$). This finding aligned with the general rule where hydrophobic bacteria (*S. aureus*) were better colonisers than hydrophilic species (*E. coli*), thus adhering best on hydrophobic surfaces [64]. Besides that, hydrophobic-hydrophobic interaction had attracted *S. aureus* and contributed to the largest number that colonised the control surface (SS). Alam and Balani [91] reported that adhesion of *S. aureus* onto stainless steel surfaces (CAM = 48.7°) was stronger than on titanium (68.8°) with relatively similar roughness (Sa = 0.22 μm –0.29 μm), retaining more *S. aureus* on the SS surface. The force needed to remove *S. aureus* from the SS using AFM cantilever was 15.21 mN giving a pull distance of 425 nm, which was significantly higher than on titanium. *S. aureus* bonding with the surface was established within seconds–hours after contact with the surfaces, thereby preventing detachment from shear. A similar finding was observed for the metals that have undergone laser treatment, where the number of bacterial adhesions differed significantly from metal to metal, fabrications and strains. The total numbers of adhered bacteria in the four laser surfaces (Surface 1-4) with respect to air and argon exposure are summarised as follows (Table 6-6).

Table 6-6 Summations of bacteria in all process with respect to metal

Fabrication/Metal		<i>S. aureus</i> ($10^3/\text{mm}^2$)	<i>E. coli</i> ($10^3/\text{mm}^2$)
Polished (Mirror)	Stainless steel	158.1 ± 7.5	14.5 ± 2.1
	Titanium	82.6 ± 4.6	13.5 ± 1.9
Air	Stainless steel	232.7 ± 5.4	104.9 ± 4.6
	Titanium	263.9 ± 4.3	80.7 ± 2.1
Argon	Stainless steel	90.7 ± 3.5	54.2 ± 4.1
	Titanium	157.5 ± 2.1	51.1 ± 3.2

The mechanism for bacterial adhesion works differently with different types of bacteria or surfaces [161]. The current findings produced almost similar trends with previous data following femtosecond laser fabrication. Chik et al. (2018) reported that *S. aureus* and *E. coli* provided opposite trends towards adherence preference on different metal surfaces. Previous findings showed that higher *E. coli* retention was observed on titanium, while *S. aureus* was attracted towards stainless steel surfaces, with respect to similar fabrication methods. Following the laser modification in air and argon, more *S. aureus* was recorded on the titanium surfaces compared to stainless steel, with an increase of between 14% to ~ 98% (Table 6-6). In contradiction with *S. aureus*, *E. coli* showed a preference towards stainless steel surfaces in both fabrication methods, however the differences were relatively low, between 6%–25% (Table 6-5). It is noteworthy that even though the repulsion ability of the SS (SSL-Air) with respect to the control surface was quantitatively higher than TI that has undergone a similar process, the average number of the attached bacteria counted on the surface remained relatively equivalent for both metals. Adhered *S. aureus* cells marked between $42 \times 10^3/\text{mm}^2 - 65 \times 10^3/\text{mm}^2$ and $57 \times 10^3/\text{mm}^2 - 77 \times 10^3/\text{mm}^2$ for stainless steel and titanium, respectively, showing that a significant difference between these surfaces was not observed. However, a marked reduction of retained *S. aureus* relative to control surface/SSL-Air/TiL-Air provided significant differences between treatment methods ($p < 0.05$) for both metal surfaces that have undergone laser-argon fabrication. The drastic changes in the adhesion numbers were probably contributed by the differences in surface chemistry (not evaluated), and the skewness of the surface, since the other parameters, i.e *Sa*, *Sq*, *Sds* and CA were not significantly different. Surface chemistry and/or atomic ordering had a very strong influence on the magnitude of adhesion for a surface with roughness below submicron

level, while highly coarse surfaces were dictated by the degree of *Sa* [162]. Oxidation of the SSL and TIL fabricated in air might have increased biocompatibility of the bacteria with the surfaces, thus increasing the adhesion.

To search for the hidden details regarding the contribution of the modified surface properties towards reducing the bacterial adhesion, an assessment of the *S. aureus* on stainless steel was discussed in detail to explain the underlying phenomenon. The hydrophobicity was long thought to be the driving factor that encouraged the preliminary adhesion between bacterial and inert surfaces. Being the dominant factor, this property was assessed to search for reasons how the adhesion mechanism worked out after any surface modifications. According to the Katsikogianni [163], surface hydrophobicity had a superior impact than the CSH of the bacteria in determining the adhesion mechanism and magnitude. The current study revealed both properties works synergistically and affecting the adhesion. Referring to Table 6-4, SSL-02-Air and SSL-03-Air, both have nearly similar *Sa* and *Sds* but different CA. Owing to the high scanning rate (50 mm/s), the wettability of SSL-02-Air (CAM = 104.4°) increased thus retaining more *S. aureus* ($65.0 \times 10^3/\text{mm}^2$) than in SSL-03-Air ($42.0 \times 10^3/\text{mm}^2$, CAM = 138.8°) (Rajab et al., 2018). Referring to similar metals, the adhesion of *E. coli* was much lower than *S. aureus*, contributing to more than 40% differences, owing to its hydrophilic properties which naturally made it appear as a less adhesive strain, but can pose a stronger bond than the hydrophobic-hydrophobic interaction after prolonged incubation.

A modification of the metal surfaces has been reported following treatment with microsecond, nanosecond, femtosecond, and picosecond lasers using various parameters to achieve either more hydrophobic or hydrophilic surfaces Cunha, Elie [54], Bagherifard, Hickey [164], Rajab F. [165]. Treatment with picosecond laser produces hydrophobic SS surfaces with CA between 99.6° – 160.0° and *Sa* in a range of 0.02 mm – 1.16 mm Rajab F. [165]. Exposure to *E. coli* suspension followed by a washing step reduced the number of retained bacteria on all modified surfaces relative to polished SS (control). They also reported that a surface with CA = 154° and *Sa* = 1.16 μm, encouraged the highest detachment of *E. coli* with only $4.2 \times 10^4/\text{cm}^2$ retained on the surface, while polished surfaces showed the greatest number of bacteria ($1.1 \times 10^4/\text{cm}^2$), thus concluding that the superhydrophobic surfaces was not always effective to prevent bacterial adhesion.

The ability of the lasered surface to repel *S. aureus* might be contributed by the reduced wettability. After laser fabrication, all surfaces exhibited higher hydrophobicity with high surface roughness compared to polished surfaces, but in varying degrees. Increasing the hydrophobicity of the surface would attract more cells due to the hydrophobic-hydrophobic interaction, but the adhesion force was jeopardised, therefore resulting in lower cells remaining on the surface. The higher wettability of the control SS and TI (CA < 75°) encouraged a stronger bonding of the bacteria with the surface, thus retaining more cells on the surfaces after four-hour exposure to bacterial suspension. In addition, the increase in roughness of all the lasered surfaces for both SS and TI but no greater than the size of the *S. aureus* (< 0.6 µm), presumably was a strong factor that contributed towards repelling the adhesion. Increased roughness without exceeding the size of the bacteria is beneficial for reducing the adhesion. This was achieved because the contact area/point between the bacteria and the original surfaces was reduced which made the adhered cells susceptible. The loosely bound cells can be easily removed with minimal force by shear stress.

The adhesion of bacteria on stainless steel materials has been studied with many reporting a positive correlation between bacterial hydrophobicity with increased degree of adhesion. The adhesion on the hydrophobic stainless steel was governed by the hydrophobicity of the bacteria and will increase with increased CSH of the individual strain within the *S. aureus* group [166]. In order to reduce adhesion of hydrophobic bacteria on the hydrophobic surfaces, a modification of the surface must be carried out to increase the surface properties to superhydrophobic level. These results suggested that when super hydrophobicity was achieved after the laser treatment, the surface may have worked as *self-cleaning* surface where it prevented water from sticking to the surface. The water was presumably rolled on the surface, thus preventing the nutrients from reaching the adhered bacteria, subsequently reducing the rate of growth. The water rolling effect also prevented the bacteria from reaching the surface, thus preventing adhesion. Besides that, there is the possibility that the additional surfaces and grooves of the 3D features have triggered the trapping of air between its nano peaks, thereby reducing the contact area between the bacteria and the surfaces.

The current finding revealed that the attachment of *E. coli* in all titanium surfaces was higher than the control process. Recent data suggested that the adhesion of *E. coli* increased in all surfaces with $SaL > SaP$, except for TL3-Ar and TL4-Ar. Increase of adhesion in *E. coli* was also reported by many authors due to roughened surfaces, where cells begin their attachment at the textured surface Rajab F. [165] Almaguer-Flores A. [162] reported that reduced roughness to a size lower than the bacteria size was beneficial for decreasing adhesion while the ratio of roughness: bacterial size ≥ 1 will facilitate the adhesion process. In addition, a high surface roughness to few micrometres away would enhance the adhesion of bacteria Braem, Mellaert [167] due to i) additional effective surface area for securing adhesion, ii) 3D features providing protection towards detachment by external forces and iii) the non-regularities of the surface i.e. crack and grooves will act as sinks to entrap the bacteria within its cavities. Some authors reported that roughness plays an important role to control adhesion, but it works differently with different strain types and bacteria shape [64]. Increased surface roughness generally enhances the bacterial adhesion, while roughness less than 400 nm reduced the adhesion of *S. aureus*, *B. cereus*, *E. coli* and *P. aeruginosa*. Adhesion of *E. coli* and *S. aureus* on nano surfaces of titanium with controlled roughness $Sq = 2.3 \text{ nm} - 6.1 \text{ nm}$ provided a contradictory trend towards adhesion [168]. The number of adhered *E. coli* increased proportionally with surface roughness, while *S. aureus* declined gradually with increasing nanometre roughness. Braem, Mellaert [167] reported that *S. aureus* adhesion was facilitated when Sa ranged between 5–8 μm , far exceeding the adhesion on the polished surface with $Sa = 30 \text{ nm}$. In contrast, Ludecke C. [168] found that the greatest number of *S. aureus* adhesion was achieved with a polished surface with $Sa = 2 \text{ nm}$.

Sa values higher than the size of the bacteria might facilitate the adhesion by providing protection towards shear stress, especially for bacteria located at the grooves and the valleys of the microstructures. According to Ortega MP [169] the surface roughness does not affect the adhesion of the *E. coli* on the stainless steel ($Sa = 0.14 - 1.37 \mu\text{m}$), but is highly influential for securing adhesion when external force was applied during rinsing. The ability to retain the adhered bacteria was contributed by the surface with highest surface roughness where the peak served as a shield to prevent the cell from detachment. In agreement with the findings, De Giorgi, Furlan [170] also reported that *E. coli* retention on stainless steel AISI 304 was the lowest with the smoothest surface ($Sa = 34 \text{ nm}$) attained using laser micro-polishing. The current study revealed that Sa less than

sub-micro-meter and negatively skewed surfaces has successfully prevented the adhesion of *S. aureus* in SS and TI fabricated in argon, thus depicting a reduction of bacteria on its surface relative to control surfaces (Table 6-4 and Table 6-5).

Decreased adhesion of *E. coli* onto TL3-Ar was presumably contributed by the high CA (141.8°) while the TL4-Ar (CA= 102.8°, $Sa = 0.07 \mu\text{m}$, $Sds = 24300/\text{mm}^2$) could be coming from the synergistic effect of a higher hybrid area, with reduced roughness and increased CA (discussed later). However, when comparing the surface characteristics for the same metal treated in air (TL4-Air, CA= 101.1°, $Sa = 0.07 \mu\text{m}$, $Sds = 24800/\text{mm}^2$), the adhesion of *E. coli* increased by 10% compared to the control titanium. With almost similar properties, the possibility of reduced adhesion achieved in TL4-Ar was most likely to be enhanced because of the different chemical compositions. Reduced oxidation for samples fabricated in argon might have reduced the attraction towards the surfaces. Cunha, Elie [54] reported that an oxidised layer was observed in a SS surface after undergoing femtosecond laser fabrication which might facilitate the adhesion. In contrast, De Giorgi, Furlan [170] reported that significant changes in surface chemistry were not observed for lasered titanium exposed to nitrogen at different power levels, $P = 0.14\text{--}0.47 \text{ mJ}$, where oxidation had been successfully suppressed. In this case, the oxidation of metal fabricated in argon had been successfully controlled thereby suppressing the bacterial adhesion compared to the metal treated in air. In the current study, it was expected that changes in chemical surface properties between air and argon-laser fabrication were significant enough to control the adhesion mechanism for both *S. aureus* and *E. coli*.

When comparing laser fabrication regarding exposure to air and argon that affected the rate of adhesion, the discussion was focused on the contribution of the oxide layer. The probability of the TI metal to change to TiO , TiO_2 or Ti_2O_3 upon exposure to air during laser treatment was very high, but unfortunately not covered in this study. A study by Shiau [100] proved that titanium implants undergoing the oxygen-plasma ion immersion managed to increase the clotting of blood responses whilst hindering the adhesion of *Streptococcus mutans* due to the presence of a TiO_2 layer. The increased negativity value of the TiO_2 layer promotes repulsion of the bulk properties of *S. mutans* due to electrostatic repulsion between similar charges of the two surfaces. Exposure to nitrogen results in the formation of nitride on titanium surfaces, which increased

resistance towards bacterial adhesion [171]. Works by Cunha, Elie [54] confirmed that femtosecond laser irradiation in air altered the surface chemistry of the LIPSS, by thickening the oxide layer with TiO₂ while reducing the portions of Ti₂O₃ relative to a polished sample. The effects of an oxide layer partly increased the anti-bacterial properties of the modified surfaces and roughness was claimed to be the primary factor for reduced adhesion.

6.7 Viewing the adhesion patterns using SEM

The results presented in section 6.5 and section 6.6 revealed promising data on the ability of the lasered surface to reduce the adhesion of *S. aureus* and *E. coli* in both stainless steel and titanium. Bohinc [64] and the reference therein mentioned that the ability of the surfaces to remove more than 60% of the bacteria was often termed as self-cleaning surfaces and would draw much interest in the commercial scale. Apart from quantitative analysis (determination of the adhered cell), it is important to examine how these bacteria positioned themselves on the fabricated surfaces before any correlation with the surface properties, particularly the surface topographies and CAM can be derived. Figure 6-13 to Figure 6-16 show the adhesion of *S. aureus* on the lasered surfaces at various spots on stainless steel and titanium metals, while Figure 6-17 to Figure 6-20 depicts the images for *E. coli*. It was speculated that bacterial cells actively choose the initial position to settle on the smoother surface rather than spatially organised contour lines, while avoiding the area with protruding nano-meter grains. By rough estimation, the density of bacteria per square area was often 5-15% higher than the bacteria settling on the LIPSS. Focusing on the LIPSS area, generally both bacteria prefer to find their best spots at the valley/crevices between two macro-topographies, which was extensively observed for the *E. coli* (Figure 6-17 to Figure 6-20). The flat area of the valley may provide the maximum contact point with the surfaces, where the bacteria established contact with the surface, while providing protection from hydrodynamic forces due to hydrodynamic force [64, 122].

In general, the presence of the textured surface, for both stainless steel and titanium altered the behaviour of the *S. aureus*. When referring to Figure 6-13 (a) and Figure 6-15 (a), it can be clearly seen that the unstructured surfaces allowed the formation of clusters, where the bacteria attached closely to each other forming a group of cells of more than 20 after 4 hours of exposure to bacterial suspension. This was a common view in most of the stainless steel and titanium fabricated in air in all four laser parameters. However, large cell clusters were almost absent in all stainless and titanium surfaces fabricated in argon (Figure 6-14 and Figure 6-16), replaced by either individuals/pairs or by smaller groups or clusters of less than 10 ten cells. Apart from that, it is best to emphasise that the textured surface might prevent the formation of cell clusters in both air and argon fabrication. In all eight stainless steel surfaces, the presence of cell clusters was not detected, replaced by a small number of cells attached onto the micro-topographies and onto individual contour lines. Quite often, but not always, *S. aureus* attached individually or in pairs and located themselves on top of the contour lines. It is believed that the topographies played an important role that forbids cell to cell communication, thus eliminating the formation of cell clusters. Other than that, owing to its size, shape and super-adhesive membrane structure, the attachment of *S. aureus* was not limited to valleys and crevices, in fact, it can easily position itself at any location on the structured area. The steepness of the convex micro-surfaces does not prevent the attachment of cells, where cells adhered easily on single or two contour line(s), as depicted in Figure 6-13 (c) and Figure 6-15 (d) and securing themselves from detachment.

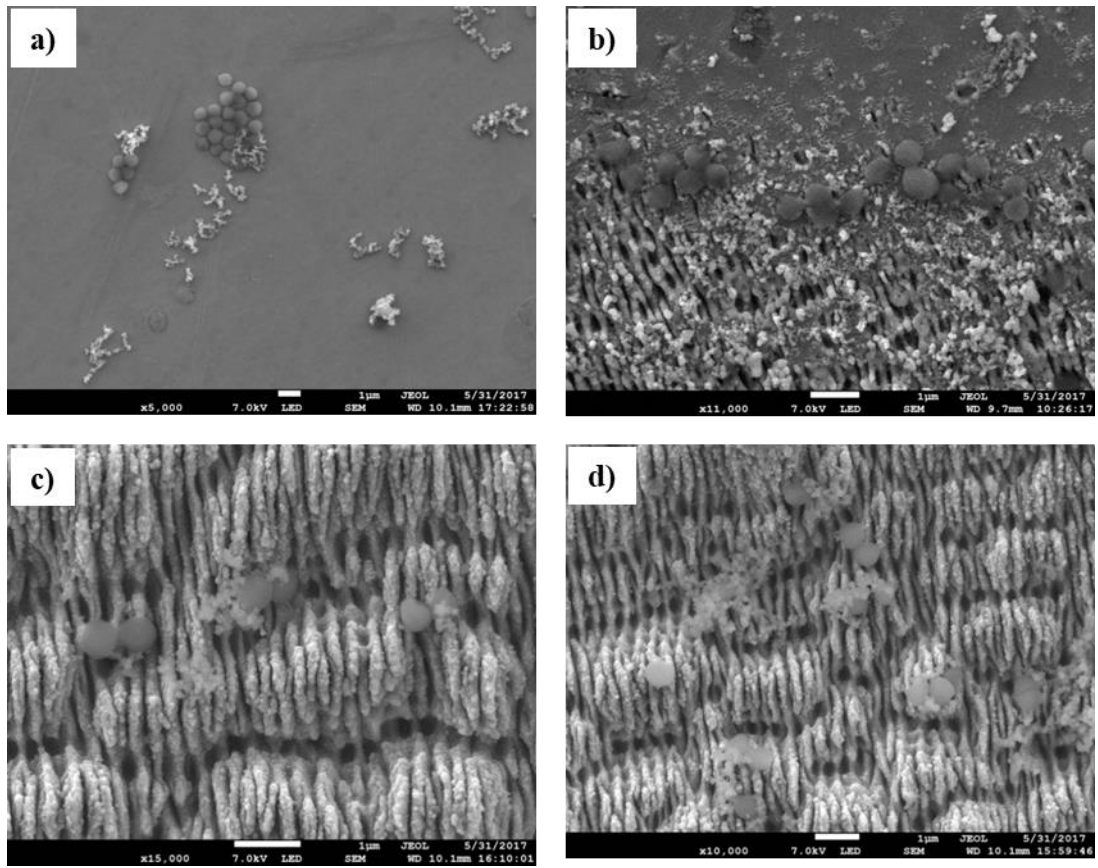


Figure 6-13 Adhesion of *S. aureus* on three different parts of the multi scales stainless steel surfaces undergone laser treatment (air)

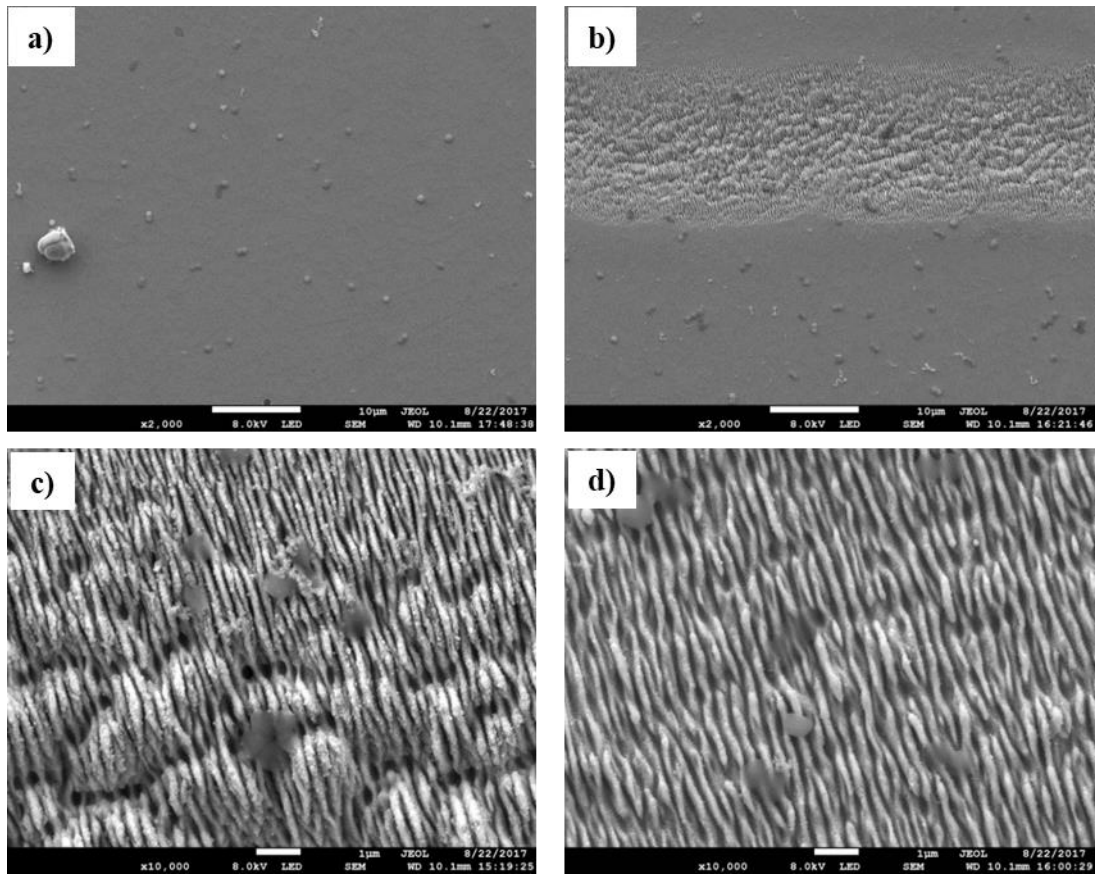


Figure 6-14 Adhesion of *S. aureus* on three different parts of the multi scales stainless steel surfaces undergone laser treatment (argon)

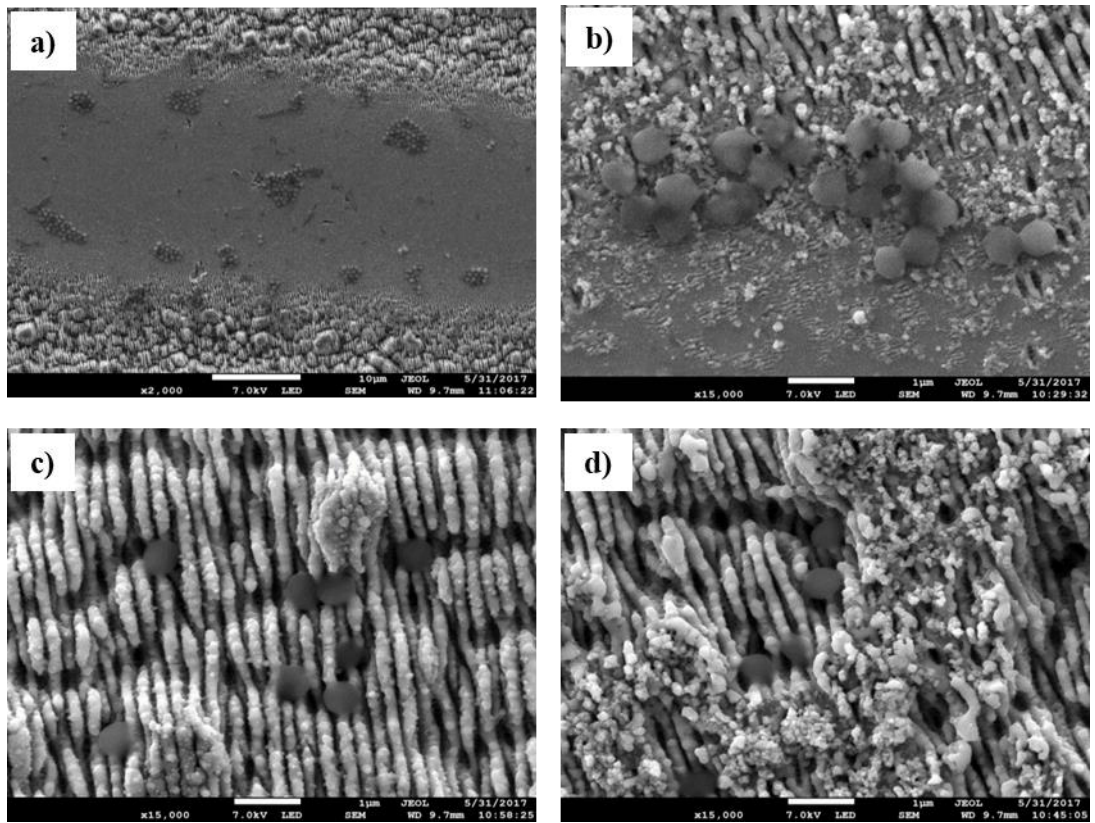


Figure 6-15 Adhesion of *S. aureus* on three different parts of the multi scales titanium surfaces undergone laser treatment in (air)

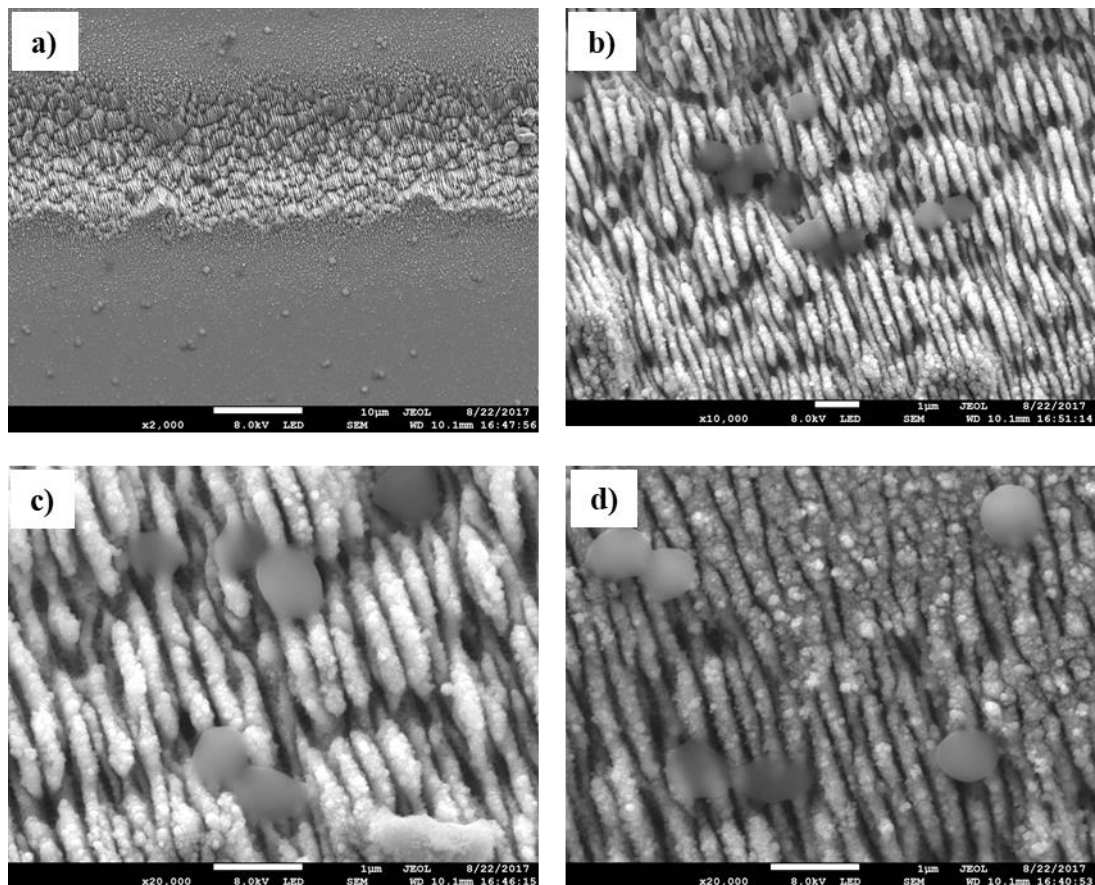


Figure 6-16 Adhesion of *S. aureus* on three different parts of the multi scales titanium surfaces undergone laser treatment in (argon).

Being a slow biofilm former, retention of *E. coli* on the lasered surface was very few and difficult to observe. Cells appeared individually with no sign of the formation of cell clusters (Figure 6-17 to Figure 6-20). No distinguished features were observed in the *E. coli* adhesion pattern between either two different metals or two different treatments. However, it was interesting to note that the adhesion of *E. coli* on the structured surface might have been prevented due to various factors. Firstly, the size and the shape of *E. coli* limits the contact point with the surface owing to the multi-contours, multi-size, and multi steepness of the surfaces. Referring to Figure 6-17 (b & c) Figure 6-18 (c), *E. coli* tends to position themselves by intersecting with the contour lines, where maximum contact area can be attained. This arrangement is the best position as *E. coli* seems to avoid the multiple heights variations, if they aligned their position parallel to contour lines. The waviness and the multiple steepness of the individual lines on the laser direction may limit the contact point as well as the strength (adhesion force). It was speculated that the *E. coli* will avoid multi contour areas and would prefer to position themselves on the

flattened surface, as it will provide a maximum contact area, although it would not guarantee the detaching effect due to hydrodynamic forces. In all SEM images, there was no *E. coli* adhering onto the contour lines in the laser direction observed in this study in all samples. The intersecting positioning of *E. coli* on the LIPSS area was observed in all SS and titanium, irrespective of the exposure towards air and argon.

Cracks, non-regular surface and grooves have been widely reported to attract more cells compared to flat surfaces [64]. Adhesion of the bacteria on the structured section of the surfaces often takes place within the valley of the LIPSS and also depending on the size and shapes of the bacteria. The coccoidal shapes of *S. aureus* with submicron sizes enables the bacteria to securely adhere to the grooves of the LIPSS (Figure 6-1). The presence of the valley serves as a basin which trap the bacteria, thus providing additional protection from shear stress while strengthening the bonding. It is interesting to mention that very often *S. aureus* appeared either individually or in a small number of cells (less than five) in all SSL and TIL fabricated in argon. Besides that, *S. aureus* was also observed on top of the microgrooves and scattered on the LIPSS. The crucial important feature of the LIPSS is that it might prevent the proliferation of the adhered bacteria, because it might cause certain damage to the cells, therefore preventing further formation of the biofilms. Meanwhile, the smooth surfaces at the unstructured area (Figure 6-13) allowed *S. aureus* to form big clusters/colonies (within 20-50 cells), thus maintaining the rigidity and survival rate of the bacteria species. Smaller colonies of *S. aureus* were also observed at the boundary layers due to increased roughness of the surfaces, where particles of molten metal grains were marked on the smooth unstructured location.

It is interesting to note that the formation of big colonies of *S. aureus* on all four types of stainless steel fabricated in argon was arrested, in both structured and unstructured areas. In SSL-Ar and TIL-Ar, cells attached either individually or less than 5 cells at the same spots, and the reason for this behaviour was not explored. When the number of adhered bacteria were counted based on the adhesion on structured and unstructured areas, the domination was obvious in the unstructured surfaces, showing an increase of 5-20% higher than cells in the LIPSS area. The ability to expel adhesion was enhanced with LIPSS in both air and argon fabrication. The presence of cell clusters was negligible, replaced by small numbers of cells attached onto the micro-topographies and

onto individual contour lines. Quite often, but not always, *S. aureus* attached individually or in pairs, and located themselves on top of the contour lines. It is believed that the topographies played an important role that forbids cell to cell communication, thus eliminating the formation of cell clusters. Other than that, owing to its size, shape and super-adhesive membrane structure, the attachment of *S. aureus* was not limited to valley and crevices, in fact, it can easily position itself at any location on the structured area. The steepness of the convex micro-surfaces does not prevent the attachment of cells, where cells adhered easily on single or two contour line(s), as depicted in Figure 6-13 (c) Figure 6-14 (d) and securing themselves from detachment.

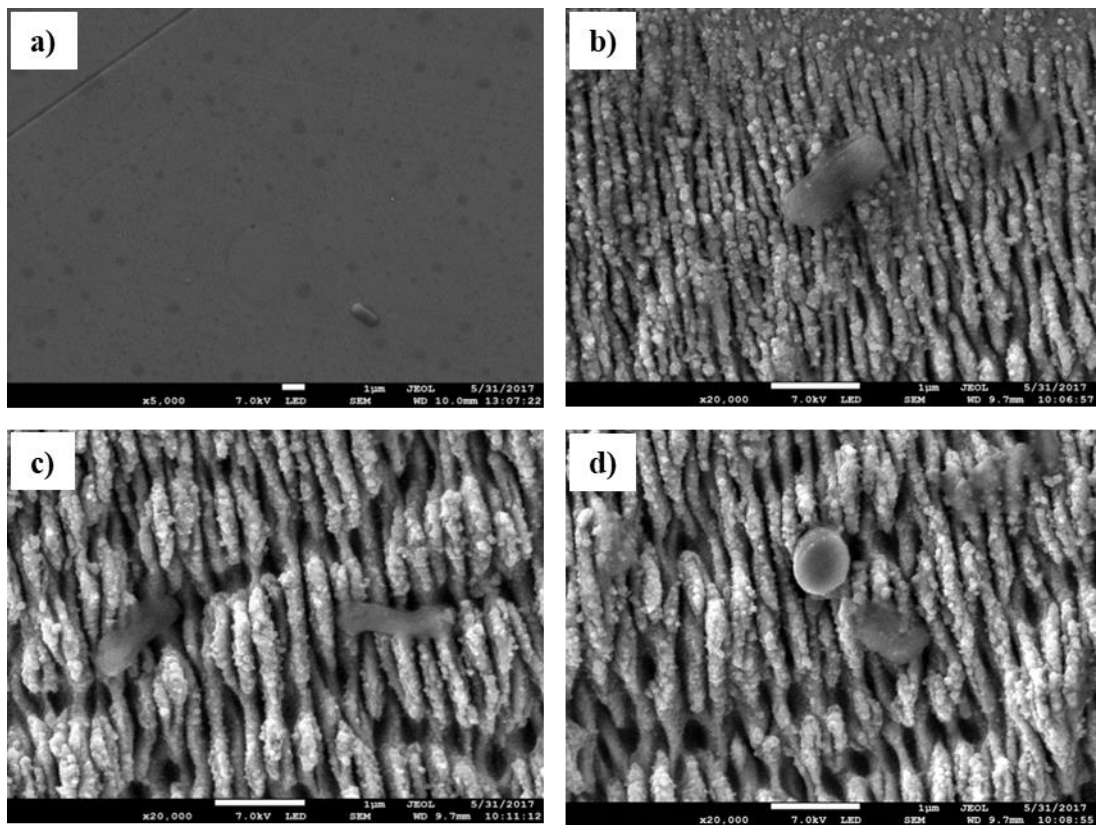


Figure 6-17 Adhesion of *E. coli* on three different parts of the multi scales stainless steel surfaces undergone laser treatment (air)

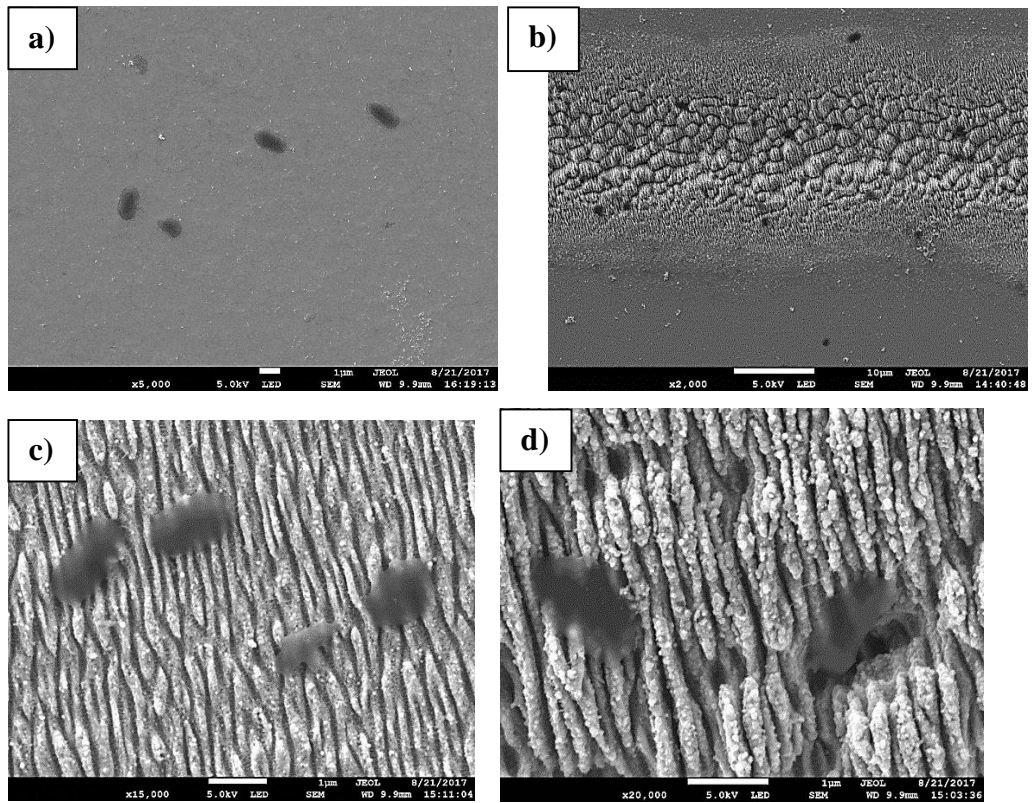


Figure 6-18 Adhesion of *E. coli* on three different parts of the multi scales stainless steel surfaces undergone laser treatment (argon)

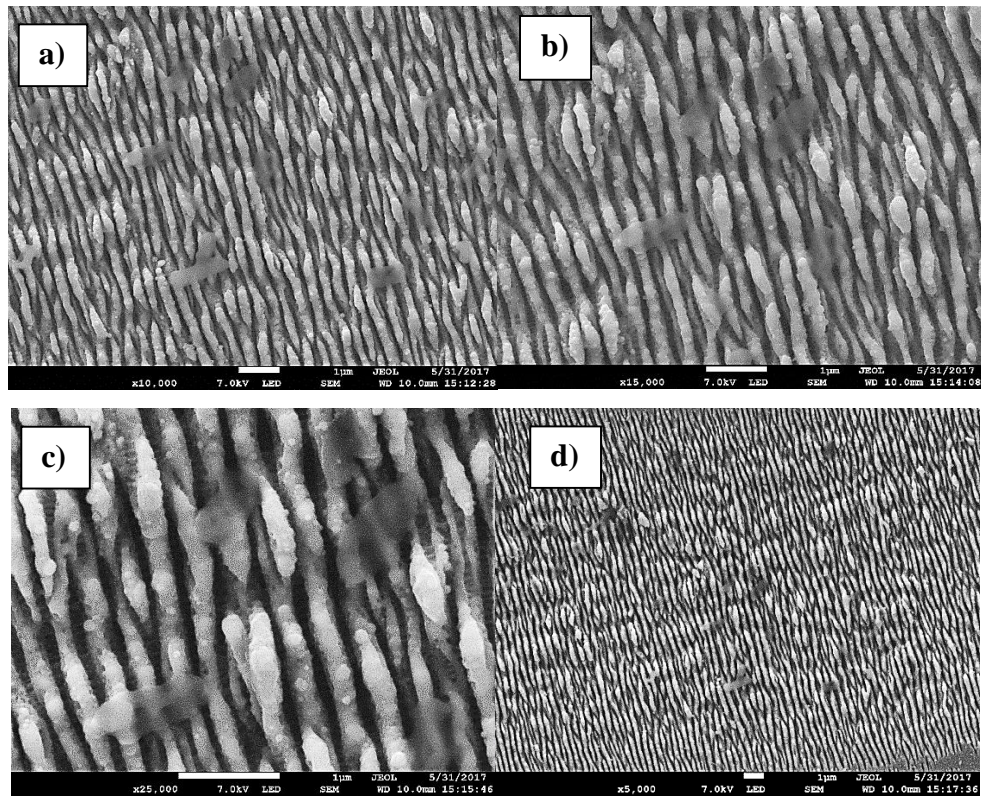


Figure 6-19 Adhesion of *E. coli* on three different parts of the multi scales titanium surfaces undergone laser treatment (air)

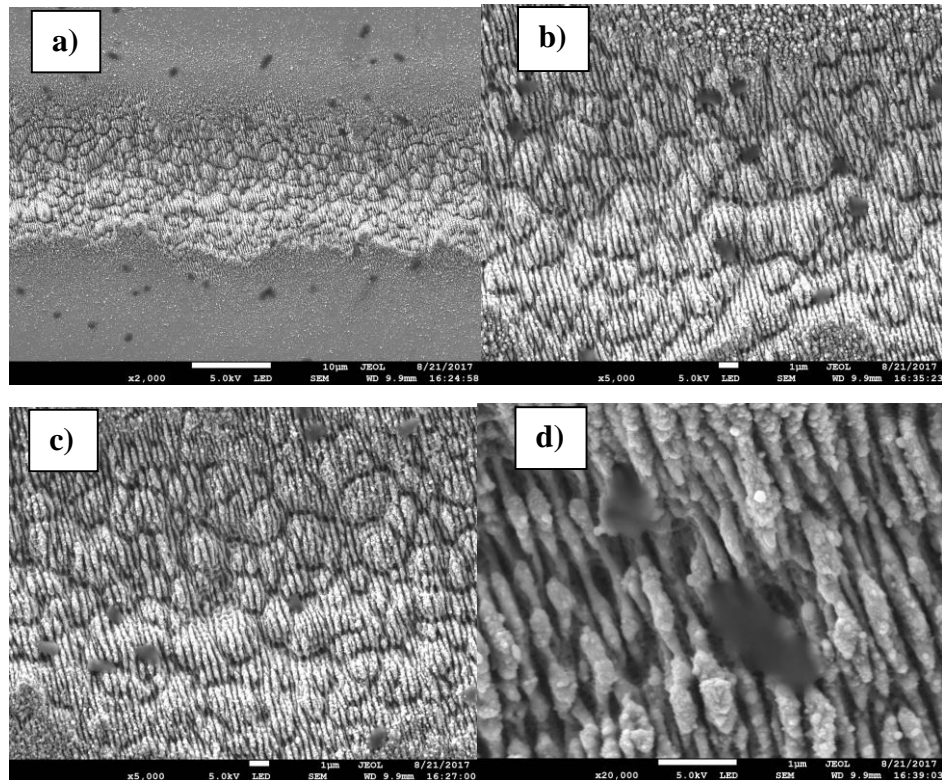


Figure 6-20 Adhesion of *E. coli* on three different parts of the multi scales titanium surfaces undergone laser treatment (argon)

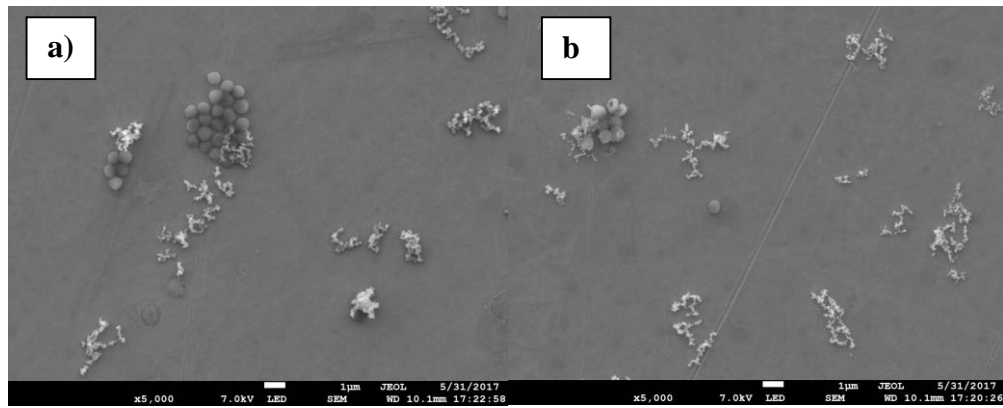


Figure 6-21 Formation of cells clusters by *S. aureus* on the unstructured area of a) SS and b) TI fabricated in air.

Preliminary works by Epperlein, Menzel [161] reported the LIPSS of stainless steel facilitated the adhesion of *S. aureus* within 3 hours of exposure, with a denser population observed on the LIPSS area than the unmodified area. In contrast to *S. aureus*, the *E. coli* adhesion was successfully prevented, where more cells were retained on the unmodified surfaces. The reduction was partly contributed by its rod shape, which increased the difficulty to position itself on the LIPSS structure, thus reducing the adhesion. Referring to fluorescence images in Figure 6-22, the LIPSS for SSL-02-Ar and TIL4-Ar repelled the adhesion of both *S. aureus* and *E. coli*, where a denser population was observed on the unstructured area. This presented a 5-15% reduction of bacteria settling on the LIPSS against the unstructured area in most of the lasered metal, but the results were not statistically significant (data not shown).

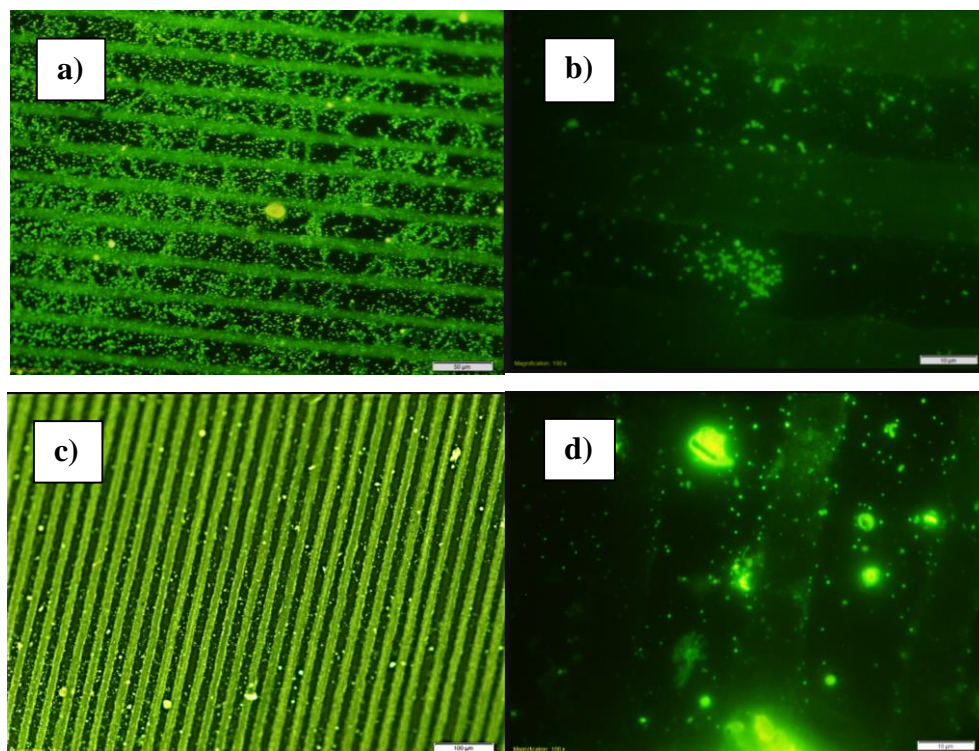


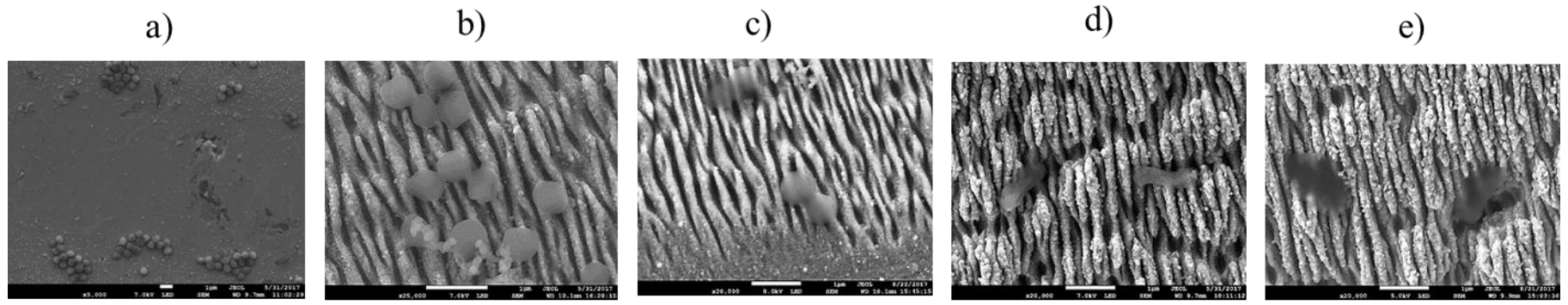
Figure 6-22 Fluorescence images of *S. aureus* on the SSL-02-Ar (a-b) and *E. coli* on the TIL4-Ar (c-d) showing more cells were retained on the unstructured area than the LIPSS.

A thorough observation of the close-up images on the bacterial shape in Figure 6-23, show clear evidence that the micro and nanostructures of the LIPSS were effective in deforming the bacterial membrane structures. The malformed membrane cells probably occurred because of the sharp contours of the LIPSS, which ruptured and lysed the cells, causing the leaking of the cell components. If this continues, the cells will lose the ability to reproduce and subsequently leads to death. It is presumed that the brushing effect between the cells and the surface due to hydrodynamic forces increased the chance of membrane deformation. It is very clear that the effect of nano grains on the LIPSS were more severe for the rod shaped bacteria, *E. coli* rather than *S. aureus* (Figure 6-23). This could be attributed to the very thin peptidoglycan of the Gram-negative bacteria; thus it can easily disrupt the outer membrane causing the leakage of the cell components and shrinking the cell envelope. However, the effects were less pronounced in the *S. aureus* where the shape remained intact, which could be attributed to its thick membrane structure. The nano-grains on the top of the LIPSS were responsible for rupturing the membrane cells, while the variables contour of the LIPSS limited the attachment of the both *S. aureus* and *E. coli*. The geographical limitations for aiding the adhesion were more severe for *E. coli* due to its size and shape. Although the effect of nano grains was

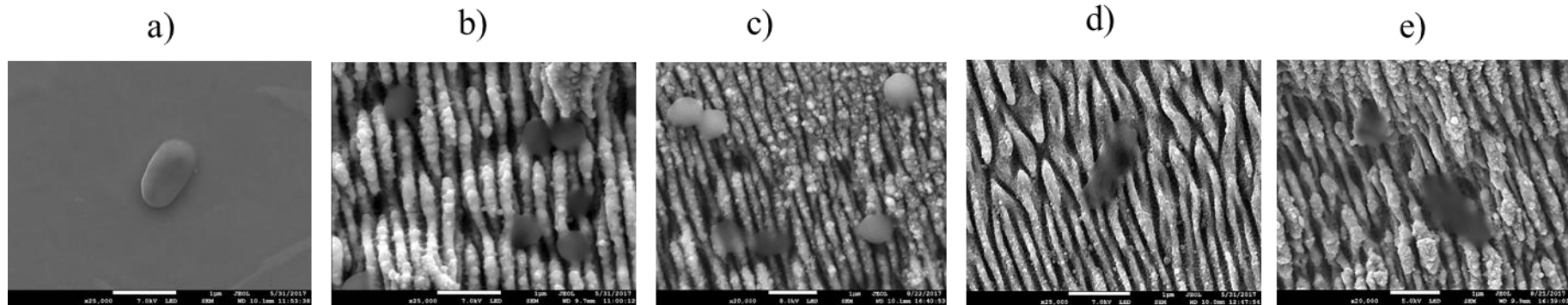
most unlikely to disrupt the surface integrity of the *S. aureus*, our observations revealed that the LIPPS were efficient for preventing colonisation thus also reducing the overall number of the adhered cells when compared with a polished surface. Therefore, the lasered surfaces have excellent capability to control the adhesion, growth and colonisation of both *E. coli* and *S. aureus* in the long run.

6.8 Correlation of Wettability and Surface Topographies with Bacterial Adhesion

Surface contact angle, nano structures, and chemical composition have been reported to be determining factors contributing to either attachment or detachment of bacteria on solid surfaces [172]. Most authors claimed that the changes towards adhesion magnitudes was contributed by the synergistic effect of two or more factors. It was difficult to derive a concrete conclusion towards determining the utmost influential factor which dictates the adhesion due to lack of information on the overall characterisation of either bacteria or the surface properties. The current finding revealed that all 16 lasered surfaces that have undergone significant changes in terms of surface properties relative to the control, subsequently affected the adhesion of *S. aureus* and *E. coli*. The correlation between surface properties were plotted using linear regression and presented in Figure 6-24 and Figure 6-25.



Stainless-steel



Titanium

Figure 6-23 The SEM images showing the shape of *S. aureus* and *E. coli* on the structured (LIPSS) and unstructured stainless steel and titanium fabricated in air and argon. a) Polished sample, b) *S. aureus*-air, c) *S. aureus* -argon, d) *E. coli* air and e) *E. coli*-argon

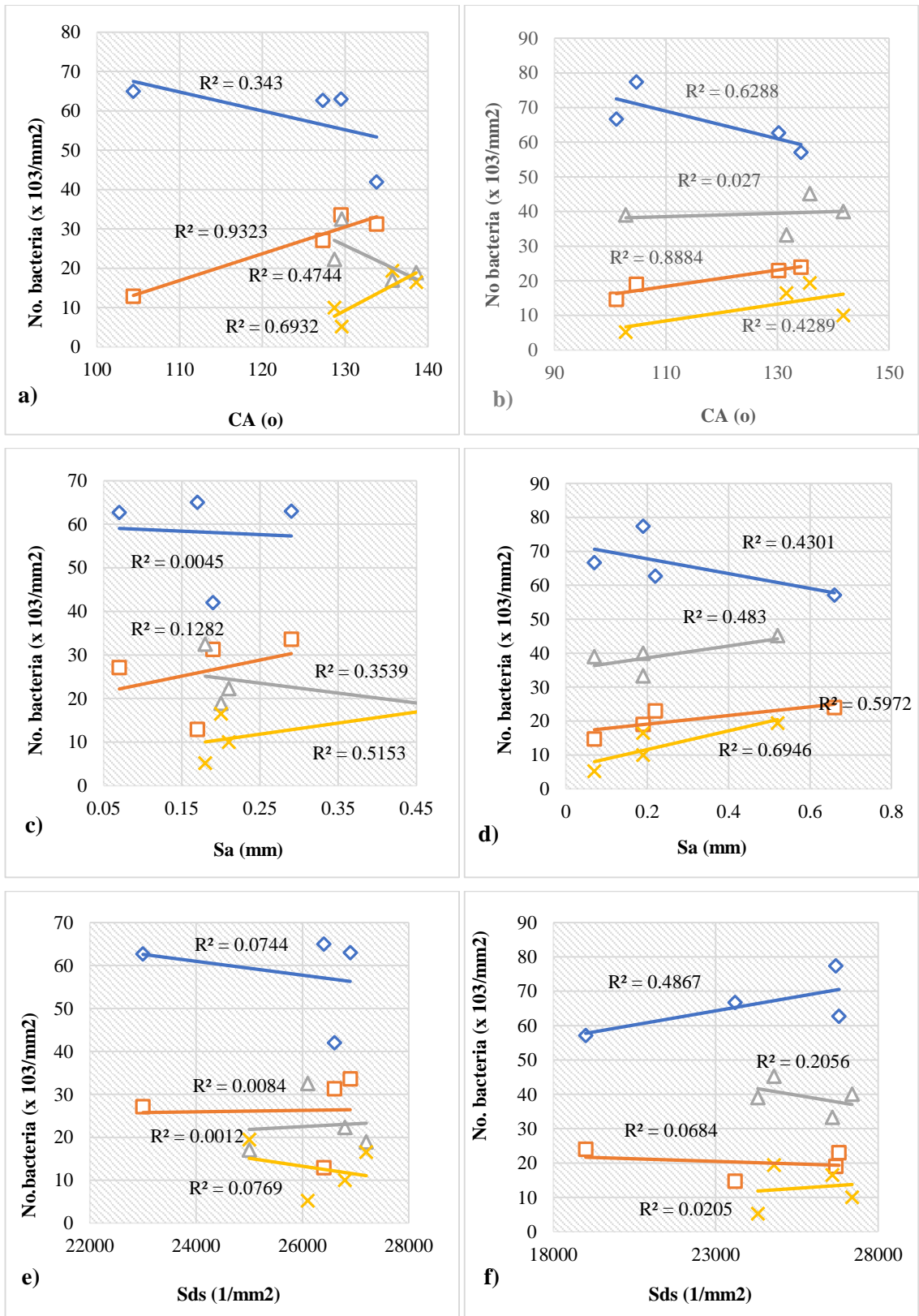


Figure 6-24 Correlation between CA, S_a and S_{ds} on the adhesion of *S. aureus* and *E. coli* on SS (a, c, and e) and TI (b, d and f) in air and argon fabrication. (◇) SA-Air, △ SA-Ar, □ SA- AR, (∧) EC-Air and (X) EC-AR.

The effect of surface properties on bacterial adhesion with respect to metal types and fabrication in air/argon were presented in Figure 6.24 and Figure 6.25. The number of adhered *S. aureus* and *E. coli* were plotted against CA, S_a , S_{ds} , S_{sk} and S_{ku} and linear regression was plotted to represent the data. The regression (R^2) value was displayed to indicate the accuracy of the correlation. The R^2 value between 0.7 – 1.0 represented a strong correlation, $R^2 = 0.50 - 0.69$ for moderate, $R^2 = 0.3 - 0.49$ for poor and $R^2 < 0.29$ as no correlation observed with the responses. Variations in responses with correlation between 0.04 to 1.0 was observed towards the surfaces. The correlation of adhesion with the CA (Figure 6.24 a & b) was moderate to strongly influenced by surface wettability within the range tested ($101.1^\circ - 141.1^\circ$). *E. coli* adhesion on SS and TT in air-laser fabrication provided the strongest correlation with R^2 of 0.89 and 0.93, respectively, showing increased adhesion with increased hydrophobicity. Much lower R^2 values was observed for the *E. coli* responses for SSL-Ar and TL-Ar but was still moderately correlated. On the other hand, the responses of the hydrophobic bacteria with CA was poorly to moderately interrelated. With the exception of TTL-Ar, the adhesion of SA was inversely correlated with increasing CA.

Surface roughness parameter was one the most important features that has been reported to affect adhesion mechanism [54]. The effect of roughness, occasionally write-off the influence of surface wettability, thus dictating the adhesion. Like the effect of wettability, adhesion of *E. coli* increased with increasing S_a , at values below submicron level on both SSL-Ar and TI-Ar but was moderately interrelated ($R^2 = 0.52 - 0.69$). The contribution of S_a and CA with respect to *S. aureus* adhesion onto all four surfaces provided similar trends for both SS and TI surfaces. Interestingly, although the properties of hybrid parameter (S_{ds}) strongly represented and proportionally increased with increasing surface hydrophobicity, the adhesion of both *S. aureus* and *E. coli* were independent of this factor (Figure 6.24 e & f). With the exception of the *S. aureus* adhesion onto TIL-Air, all correlation showed very low R^2 , thus indicating that adhesion was not affected by the values of summit density (S_{ds}) for surfaces.

Skewness contributed towards adhesion of *S. aureus* on SSL and TIL fabricated in Argon, with $R^2 = > 0.80$, showing a strong correlation existed between the number of adhered bacteria and *Ssk*. The skewness of the metal differed significantly with respect to the fabrication method. Air fabrication produced positively skewed surfaces, while argon fabrication was negatively skewed for both SS and TI. In conjunction with $S_a <$ bacteria size, the increase of pitting on the surface reduced the adhesion while the shorter peak height does not provide protection from hydrodynamic forces. The other possibility was that the *S. aureus* adhesion on the contour surface was weakened (comparative to SS control) because surface-bacteria contact area was reduced, thereby decreasing the adhesion. Focusing on the surface with skewness < 0 , it was shown that the ability of the surface to repel adhesion (SA-Ar) was more pronounced with reducing *Ssk* negativity (Figure 6.25 a & b).

Surface kurtosis for TIL in argon provided the highest correlation with *S. aureus* adhesion. The *S. aureus* indicated that the adhered cell proportionally increased with increasing *Sk_u* in both SSL and TIL, with the highest regression achieved with the latter. It is interesting to note that the correlation adhesion of both *S. aureus* and *E. coli* with all parameters studied, were either poorly correlated or independently related for all surfaces fabricated in air. On the other hand, adhesion onto surfaces fabricated in Argon produced a moderate to strong correlation with surface topographies especially for the *S. aureus*. This finding might support the hypothesis that the adhesion may not only be affected by the surface topography but also by the chemical surface composition. A strong correlation was produced and might have suggested that in Argon fabrication, the foundation of adhesion was based on the changes of topographies, with no implication/synergistic effect arising from the differences with respect to chemical compositions. However, the adhesion of *E. coli* was too complicated to be discussed thoroughly presumably because the bacteria employed a different mechanism (in comparison with *S. aureus*) arising from the hydrophobic-hydrophilic interaction which often induced repulsion towards the adhesion mechanism (*E. coli*-hydrophilic, SSL/TIL- hydrophobic).

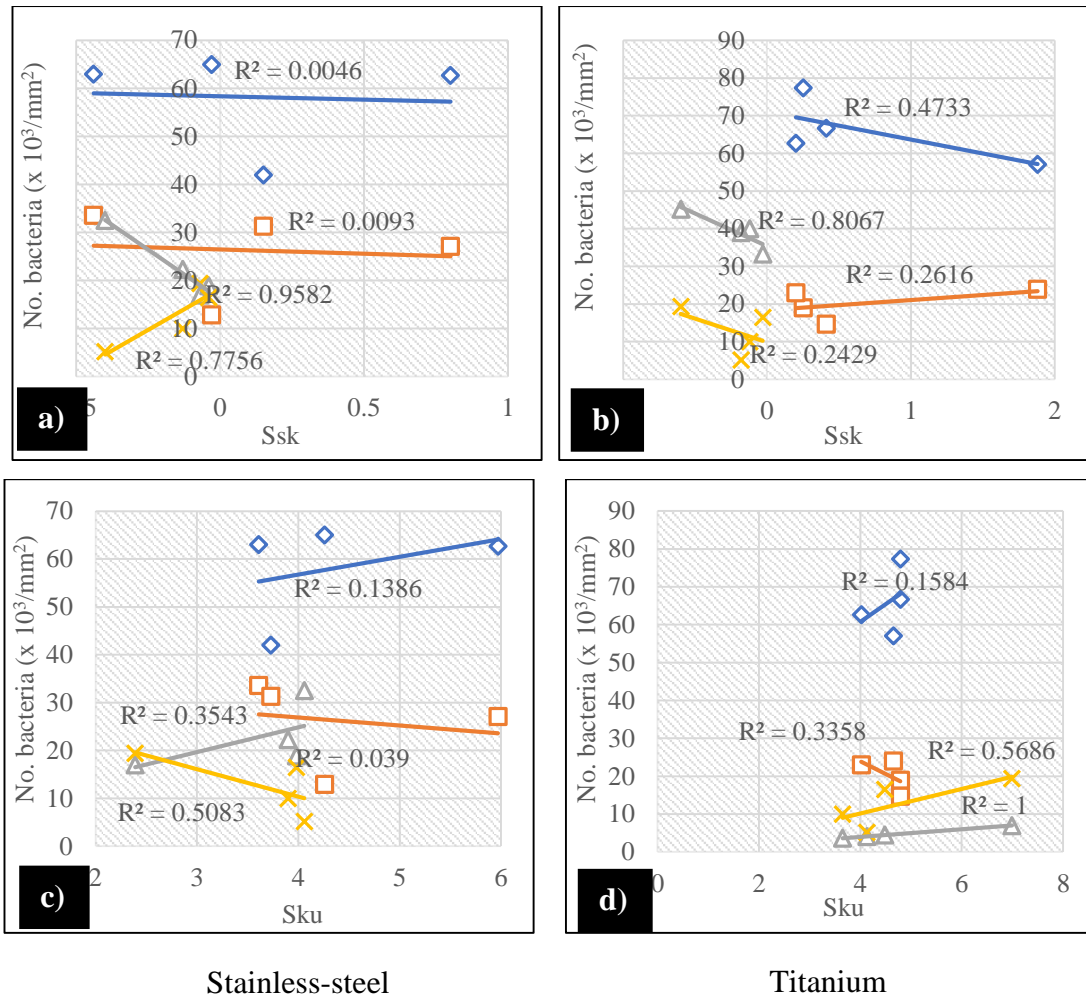


Figure 6-25 Correlation between *Ssk* and *Sku* on the adhesion of *S. aureus* and *E. coli* on SS (a and b) and TI (c and d) in air and argon fabrication. (◇) SA-Air, (△) SA-AR, (□) EC -Air and (X) EC-AR. $R^2 > 0.7$ indicated strong correlation, $R^2 = 0.5 - 0.69$ represented moderate correlation and $R^2 = 0.49 - 0.3$ poorly correlated and $R^2 < 0.29$ provided no correlation.

6.9 Chapter Summary

Toward minimising the bacterial colonisation of surfaces, this chapter presented a laser fabrication technique that not only produced a surface with micro- and nano-scale roughness, but also a slight change towards surface composition that was able to change the rate of adhesion of both *S. aureus* and *E. coli*. Such a multi-scale surface (LIPSS) topography exhibited enhanced antibacterial effect against a range of pathogens, both from Gram-positive and Gram-negative types. This chapter showed that the laser fabrication managed to reduce the adherence of *S. aureus* on the control sample by more than 50% compared to control. The lowest adhesion was attained with SSL-Ar with retained bacteria of $17.0 \times 10^3/\text{mm}^2$, depicting the lowest value for *S. aureus* throughout the study. SS and TI that underwent laser parameter 4 in argon showed a reduced biocompatibility of *E. coli* with the surface. It was presumably contributed by the LIPSS surface, where the impact for multi-height variation was reduced, and the protruding nanograins increased resistance for the adhesion, thereby preventing the bacteria from retaining on the surface. This contributed to the lowest *E. coli* adhesion on the all metal surfaces tested (including with polished and WEDM samples), with only $3.3 \times 10^3/\text{mm}^2$ retained on the surface.

Chapter 7

Conclusions and Recommendations

7.1 Conclusions

The aims of this research were to study the effect of surface topography parameters (with respect to its modified properties) towards the surface wettability and bacterial adhesion of Gram-positive and Gram-negative bacteria. To achieve a surface with the ability to influence wettability and suppressing bacterial adhesion, a deep understanding of the behaviour of the bacteria needs to be addressed prior to commencing work. Therefore, the study involved three important scopes, i) bacterial characterisations, ii) surface fabrication and characterisation and iii) adhesion study and analysis of the contributing factors.

The first part of the research was focused on evaluating the behaviours of the selected bacteria when exposed to inert surfaces. A preliminary study involved the selection and partial characterisation of the bacteria, where CSH, Gram types, surface charge, sizes and shapes were determined prior to adhesion work. The study was carefully aligned to observe the responses of bacteria towards adhesion, where changes in bacterial surface properties were determined beforehand. Three types of bacteria were used, two Gram-positive (*S. aureus* and *B. subtilis*) and *E. coli* (Gram-negative). The adhesion was studied on glass substrates and the effects of exposure time; cell density bacterial age was successfully explored and a correlation between affinity towards adhesion was assessed. Adhesion on glass provided an insight that adhesion behaviour was contributed by the properties of the bacteria and can largely influence the adhesion, before taking an effect from the substrate's properties. The information gathered in this part was compared with adhesion on metallic surfaces.

The second part involved the selection of surface fabrication techniques to produce metallic samples (Stainless steel 316L and titanium Ti6Al4V) with micro and sub-micro roughness. Grinding method (polished), wired electro-erosive discharge machine (WEDM) and laser-assisted techniques were chosen to produce the surfaces of interest. Utilising simple mechanical polishing by grinding with different grit paper produced hydrophilic surfaces with sub-micron sizes, displaying Sa between 0.10 to 0.20 μm . Meanwhile, WEDM fabrication was carried out by varying the machine feed rate (10 mm/min - 22 mm/min), producing mild hydrophobic to hydrophobic surfaces and Sa between 2.00 to 4.00 μm . When femtosecond laser was used, the parameter process was varied in terms of power, scan speed and number of repetitions, and textural surfaces with nanograins were produced. The roughness of the surface for SSL and TIL ranged between 0.01 - 0.66 μm , with increased wettability, higher than the previous two methods. Therefore, the study tested the behaviour of the surface with Sa from 0.01 to 4.00 μm with the different machine approaches. Without limiting Sa values, the fabrication approach also produced two types of surfaces, surface with dominant lay (Str approaches 1) and surfaces with isotropic texture (Str approaching 0).

The third part of the study was to identify the degree of correlation between the surface parameters (Sa , Sku , Ssk , Sal , Sdq , Str , Sdr and Sds) with water contact towards the number of cells attached to the modified surfaces. In previous studies, Sa was considered as the main influential parameter towards hydrophobicity. However, we unexpectedly we found that summit density showed a strong correlation for all fabrication techniques (polished, WEDM and Laser-assisted).

Polished specimens showed a strong correlation with Sa , Sal and Sds . As reported in Chapter 5, the surfaces of polished specimens were flattened with negative skewed distribution and higher Sds values. For WEDM, all parameters showed moderate and poor correlation except Sds with a strong correlation for both metals' specimens. But the value of Sds was relatively lower compared to the polished specimen. Therefore, the influential factor contribution may come from the surface roughness. And finally, for the third technique, laser-assisted showed a high correlation with Sds for both metals treated with

Air and Argon gas. Therefore, it was evident in this study that surface density played an important role towards the hydrophobicity of the metallic surfaces with respect to the structure of the surfaces (smooth and rough).

The adhesion study on the metallic surfaces that underwent polishing, WEDM and laser-assisted techniques were compared with the adhesion onto mirror-finish-polished stainless steel (SS) and titanium (Ti). Following a similar fabrication process, the adhesions of most bacterial species on the SS were much higher than those on titanium. Most of the polished and WEDM surfaces managed to reduce the adhesion of *S. aureus* but failed to produce any significant effects on the *E. coli* adhesion. Instead, more *E. coli* were retained on all stainless steel and titanium surfaces that underwent polishing and WEDM as opposed to controlling. Meanwhile, *B. subtilis* adhesion was varied, where some surfaces reduced the adhesion while other promoted more cell attachment. The study on these two fabrication methods revealed that *S. aureus* contributed to the highest population, followed by *B. subtilis* and *E. coli*. This was true for most SSP, TiP, SSE and TiE surfaces.

Failure to remove *E. coli* in the previous two methods was continuously investigated using metallic surfaces that have undergone the laser-assisted technique. At this stage, the study of *B. subtilis* was omitted since investigation on Gram-positive bacteria can be carried out with *S. aureus* alone. From previous findings, it was speculated that the effect from oxidised surfaces controlled the adhesion, resulting in poor control towards adhesion. Moreover, oxidised surfaces reduced the consequences from varying surface properties. i.e. CA, SA, Ssk and Sku showing very poor correlations with several adhered bacteria. Thereby, two types of fabrication methods were proposed in the study, i) Air fabrication and ii) Argon fabrication. The use of Argon gas as a shielding gas was proposed to cease the formation of an oxidation layer and successfully controlled the adhesion by augmenting other parameters that affected the bacterial behaviour.

The ability of TIL-Ar to suppress adhesion was contributed by the textural LIPSS organisation, where the gap between individual contours lines reduced the contact point of the bacteria and surfaces, minimising adhesion strength, thereby encouraging bacterial detachment from the surface. However, the gap width must be maximised but must not exceed the size/diameter of the bacteria to prevent the trapping of bacteria especially for *E. coli* species. Viewing with SEM confirmed that the grooves or valleys trapped the bacteria and protects them against detachment, thus initiating the colonisation of bacteria. This problem was eliminated when the scan speed was increased to 50 mm/s whilst maintaining the laser power at 120 mW, as in SSL2-TIL2 and SSL4-TIL4 where the number of *E. coli* retained on the surface was reduced up to ~69% in contrast to the same metal at $V = 10$ mm/s. However, the reduced microwaviness and flattened LIPSS did not improve the repellence towards *S. aureus*. In fact, more *S. aureus* was retained on the flattened LIPSS surfaces ($V = 50$ mm/s), marking up to a 50% increase compared to the surface at $V=10$ mm/s. The impact of increased bacterial adhesion was more severe on SS surfaces than on the TI, and independent with respect to air or argon-fabrication.

Overall, the objective of the present work was successfully achieved. The current findings confirmed that using laser fabrication with surface texturing while controlling the surface oxidation using Argon gas has successfully combatted the adhesion of both *S. aureus* and *E. coli*. The TIL-Ar fabrications provided the lowest adhesion for *S. aureus* and *E. coli*, with only $17.2 \times 10^3/\text{mm}^2$ and $3.3 \times 10^3/\text{mm}^2$ cells retained on the surface, respectively. The effect of fabrication method, surface properties and bacterial properties were successfully linked and discussed. In addition, the following conclusions may be drawn from this study:

- ❖ The properties of *S. aureus* as a hydrophobic bacterium proved that Gram-positive bacterium was always a greater coloniser, while the hydrophobic character enhanced its adhesive property. Throughout this study, surfaces were exposed to a similar number of bacteria, but the density for *S. aureus* adhesion was always the highest compared to other bacteria. It is possible to conclude that the abilities of *S. aureus* to be a higher coloniser on a surface are independent of surface finishing, textures, wettability, topography, features, surface chemical and surrounding factors.

- ❖ In addition, it may be appropriate to suggest that the behaviour of adhesion is, firstly, governed by interaction between two similar surfaces, either hydrophobic-hydrophobic or hydrophilic-hydrophilic surfaces. When the hydrophilic surface was used, only bacteria with hydrophilic CSH (*B. subtilis*) would correspond to changes in surface parameters (CA and Sa) which were observed in the polishing study. When mild hydrophobic to hydrophobic ($80^\circ < CA < 100^\circ$) surfaces from WEDM fabrications were used, no correlation was observed for gram-negative/hydrophilic bacteria. Following laser fabrication, the adhesion of *S. aureus* provided a strong correlation with the surface properties of TIL.

Although certain polishing and WEDM surfaces provide better control for the bacterial adhesion, laser fabrication offered advantages over these processes. Laser processing offers flexibility with control elements to produce a surface for a specific property, repeatable with high accuracy. Unlike polishing, laser fabrication does not produce any waste elements since this process only involved the removing, reorganisation and restructuring of the affected area, thereby is considered as a clean process. Besides that, the increased hydrophobicity level of the lasered fabricated surface reduces the friction coefficient and minimises the contact of particles onto the surface, thereby prolonging the shelf life of the materials. This leads to increasing resistance for mass transfer, subsequently reducing the adhesion. Current observations on the impact of surface engineering revealed that there is a possibility that the outer structure of the bacterial surface was damaged due to the brushing effect with the coarse surface that

emerged from the nano structures (grains). The ruptured membrane may cause leakage of the cell content, consequently reducing the chance of survival and proliferation. However, care should be taken related to its contact killing mode as upon prolonged exposure to bacterial suspension, the dead bacteria can serve as a conditioning film and provide a new platform for subsequent bacterial adhesion.

7.2 Recommendations for future studies

The purpose of this study was to develop a surface with certain characteristics that would repel most of the bacteria species, with the ability to carry on the appropriate task with the materials. Before deriving any conclusion relating to surfaces with such criteria, a more thorough study must be carried out for such cases to strengthen the understanding on the adhesion mechanism. Interactions between bacteria and surface are time-dependent, therefore, a continuity study based on a prolonged exposure must be carried out whilst changing the environmental factors i.e. medium types, pH, salinity, etc. Prolonged adhesion to 72 hours might assist to provide better insights into the adhesion capability of the slow binding bacteria. Furthermore, the surface should be tested with different strains of bacteria to test its true capability to reduce bacterial adhesion. It might be beneficial to study Gram-positive and Gram-negative bacteria with different hydrophobicity levels from the current study, i.e. hydrophobic bacteria for Gram-negative, and hydrophilic species for Gram-positive.

Detailed surface and bacteria characterisation should be embarked to gain more information on the adhesion directions. Analysis of surface properties inclusive of surface energy, surface charge, chemical composition (EDX, XPS, FTIR, Raman, NMR) will help to give a better conclusion on the possible factors that are more dominant for the bacterial adhesion. Besides that, AFM and TEM analysis will prove whether the modified surface would be able to reduce the adhesion strength of the bacteria whilst the latter would be able to confirm whether the cell of the bacteria was damaged due to the surface

texture. Data collection also will be beneficial if bacterial count can be distinguished by the number of live and dead bacteria (dead and live cells dye instead of general fluorescent) which will reconfirm the ability of the surface to serve as a contact-mode-killing surface. A study on the bacteria molecular structure and its contribution to the adhesion i.e.: the-EPS-mediated-adhesion, where the composition of polysaccharides and proteins has been reported to facilitate the binding process on the surface. Analysis on the surface protein and carbohydrate would benefit the most especially when employing the chemical functionalisation, which will help in choosing the best chemical that will resist the protein/carbohydrate adsorption.

Surface modification under laser treatment can be directed towards producing a texture with more nanograins on the LIPSS area but with fewer valleys and crevices. Besides that, it is best if the width between two control lines can be controlled between 0.4 – 0.5 μm that will not only increase the resistance for adhesion, but also avoid trapping cells between these features. This surface can be achieved by controlling the laser pulses, scanning speed, the BET and the energy fluence of the laser. Besides that, varying the surface structure with the specific patterns (3D shape) can be achieved from a wide array of modifications from those proposed in the study. Special lithography and plasma techniques with different types of gas exposure can be employed not only to produce surfaces with different texture and roughness, but also may modify the chemical composition that might increase the wettability of the surface without changing its topography. Increasing hydrophobicity can also be modified using different types shielding gas such as fluorocarbons, but it might well increase the overall cost. On top of this, laser fabrication can also be aligned with a chemical modification to provide a surface with specific functionalisation. Embedding special chemical or biological compounds would be very advantageous field to be explored in the future that will increase the ability of the surface to combat bacterial adhesion while enhancing the growth of any tissue for the development of implants. Further coating with materials with low surface energy may be beneficial in combating the bacterial adhesion.

REFERENCES

1. Paul Dunne, E.N., Ron Smith, *Military Spending, Investment and Economic Growth in Small Industrialising Economies*, in *African Econometrics Society Conference*. 2002: University of Witwatersrand, Johannesburg, South Africa.
2. H.C.Flemming, *Microbial Biofouling: Unsolved Problems, Insufficient Approaches, and Possible Solutions*. *Biofilm Highlights*, Springer Series on Biofilms, 2011. **5**: p. 81 - 109.
3. Szewzyk, U., et al., *Microbiological safety of drinking water*. *Annu Rev Microbiol*, 2000. **54**: p. 81-127.
4. Ralph Jimenez, G.R.F., P. V. Kumar & M. Maroncelli, *Femtosecond solvation dynamics of water*. *Nature: International Journal of Science*, 1994. **369**: p. 471-473.
5. Jonah Erlebacher, M.J.A., Alain Karma, Nikolay Dimitrov & Karl Sieradzki, *Evolution of nanoporosity in dealloying*. *Nature: International Journal of Science*, 2001. **410**: p. 450-453.
6. Brendan Drumm, A.W.N., Zdenka Policova, Philip M.Sherman, *Bacterial Cell Surface Hydrophobicity Properties in the Mediation of In Vitro Adhesion by the Rabbit Enteric Pathogen Escherichia coli strain RDEC-1*. *The American Society for Clinical Investigation, Inc*, 1989. **84**: p. 1588 - 1594.
7. Technology, A.C.o.S.a., *Developments in biotechnology*. 1990, HMSO: London.
8. Julian F.V. Vincent, O.A.B., Nikolaj R. Bogatyrev, Adrian Bowyer, Anja-Karina Pahl, *Biomimetics: its practice and theory*. *Journal of The Royal Society Interface*, 2006. **3**: p. 471 - 482.
9. Gebeshuber, I.C., *Biotribology inspires new technologies*. *nanotoday*, 2007. **2**(5): p. 30 - 37.
10. Bhushan, B., *Biomimetics: lessons from nature - an overview*. *Philosophical Transactions of The Royal Society A*, 2009. **367**: p. 1445 - 1486.
11. Bhushan, B., *Biomimetics: lessons from nature--an overview*. *Philos Trans A Math Phys Eng Sci*, 2009. **367**(1893): p. 1445-86.
12. Bar-Cohen, Y., *Biomimetics: Biologically Inspired Technologies*. 2006, United States of America: Taylor & Francis Group, LLC.
13. DAI Zhendong, T.J., Ren Luquan, *Researches and developments of biomimetics in tribology*. *Chinese Science Bulletin*, 2006. **51**(22): p. 2681 - 2689.
14. Vincent, J.F., et al., *Biomimetics: its practice and theory*. *J R Soc Interface*, 2006. **3**(9): p. 471-82.
15. T.D Morgan, M.W., *The effects of surface roughness and type of denture acrylic on biofilm formation by Streptococcus oralis in a constant depth film fermentor*. *Journal of Applied Microbiology*, 2001. **91**: p. 47 - 53.
16. Xi Zhang, F.S., Jia Niu, Yugui Jlang, Zhiqiang Wang, *Superhydrophobic surfacesL from structural control to functional application*. *Journal of Materials Chemistry*, 2007. **18**: p. 621 - 633.
17. Michael Nosonovsky, B.B., *Superhydrophobic surfaces and emerging applications: non-adhesion, energy, green engineering*. *Current Opinion in Colloid & Interface Science*, 2009. **14**: p. 270 - 280.
18. Gu, Z.Z., et al., *Structural color and the lotus effect*. *Angewandte Chemie International Edition*, 2003. **42**(8): p. 894-897.
19. Barry, T.N. and D.A. Forss, *The condensed tannin content of vegetative Lotus pedunculatus, its regulation by fertiliser application, and effect upon protein solubility*. *Journal of the Science of Food and Agriculture*, 1983. **34**(10): p. 1047-1056.
20. Barthlott, W. and C. Neinhuis, *Purity of the sacred lotus, or escape from contamination in biological surfaces*. *Planta*, 1997. **202**(1): p. 1-8.
21. Patankar, N.A., *Mimicking the lotus effect: influence of double roughness structures and slender pillars*. *Langmuir*, 2004. **20**(19): p. 8209-8213.

22. Spori, D.M., et al., *Beyond the lotus effect: roughness influences on wetting over a wide surface-energy range*. Langmuir, 2008. **24**(10): p. 5411-5417.
23. Spaeth, M. and W. Barthlott, *Lotus-Effect®: Biomimetic Super-Hydrophobic Surfaces and their Application*. Advances in Science and Technology, 2009. **60**: p. 38-46.
24. Koch, K. and W. Barthlott, *Superhydrophobic and superhydrophilic plant surfaces: an inspiration for biomimetic materials*. Philos Trans A Math Phys Eng Sci, 2009. **367**(1893): p. 1487-509.
25. Bhushan B, K.K., Jung YC, *Nanostructures for superhydrophobicity and low adhesion*. Soft Matter, 2008. **4**: p. 1799 - 804.
26. Nosonovsky M, B.B., *Multiscale Dissipative Mechanisms and Hierarchical Surfaces: Friction, Superhydrophobicity, and Biomimetics*. 2008, Heidelberg, Germany: Springer-Verlag.
27. Guo, Z., W. Liu, and B.L. Su, *Superhydrophobic surfaces: from natural to biomimetic to functional*. J Colloid Interface Sci, 2011. **353**(2): p. 335-55.
28. Watson, G.S., et al., *A gecko skin micro/nano structure – A low adhesion, superhydrophobic, anti-wetting, self-cleaning, biocompatible, antibacterial surface*. Acta Biomaterialia, 2015. **21**: p. 109-122.
29. Peifu Tang, W.Z., Yan Wang, Boxun Zhang, Hao Wang, Changjian Lin, Lihai Zhang, *Effect of Superhydrophobic Surface of Titanium on Staphylococcus aureus Adhesion*. JOURNAL of Nanomaterials, 2011. **2011**: p. 1 - 8.
30. Stephen L.Hodson, T.E.L., Christopher M.Burke, *Biofouling of fish-cage netting: efficacy and problems of in situ cleaning*. Aquaculture, 1997. **152**: p. 77 - 90.
31. Minglin Ma, R.M.H., *Superhydrophobic Surfaces*. Current Opinion in Colloid & Interface Science, 2006. **11**: p. 193 - 202.
32. Toumey, C., *Apostolic Succession*, in *Engineering & Science*. 2005.
33. Roukes, M., *Plenty of Room Indeed*, in *Sci Am*. 2001, Scientific American, Inc. p. 48 - 57.
34. Breton, P.J., *From microns to nanometers: early landmarks in the science of scanning electron microscope imaging*. Scanning Microsc., 1999. **13**(1): p. 1 - 6.
35. Weillie Zhou, Z.L.W., *Scanning Microscopy for Nanotechnology: Techniques and Applications*. 2007: Springer.
36. Jiang, K., Qunqing Li, Shoushan Fan, *Nanotechnology: spinning continuous carbon nanotube yarns*. Nature, 2002. **419**: p. 801.
37. Yu, M., Mark J. Dyer, George D. Skidmore, Henry Q. Rohrs, XueKun Lu, Kevin D. Ausman, James R. Von Ehr, Rodney S. Ruoff, *Three-dimensional manipulation of carbon nanotubes under a scanning electron microscope*. Nanotechnology, 1999. **10**(3): p. 244.
38. Wang, Z.L., *New developments in transmission electron microscopy for nanotechnology*. Advanced Materials, 2003. **15**(18): p. 1497-1514.
39. Bhushan, B. and Y.C. Jung, *Natural and biomimetic artificial surfaces for superhydrophobicity, self-cleaning, low adhesion, and drag reduction*. Progress in Materials Science, 2011. **56**(1): p. 1-108.
40. Forbes, P., *The Gecko's Foot: Bio-inspiration : Engineering New Materials from Nature*. 2005: W W Norton & Company Incorporated.
41. Mukherjee, P.K., Debaijyoti Mukherjee, Amal K. Maji, S. Rai, Michael Heinrich, *The sacred lotus (Nelumbo nucifera) - phytochemical and therapeutic profile*. Journal of Pharmacy and Pharmacology, 2009. **61**(4): p. 407 - 422.
42. Waldron, K.J. *A Brief History of Biomimetic Robotics*. in *International Symposium on History of Machines and Mechanisms Proceedings HMM 2000*. 2000. Springer Netherlands.
43. Mohammad Shateri Khalil-Abad, M.E.Y., *Superhydrophobic antibacterial cotton textiles*. J Colloid Interface Sci, 2010. **351**: p. 293 - 298.
44. Borsellino, C., G. Di Bella, *Paper-reinforced biomimetic cellular structures for automotive applications*. Materials & Design, 2009. **30**(10): p. 4054 - 4059.

45. Pang, J.W.C., I.P. Bond, *Bleeding composites - damage detection and self-repair using a biomimetic approach*. Composites Part A: Applied Science and Manufacturing, 2005. **36**(2): p. 183 - 188.
46. Ghasemi-Varnamkhasti, M., Seyed Saeid Mohtasebi, Maryam Siadat, *Biomimetic-based odor and taste sensing systems to food quality and safety characterisation: An overview on basic principles and recent achievements*. Journal of Food Engineering, 2010. **100**(3): p. 377 - 387.
47. Tang, Z., Ying Wang, Paul Podsiadlo, Nicholas A. Kotov, *Biomedical Applications of Layer-by-Layer Assembly: From Biomimetics to Tissue Engineering*. Advanced Materials, 2006. **18**(24): p. 3203 - 3224.
48. Badilescu, S. and M. Packirisamy, *BioMEMS : science and engineering perspectives*. 2011, Boca Raton: CRC Press. xvii, 329 p.
49. Kowalczyk, S.W., T.R. Blosser, and C. Dekker, *Biomimetic nanopores: learning from and about nature*. Trends in biotechnology, 2009. **29**(12): p. 607-614.
50. Dufrene, Y.F., Vermeiren, H., Van der Leyden, J., Rouxhet, P.G, *Direct evidence for the involvement of extracellular proteins in the adhesion of Azospirillum brasilense*. Microbiology, 1996. **142**: p. 855 - 865.
51. Dr. Mortimer L. Downey, D.D.T.M., Gary R. Bachula, Delores M. Etter, Dr. E. Fenton Carey, Lori A. Perine, *National Nanotechnology Initiative: Leading to the Next Industrial Revolution*, C.o.T.N.S.a.T. Council, Editor. 2000, Interagency Working Group on Nanoscience, Engineering and Technology: Washington D.C.
52. Nosonovsky, M. and B. Bhushan, *Superhydrophobic surfaces and emerging applications: Non-adhesion, energy, green engineering*. Current Opinion in Colloid & Interface Science, 2009. **14**(4): p. 270-280.
53. Hu, X., et al., *Bacterial and osteoblast behaviour on titanium, cobalt–chromium alloy and stainless steel treated with alkali and heat: A comparative study for potential orthopedic applications*. Journal of Colloid and Interface Science, 2014. **417**: p. 410-419.
54. Cunha, A., et al., *Femtosecond laser surface texturing of titanium as a method to reduce the adhesion of Staphylococcus aureus and biofilm formation*. Applied Surface Science, 2016. **360**: p. 485-493.
55. Jing, H., E. Sahle-Demessie, and G.A. Sorial, *Inhibition of biofilm growth on polymer-MWCNTs composites and metal surfaces*. Science of The Total Environment, 2018. **633**: p. 167-178.
56. Shuai, C., et al., *Microstructure, biodegradation, antibacterial and mechanical properties of ZK60-Cu alloys prepared by selective laser melting technique*. Journal of Materials Science & Technology, 2018. **34**(10): p. 1944-1952.
57. Wenzel, R.P., *Health Care–Associated Infections: Major Issues in the Early Years of the 21st Century*. Clinical Infectious Diseases, 2007. **45**(Supplement_1): p. S85-S88.
58. Godoy-Gallardo, M., et al., *Covalent immobilization of hLf1-11 peptide on a titanium surface reduces bacterial adhesion and biofilm formation*. Acta Biomaterialia, 2014. **10**(8): p. 3522-3534.
59. Askeland, D.R., *The Science and Engineering of Materials*. 1991: Springer, Dordrecht.
60. Donald M, B., Pentti Tengvall, Marcus Textor, Peter Thomsen *Titanium in Medicine: material science, surface science, engineering, biological responses and medical applications*. Formatex Research Center ed. 2001: Springer Verlag Berlin Heidelberg.
61. Liam Blunt, X.J., *Advanced Techniques for Assessment Surface Topography Development of a Basis for 3D Surface Texture Standards “SURFSTAND”*. 2003, Kogan Page Limited.
62. X. Liu, F.G., *A novel multi-function tribological probe microscope for mapping surface properties*. Measurement Science and Technology, 2004. **15**: p. 91 - 102.
63. Loredana Santo, J.P.D., *Surface Engineering Techniques and Applications: Research Advancements*. IGI Global, 2014.

64. Bohinc, K., Drazic G., Abram A., Jevsnik M., Jersek B., Nipic D., Kurincic M and Raspor P. , *Metal surface characteristics dictate bacterial adhesion capacity*. International Journal of Adhesion & Adhesives, 2016. **68**: p. 39-46.
65. Kaushik, R.M., A.B. Bhandakkar, and T.U. Patro, *Solution of emulsifiable oil and hydrogen peroxide for chemical–mechanical polishing of Ti alloy—A green approach*. Materials Letters, 2014. **122**: p. 252-255.
66. Heimer, S., et al., *Surface properties of polyetheretherketone after different laboratory and chairside polishing protocols*. The Journal of Prosthetic Dentistry, 2017. **117**(3): p. 419-425.
67. Chegiani, F., S.T.S. Bukkapatnam, and M.E. Mansori, *Thermo-mechanical Effects in Mechanical Polishing of Natural Fiber Composites*. Procedia Manufacturing, 2018. **26**: p. 294-304.
68. Yang N, Z.W., L Z and Sun T *Wear process of single crystal diamond affected by sliding velocity and contact pressure in mechanical polishing*. Diamond and Related Material, 2015.
69. Ozdemir, Z., A. Ozdemir, and G.B. Basim, *Application of chemical mechanical polishing process on titanium based implants*. Materials Science and Engineering: C, 2016. **68**: p. 383-396.
70. Skovager, A., et al., *A comparative study of fine polished stainless steel, TiN and TiN/Ag surfaces: Adhesion and attachment strength of Listeria monocytogenes as well as anti-listerial effect*. Colloids and Surfaces B: Biointerfaces, 2013. **109**: p. 190-196.
71. Kang, D.-H., et al., *Effect of polishing method on surface roughness and bacterial adhesion of zirconia-porcelain veneer*. Ceramics International, 2017. **43**(7): p. 5382-5387.
72. Hu, L., et al., *Fabrication of biomimetic superhydrophobic surface based on nanosecond laser-treated titanium alloy surface and organic polysilazane composite coating*. Colloids and Surfaces A: Physicochemical and Engineering Aspects, 2018. **555**: p. 515-524.
73. Kulkarni, O. and S. Kulkarni, *Process Parameter Optimisation in WEDM by Grey Wolf Optimiser*. Materials Today: Proceedings, 2018. **5**(2, Part 1): p. 4402-4412.
74. Tejas Ajay, B., P. Mayur Vitthal, and G. Rajyalakshmi, *WEDM machining on Aerospace Materials for improving Material Properties*. Materials Today: Proceedings, 2017. **4**(8): p. 9107-9116.
75. Choudhuri, B., et al., *Modelling of Surface Roughness and Tool Consumption of WEDM and Optimisation of Process Parameters Based on Fuzzy-PSO*. Materials Today: Proceedings, 2018. **5**(2, Part 2): p. 7505-7514.
76. Muralova, K., et al., *Analysis of surface morphology and topography of pure aluminium machined using WEDM*. Measurement, 2018. **114**: p. 169-176.
77. Zhang, Z., et al., *Study on machining characteristics of WEDM with ultrasonic vibration and magnetic field assisted techniques*. Journal of Materials Processing Technology, 2016. **234**: p. 342-352.
78. Torres, A., I. Puertas, and C.J. Luis, *Modelling of surface finish, electrode wear and material removal rate in electrical discharge machining of hard-to-machine alloys*. Precision Engineering, 2015. **40**: p. 33-45.
79. Pramanik, A. and A.K. Basak, *Sustainability in wire electrical discharge machining of titanium alloy: Understanding wire rupture*. Journal of Cleaner Production, 2018. **198**: p. 472-479.
80. Cheng, X., et al., *Development of ultra-precision machining system with unique wire EDM tool fabrication system for micro/nano-machining*. CIRP Annals, 2008. **57**(1): p. 415-420.
81. Ma, Q., et al., *Fabricating robust and repairable superhydrophobic surface on carbon steel by nanosecond laser texturing for corrosion protection*. Applied Surface Science, 2018. **455**: p. 748-757.

82. Cunha A., E., AM, Plawinski L., Serro, A.P, do Rego A.M., Almeida A., Urdaci M.C., Durrieu M.C and Vilar R, *Femtosecond laser surface texturing of titanium as a method to reduce the adhesion of Staphylococcus aureus and biofilm formation*. Applied Surface, 2016. **360**(485 - 493).
83. Giorgi, C.D., Furlan V., Demir, A.G, Tallarita E., Candiani G., and Previtali B, *Laser micropolishing of AISI304 stainless steel surfaces for cleanability and bacteria removal capability*. Applied surface science, 2017. **406**: p. 199-211.
84. Liu, X. and H.C. Man, *Laser fabrication of Ag-HA nanocomposites on Ti6Al4V implant for enhancing bioactivity and antibacterial capability*. Materials Science and Engineering: C, 2017. **70**: p. 1-8.
85. Maragkaki, S., et al., *Wavelength dependence of picosecond laser-induced periodic surface structures on copper*. Applied Surface Science, 2017. **417**: p. 88-92.
86. Du, Q., et al., *Fabrication of superhydrophobic/superhydrophilic patterns on polyimide surface by ultraviolet laser direct texturing*. Journal of Materials Processing Technology, 2018. **251**: p. 188-196.
87. Katsutoshi Hori, N.H., Mari Nannbu, Kei Kanie, Mina Okochi, Hiroyuki Honda, Hisami Watanabe, *Drastic change in cell surface hydrophobicity of a new bacterial strain, Pseudomonas sp. TIS1-127, induced by growth temperature and its effects on the toluene-conversion rate* Journal of Bioscience and Bioengineering, 2009. **107**(3): p. 250-255.
88. van Hoogmoed, C.G., et al., *Inhibition of *Streptococcus mutans* NS Adhesion to Glass with and without a Salivary Conditioning Film by Biosurfactant-Releasing *Streptococcus mitis* Strains*. Applied and Environmental Microbiology, 2000. **66**(2): p. 659-663.
89. Garrett, T.R., M. Bhakoo, and Z. Zhang, *Bacterial adhesion and biofilms on surfaces*. Progress in Natural Science, 2008. **18**(9): p. 1049-1056.
90. Al-Abbas, F.M., Spear, J. R., Kakpovbia, A., Balhareth, N. M., Olson, D. L., and Mishra, B, *Bacterial attachment to metal substrate and its effects on microbiologically-influenced corrosion in transporting hydrocarbon pipelines*. Journal of pipeline engineering, 2012. **11**: p. 63-72.
91. Alam, F. and K. Balani, *Adhesion force of staphylococcus aureus on various biomaterial surfaces*. Journal of the Mechanical Behaviour of Biomedical Materials, 2017. **65**: p. 872-880.
92. Hermansson, M., *The DVLO theory in microbial adhesion*. Colloids and Surfaces B: Biointerfaces, 1999. **14**: p. 105 - 119.
93. Shaikh, S., et al., *Femtosecond laser induced surface modification for prevention of bacterial adhesion on 45S5 bioactive glass*. Journal of Non-Crystalline Solids, 2018. **482**: p. 63-72.
94. Faisal M AlAbbas, J.R.S., Anthony Kakpovbia, Nasser M Balhareth, David L Olson, and Brajendra Mishra, *Bacterial attachment to metal substrate and its effects on microbiologically-influenced corrosion in trasporting hydrocarbon pipelines*. The Journal of Pipeline Engineering, 2012: p. 63 - 72.
95. Han, A., et al., *Bacterial adhesion mechanisms on dental implant surfaces and the influencing factors*. International Journal of Adhesion and Adhesives, 2016. **69**: p. 58-71.
96. Yang, M., et al., *Control of bacterial adhesion and growth on honeycomb-like patterned surfaces*. Colloids and Surfaces B: Biointerfaces, 2015. **135**: p. 549-555.
97. Nguyen, D., et al., *Adhesion and surface energy of shale rocks*. Colloids and Surfaces A: Physicochemical and Engineering Aspects, 2017. **520**: p. 712-721.
98. Zhu, C., et al., *Antimicrobial design of titanium surface that kill sessile bacteria but support stem cells adhesion*. Applied Surface Science, 2016. **389**: p. 7-16.
99. Yoon, S.H., et al., *Superhydrophobic and superhydrophilic nanocomposite coatings for preventing Escherichia coli K-12 adhesion on food contact surface*. Journal of Food Engineering, 2014. **131**: p. 135-141.

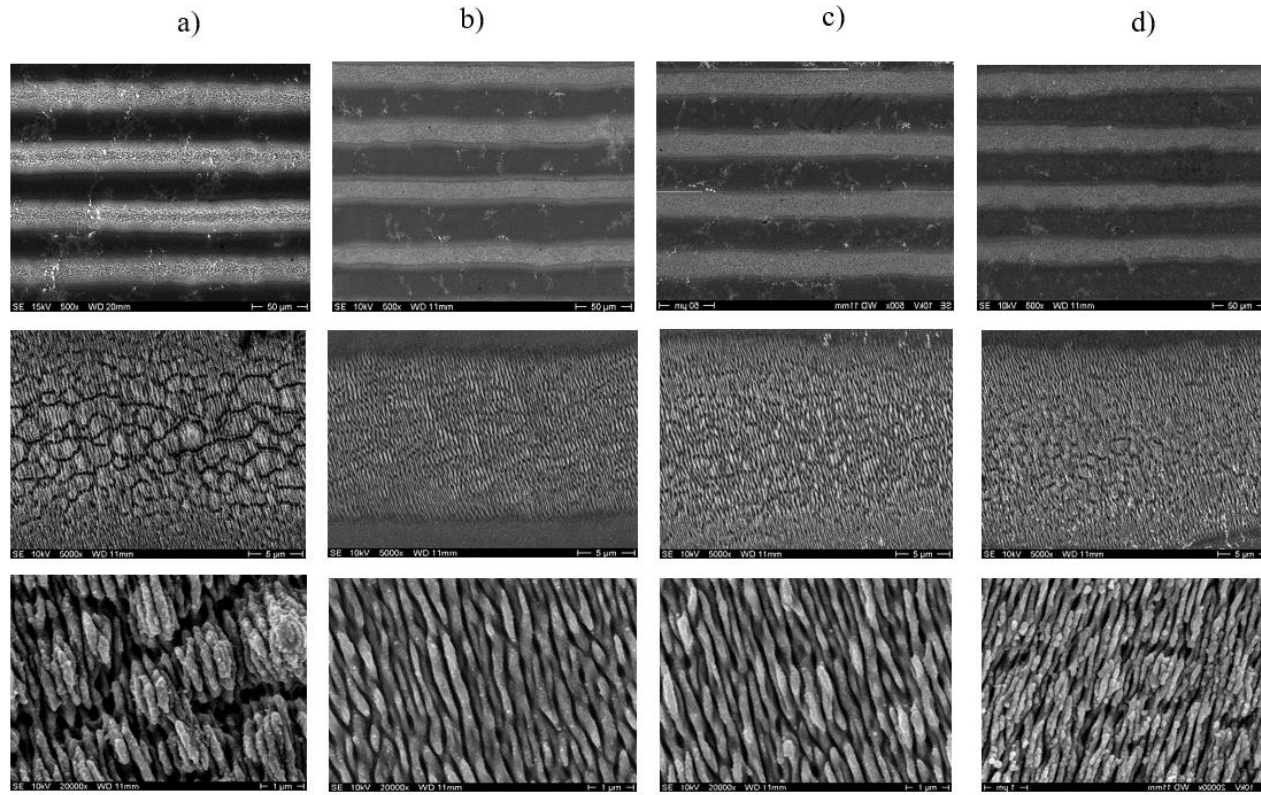
100. Shiau, *Plasma -chemical improvements* 2018.
101. Alam, F. and K. Balani, *Role of silver/zinc oxide in affecting de-adhesion strength of Staphylococcus aureus on polymer biocomposites*. Materials Science and Engineering: C, 2017. **75**: p. 1106-1114.
102. Lu, N., et al., *Fabrication of PDMS surfaces with micro patterns and the effect of pattern sizes on bacteria adhesion*. Food Control, 2016. **68**: p. 344-351.
103. Truong, V.K., et al., *The influence of nano-scale surface roughness on bacterial adhesion to ultrafine-grained titanium*. Biomaterials, 2010. **31**(13): p. 3674-3683.
104. Korber, D.R., et al., *Substratum topography influences susceptibility of Salmonella enteritidis biofilms to trisodium phosphate*. Applied and Environmental Microbiology, 1997. **63**(9): p. 3352-3358.
105. Little, E.B., G.M. Edelman, and B.A. Cunningham, *Palmitoylation of the Cytoplasmic Domain of the Neural Cell Adhesion Molecule N-CAM Serves as an Anchor to Cellular Membranes*. Cell Adhesion and Communication, 1998. **6**(5): p. 415-430.
106. Sheng, X., Y.P. Ting, and S.O. Pehkonen, *The influence of ionic strength, nutrients and pH on bacterial adhesion to metals*. Journal of Colloid and Interface Science, 2008. **321**(2): p. 256-264.
107. Dewald, C., et al., *Gold nanoparticle contact point density controls microbial adhesion on gold surfaces*. Colloids and Surfaces B: Biointerfaces, 2018. **163**: p. 201-208.
108. Morgan, T.D. and M. Wilson, *The effects of surface roughness and type of denture acrylic on biofilm formation by Streptococcus oralis in a constant depth film fermentor*. Journal of Applied Microbiology, 2001. **91**(1): p. 47-53.
109. Doyle R.J., N.-H.F., Singh J.S., *Hydrophobic characteristics of Bacillus spores*. Current Microbiology, 1984. **10**: p. 329 - 332.
110. Harimawan, A. and Y.-P. Ting, *Investigation of extracellular polymeric substances (EPS) properties of P. aeruginosa and B. subtilis and their role in bacterial adhesion*. Colloids and Surfaces B: Biointerfaces, 2016. **146**: p. 459-467.
111. Ribeiro, M.C., et al., *Preconditioning of the stainless steel surface affects the adhesion of Bacillus cereus spores*. International Dairy Journal, 2017. **66**: p. 108-114.
112. C.A Huang, C.C.H., H.H Kuo, *The surface characteristics of P/M high-speed steel (ASP 23) multi-cut with wire electrical discharge machine (WEDM)*. Journal of Materials Processing Technology, 2003. **140**(1 - 3): p. 298 - 302.
113. S. Mahendran, D.R. *Micro-EDM: Overview and Recent Developments*. in *National Conference in Mechanical Engineering Research and Postgraduate Students (NCMER)*. 2010. FKM Conference Hall, UMP Kuantan Pahang: Universiti Malaysia Pahang.
114. Xiong, Y.Q., et al., *Influence of pH on adaptive resistance of Pseudomonas aeruginosa to aminoglycosides and their postantibiotic effects*. Antimicrobial Agents and Chemotherapy, 1996. **40**(1): p. 35-39.
115. Beveridge, T., *Use of the Gram stain in microbiology*. Biotechnic & Histochemistry, 2009. **76**(3).
116. Habimana, O., Semião, A. J.C., and Casey, E, *The role of cell-surface interactions in bacterial initial adhesion and consequent biofilm formation on nanofiltration/reverse osmosis membranes*. Journal of Membrane Science, 2014. **454**: p. 82-96.
117. Schöler, A., et al., *Analysis of soil microbial communities based on amplicon sequencing of marker genes*. Biology and Fertility of Soils, 2017. **53**(5): p. 485-489.
118. Yang, H., et al., *Characterisation of Multiple-Antimicrobial-Resistant Escherichia coli Isolates from Diseased Chickens and Swine in China*. Journal of Clinical Microbiology, 2004. **42**(8): p. 3483-3489.
119. Barton, L.L., *Structural and Functional Relationships in Prokaryotes*. 2005: Springer New York.
120. Sharon L. Walker, J.E.H., 2 Jeremy A. Redman, and Menachem Elimelech, *Influence of Growth Phase on Adhesion Kinetics of Escherichia coli D21g*. APPLIED AND ENVIRONMENTAL MICROBIOLOGY, 2005. **71**(6): p. 3093-3099.

121. N. O. Kjeldgaard, O.M., M. Schaechter*, *The Transition Between Different Physiological States During Balanced Growth of Salmonella typhimurium*. Microbiology, 1958. **19**: p. 607-616.
122. Vadia, S. and P.A. Levin, *Growth rate and cell size: a re-examination of the growth law*. Current Opinion in Microbiology, 2015. **24**: p. 96-103.
123. Vázquez-Juárez, R., T. Andlid, and L. Gustafsson, *Cell surface hydrophobicity and its relation to adhesion of yeasts isolated from fish gut*. Colloids and Surfaces B: Biointerfaces, 1994. **2**(1): p. 199-208.
124. Hilal, N. and W.R. Bowen, *Atomic force microscope study of the rejection of colloids by membrane pores*. Desalination, 2002. **150**(3): p. 289-295.
125. Jones, D.S., et al., *Standardisation and comparison of methods employed for microbial cell surface hydrophobicity and charge determination*. International Journal of Pharmaceutics, 1996. **131**(1): p. 83-89.
126. M. Rosenberg, D.G.a.E.R., *Adherence of Bacteria to Hydrocarbons: A simple method for Measuring Cell-Surface Hydrophobicity*. FEMS Microbiology Letters, 1980. **9**: p. 29-33.
127. Toranzo, I.B.Y.S.J.L.B.A.E., *Influence of the growth conditions on the hydrophobicity of Renibacterium salmoninarum evaluated by different methods*. FEMS Microbiology Letters, 1989. **60**(1).
128. Ahimou, F., et al., *Influence of electrical properties on the evaluation of the surface hydrophobicity of Bacillus subtilis*. Journal of Microbiological Methods, 2001. **45**(2): p. 119-126.
129. Hamadi F., a.L.H., *Comparison of contact angle measurement and microbial adhesion to solvents for assaying electron donor-electron acceptor (acid-base) properties of bacterial surface*. Colloids and Surfaces B: Biointerfaces, 2008. **65**(1): p. 134-139.
130. Kilonzo, P., A. Margaritis, and M. Bergougnou, *Effects of surface treatment and process parameters on immobilization of recombinant yeast cells by adsorption to fibrous matrices*. Bioresource Technology, 2011. **102**(4): p. 3662-3672.
131. Hamadi, A., et al., *Regulation of focal adhesion dynamics and disassembly by phosphorylation of FAK at tyrosine 397*. Journal of Cell Science, 2005. **118**(19): p. 4415-4425.
132. Mitik-Dineva N1, W.J., Mocanasu RC, Stoddart PR, Crawford RJ, Ivanova EP., *Impact of nano-topography on bacterial attachment*. Biotechnol, 2008(April): p. 536-544.
133. Morra, M. and C. Cassinelli, *Bacterial adhesion to polymer surfaces: A critical review of surface thermodynamic approaches*. Journal of Biomaterials Science, Polymer Edition, 1998. **9**(1): p. 55-74.
134. Hamadi, F. and H. Latrache, *Comparison of contact angle measurement and microbial adhesion to solvents for assaying electron donor-electron acceptor (acid-base) properties of bacterial surface*. Colloids and Surfaces B: Biointerfaces, 2008. **65**(1): p. 134-139.
135. Geertsema-Doornbusch, G.I., H.C. van der Mei, and H.J. Busscher, *Microbial cell surface hydrophobicity The involvement of electrostatic interactions in microbial adhesion to hydrocarbons (MATH)*. Journal of Microbiological Methods, 1993. **18**(1): p. 61-68.
136. Zikmanis P., S.L., Auzina L. and Andersone, *Hydrophobicity of bacteria Zymomonas mobilis under varied environmental conditions*. Process Biochemistry **42**(4): p. 745-750.
137. Werner-Washburne, M., et al., *Stationary phase in the yeast Saccharomyces cerevisiae*. Microbiological Reviews, 1993. **57**(2): p. 383-401.
138. Ranu, B.C., A. Hajra, and U. Jana, *Indium(III) Chloride-Catalyzed One-Pot Synthesis of Dihydropyrimidinones by a Three-Component Coupling of 1,3-Dicarbonyl Compounds, Aldehydes, and Urea: An Improved Procedure for the Biginelli Reaction*. The Journal of Organic Chemistry, 2000. **65**(19): p. 6270-6272.
139. Yen, M.-T., J.-H. Yang, and J.-L. Mau, *Physicochemical characterisation of chitin and chitosan from crab shells*. Carbohydrate Polymers, 2009. **75**(1): p. 15-21.

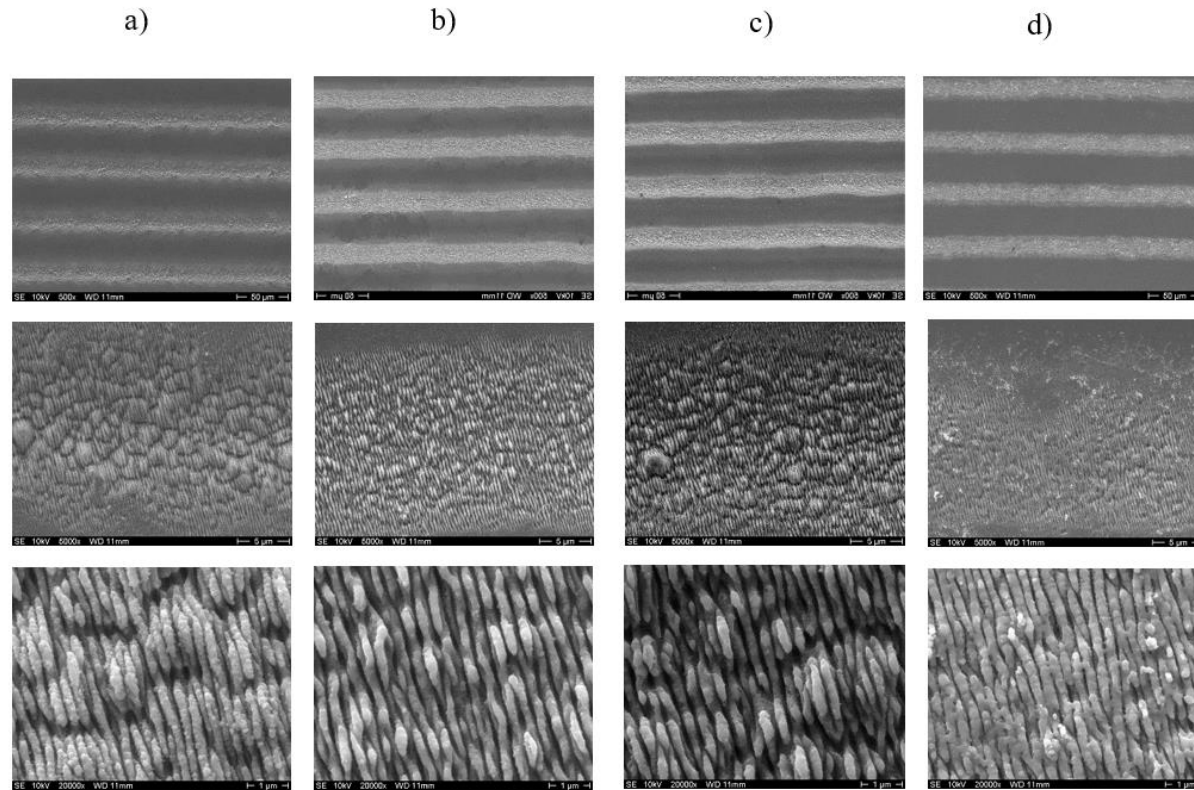
140. Warth, A.D., *Relationship between the heat resistance of spores and the optimum and maximum growth temperatures of Bacillus species*. Journal of Bacteriology, 1978. **134**(3): p. 699-705.
141. Rose, A.H. and G.M. J, *Advances in Microbial Physiology*. 1978: Elsevier Science.
142. Zhenyong Zhao, A.S., Jonathan Woon-Chung Wong, *Effects of rhamnolipids on cell surface hydrophobicity of PAH degrading bacteria and the biodegradation of phenanthrene*. Bioresource Technology 2011. **102**: p. 3999-4007.
143. Jana, N.R., et al., *Polyglutamine length-dependent interaction of Hsp40 and Hsp70 family chaperones with truncated N-terminal huntingtin: their role in suppression of aggregation and cellular toxicity*. Human Molecular Genetics, 2000. **9**(13): p. 2009-2018.
144. Baikun Li, B.E.L., *Bacterial adhesion to glass and metal-oxide surfaces*. Colloids and Surfaces B: Biointerfaces 2004. **36**: p. 81-90.
145. Yea-Ling Ong, A.R., George Georgian, Mukl M. Sharma, *Adhesion forces between e.coli bacteria and biomaterial surfaces*. Langmuir, 1999. **15**(8): p. 2714 - 2725.
146. Cunliffe, D., et al., *Bacterial Adhesion at Synthetic Surfaces*. Applied and Environmental Microbiology, 1999. **65**(11): p. 4995-5002.
147. Chan, C.-W., et al., *Enhancing the antibacterial performance of orthopaedic implant materials by fibre laser surface engineering*. Applied Surface Science, 2017. **404**: p. 67-81.
148. Bellon-Fontaine, M.N., J. Rault, and C.J. van Oss, *Microbial adhesion to solvents: a novel method to determine the electron-donor/electron-acceptor or Lewis acid-base properties of microbial cells*. Colloids and Surfaces B: Biointerfaces, 1996. **7**(1): p. 47-53.
149. Hogan, D.A., *Quorum Sensing: Alcohols in a Social Situation*. Current Biology, 2006. **16**(12): p. 457-458.
150. Fan, L.-J., Karinp, T., *Effect of serum concentration on adhesion of monocytic THP-1 cells onto cultured EC monolayer and EC-SMC co-culture*. Journal of Zhejiang University SCIENCE B, 2008. **9**(8): p. 623 - 629.
151. Fletcher, S.M.M., *The effect of temperature and relative humidity on the survival of bacteria attached to dry solid surfaces*. JOurnal of Applied Microbiology, 1988. **7**(4).
152. Kerro Dego, J.E.v.D.a.H.N., *Factors involved in the early pathogenesis of bovine Staphylococcus aureus mastitis with emphasis on bacterial adhesion and invasion A review*. 24, 2002. **4**(181-198).
153. G. Harkes, J.F.a.J.D., *Adhesion of Escherichia coli on to a series of poly(methacrylates) differing in charge and hydrophobicity* **Biomaterials**, 1991. **12**: p. 109-122.
154. van Loosdrecht, M.C., et al., *Influence of interfaces on microbial activity*. Microbiological Reviews, 1990. **54**(1): p. 75-87.
155. Whitehouse, D.J., *Handbook of Surface Metrology*. 1994: CRC Press.
156. Bhusan, B., *Surface Roughness Analysis and Measurement Technique*, in *Modern Tribology Handbook*, B. Bhusan, Editor. 2001, CRC Press Taylor & Francis Group.
157. Pragya Shandilya, P.K.J., N. K. Jain, *Parametric optimisation during wire electrical discharge machining using response surface methodology*. SciVerse ScienceDirect - Procedia Engineering, 2012. **38**(2012): p. 2371 - 2377.
158. Aniza Alias, B.A., Norliana Mohd Abbas, *Influence of Machine Feed Rate in WEDM of Titanium Ti-6Al-4v with constant current (6A) using Brass Wire*. SciVerse ScienceDirect - Procedia Engineering, 2012. **41**(2012): p. 1806 - 1811.
159. Bohinc, K., et al., *Metal surface characteristics dictate bacterial adhesion capacity*. International Journal of Adhesion and Adhesives, 2016. **68**: p. 39-46.
160. Bernardes, P.C., et al., *Assessment of hydrophobicity and roughness of stainless steel adhered by an isolate of Bacillus cereus from a dairy plant*. Brazilian Journal of Microbiology, 2010. **41**: p. 984-992.

161. Epperlein, N., et al., *Influence of femtosecond laser produced nanostructures on biofilm growth on steel*. Applied Surface Science, 2017. **418**: p. 420-424.
162. Almaguer-Flores A., S.-B.P., Galicia R and Rodil S.E. , *Bacterial adhesion on amorphous and crystalline metal oxide coatings*. Materials Science and Engineering C. , 2015. **57**: p. 88-89.
163. Katsikogianni, Y.F.M.M., *Theoretical and experimental approaches of bacteria-biomaterial interactions*. JOurnal of Recommendation Service, 2007. **38**(12).
164. Bagherifard, S., et al., *The influence of nanostructured features on bacterial adhesion and bone cell functions on severely shot peened 316L stainless steel*. Biomaterials, 2015. **73**: p. 185-197.
165. Rajab F., L., C.M., Benson P.S. Li L. and Whitehead K.A, *Picosecond laser treatment production of hierarchical structured stainless steel to reduce bacterial fouling*. Food and Bioproducts processing, 2018. **109**: p. 29-40.
166. Q.Zhao, Y.L., C.Wang, S.Wang, N.Peng, C.Jeynes, *Bacterial Adhesion on ion-implanted stainless steel surfaces*. Applied Surface Science, 2007. **253**: p. 8674 - 8681.
167. Braem, A., et al., *Staphylococcal biofilm growth on smooth and porous titanium coatings for biomedical applications*. Journal of Biomedical Materials Research Part A, 2014. **102**(1): p. 215-224.
168. Ludecke C., R.M., Yu W., Horn U., Bossert J and Jandt K.D Colloids and Surfaces B: Biointerfaces, 2016. **145**: p. 617-625.
169. Ortega MP, H.T., Watanabe H and Sakiyama T, *Adhesion behaviour and removability of Escherichia coli on stainless steel surface*. Food Control, 2010. **21**: p. 573-578.
170. De Giorgi, C., et al., *Laser micropolishing of AISI 304 stainless steel surfaces for cleanability and bacteria removal capability*. Applied Surface Science, 2017. **406**: p. 199-211.
171. Garson, M.J., et al., *A sponge/dinoflagellate association in the haplosclerid sponge Haliclona sp.: cellular origin of cytotoxic alkaloids by Percoll density gradient fractionation*. Cell and Tissue Research, 1998. **293**(2): p. 365-373.
172. Niaa, S.R.A.A.D., *Chemical composition and evolution of the garnets in the Astamal Fe-LREE distal skarn deposit, Qara-Dagh–Sabalan metallogenic belt, Lesser Caucasus, NW Iran*. Ore Geology Review, 2016. **78**(October): p. 166.175.

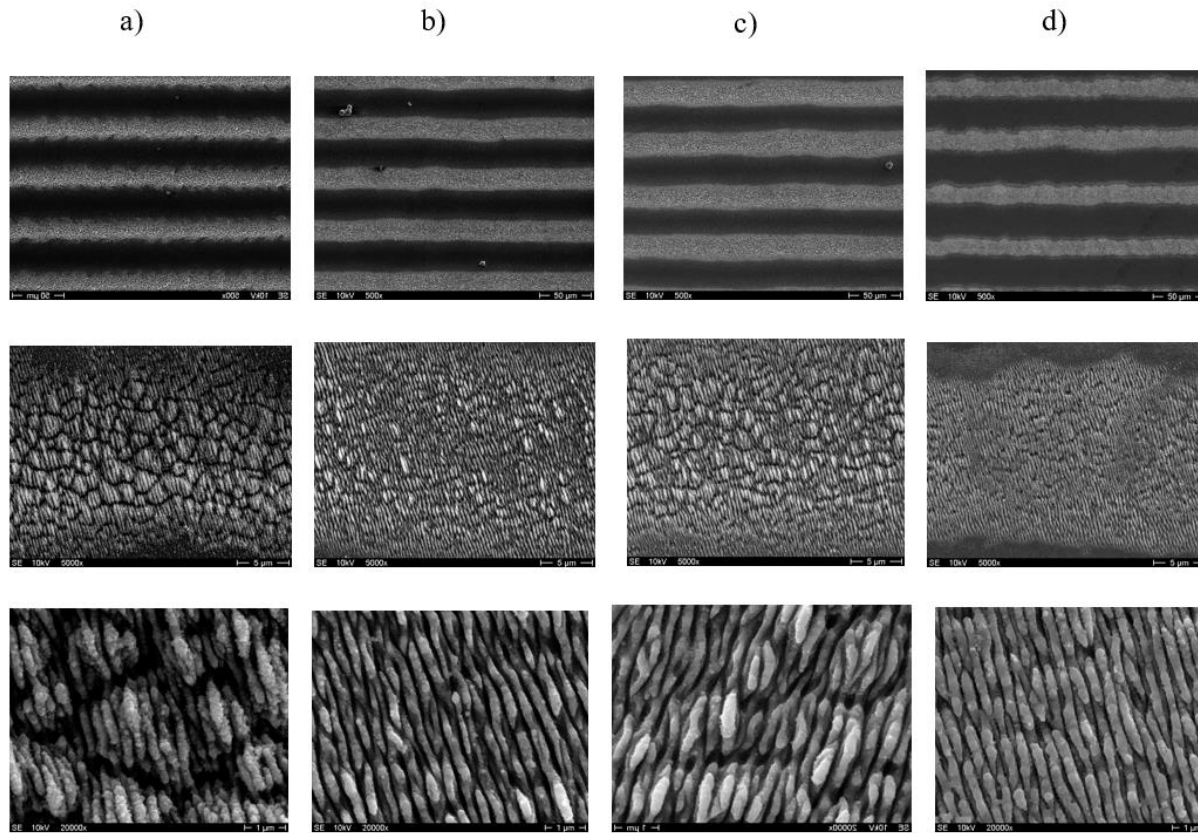
APPENDIX



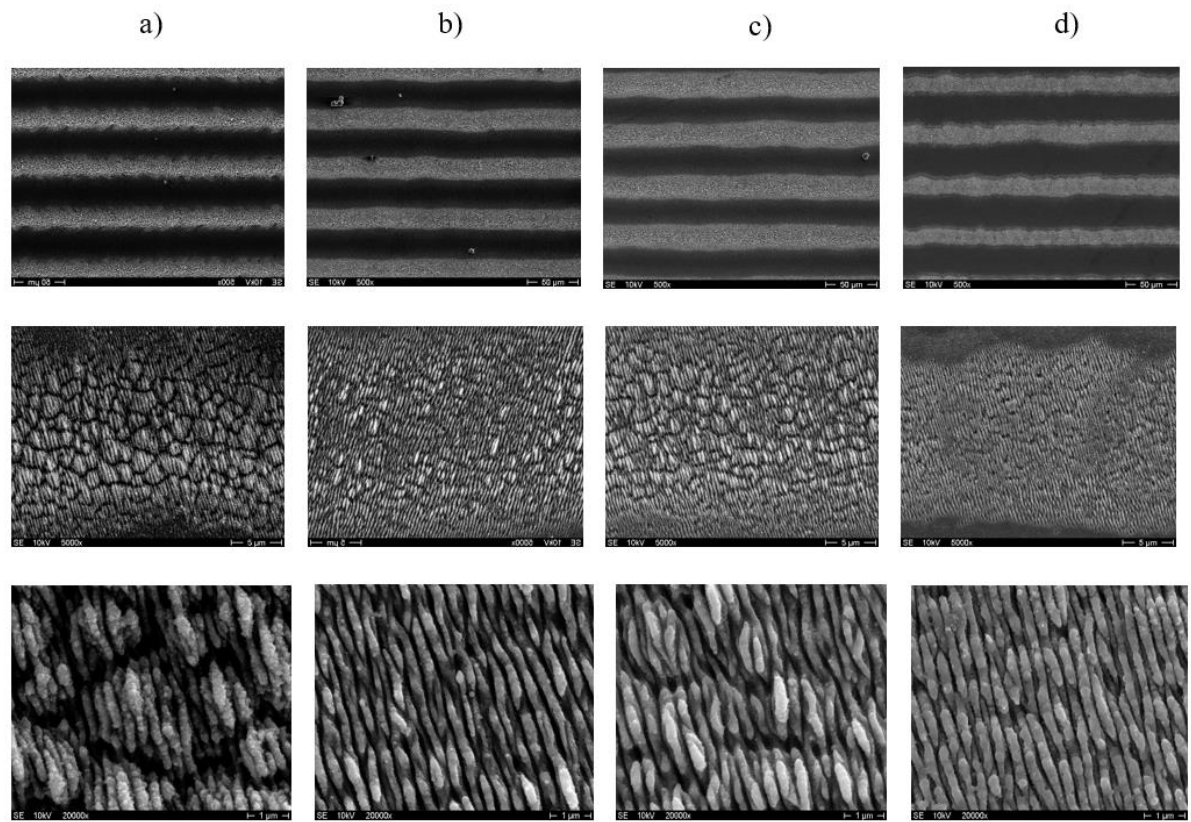
A-1.0: Stainless steel surfaces fabricated in air using femtosecond laser. Figures represented a) SSL-01-Air, b) SSL-02-Air, c) SSL-03-Air and d) SSL-04-Air.



A-1.1: Stainless steel surfaces fabricated in argon using femtosecond laser. Figures represented a) SSL-01-AR, b) SSL-02-AR, c) SSL-03-AR and d) SSL-04-AR



A-1.2: Titanium surfaces fabricated in air using femtosecond laser. Figures represented a) TTL1-Air, b) TTL2-Air, c) TTL3-Air and d) TTL4-Air.



A-1.2: Titanium surfaces fabricated in argon using femtosecond laser. Figures represented a) TTL1-Air, b) TTL2-Air, c) TTL3-Air and d) TTL4-Air.